CO2 Capture for Cement Technology

Pathi, Sharat Kumar; Dam-Johansen, Kim; Illerup, Jytte Boll; Lin, Weigang; Hjuler, Klaus

Publication date:
2013

Document Version
Publisher's PDF, also known as Version of record

TECHNICAL UNIVERSITY OF DENMARK

CO_2 Capture for Cement Technology

Ph.D. Thesis

Sharat Kumar Pathi
2013

Supervisors:
Kim Dam-Johansen (DTU)
Jytte Boll Illerup (DTU)
Weigang Lin (DTU)
Klaus Hjuler (FLSmidth A/S)

Combustion and Harmful Emission Control Research Centre

Department of Chemical and Biochemical Engineering

Preface

This thesis is the outcome of research work carried out at the Combustion and Harmful Emission Control (CHEC) research center at the Department of Chemical and Biochemical Engineering of the Technical University of Denmark (DTU) in the period from January 2010 to June 2013. The thesis was written in partial fulfillment for obtaining a Ph.D. degree at the DTU. The project work was supervised by Kim Dam-Johansen (DTU), Jytte Boll Illerup (DTU), Weigang Lin (DTU) and Klaus Hjuler (FLSmidth A/S). The project was financially supported by The Danish National Advanced Technology Foundation, FLSmidth A/S and the DTU.

I am very grateful to Kim Dam-Johansen for giving me the opportunity to work on this challenging project and for his belief in me. I am thankful to Jytte Boll Illerup for her guidance and support during the project. I owe my thanks to Weigang Lin for critical evaluation of my work and encouraging me to perform a detailed evaluation of the problems that came up, and for guiding me toward simplified working solutions. I am also very thankful to Klaus Hjuler for his precise comments and guidance, which really helped me to move forward in my project. Finally, I would like thank my entire supervisory team for their inspiration and patient review of my work. Discussions with them were interesting and challenging, which drove me to think further, to look at the bigger picture and to attain greater depth of knowledge.

I also thank my colleagues, especially the members of the cement research platform, the technical staff and the KT workshop. I would also like to thank Rolf Jensen from Mechanical Engineering (DTU) for his help with SEM analysis and Kenny Ståhl from the Chemistry Department (DTU) for his guidance on XRD pattern analysis. I would also like to thank Kirsten Theisen from FLSmidth A/S for suggestions on XRD analysis.

Finally, I would like to thank my family and friends: Pavle Ándric, Rama, Premsagar, Raghav, Prem, Ravi, Amar, Siva, Jakob and Vikas for their support during my Ph.D. studies. Last but not the least, I thank Anupama and my family for being there for me and supporting me in every possible way.

Kgs Lyngby, 27th June 2013,

Sharat Kumar Pathi.

Summary

Production of cement is an energy intensive process and is the source of considerable CO_2 emissions. It is estimated that the cement industry contributes around 8% of total global CO_2 emissions. CO_2 is one of the major greenhouse gases. In the atmosphere, the CO_2 concentration has increased from 310 ppmv in 1960 to 390 ppmv in 2012, probably due to human activity. A lot of research is being carried out for reducing CO_2 emissions from large stationary sources. Of which, the carbonate looping process is a new process and has the potential to reduce CO_2 emissions with lower energy penalties. Most of the work performed recently has focused on CO_2 capture from fossil fuel-based power plants. Inherently, this process is especially suitable for cement plants, as CaO used for CO_2 capture is also a major ingredient for clinker production. Thus, a detailed investigation was carried out to study the application of the carbonate looping process to the cement industry. In order to study the application of the carbonate looping process to cement industry, the project work is divided into three scales: 1) at particle scale (TGA), 2) at reactor scale (Fluid-bed) and 3) at process scale (process modeling Pro/II).

The results from TGA revealed that the CO_2 capture capacity of cement raw meal as a function of cycle number had a similar trend to that of limestone, i.e. the CO_2 capture capacity decreased with increasing cycle number. However, the maximum CO_2 capture capacity of calcined cement raw meal (17%, first cycle) was much lower compared to natural limestone (28%, first cycle), where calcination was carried out under realistic conditions (950°C, CO_2). After changing the calcination atmosphere from CO_2 to N_2, the difference in the CO_2 capture capacity of the sorbents was large, but the capture capacities increased for both limestone (58%) and raw meal (28%). To investigate the influence of temperature, calcination was carried out at 850°C in N_2. The results (limestone 65% and raw meal 63%) show that there was no significant difference in the CO_2 capture capacities under these conditions.

To reveal the reason behind this difference in the CO_2 capture capacity of limestone and cement raw meal, experiments were performed under realistic conditions to investigate the influence of the main components (Al_2O_3, Fe_2O_3, SiO_2) of cement raw meal on the major component i.e. limestone. The results show that each component had a unique effect on the CO_2 capture capacity of limestone. BET surface area measurements, SEM analysis and XRD analysis techniques were carried out on calcined samples to estimate the surface area of the raw meal (2 m^2/g) compared to limestone (4 m^2/g), to visualize the surface morphology of calcined limestone in the raw meal, which indicated larger grains compared to the grains of calcined natural limestone, and to investigate any interactions between limestone and other components in the raw meal, which showed no significant interactions between the components, respectively.

In the fluidized bed reactor, cycle and continuous carbonation experiments were carried out. Cycle experiments results on the trend in CO_2 capture capacity of sorbent (limestone and simulated raw meal) was similar to the TGA experimental results. Further, the fluidized bed cyclic experiment results show that the CO_2 capture capacity of cement raw meal was similar to limestone, as a function of cycle number because the calcination conditions were mild (800°C in air). The reaction rate constant was estimated as a function of the conversion of bed. In the fluidized bed reactor reaction rate constant in the initial fast reaction regime relevant for the carbonate looping process is 2 [$m^3/kmol{\cdot}s$] which drops with conversion and this rate constant is comparable to the value estimated from the TGA, which is 3.5 [$m^3/kmol{\cdot}s$].

Continuous carbonation experiments were carried out to investigate the performance of carbonator as a circulating fluidized bed reactor. A new experimental method was applied for accurate measurement of the particle recirculation rate which is the key parameter in a circulating fluidized bed reactor. The experimental results show that the most influencing parameter on the performance of carbonator is the

inlet Ca to C molar ratio. In this experiment, more than 80% of the inlet CO_2 was captured by highly deactivated limestone, which had a maximum CO_2 capture capacity of 11.5%, with an inlet Ca/C ratio of 13. So, the performance of the carbonator can be defined by the inlet Ca/C ratio, which can be estimated if the maximum capture capacity of limestone is known. A circulating fluidized bed reactor model was proposed where the particle distribution profile along the reactor height was estimated from the experiments. The reactor model was validated with experimental results, and it was used to simulate different operating conditions for the carbonator. Based on the model simulation results a particle recirculation of 2-5 kg/m^2s is sufficient for 90% CO_2 capture efficiency depending on active fraction, inlet CO_2 concentration and composition of particle stream.

Based on the main experimental results, i.e. the CO_2 capture capacity of raw meal as a function of cycle number and the main parameter that controls the performance of the carbonator, a process model integrating the carbonate looping process with the cement pyro-process was simulated. The process simulation results indicate that the CO_2 emission was only 0.07 kg/ kg cl, with an energy penalty of 2 MJ/kg CO_2 captured, whereas in a normal cement plant, it is 0.9 kg/ kg cl. However the thermal energy demand in the integrated plant increases from 3.9 MJ/ kg cl to 5.6 MJ/ kg cl. But on the other side this additional energy spent can be recovered as a high quality heat to generate electricity. The potential to generate electricity depends on the scale of the plant, the bigger the production capacity of cement plant the better, with capacity higher than 3400 tons of clinker/day is required to produce captive electricity to meet the demand both from the cement plant operations and from the CO_2 capture system operations.

Dansk resume

Fremstillingen af cement er en energiintensiv proces, der også udleder store mængder CO_2. Det er estimeret, at cementindustrien står for omkring 8% af den samlede, globale udledning af CO_2, der er en af de vigtigste drivhusgasser. Koncentrationen af CO_2 i atmosfæren er steget fra 310 ppmv i 1960 til 390 ppmv i 2012, hvilket hovedsageligt tilskrives menneskelige aktiviteter. Karbonat-looping processen er en ny proces, som potentiaelt kan nedbringe CO_2-udledningen med et mindre energitab end andre CO_2-opsamlingsprocesser. Processen er specielt egnet til cementfremstillingsanlæg, da den anvendte sorbent er kalksten, der også er en det primære råmateriale ved fremstilling af cementklinker.

For at undersøge anvendelsen af karbonat-looping-processen i cementindustrien, har arbejdet i nærværende projekt fokuseret på tre forskellige skalaer: 1) partikel-skala (TGA), 2) reaktor-skala (Fluidbed) og 3) proces-skala (procesmodellering Pro / II).

Resultaterne fra TGA-undersøgelserne viser, at CO_2-opsamlingskapaciteten for cementråmel og ren kalksten udvikler sig ens over tid, det vil sige, at opsamlingskapaciteten falder med et stigende antal cyklusser. Den maksimale CO_2-opsamlingskapacitet for cementråmel (17% i første cyklus) er imidlertid meget lavere end for ren kalksten (28% i første cyklus), når kalcineringen bliver udført ved realistiske procesbetingelser (950°C og CO_2-rig atmosfære). Ved ændring af kalcineringsatmosfæren fra CO_2 til N_2 er der stadig stor forskel i opsamlingskapaciteten af sorbenterne, men generelt stiger kapaciteten for kalksten (58% i første cyklus) og råmel (28% i første cyklus). For at undersøge indflydelsen af kalcineringstemperaturen blev der også udført kalcineringer ved en lavere temperatur (850°C, i ren N_2). Resultater fra dette forsøg viser ikke nogen stor forskel i CO_2 opsamlingskapaciteten for de 2 materialer (kalksten 65% og råmel 63%), det vil sige at råmelets kapacitet stiger til samme niveau som kalkstenens.

For at klarlægge årsagen til denne forskel i CO_2-opsamlingskapacitet mellem kalksten og cementråmel ved realistiske betingelser (høj temperatur og CO_2-koncentration), blev indflydelsen af de vigtigeste komponenter (Al_2O_3, Fe_2O_3, SiO_2) i cementråmel på hovedkomponenten (kalksten) undersøgt eksperimentelt. Resultaterne viser, at hver komponent har en unik effekt på opsamlingskapaciteten af kalksten. Mekanismerne bag effekten af de forskellige komponenter blev undersøgt for kalcineret kalksten og råmel ved hjælp af forskellige analysemetoder: Brunauer-Emmett-Teller (BET) overfladearealbestemmelse, elektronmikroskopi (SEM) og røntgendiffraktion (XRD). BET-målingerne viste, at overfladearealet af råmel kun var 2 m^2/g, mens det var 4 m^2/g for kalksten, og SEM-analyserne viste at kalkstenmikrokornene i råmel var større end mikrokornene i ren kalksten. Ud fra XRD-analyserne kunne der ikke ses tegn på betydelige interaktioner mellem komponenterne. Graden af sintring afhænger af de komponenter, der findes sammen med kalksten i råmelet.

I fluidbed-reaktoren blev der udført cykliske og kontinuerte kaboneringsforsøg med kalksten og råmel. Resultaterne viser, at CO_2-opsamlingskapaciteterne, for de to sorbenter, er de samme som opnået i TGA-forsøgene. Desuden viser forsøgene, at opsamlingskapaciteten, som funktion af antallet af cyklusser, er den samme for kalksten og råmel, når forsøgene udføres ved milde kalcineringsbetingelser (800°C i luft). Reaktionshastighedskonstanterne er beregnet som en funktion af sorbentens omdannelsesgrad i de to forsøgsopstillingers bedmateriale. Ud fra fluidbedforsøgene blev den initiale hurtige hastighedskonstant, som er relevant for karbonat-looping processen, beregnet til 2 $m^3/(kmol\ s)$, hvilket er samme størrelsesorden som hastighedskonstanten på 3,5 $m^3/(kmol\ s)$ beregnet ud fra TGA-forsøgene,

Kontinuerte karboneringsforsøg blev udført for at undersøge karbonatorens ydeevne, når reaktoren anvendes som en cirkulerende fluidbedreaktor. Partikelcirkulationshastigheden, som her er en vigtig parameter, blev målt ved hjælp af en ny eksperimental metode. Resultaterne viser, at den vigtigste

parameter for reaktorens ydeevne er Ca/C-forholdet ved indgangen til reaktoren. Når forholdet er ca. 13 kan der opnås en reduktion af det tilførte CO_2 på mere end 80%, selvom kalkstenen er deaktiveret, og derfor kun har en maksimal absorptionskapacitet på 11,5 %. En matematisk model for en cirkulerende fluidbedreaktor er blevet opbygget, hvor partikelfordelingsprofilen som funktion af reaktorhøjden er bestemt ud fra eksperimentelle forsøg. Modellen er valideret og anvendt til at simulere karbonatoren ved forskellige forsøgsbetingelser. Modelsimuleringerne viser, at der kan opnås en CO_2-reduktion på 90 % ved en cirkulationshastigheden på 2-5 kg/m^2/s. Cirkulationshastigheden vil afhængige af andelen af aktiv sorbent, indgangs CO_2-koncentrationen samt den kemiske sammensætning af partikelstrømmen.

En matematisk model er opbygget til simulering af integrationen afkarbonat-looping-processen med et cementanlæg. Modellen er baseret på hovedresultaterne fra de eksperimentelle forsøg, der omhandler CO_2-opsamlingskapaciteten af råmel som funktion af antallet af cyklusser, samt den parameter, der er vigtigst for karbonatorens opsamlingskapacitet – forholdet mellem Ca og C ved indgangen til reaktoren. Resultaterne fra anvendelse af modellen til processimuleringer indikerer, at CO_2-emissionen kan reduceres fra 0,9 kg/(kg klinker) til 0,07 kg/(kg klinker) ved anvendelse af karbonat-looping-processen. Umiddelbart stiger energiforbruget fra 3,9 MJ/(kg klinker) til 5,6 MJ/(kg klinker); dette vil dog i nogen grad kunne genindvendes til produktion af elektricitet. Potentialet for produktion af elektricitet vil afhænge af cementanlæggets størrelse. For at kunne dække strømforbruget til et cementproduktionsanlæg og en CO_2-opsamlingsprocesse, skal cementanlægget have en kapacitet på mindst 3400 tons klinker pr. dag.

Table of Contents

List of Figures

List of Tables

Abbreviations

AC: Avoided Cost

ASU: Air Separation Unit

BET: Brunauer-Emmett-Teller

CANMET: Natural Resources Canada

CCS: Carbon Capture and Sequestration

CFB: Circulating Fluidized Bed

CIS: Commonwealth of Independent States

CLP: Carbonate Looping Process

CO_2-CPU: CO_2 Compression and purification Unit

COE: Cost of Electricity

CSIC: Spanish National Research Council

ECRA: European Cement Research Academy

FWHM: Full Width at Half Maximum intensity

ICDD: International Centre for Diffraction Data

IEA: International Energy Agency

IFK (Germany): Institute of Power Plant Technology (Stuttgart)

ILC: In Line Calciner

INCAR: Instituto Nacional del Carbón

IPCC: Intergovernmental Panel on Climate Change

ITRI (Taiwan): Industrial Technology Research Institute

K-L: Kunii Levenspiel

KIER: Korean Institute of Energy research

OSU: Ohio State University

SEM: Scanning Electron Microscopy

SLC: Separate Line Calciner

TGA: Thermo-Gravimetric Analyzer

TU (China): Tsinghua University

TUD (Germany): Technical University of Darmstadt

WHRS: Waste Heat Recovery System

XRD: X-Ray Diffraction

Notation

$P_{CO_2,eq}$: CO_2 thermodynamic equilibrium pressure over CaO [pa] or [atm].

$X_{carb,N}$: Conversion of CaO to $CaCO_3$ carbonation or CO_2 capture Capacity in the N^{th} cycle [-].

$n_{CO_2,N}$: Number of moles of CO_2 captured at the end of carbonation in the N^{th} cycle [mol].

$n_{CaCO_3,0}$: Initial number of moles of $CaCO_3$ [mol].

$m_{sample,N}$: Weight of the sample at the end of the N^{th} carbonation cycle [mg].

$m_{CaO,1}$: Weight of the sample at the end of the 1^{st} calcination cycle [mg].

$w_{in,N}$: Weight of the sample before analysis [mg].

$w_{f,N}$: Final weight of the sample [mg].

D : Crystallite size [nm].

K : Crystallite-shape factor = 0.9 [-].

λ : X-ray wavelength, 0.15418 [nm].

θ : Observed peak angle, [radians].

β : X-ray diffraction broadening (FWHM) [radians].

X_N : CO_2 capture capacity in the N^{th} cycle [-].

$X_{\max}$: Maximum CO_2 capture capacity [-].

X_r : Residual CO_2 capture capacity [-].

k : CO_2 capture capacity decay constant [-].

$V_{CO_2,total}$: Volume of CO_2 in the fresh limestone [NL].

w_{CaCO_3} : Weight of limestone fed in to the reactor [g].

ρ_{CO_2} : Density of CO_2 gas [1.97 g/NL].

M_{CO_2} : Molecular weight of CO_2 [mol/g].

M_{CaCO_3} : Molecular weight of $CaCO_3$ [mol/g].

ϕ_i : Volumetric flow rate gas "*i*" [NL/min].

$x_{CO_2,inlet}$: Inlet volume fraction of CO_2 in the fluidizing gas [vol.%].

$x_{CO_2,outlet}$: Outlet volume fraction of CO_2 in the exit gas [vol.%].

X_{cal} : Degree of calcination $CaCO_3$ to CaO carbonation [-].

x_{SO_2}, : Concentration of SO_2 in the exit gas in [ppmv].

X_{SO_2} : Conversion of SO_2 gas based on inlet and outlet molar flows [-].

$\phi_{SO_2,in}$: Inlet flow rate of SO_2 gas [NL/min].

k_a : Attrition rate constant [1/s].

W : Bed weight [g].

$W_{\min}$: Minimum bed weight [g].

Ecarb : CO_2 capture efficiency [-].

C_{CO_2} : CO_2 concentration [mol/m^3].

$C_{CO_2,eq}$: Equilibrium CO_2 concentration [mol/m^3].

δ : Bubble fraction in the fluid bed [-].

$(1-\delta)$: Emulsion fraction in the fluid bed [-].

γ_e : Particle fraction in the emulsion region [-].

K_{be} : Gas transfer co-efficient from bubble to emulsion region [1/s].

u_{mf} : Minimum fluidization velocity [m/s].

u_o : Superficial gas velocity [m/s].

u_b^* : Bubble rise velocity [m/s].

d_b : Bubble diameter [m].

R : Gas constant [m^3atm/kmol K].

k_s : Carbonation rate constant [m^4/kmol·s]

k_f : Carbonation rate constant [m^3/kmol·s]

δ_{cd} : Bubble or core region in dense bed [-].

ε_s : Particle fraction [-].

ε_{sd} : Particle fraction in the dense bed [-].

ε_{se} : *P*article fraction at the reactor exit [-].

a : Particle distribution decay constant [1/m].

η_l : contact efficiency in the freeboard [-].

η_d : contact efficiency in the dense bed [-].

H_t : Reactor height [m].

$H_l or H_f$: Height of free board region [m].

H_d : Height of dense bed [m].

A_t : Cross sectional area of reactor [m^2].

K_r : Carbonator reaction rate [1/s].

1. Introduction

1.1 Background

Carbon dioxide (CO_2) is one of the major greenhouse gases. The concentration of CO_2 in the atmosphere tends to rise, which needs to be controlled to mitigate climate change. The rise in CO_2 concentration is mainly due to anthropogenic sources, of which the cement industry was estimated to contribute around 5% of total global CO_2 emissions in 2001[1] and above 8% by 2012[2,3]. The cement industry has been growing steadily and this is expected to accelerate in coming decades, since major growth is foreseen in countries such as China, India and other economically growing countries. Cement production is both energy- and emissions-intensive, and the CO_2 emissions are both energy use- and process-related[4]. According to the Intergovernmental Panel on Climate Change (IPCC), carbon capture and sequestration (CCS) from large stationary sources is considered the best mid-term mitigation option to avoid climate change[5].

The first step in CCS is to separate CO_2 from the flue gas. One of the emerging new technologies for capturing CO_2 is the carbonate looping process (CLP)[6]. This process is expected to have huge potential as an alternative to other CO_2 capture processes, especially in terms of its lower energy penalty. In this process, a sorbent material is looped between two reactors, one for capturing CO_2 from the flue gas and the other for releasing concentrated CO_2 gas from the sorbent regenerator. A schematic diagram of the CLP integrated to the cement pyro-process is presented in Figure 1-1. The CLP is especially suitable for the cement industry because:

1. Limestone, the main component in the raw meal for cement production, is used as a sorbent.

2. High quality energy can be extracted from the process as this process takes place at a high temperature.

However, there are many unknown factors in adapting this process for industrial applications, such as:

1. Can cement raw meal be used as a sorbent in the looping process?
2. What is the influence of the raw meal composition on the CO_2 capture capacity?
3. What are the important operating parameters in the reactor design for using raw meal as a sorbent?
4. How can the looping process be integrated into the cement pyro-process?

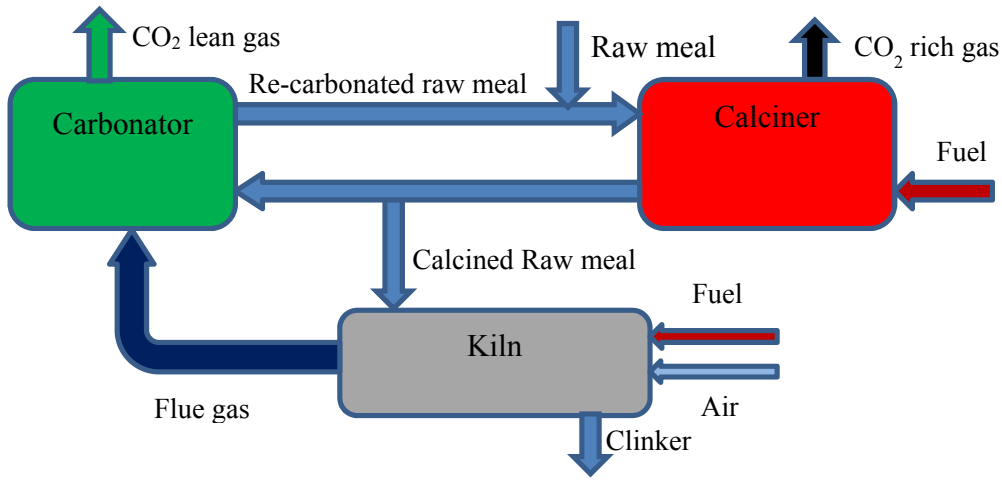

Figure 1-1: Schematic diagram of the carbonate looping process integrated into the cement pyro-process.

1.2 Scope of Work

In order to evaluate these unknown factors, the present work is divided into an experimental and a modeling part, where the experimental results are used for model development and optimization. In the experimental work, investigations were carried out in a small thermo-gravimetric analyzer (TGA)

apparatus and in a lab scale fluidized bed reactor. A TGA apparatus was used to study the application of the cement raw meal as a CO_2 sorbent under controlled reaction conditions, i.e. temperature, CO_2 concentration, heating rate and time. The results from these experiments, along with detailed particle analyses, were used to understand the mechanism underlying the CO_2 capture capacity of a calcined raw meal in the looping process. In the fluidized bed reactor setup, experiments were carried out to simulate the looping process in batch mode and in continuous mode to evaluate reactor performance. In batch mode, cyclic experiments were performed to simulate looping reaction conditions in the fluidized bed reactor. Continuous mode experiments were performed to study the influence of operating parameters on the performance of the carbonator.

In the modeling work, the carbonator reactor was modeled as a bubbling fluidized bed reactor to describe the carbonation of calcined limestone in the bed from cyclic experiments and as a circulation fluidized bed (CFB) reactor to evaluate the performance of the carbonator in the steady state. The model predicted results were validated with the experimental results. A correlation equation was used to describe the CO_2 capture capacity of the raw meal as a function of looping cycle number from the TGA experiments. The correlation equation fitted to the experimental data was used in process modeling to simulate carbonate looping integrated with a cement clinker production process. The integrated process model was used as a tool to evaluate the energy penalty for CO_2 capture from the cement production process.

1.3 Objectives

The main objective of this thesis was to provide scientifically-based knowledge regarding the carbonate looping process for reducing CO_2 emissions by the cement industry. This is sought through

experimental investigations under controlled conditions and by mathematical modeling to evaluate important parameters.

The thesis is intended to provide knowledge on the application of raw meal as a sorbent, which could pave the way to easy integration of the carbonate looping process into the cement pyro-process for reducing CO_2 emissions from the cement production process. Furthermore, it could form the basis for redesigning cement clinker production and thereby improve the efficiency of the process along with lowering CO_2 emissions.

The focus is on the cement industry, but these results could also be used for other processes related to CO_2 capture by limestone, like the fossil fuel-based power sector and hydrogen production from biomass.

1.4 Structure

Chapter 2 of the thesis provides the background on cement production and CO_2 emissions, and summarizes the literature with a description of the carbonate looping process and its status in terms of research and industrial applications.

Chapter 3 focuses on the application of raw meal as a sorbent in the CLP. The emphasis is on the CO_2 capture capacity of the limestone in the raw meal, and the mechanism for decay in the CO_2 capture capacity was investigated in detail. The results from the CO_2 capture capacity of the raw meal with respect to the looping cycle number was described by a correlation, which was used later in process modeling for the integration of the carbonate looping process with the cement production process.

Chapter 4 presents the cycle experiments to simulate the carbonate looping processes in a fluidized bed reactor with limestone and raw meal. The cyclic carbonation behavior was investigated in the fluidized reactor as a function of various operating parameters.

Chapter 5 includes the results of the continuous carbonation experiments from the fluidized bed reactor simulated as a CFB reactor. The experiments were performed to investigate the influence of the main operating parameters on the performance of the carbonator. Key parameters estimated from the experiments were used for the development of the K-L steady state carbonator reactor.

Chapter 6 is on process modeling of integrating the carbonate looping process with a cement production process. This model was simulated using the experimental results, and an evaluation of the entire process was performed based on the additional thermal energy supplied along with cogeneration potential.

Chapter 7 contains the overall conclusions and suggestions for future work.

2. Literature Review

2.1 Cement Industry

Cement is one of the most abundantly consumed products, and is one of the primary components of concrete, which is used globally for construction and the development of infrastructure. The production of cement has been increasing rapidly since the late 1990s, and it is estimated that global production increased from around 1.6 to 3.6[7] billion metric tons from 2001 to 2011. The trend in cement production is shown in Figure 2-1, where 100 units are considered as the reference point in 2001. Cement production increased in all regions until 2007, then decreased in some regions due to the economic slowdown in 2008 and 2009; however, cement production in rapidly growing economies continued the accelerating trend. The major share of cement production in 2011 was in China (>50%), followed by India (6.2%)[7]. Cement production in the coming decades is also expected to increase further due to huge developments in infrastructure projects, especially in emerging economies.

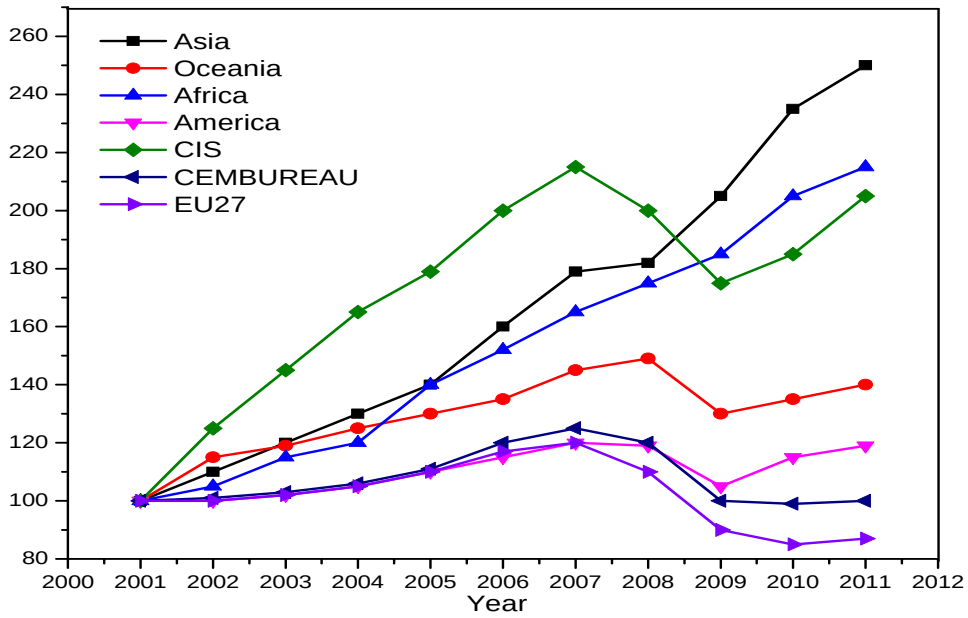

Figure 2-1: World cement production by region from 2001-2011; Index 2001=100[7].

Cement manufacture is an energy-intensive process. The energy consumption by the cement industry is estimated to be 8% of the global industrial energy consumption[2], including the combustion of fuels and use of electricity. The specific thermal energy for clinker production has decreased significantly over the last 50 years. This is mainly attributable to improved process technology[8]. The energy demand depends on the type of kiln, from 5-6 MJ/kg clinker in a long kiln to 3-4 MJ/kg clinker in a modern kiln with pre-heaters and a pre-calciner[9]. Even though the specific thermal energy has decreased, the cement production process is still considered an energy- and emission-intensive process.

The basic principle of the cement production process is presented briefly in the following sections. This section gives general information to understand the cement production process and sources of CO_2 emissions.

2.1.1 Cement Production

There are many types of cement, depending on the end use, but the main content of these cements is the cement clinker. One of the highly produced cement types is Portland cement (95% clinker), which is produced by burning limestone with sand and clay. The input material, also called cement raw meal, mostly contains calcium carbonate ($CaCO_3$), silica (SiO_2), aluminum oxide (Al_2O_3) and iron oxide (Fe_2O_3). The cement raw meal is heated to 1450°C in the kiln, which results in a series of chemical and physical processes, forming granules/nodules termed clinker. The clinker is cooled and ground along with 5% gypsum to form a fine powder called cement. The main steps in cement production are quarrying of the raw materials, pre-treating the raw material, pyro-processing, cooling, grinding with gypsum and shipping. The central step in the cement production process from a chemical perspective is the pyro-process, shown in Figure 2-2, where a series of steps takes place with changes in the temperature of the raw meal. These steps include drying the raw materials, calcination of limestone in

the raw material, clinker formation at the highest temperature and controlled cooling of the sintered product to obtain the desired components. Clinker production can be categorized based on the moisture content of the feed going into the kiln as a wet, semi-wet, semi-dry or dry process[10]. The pyro-process in a modern kiln uses cyclone pre-heaters, a calciner and a rotary kiln to form clinker components. The main components of clinker are belite ($2CaO{\cdot}SiO_2$, 7-32%), alite ($3CaO{\cdot}SiO_2$, 45-75%), aluminate ($CaO{\cdot}Al_2O_3$, 1-18%) and ferrite ($4CaO{\cdot}Al_2O_3{\cdot}Fe_2O_3$, 1-18%)[11].

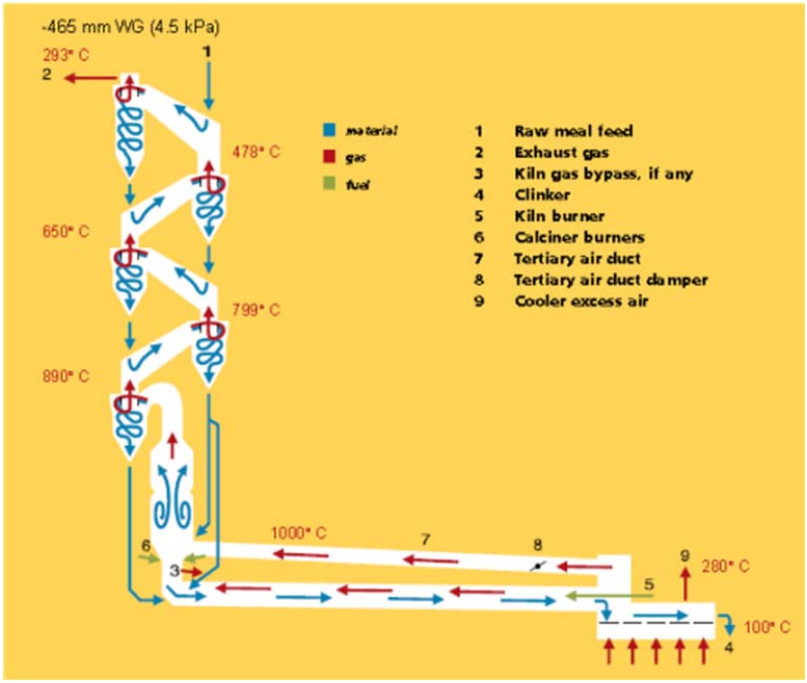

Figure 2-2: A typical schematic representation of a modern large kiln system (FLS design)[12].

2.1.2 Pyro-process

In the pyro-process, the cold raw meal is heated and calcined in the calciner. Calcination is the major chemical step in the thermal treatment of raw meal, where $CaCO_3$ decomposes into CaO and CO_2 as shown in equation (2-1):

$$CaCO_3 \rightleftharpoons CaO + CO_2 \qquad \Delta H = 1782 kJ / kg CaCO_3 \qquad \text{2-1}$$

Calcination is highly endothermic, and the energy for this reaction is supplied by the combustion of fuel in the calciner, where the temperature is around 870°C. This reaction is controlled by the equilibrium relationship between the temperature and the CO_2 partial pressure in the calciner. The next step in pyro-processing after calcination is the clinker reactions, which occur between 700 and 1450°C, where calcined raw meal is converted into the cement clinker product. This process is initiated at the calciner stage, where the temperature is around 870°C, and continues in the rotary kiln, where the temperature of the material increases to 1450°C. The series of clinker reactions with respect to temperature range is summarized below[9]. At temperatures above 700°C, calcined limestone reacts with silica to form belite:

$$2CaO + SiO_2 \rightarrow 2CaO \cdot SiO_2 \qquad \text{2-2}$$

At temperatures above 900°C, calcined limestone reacts with alumina or iron oxide to form the compounds aluminate and ferrite according to equations (2-3, 2-4):

$$3CaO + Al_2O_3 \rightarrow 3CaO \cdot Al_2O_3 \qquad \text{2-3}$$

$$4CaO + Al_2O_3 + Fe_2O_3 \rightarrow 4CaO \cdot Al_2O_3 \cdot Fe_2O_3 \qquad \text{2-4}$$

At temperatures above 1300°C in the melt phase, lime (CaO) reacts with belite to form alite according to equation (2-5):

$$CaO + 2CaO \cdot SiO_2 \rightarrow 3CaO \cdot SiO_2 \qquad \text{2-5}$$

The set of reactions mentioned above present only the main components in the final clinker, but during the process, intermediate compounds are involved, and the clinker reactions are affected by minor compounds in the feedstock. The details of these reactions are presented in the literature.[11] The main

parameter of these clinker reactions is the temperature, which initiates the solid-solid reactions, the liquid phase sintering and the final cooling with reorganization of the clinker microstructure.

2.1.3 Pyro-processing Systems

The pyro-processing systems, which carry out the sequence of steps for clinker production, have multiple objectives: high production rate, high energy efficiency and low emissions levels. The pyro-process system in the modern kiln system can be divided into four sections, each performing a specific task, while improving the overall process efficiency. These sections are the pre-heater, pre-calciner, rotary kiln and cooler.

The pre-heater systems are designed and operated on the principle of counter-current flow of cold material and hot gases. The pre-heater system is divided into four to six stages, which are plant-specific depending on the moisture content, the plant capacity and the operating conditions. The pre-calciner effectively expands the system capability through a second firing stage. The heat consumption in the pre-calciner is typically 60% of the total heat input due to the endothermic calcination reaction. These systems are designed for at least 85% calcination of the raw meal. There are different types of calciner, such as an *in-line calciner* (ILC; Figure 2-2) and a *separate line calciner* (SLC; Figure 2-3). The general aims of the pre-heater and pre-calciner systems are:

- Complete combustion of calciner fuel
- Reducing the thermal load in the rotary kiln
- Obtaining a high degree of calcination
- Limiting harmful emissions
- Fuel flexibility-including alternative fuels

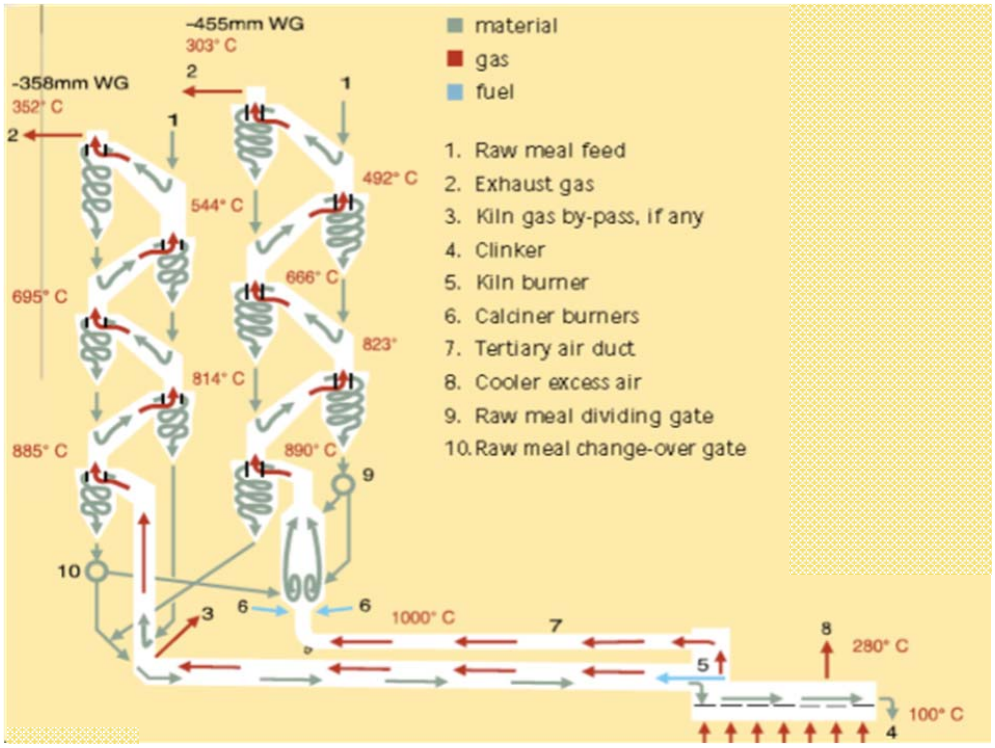

Figure 2-3: A typical schematic representation of a modern large pyro-process system with an SLC (FLS design: SLC)[12].

The next section in line is the rotary kiln, where the calcined raw meal passes through the kiln towards the burning zone and then to the cooling zone. In the rotary kiln, the heat is transferred from the gas to the solid material, but due to the flow profile, the efficiency of heat transfer is much lower than in suspension systems. New systems for the clinkering reaction with high energy efficiency are still at a research stage[13]. The most significant development in rotary kiln system was the design of two supporting short kilns with a length to internal diameter ratio of 10 to 14. This is considerably lower than the typical ratio of 16 to 18 of the three support systems. Furthermore, shorter kilns have lower thermal loading compared to longer kilns for the same production capacity[14].

The next section is the clinker cooling, which is divided into two steps: cooling inside the kiln from the maximum temperature to about 1200°C, while in the second step which takes place in the cooler, the

cooling process continues to about 100°C. The cooling process is not only for cooling and freezing clinker phases and microstructures, but also for pre-heating the combustion air, thereby improving the overall energy efficiency of the process.

2.2 CO_2 Emissions and Reductions

Figure 2-4 presents the CO_2 emissions from the top 25 countries in the world from fossil fuel combustion and cement production. The major EU countries are given separately for relative comparison with other countries.

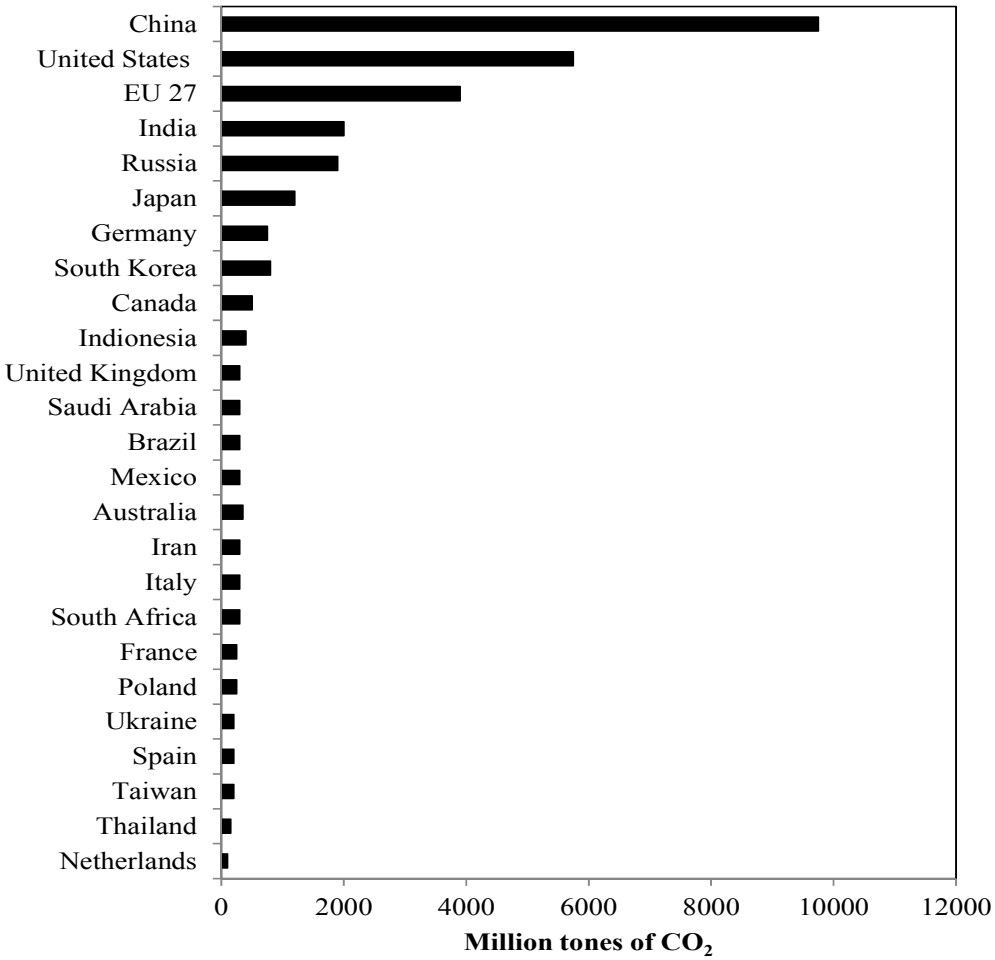

Figure 2-4: CO_2 emissions from fossil fuel combustion and cement production from the top 25 countries in 2011[2].

The production of 1 kg of cement releases about 0.7-0.9 kg CO_2, depending on the clinker to cement ratio and other factors like plant efficiency, the type of fuel and the raw material composition.

Even though cement production is an energy-intensive process, fuel combustion is not the major source of CO_2 emissions. More than 50% of the CO_2 emissions are from the process of calcination, according to eq. (2-1), as 1 kg of $CaCO_3$ releases of 0.44 kg of CO_2. The CO_2 emissions from a cement plant can be classified as direct energy–related emissions, indirect emissions from electricity consumption and process-related emissions due to the calcination of limestone. In 2011, total cement production was 3.6 billion tons, so the total CO_2 emissions from the cement industry were around 2.5-3 billion tons.

In order to reduce CO_2 emissions by the cement industry, the most feasible options are post-combustion technologies and oxy-fuel technologies. The suitable alternative for CO_2 emission reduction from a cement plant is post-combustion technologies, which do not alter the existing pyro-process because they are end-of-pipe technologies. These technologies are suitable for new kilns as well as for retrofitting. In post-combustion technologies, CO_2 capture by amines or other solvents is fairly well-developed for industrial applications[6]. In these processes, CO_2 in the flue gas is absorbed by solvents, which are then regenerated for reuse. The solvent-based process also requires a significant amount of energy for regeneration, which results in a much higher energy penalty compared to oxy-fuel technology. Oxy-fuel technology uses oxygen instead of air for the combustion of fuel, which results in a CO_2-rich exhaust stream for sequestration. Oxy-fuel technology for CO_2 emission reduction from cement plants is still under investigation[10,15]. Until now, two basic possibilities have been considered for applying this technology to cement kilns: 1) the full oxy-fuel technology, where the kiln, pre-calciner and pre-heater tower are operated in a CO_2-rich atmosphere, which results in total capture of emitted CO_2 and 2) partial oxy-fuel technology, applied only to the calciner and pre-heater tower to abate the major fraction of the CO_2 emissions and where the emissions from the kiln are released, as

occurs in a normal plant. The advantage of the latter technology compared to the former is that it can be applied with fewer plant modifications. However, the disadvantage is that it cannot reduce CO_2 emissions completely. Figure 2-5 shows the arrangement of two pre-heater towers applying partial oxy-fuel technology.

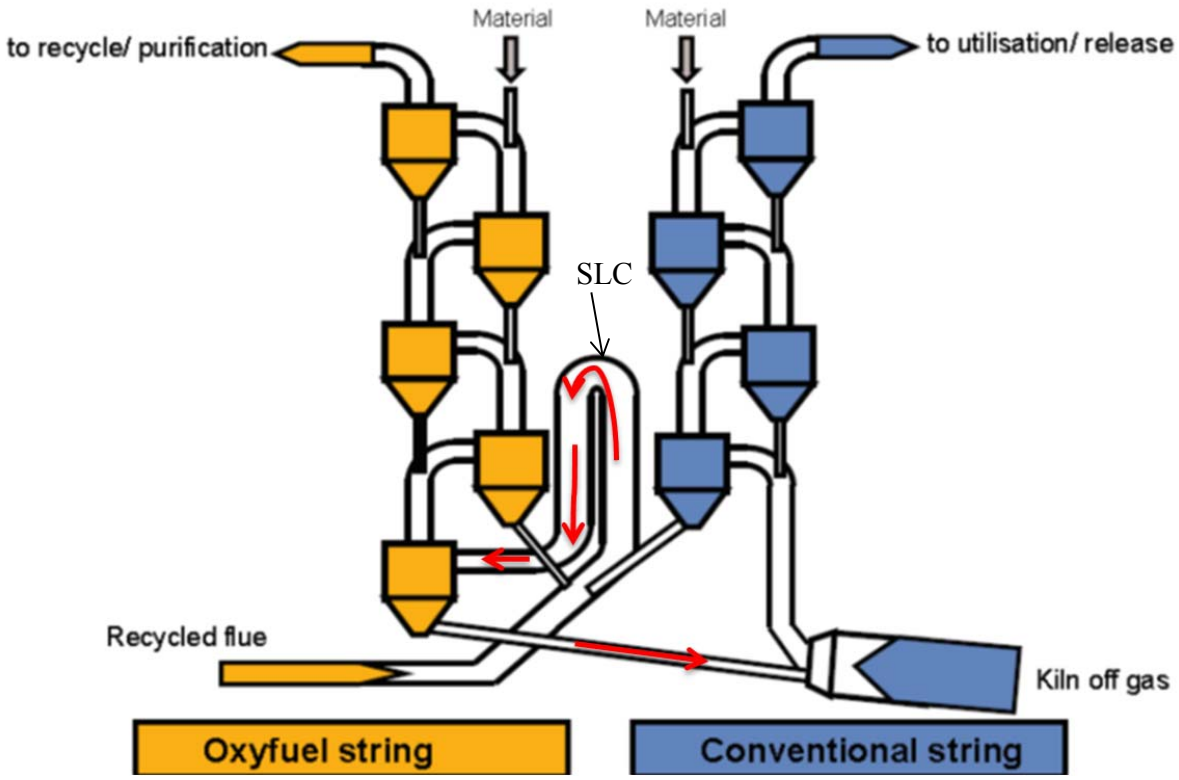

Figure 2-5: Pre-heater tower arrangement in partial oxy-fuel technology, where the material enters kiln through separate calciner line (SLC) indicated by red arrows[15].

The European Cement Research Academy (ECRA) compared both partial oxy-fuel technology and full oxy-fuel technology in their technical report[15]. The conclusion from their study indicated that both technologies have similar abatement costs (34-36 €/ton CO_2), with the partial oxy-fuel being slightly higher along with allowing higher CO_2 emissions, but the estimated investment costs can be up to 35 m€ lower for partial oxy-fuel technology. The additional electricity demand for both cases was almost

double compared to a normal plant, with the full oxy-fuel technology being 10% higher than the partial oxy-fuel technology. Furthermore, the option to retrofit for the application of partial oxy-fuel technology is considered to be less complex compared to the full oxy-fuel technology. The other alternative option for CO_2 capture is the carbonate looping process, where limestone can be used as a sorbent for CO_2 capture. This is a rather new technology, and its potential has been recognized by the ECRA[15] and the International Energy Agency (IEA)[10]. The carbonate looping process inherently includes partial oxy-fuel technology in addition to a carbonator for CO_2 capture from the flue gas. Thus, the carbonate looping process has the potential to build on the advantages of partial oxy-fuel technology and to eliminate some of its disadvantages compared to full oxy-fuel technology.

In the following sections, a literature review of the carbonate looping process is presented to understand the process and the challenges that this process poses for industrial application along with the status of current research.

2.3 Carbonate Looping Process

The main reaction governing the carbonate looping process is the reversible reaction given in eq. (2-1)[16]. The forward reaction is the calcination of limestone, which is an endothermic reaction, for the generation of a sorbent material. The reverse reaction is the carbonation of calcined limestone, an exothermic reaction, for capturing CO_2 from the flue gas. The forward and reverse reactions are dependent on the partial pressure of CO_2 and the temperature. The decomposition pressure is determined by the thermodynamic equilibrium conditions and is given as[17] :

$$P_{CO_2,eq} = 4.137 \cdot 10^{12} \exp(-20474 / (T + 273)) \qquad \text{2-6}$$

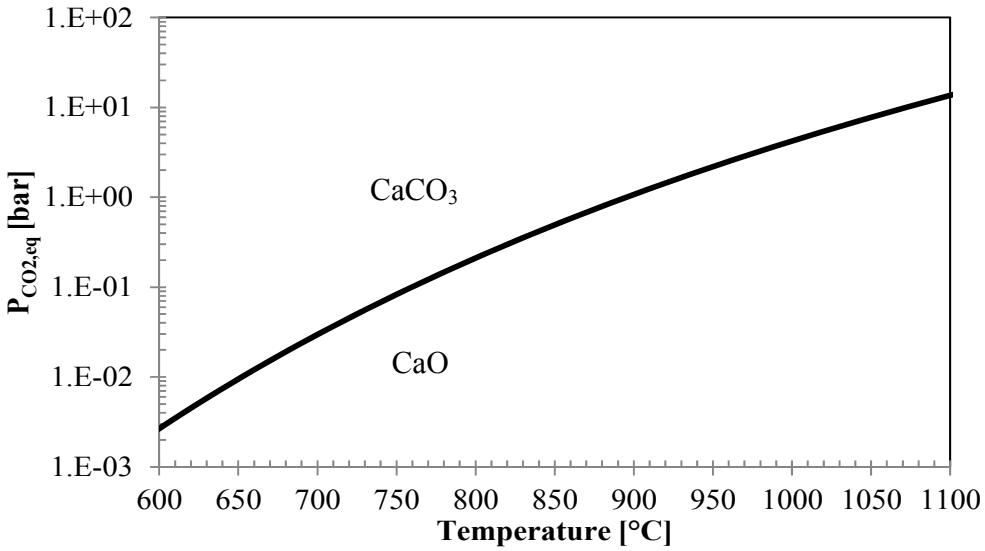

Figure 2-6: Decomposition pressure of CO_2 over CaO as a function of temperature.

$P_{CO_{2},eq}$ is in *Pa* while the temperature *T* is in ^{o}C. The equilibrium partial pressure of CO_2 over CaO increases with temperature, from ~0.003 bar at 600^{o}C to 1 bar at 900^{o}C (Figure 2-6). The partial pressure of CO_2 should always be below the equilibrium pressure for limestone calcination to take place. Conversely, for the carbonation of calcined limestone, the partial pressure of CO_2 should be higher than the equilibrium partial pressure.

In the carbonate looping process, the calcination of limestone has to be carried out at temperatures above 900°C for the generation of a sorbent in a CO_2-rich atmosphere, and carbonation has to be carried out at a temperature around 600°C for high thermodynamic capture efficiency.

2.3.1 Status on Research and Industrial Application of the Carbonate Looping Process

The carbonate looping process for capturing CO_2 from a flue gas was first proposed by Shimizu et al. in 1999[18]. Dual fluidized bed reactors are considered a suitable system for the looping process.

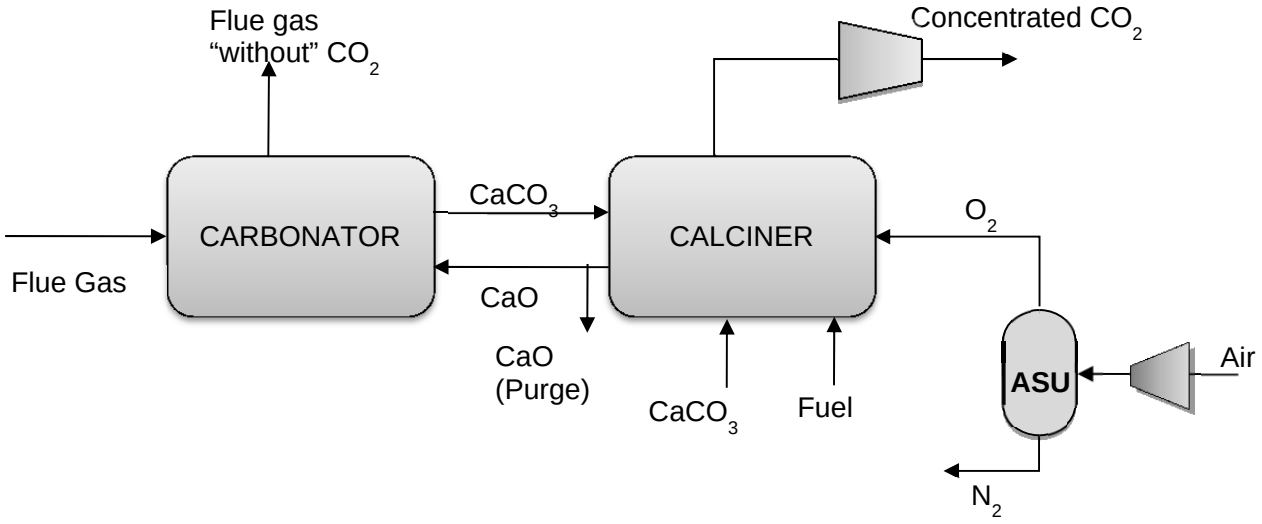

Figure 2-7: Schematic of the carbonate looping process[18].

In this process, CO_2 in the flue gas can be captured by calcined limestone particles as a sorbent material in a fluidized bed carbonator. The stream of partly carbonated sorbent particles leaving the carbonator is transferred to a second fluidized bed reactor, where the sorbent particles are regenerated to calcined limestone. The regeneration of the sorbent particles is carried out in a CO_2-rich atmosphere to release the captured CO_2 in a concentrated form, which can be further processed, compressed and transported for sequestration. The energy for regeneration of a sorbent can be supplied by the combustion of fuel under oxy-fuel conditions. Furthermore, the carbonate looping process is carried out at a high temperature (600-950^{o}C), meaning that high quality energy can be extracted from the process, suitable for electricity generation. Thus, the energy penalty for capturing CO_2 can be reduced. Figure 2-7 shows the schematic diagram of the carbonate looping process.

The carbonate looping process is considered to be an alternative option for capturing CO_2 from fossil fuel-based power plants, but it can also be applied to any process industry. This process appears to be applicable not only to new plants, but also as a retrofit to existing plants. The potential of this process

to reduce the CO_2 emissions from fossil fuel-based power plants at a lower energy penalty compared to the other alternatives was soon recognized by many research groups across the globe, i.e. INCAR (Spain) in 2002[19], Ohio State University (US) in 2002[20], CANMET (Canada) in 2003[21], Tsinghua University (China) in 2007[22], TUD (Germany) in 2009[23], IFK (Germany) in 2010[24], the Korean Institute of Energy Research in 2007[25], ITRI (Taiwan) in 2011[26]).

In the early 2000s, a number of the experiments were carried out in a small TGA and in a fixed bed apparatus to investigate the influence of reaction conditions[19,21,25,27-35]. The results from these experiments were used to understand the reaction kinetics and established the effects of reaction conditions on the CO_2 capture capacity of the sorbent as a function of looping cycle number. The main observation from these results was that the CO_2 capture capacity decreases with an increasing number of looping cycles. The impact of this result on the process is that the sorbent material in the looping process has to be replaced after some time to maintain a high CO_2 capture efficiency. This is one of the challenges in applying the carbonate looping process. However, research is being carried out to improve the CO_2 capture capacity of the sorbent material by different methods, such as doping[36,37] thermal pre-treatment[38] and reactivation of the sorbent[39].

Since the carbonate looping process is a heterogeneous, gas-solid reaction, fluidized bed reactors are considered to be the most appropriate for industrial application. So, carbonate looping experiments were carried out in a single fluidized bed reactor from 2004 onwards[22,25,40-43] and later on in dual fluidized bed reactors from 2009[44-48]. The tests in dual fluidized bed reactors were performed in the range from 10 kW-1.7 MW_{th}[26,49-56] to investigate the feasibility, hydrodynamic stability and influence of operating parameters. Lately, scale-up tests in pilot plants (0.2-1.7 MW_{th}) have been carried out by the CSIC-INCAR (Spain)[56], IFK[52] and TUD[55].

Most research groups are focusing on implementing the carbonate looping process in fossil fuel-based power plants, which is the natural choice based on the amount of CO_2 emitted from this sector. There is also growing interest in applying this process to other sectors like the cement industry. Research groups in the UK (the University of Edinburgh) and in Spain (CSIC)[57] are investigating the carbonate looping process for CO_2 capture from the cement industry. Their studies have mainly focused on process modeling[58,59].

2.3.2 Calcination

The calcination reaction is the primary step for CO_2 capture from a flue gas using calcium carbonate as a sorbent. After calcination, the produced calcium oxide has only 56% of the mass of the initial parent carbonate, since the relative molar volume of calcium carbonate is 36.9 cm^3/mol, whereas for calcium oxide this is only 16.9 cm^3/mol. If there is negligible particle shrinkage, the porosity of calcium oxide from a non-porous carbonate will increase to a theoretical value of 0.55. In reality, the final porosity will depend on the type of limestone, as different limestones have different initial porosity and composition[60], which affects the final structure of a calcined limestone under calcination conditions (temperature, reaction atmosphere and time). The final porous structure of a calcined limestone, which determines the surface area, plays an important role in the CO_2 capture capacity, since the CO_2 gas reacts with active sites on the surface of a calcined limestone and accessibility to these sites is an important parameter.

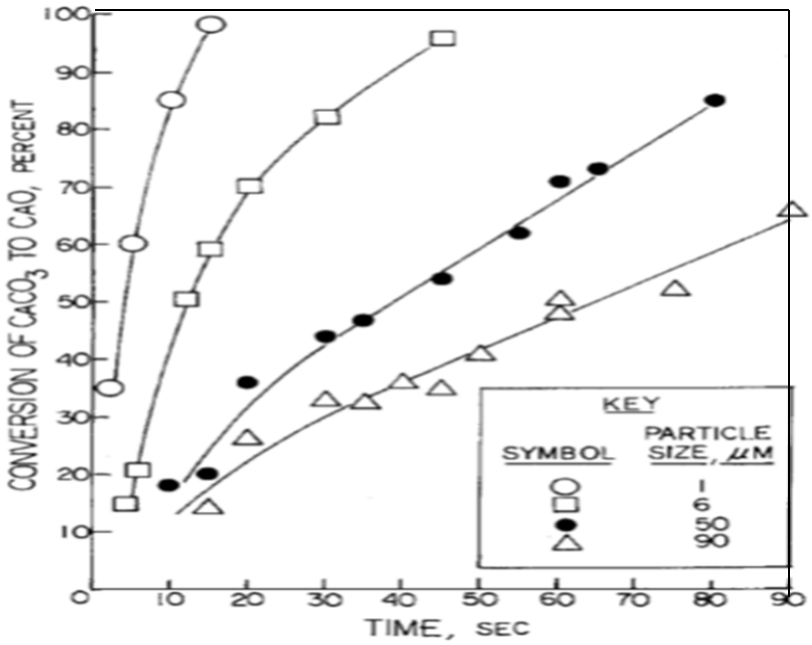

Figure 2-8: Effect of particle size on the rate of calcination at 710°C under a flow of nitrogen [61].

The calcination reaction is discussed to understand the mechanism and its effects on the CO_2 capture capacity of limestone. During calcination, two things occur: 1) CO_2 release and 2) sintering of the particle. The rate of calcination of a limestone particle depends on the particle size, the CO_2 partial pressure and the temperature at the reaction front. The size of the particle is an important factor that determines the kinetics of calcination, as a smaller particle results in a higher reaction rate and vice versa, as can be observed in Figure 2-8. Diffusion of CO_2 from the reactant surface through the porous structure of the particle to the bulk gas surrounding the particle will significantly affect the rate of reaction, as the size of the particle increases. For particles in the size range of 1-90 μm, the chemical reaction controls the calcination rate[17,61], whereas for particles above 6 mm, the heat transfer rate becomes the controlling parameter[62]. For particles between these sizes, the chemical reaction and internal mass transfer are the main resistances that control the calcination rate. Thus, the relative importance of each resistance depends on the particle size and on the porous structure of the particle.

The calcination reaction rate equations established by different researchers are compiled in Table 2-1. The rate of calcination is an important factor, because it effects the time for calcination, and it has an indirect effect on the final structure of the calcined particle, which affects the CO_2 capture capacity.

Table 2-1: Calcination reaction rate expressions from the literature.

Rate equation	Constant	Ref.
$r_{cal} = k_{s\_B} A_{CaCO_3} [mol/s]$	$k_{s\_B} = 6.078e7 \exp(-205/RT)[mol/m^2 s]$ $A_{CaCO_3}[m^2]$	Borgwardt[61]
$r_{cal} = k_{s\_B}(1 - P/P_{eq}) A_{CaCO_3}[mol/s]$	$0.01P_{eq} < P < P_{eq}[atm]$	Hu& Scaroni[63]
$r_{cal} = V_{M\_CaCO_3} k_D (P_{eq} - P)$ [m/s]	$k_D = 0.00122 \exp(-4026/T)[kmol/m^2 s \cdot atm]$ $P_{eq}[atm]$	Silcox[17]
$r_{cal} = 3K_{r\_R} V_{M\_CaCO_3} (1-X)^{2/3} / R_p$ $[1/s]$	$K_{r\_R} = 16.68 \exp(-1.186e8/RT)[kmol/m^2 s]$ $R_p[m]$	Rao[64]
$r_{cal} = k_{d\_S}(P_{eq} - P)$ $[mol/m^2 s]$	$k_{d\_S} = 0.0012 \exp(-33.47/RT)[mol/m^2 s \cdot kPa]$ $P_{eq}[kpa]$	Stanmore & Gilot[65]

In the carbonate looping process, calcination (regeneration) of limestone has to be carried in a CO_2-rich atmosphere and energy has to be supplied for the endothermic calcination reaction. In the literature, different options have been proposed, such as: i) energy transfer using heat-carrying particles, ii) direct heat transfer, iii) chemical looping combustion and iii) oxy-fuel combustion[66]. Of these different methods, each has its limitations, but the oxy-fuel combustion method appears to be technically feasible at this stage. The reaction atmosphere of the regenerator will influence limestone calcination. Under realistic calcination conditions, the concentration of CO_2 will be the major fraction, followed by H_2O, SO_2 and the other minor components depending on the composition of the fuel.

Chen et al.[67] and Wang et al.[68] investigated the calcination characteristics of limestone under oxy-fuel combustion conditions. The time for complete calcination increased from 2 to 10 min after increasing the CO_2 concentration from 0 to 80% at a reactor temperature of 950°C[67-69]. The main parameter controlling the calcination reaction rate is the difference between the partial pressure of CO_2 and the equilibrium CO_2 pressure. Similar experiments were also performed by Wang et al.[68] in a fluidized bed reactor. The time required for complete calcination was different, which was due to the type of reactor used, but the results were qualitatively similar to those of Chen et al.[67] Increasing the H_2O concentration theoretically lowers the calcination temperature, and it could be favorable to have a high concentration of H_2O[70]. However, there might be other problems in the presence of steam, such as sintering[71] and the mechanical stability of limestone, which still need to be evaluated thoroughly. SO_2 generated from fuel combustion under oxy-fuel conditions can react with limestone or calcined limestone to form calcium sulfite/sulfate[72]. Calcium sulfate forms a dense layer on the surface of lime, since the molar volume of $CaSO_4$ (46 cm^3/mol) is much higher than the parent $CaCO_3$ (36.9 cm^3/mol). The effect of SO_2 on the calcination reaction has not been investigated in detail, and it is expected that it may not have any significant effect on the calcination of limestone, but it might affect the CO_2 capture capacity. The ash content present in the fuel is another important factor that has not been investigated in the carbonate looping process.

2.3.3 Sintering

Sintering is the process of reducing the total surface area of a particle, which takes place at a high temperature. The sintering process affects the internal porous structure of the particles, because necks develop between adjacent grains and the grains continue to grow in size. Since the growth in grain size is fed by adjacent grains, it results in a decrease in the total surface area of the particle. In this process,

the distribution of the pore sizes changes, the number of micro-pores decreases and there is a relative increase in number of macro-pores. The change in the internal structure of limestone is influenced by the temperature, time, sintering atmosphere and the composition of the particle.

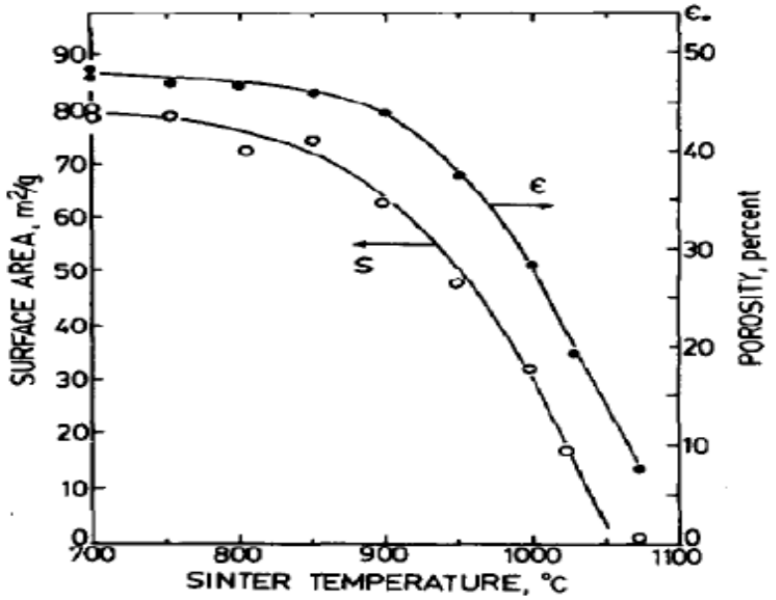

Figure 2-9: Porosity and surface area of 2 μm limestone-derived CaO particles (250 mg) after 15 minutes of sintering in a N_2 atmosphere[73].

Borgwardth[73] investigated the degree of sintering of freshly calcined limestone at different temperatures. Figure 2-9 summarizes the influence of temperature on the porous structure of calcium oxide. The porosity and surface area were to decrease with increasing temperature.

The influence of the atmosphere on CaO sintering was investigated by Fuertes[74] and Borgwardt[75]. Sintering of CaO in the presence of CO_2 in N_2 resulted in a drop in the specific surface area compared with sintering in only N_2. Similarly, the presence of water vapor in the sintering atmosphere also enhanced the sintering of CaO[75]. This effect was more pronounced in the presence of both CO_2 and

H_2O in the sintering atmosphere[75]. The change in surface area with sintering time can be described by the German-Munir model[73-75].

$$\left(\frac{S_o - S}{S_o}\right)^{\gamma} = k_s t \qquad 2\text{-}7$$

In this equation, S_o and S[m^2/g] are the initial surface area and the surface area at time t, respectively. k_s [1/s] is the sintering rate constant depending on the temperature and γ is a parameter which depends on the type of transport mechanism between the grains during the sintering process.

The rate of sintering of CaO prepared from pure $CaCO_3$ is 10 times lower than for CaO prepared from a natural limestone[65]. This was attributed to the presence of foreign ions in the natural rock. These ions produce defects in the crystal lattice, which encourage lattice diffusion. So, the composition of limestone is also a very important factor that affects the final surface area of the calcined limestone.

Agnew et al.[76] investigated the calcination and sintering of limestone in a combustion atmosphere. Their main focus was on evaluating the surface area of calcined limestone depending on the rate of calcination and the rate of sintering. An increase in the calcination temperature resulted in a higher calcination rate and reduced the time necessary for sintering, resulting in larger pore structures compared to calcination carried out at a lower rate for a longer period of time.

In the carbonate looping process, the calciner is operated in a CO_2-rich atmosphere, meaning that temperature in the calciner is higher than 900°C. Along with a high concentration of CO_2, there might be H_2O in a significant fraction due to fuel combustion. The high concentration of CO_2 and H_2O enhance sintering and reduce the surface area of the calcined particles[75]. Chen et al.[67] investigated the sintering of limestone under CO_2-rich conditions. The final surface area and the pore size of limestone calcined in a CO_2-rich atmosphere were lower than those calcined in air at the same temperature. The

influence of some of the oxy-fuel conditions on calcined limestone properties is evident, but a detailed investigation under realistic calcination conditions is still not available in the literature, except for one study by Lu et al.[77].

2.3.4 Carbonation

The efficiency of the carbonate looping process depends on the degree of carbonation of the calcined limestone particle. Carbonation is the reverse of the calcination reaction (2-1), and it is an exothermic reaction. The conditions during carbonation should have the right balance between a high temperature, which favors the rate of reaction and a low temperature, which reduces the thermodynamic equilibrium limitation (see Figure 2-6). The conversion of a calcined limestone particle is far from theoretical full conversion because CO_2 gas has to diffuse from the bulk gas to the reaction surface. The accessibility of the reaction surface to CO_2 gas is reduced due to sintering of the particle and due to product layer formation. This is one of the challenges for industrial application of the carbonate looping process.

Baker[78] investigated the carbonation reaction and found that the carbonation reaction has two characteristic stages: a rapid initial rate followed by a slower rate to a final conversion plateau. The abrupt shift in the reaction rate from fast to slow is due to a change in the reaction regime. Recently, it was revealed that the shift in the reaction rate occurs after the formation of a product layer of a critical thickness, which was estimated to be 50 nm[28]. The carbonation reaction time has an influence on sorbent conversion in the fast regime, whereas its relative influence after the shift in the reaction regime is not significant for practical application. It is natural to expect an influence of the particle size on the degree of re-carbonation at a given time. However, it has been shown that there was no significant influence in the size range tested from 74 to 149 μm[79]. The relatively limited influence in this range of particle size might be due to the reaction pattern, which is expected to be uniform

throughout the particle, unlike for the case of sulfation, which causes pore blockage due to the higher molar volume of sulfate compared to calcium carbonate. The influence of particle size in the range from 250 μm to 1 mm was investigated by Grasa et al.[34]; it was found that an increased particle size decreased the rate of carbonation due to internal mass transfer limitations.

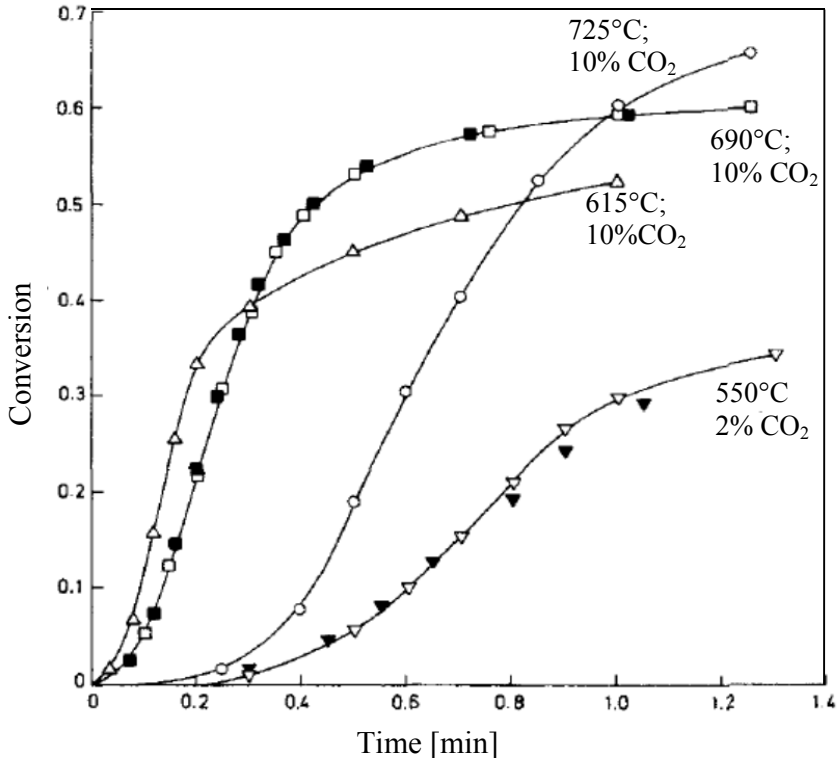

Figure 2-10: Effect of temperature and particle size (filled: 129 to 149 μm, open: 74 to 88 μm) on the carbonation conversion of calcined limestone[79].

Figure 2-10 shows the conversion of calcined limestone as a function of time for different temperatures, particle sizes and CO_2 concentrations. The influence of temperature was investigated by Bhatia and Perlmutter[79] and Wang et al.[80]. The experimental results from Wang et al.[80] showed that an increase in temperature from 500 to 800°C increased the reaction rate, whereas the results of Bhatia and

Perlmutter[79] indicated that rate of reaction increased up to 700°C and dropped with a subsequent increase in temperature[79]. An increase in the carbonation temperature increases the rate of reaction if the concentration of CO_2 is well above the equilibrium concentration in the fast reaction regime. After the shift in reaction regime from fast to slow, the influence of temperature on the rate of reaction is not significant. The major difference in reaction conditions in the studies by Wang et al.[80] and Bhatia and Perlmutter[79] was the CO_2 concentration. Wang et al. investigated carbonation at 80 vol.% CO_2 compared to 10 and 42% by Bhatia and Perlmutter[79].

The influence of the CO_2 concentration during carbonation was investigated by Sun et al.[33,81] and Grasa et al.[34,82], who concluded that the CO_2 partial pressure has no significant influence if it is above 10 vol.% at a constant temperature. If the CO_2 concentration is below 10 vol.%, then the rate of carbonation is expected to be linearly dependent on the difference between the partial pressure of CO_2 and the equilibrium partial pressure[33,79,81,82]. The reaction atmosphere is another important parameter, which may influence carbonation, especially regarding SO_2 and H_2O, which are usually present in the flue gas. Wang et al.[80] investigated the influence of H_2O on the degree of carbonation at different temperatures from 250-800°C at 80 vol.% CO_2. Their results showed that the presence of 8 vol.% H_2O had a significant influence on the rate of reaction and the final conversion at a 600°C, but further increases in the H_2O concentration up to 15 vol.% did not have any additional effect. The presence of H_2O catalyzed the carbonation reaction, which resulted in higher conversion compared to carbonation without water. However, their experiments were carried out with very high CO_2 concentrations, which may not be applicable to realistic carbonation conditions, although this has not yet been investigated.

SO_2 is usually present in the reaction atmosphere and is expected to affect carbonation since it reacts with limestone. So, there might be competition between CO_2 and SO_2 for reactions with calcined

limestone. Ryu et al.[41] investigated simultaneous CO_2 and SO_2 capture for three different types of limestones in a fluidized bed reactor. The general trend was that CO_2 capture capacity decreased with increasing SO_2 concentration, but the degree of decay was dependent of the type of limestone.

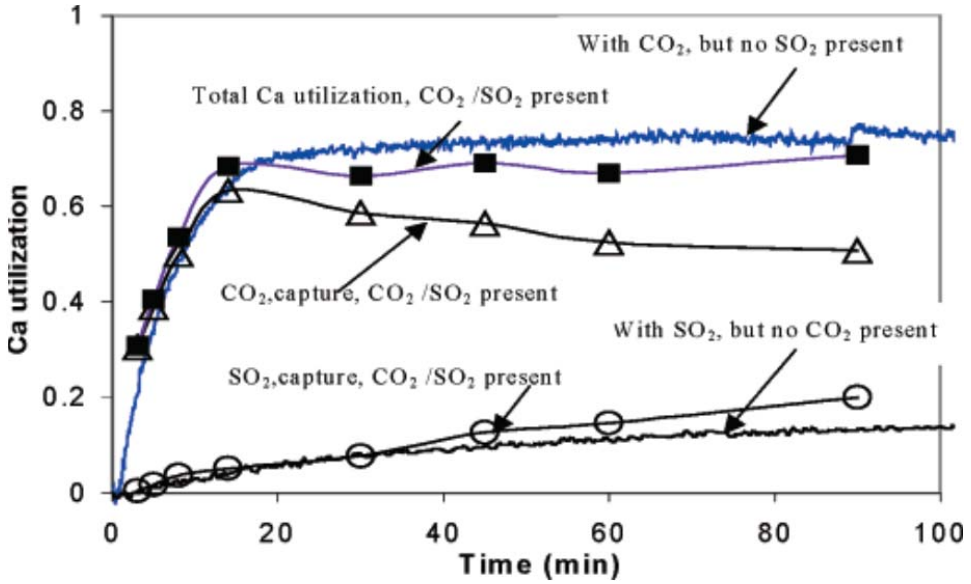

Figure 2-11: Total conversion of calcined limestone at 850°C at 1 atm with 250-215 µm Strassburg limestone. The top and bottom curves are for the limiting case where there was only CO_2 or SO_2, respectively. Points are for the simultaneous capture case showing total calcium conversion (squares), conversion due to CO_2 capture (triangles) and conversion due to SO_2 capture (circles)[83].

More detailed investigations were carried out by Sun et al.[83], presented in Figure 2-11, where the SO_2 concentration was 2900 ppmv, with 3 vol.% O_2, 80 vol.% CO_2 and the remainder as N_2. In this figure, the differences in simultaneous CO_2 and SO_2 capture were compared with only SO_2 or CO_2 capture. In the initial period, there was no effect of SO_2 on carbonation, but after the formation of the carbonate product layer on the surface, direct sulfation took place, resulting in negative conversion of carbonate. The decay in the CO_2 capture capacity was due to pore blockage, resulting from direct sulfation after

the end of the initial fast carbonation. In the carbonate looping process, it is expected that the presence of SO_2 might not influence the carbonation reaction, as the expected residence time of the particles is less compared to the reaction times presented in Figure 2-11; however, the presence of SO_2 is expected to increase the decay in CO_2 capture capacity in subsequent cycles[35,41,77,83,84]. Most of the literature data for simultaneous carbonation and sulfation were obtained with temperatures above 800°C[35,83,84], which are far from realistic carbonation conditions.

The other important factor that influences the carbonation reaction is the calcination conditions. Grasa and Abanades[31] investigated the calcination temperature on the CO_2 capture capacity of limestone. They concluded from their study that the calcination temperature does not have a significant influence on the CO_2 capture capacity until 950^{o}C, whereas above 1000^{o}C, the decay in CO_2 capture capacity is severe. This observation might be because of their experimental conditions, where calcination and carbonation were carried out in the same atmosphere, which means that carbonation might have started even before the set carbonation temperature was reached. This might have resulted in some deviations in the calcination temperature effect below 950^{o}C. Grasa and Abanades[34] later modified their experimental procedure by removing CO_2 during the temperature transition period. However, the influence of the calcination temperature on cyclic carbonation was not investigated. Christensen[85] investigated the effect of calcination conditions and showed that increasing the calcination temperature reduced the CO_2 capture capacity of limestone. Manovic et al.[36] investigated the influence of the reaction atmosphere during calcination by simulating the cyclic process in N_2 and pure CO_2 at 950^{o}C. The CO_2 capture capacity of limestone dropped significantly, when calcined in a CO_2 atmosphere compared to calcination in N_2. The calcination conditions have a significant influence on the carbonation of limestone due to sintering phenomena, which affects the final surface area of the calcined limestone and the distribution of the pore volume. If the final surface area after calcination is

high with a suitable pore size distribution, this results in a high degree of carbonation. The influence of the CO_2 concentration during calcination on the degree of re-carbonation was investigated by Bhatia and Perlmutter[79]. An increase in the concentration of CO_2 resulted in a shift in the pore size distribution of the calcined limestone from small to larger pores, which had a negative impact on the final conversion of the calcined limestone. Thus, the factors that enhance sintering during the calcination of limestone, as discussed in the sintering section, have negative effects on re-carbonation.

2.3.5 Looping Cycles

In the carbonate looping process, as said before, sorbent particles are looped continuously between a calciner and a carbonator. Baker[78] was the first to study calcination and carbonation cycles with limestone, and found a decaying trend in the CO_2 capture capacity of limestone with an increasing number of cycles. Grasa and Abanades[31] investigated a long series of experiments under conditions relevant to the carbonate looping process, which showed the decay of limestone particles with an increasing number of cycles until an asymptotic residual capacity was reached. Figure 2-12 shows the cyclic process of a carbonate looping process operated at 0.1 MPa at 10 vol.% CO_2, repeatedly cycled between 850^{o}C and 650^{o}C, where equilibrium favorable conditions imply calcination or carbonation. In these cycles, the characteristics of the looping process can be observed, in that the calcination reaction is fast with a sudden drop in weight; similarly, carbonation is a fast reaction followed by a slow carbonation reaction regime. In Figure 2-12, the sample mass after calcination remains constant, whereas the mass after carbonation decreases dramatically with an increase in the number of cycles. The decay in the CO_2 capture capacity decreases significantly in the initial 10 cycles compared to later cycles. Grasa and Abanades[31] investigated the effect of the calcination temperature on the CO_2 capture

capacity. In their study, it was found that from one cycle to the next cycle, there was a significant difference in decay with increasing calcination temperature in the initial cycles.

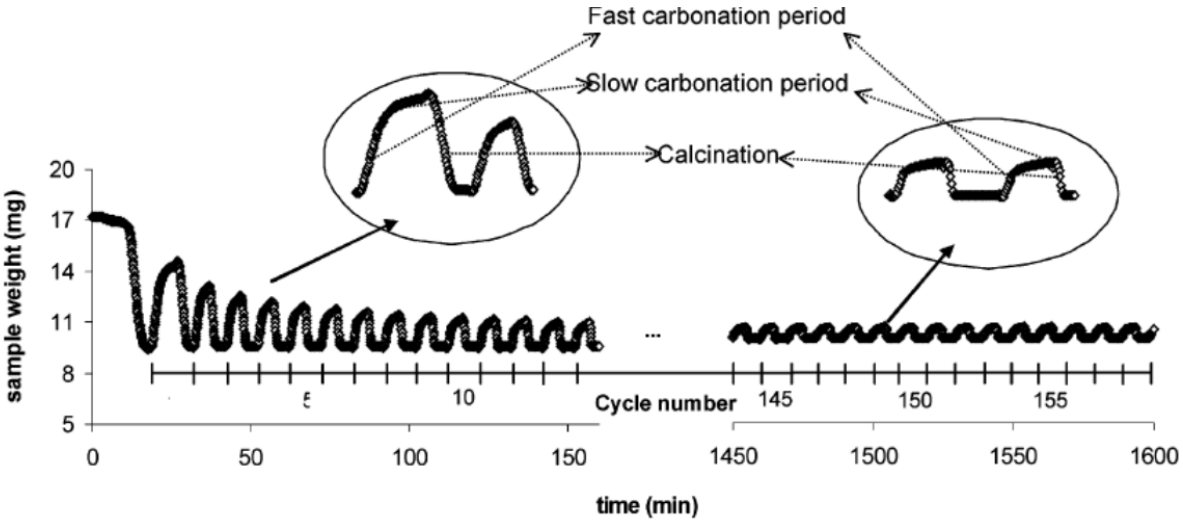

Figure 2-12: Sample mass change vs. time for carbonate looping cycles. Limestone: Piaseck, particle size 0.4-0.6 mm, calcination temperature 850°C, 5 min; carbonation temperature 650°C, 5 min; both at P_{CO2} 0.01 MPa in air[31].

Manovic et al.[36] investigated the influence of the reaction atmosphere during calcination by simulating the looping process in N_2 and pure CO_2 at 950°C. The CO_2 capture capacity of limestone from one cycle to the next cycle had no significant dependence on the reaction atmosphere. The results from Grasa and Abanades[31] and Manovic et al.[36] indicate two things: the calcination temperature influences the CO_2 capture capacity in the next cycle, whereas the calcination atmosphere does not have a significant influence. The influence of calcination time was investigated by Gonzâlez et al.[86]. With increasing calcination time, the drop in the CO_2 capture capacity from one cycle to the next cycle was higher due to increase in sintering time. At a given temperature, the effect of the calcination time on sorbent decay is still comparatively lower than the effect caused by repeated cycles, assuming a

similar cumulative calcination time during looping cycles. There is no information available on the influence of the duration of the carbonation step. The reason for this might be because the time for carbonation in the initial fast reaction regime is short and longer carbonation times are not relevant for practical applications. During cyclic processes, the internal morphology of the limestone will change continuously due to the release of CO_2 during calcination and the formation of $CaCO_3$ during carbonation. The change in morphology can be estimated by characterization of the pores in the calcined and carbonated samples[28,30]. With an increase in the cycle number, the estimated average pore diameter increases, which entails a smaller surface area. The smaller surface area influences the CO_2 capture capacity of limestone.

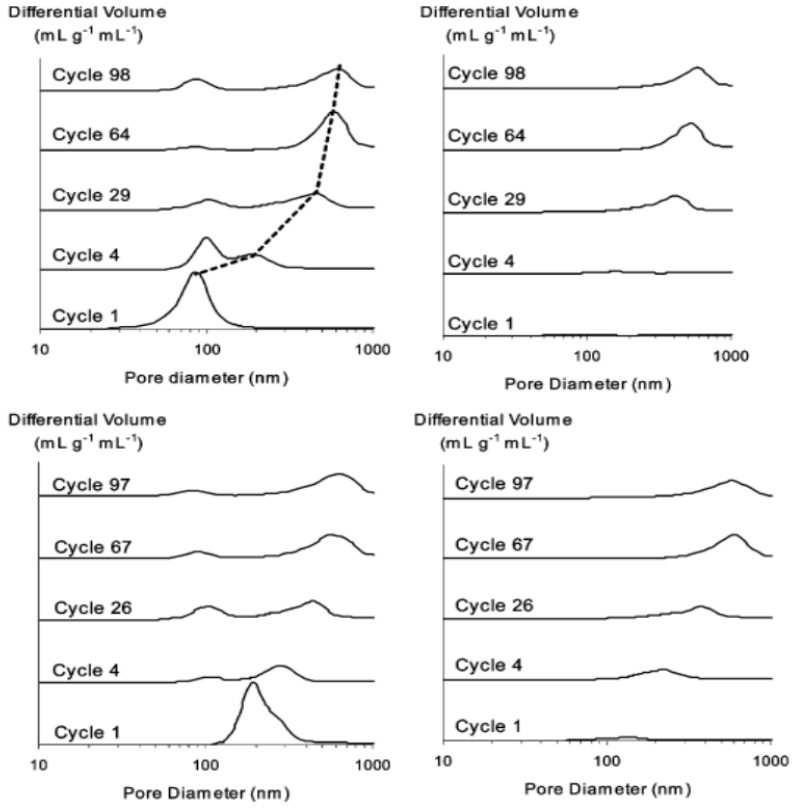

Figure 2-13: Pore size distribution in freshly calcined limestone (top) and the pre-sintered series (bottom). The curves on the left are from calcined and on those the right from carbonated samples[30].

Figure 2-13 shows the pore size distribution of the carbonate and the calcined limestone, illustrating the shift in the pore size distribution with an increasing number of cycles. There are two different scenarios possible for the decay in CO_2 capture capacity due to sintering. The first one is sintering of calcium oxide and the second one is sintering of calcium carbonate. There is no discussion or data in the literature as to whether this occurs due to the sintering of calcium oxide or calcium carbonate. Since the sintering temperature of calcium oxide is very high compared to that of calcium carbonate, the sintering phenomenon may start during the carbonation stage and accelerate during the heating of calcium carbonate until the equilibrium calcination temperature is reached.

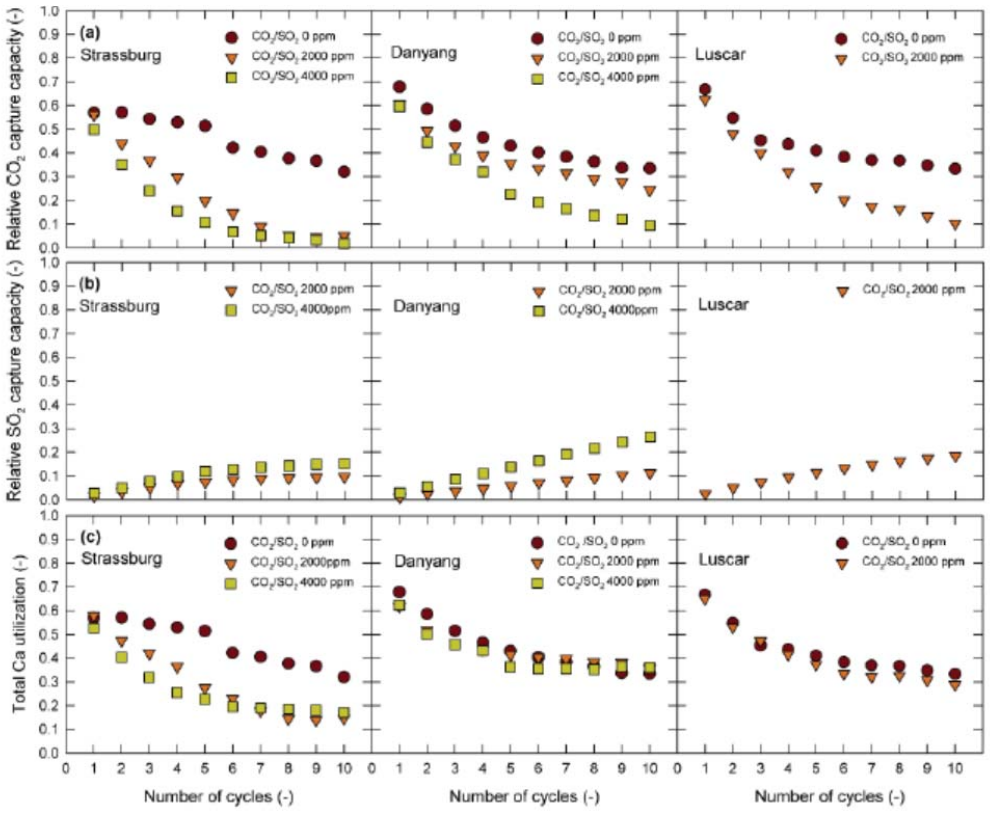

Figure 2-14: Comparison of the CO_2 capture capacity, SO_2 capture capacity, and total calcium utilization for three types of limestone[41].

The effect of looping cycles on the SO_2 retention was investigated by Grasa et al.[84], Manovic et al.[87], Arias et al.[88] and Ryu et al.[41]. With an increasing number of cycles, the decay in the CO_2 capture capacity decreased, as shown in Figure 2-14 due to the retention of SO_2. However, Grasa et al.[84] showed that spent limestone from the looping cycles tended to have a higher sulfation capacity due to changes in the texture of the limestone particles. A similar conclusion was also obtained by Manovic et al.[87], except for one type of limestone with significant particle shrinkage which resulted in lower sulfation compared to the original limestone. So, the evolution of pore structure during looping cycles also affects the SO_2 retention capacity of limestone.

2.3.6 Type of Limestone

All the above mentioned factors, such as the calcination temperature, CO_2 concentration and calcination time, influence the decay in the CO_2 capture capacity, which is further accelerated by looping between calcination and carbonation conditions. However, one other important factor, which has not been considered in depth, is the influence of other components present in natural limestone. Since natural limestone contains many other components along with calcium carbonate, even though the fractions are very small compared to calcium carbonate, these might influence the CO_2 capture capacity of the limestone in the looping process.

The type of limestone used as a sorbent for the carbonate looping process is another parameter that influences carbonate looping process system design. Different types of limestone have different compositions, which varies widely based on geographical location. Furthermore, the composition can even vary from location to location in the same quarry. Along with the composition, natural limestone particles may vary structurally in terms of the porosity distribution and the mechanical strength. Thus, different limestone samples, upon calcination, might generate different textures which might result in

different reaction patterns and influence the CO_2 capture capacity and the design of the system. There have been extensive studies on the influence of the type of limestone on sulfur capture[72,89-93] in combustion systems, where a ranking has been made for different types of limestone based on the performance of limestone in capturing sulfur[72]. Grasa and Abanades[31] studied the influence of five different types of limestones and one dolomite over a large number of looping cycles; their results showed a small difference expect for one limestone (Gotland), which had a markedly poorer performance. The deviation observed in the results was not addressed in their study. Gotland limestone was also used for investigating sulfur capture, and showed poorer performance compared most other limestones[72]. So, it seems that the classification of limestone for sulfur capture could also be applied to CO_2 capture. A certain type of limestone might have poor capture capacity, but the general trend in CO_2 capture capacity is similar to high purity carbonates[78]. Grasa et al.[34] revealed that for the five different types of limestone tested, the rate of carbonation during the fast reaction regime was similar, but during the slow reaction regime, there were significant differences resulting in differences in the final CO_2 capture capacities. Alvarez et al.[94] investigated nine different types of natural limestone classified according to the composition and parent crystal size. The objective was to classify them according to CO_2 capture capacity and mechanical strength. The limestones that were not highly crystalline or amorphous showed better performance both in terms of CO_2 capture capacity and resistance to mechanical degradation. Similar experiments were performed by Fennell et al.[42] on five different types of limestone. The CO_2 capture capacity of different limestone types was different due to differences in the pore structure evolution of the different limestone types after calcination[95]. However, all the limestones had similar reaction rates until the formation of the carbonate layer (50 nm thick and beyond), at which point the reaction rates were different. This point was also revealed earlier by

Alveraz et al.[28] for two different limestones, where the formation of the product layer was found to be characteristic of the change in the reaction regime.

Kruczek[96] investigated 16 types of natural limestone, where the evolution of the surface area, porosity and the average pore radius were plotted with respect to the looping cycle number. The trend in the evolution pattern was similar for certain types of limestone, whereas for others it was different; there was no detailed reasoning provided for this phenomenon, owing to the complexity of the composition of the different limestones. Furthermore, the change in crystal phases ($CaCO_3$/CaO) of the natural limestone after calcination and carbonation cycles was very different from the parent sample. Under ideal conditions, it is expected that the crystal phase will be similar to the parent sample, but there were many unidentified crystal phases after re-carbonation[96]. It was concluded that there could be some interaction between different compounds in natural limestone, leading to the formation of new phases, when natural limestone is subjected to high temperature. These different phases, formed at a high temperature, might also have an influence on the CO_2 capture capacity.

Most of the investigations described earlier were not carried out under realistic carbonate looping conditions; some were conducted under mild conditions[28,31,34,42], and some at unrealistic CO_2 concentrations during carbonation[94]. So, under realistic conditions, the results might differ from what was observed in those studies. The experiments by Christensen[85] (Master's thesis) were performed under realistic conditions. The CO_2 capture capacities of different limestones were different in the initial cycles, but in later cycles, the deviation in the CO_2 capture capacity was insignificant. Comparing different calcination conditions, the decay was much more severe in the study by Christensen[85] than that observed by Grasa and Abanades[31]. One reason for the decay in the CO_2 capture capacity might be structural changes, where different types of limestone develop different textures upon continuous looping. The porous structure in the limestone particle is dependent on the

looping cycle number and the degree of sintering, which shifts the average pore diameter from small to large with an increasing number of cycles, thus affecting the CO_2 capture capacity.[30]

2.3.7 Techniques for Improving the CO_2 Capture Capacity of a Sorbent

The general trend in the CO_2 capture capacity of sorbents is that it decays with increasing number of cycles. There have been efforts to improve the sorbent properties by different methods, like pre-treatment of the sorbent, intermediate reactivation steps and doping. Hydration was one of the methods chosen for improving the sulfur capture capacity of limestone[97]. Manovic et al.[98] investigated the effect of steam reactivation and showed that it had a significant effect on the CO_2 capture capacity. Arias et al.[99,100] investigated the reactivation mechanism in detail and concluded that the there was no significant influence on the rate of reaction in the fast reaction regime, but the shift in the reaction regime took place at high conversion, when the sorbent was reactivated using steam. The improved performance of the sorbent, when reactivated by steam, was due to morphological changes in the sorbent. It was observed that particles swelled instead of shrinking after reactivation, which resulted in better perforamce[101]. The other option proposed for improving sorbent capture capacity is thermal pre-treatment, where the sorbent is exposed to high temperature to form a stable structure which does not undergo further sintering at a lower temperature[102,103]. Thermally pretreated sorbents were found to have reduced capture capacity in the initial cycles which increased with the number cycles to reach a stable capture capacity. The reason for this observation was explained based on the pore-skeleton model by Manovic[102], and Okunev and Lysikov[104] explained that a new surface develops due to cyclic CO_2 capture and release, which changes the texture and improves the CO_2 capture capacity. However, there were contradictions to a generalization of this theory, as some limestones did not show any improvement in the CO_2 capture capacity[30]. The reason stated for this deviation was the difference

in the composition of the parent sorbents. The sorbent which had Al_2O_3 and SiO_2 showed a positive effect upon thermal pre-treatment, whereas the sorbent containing Na_2O showed a negative effect upon thermal treatment. Thus, the presence of other impurities also affects the CO_2 capture capacity[21,38]. The other alternative investigated for improving the CO_2 capture capacity of sorbent is the doping method by Salvador et al.[21], Manovic and Anthony[105,106] and Koirala et al.[37]. Improved CO_2 capture capacity of sorbent by the doping method was achieved by the formation of a stable compound which controls the sintering process and retains the porous structure. High CO_2 capture capacity was maintained even after 30 looping cycles, when limestone was blended with calcium aluminate cements[105]. Thus, compounds formed during the looping process might influence the CO_2 capture capacity[88]. In the doping method, the key is the formation of mayenite due to the interaction between calcium oxide and aluminum oxide. In order to evenly distribute the mayenite formed in the sorbent, two options were investigated: 1) pelletization[106] and 2) flame spray pyrolysis[37]. In the pelletization method, natural limestone is mixed with a binder, which requires doping compounds[106], and is extruded to form pellets. In the flame spray pyrolysis method, a solution is prepared with the doping element in a suitable solvent, which is fed into the flame reactor using oxygen as a dispersion agent. The doping element reacts with the sorbents at high temperature, producing a fine powder with stable sorbent characteristics.

2.3.8 Investigations in a Fluidized Bed Reactor

A suitable system for the carbonate looping process is two inter-connected fluidized bed reactors. For industrial application, it is important to understand the looping process in the fluidized bed reactor, as the operating conditions in the fluidized reactor are different from the TGA apparatus generally used to investigate the cyclic process. Experiments were performed in a single fluidized bed reactor to

investigate the behavior of a fluidized bed reactor for CO_2 capture by calcined limestone[40]. The effects of repeated cycles on the sorbent[42], the simultaneous capture of CO_2 and SO_2[41], the effect of coal ash with limestone[107] and the hydrodynamic characteristics[108] were investigated. The experiments performed in a single fluidized bed reactor are summarized in Table 2-2. Salvador et al.[21] tried to compare the CO_2 capture capacity of limestone from a TGA with that from a fluidized bed reactor and found deviations in the final CO_2 capture capacities. Abanades et al.[40] demonstrated that a fluidized bed reactor is a suitable reactor for CO_2 capture in a bed of calcined limestone. The CO_2 concentration profile in the bubbling fluidized bed reactor was measured along the bed height with respect to time. The results showed that the fluidized bed reactor was effective for CO_2 capture from the flue gas, and capture depended on the active fraction of the calcined limestone. Fennell et al.[42] investigated on the CO_2 capture capacity and attrition of the particles due to repeated cycles. The general trend in the CO_2 capture capacity was similar to the TGA apparatus, and around 10% of the mass was lost due to attrition during the 8 h operation period. Mahadzir and Zainal[108] investigated the hydrodynamic characteristics of calcined limestone mixed with sand and proposed a different mixture composition with good fluidization properties for different particle sizes with respect to the operating conditions. Galloy et al.[55] demonstrated the carbonate looping process in a single fluidized bed reactor (470 MW_{th}) to test the CO_2 capture rate as a step for industrial scale application. In this test, the carbonator was operated in a bubbling regime, but for industrial application, the carbonator has to be operated in a fast fluidization regime for continuous CO_2 capture from large volumetric gas flow rates relevant to the industrial scale. This requires continuous circulation of particles into the carbonator to replace the entrained particles. So, experiments were carried out in dual fluidized bed reactors for continuous operation. Parametric investigation of the carbonate looping process was carried out in a 10 kW_{th} scale plant[51]. One of the main challenges in the dual fluidized bed reactor is the controlled transport of

particles between the two reactors, which is critical for stable operation of the looping process. In lieu of this novel inter-connected fluidized bed system, experiments were also proposed with a focus on transporting the sorbent from one reactor to the other[45]. Charitos et al.[24] performed a hydrodynamic analysis on a dual fluidized bed reactor (IFK) to test a cone-valve to control the flow of sorbent and to determine the stable operating conditions. The pilot scale investigations were carried out by three research centers, i.e. CANMET[44], INCSAR-CSIC[53] and IFK[51]. A summary of the tests in dual fluidized bed reactors is shown in Table 2-3.

Table 2-2: Summary of experiments in a single fluidized bed reactor

Focus	Limestone	H [m]	D [m]	scale [kW]	dp [mm]	Calcination	Carbonation	Initial bed [kg]	Ref.
Reactivation of limestone	Cadomin, Havelock	5	0.1	75	0.65-1.67	850°C[1]	650°C,15%CO_2	5	Salvador et al. [21]
CO_2 profile in the bed	Cadomin, Havelock	5	0.1	75	0.65-1.68	850°C[1]	650°C,15%CO_2	5	Abanades et al. [40]
Simultaneous SO_2/CO_2	Strassburg, Luscar, Danyang	1.17	0.1	n/a	0.35-0.6	850°C[1]	700°C,16% CO_2, 2000-4000 ppmv	2	Ryu et al.[41]
Effect of cycles	Purbeck, Penrith, Cadomin, Glen-Morrison, Havelock	0.46	0.03	n/a	0.5-.71	750°C[2]	750°C,14% CO_2	30 g	Fennell et al.[42]
Cyclic characteristics	Limestone , dolomite		0.035	n/a	0.2-0.45	950°C[3]	650°C,16% CO_2	90 g	Fan et al.[109]
Effect of coal ash	Limestone , dolomite		0.035	n/a	0.2-0.45	950°C[3]	650°C,16% CO_2	105 g	Fan et al.[107]
Effect of sorbent properties	Limestone , dolomite, $CaO/Ca_{12}Al_{14}O_{33}$		0.035	n/a	0.2-0.45	950°C[3]	650°C,16% CO_2	90 g	Li et al.[110]
Particle size	Calcined dolomite	0.66	0.06	n/a	0.098,0.078,1,1.5*	850°C[2]	650°C,15% CO_2	300 g	Felice et al.[111]
Fluidization properties	Calcined limestone	0.6	0.074	3	0.1,0.5,1*		700°C,20% CO_2	1	Mahadzir et al. [108]
Pilot scale test	Calcined limestone	8.66	0.6	470	0.43*	800°C[1]	700°C,15% CO_2	150	Galloy et al.[55]

[1]: air; [2]: N_2; [3]: 90%CO_2

Table 2-3: Summary of dual fluidized bed reactor experiments and the tests conducted.

	Scale [kW_{th}]	Particle recirculation	H, i.d.	Study	Ref.
CANMET	70	Air lifting particles	5 m, 0.1	Dual bed testing and CO_2 capture from syn-gas	Lu et al. [44,112]
OSU	120	Entrained flow by induced draft fan	n/a	Parametric study	Wang et al.[54]
KIER	Cold	High velocity gas	1, 0.15	Particle transportation	Ryu et al.[45]
Tsinghua	10s	solid injection nozzle similar to KIER(0.8 kg/m^2s)	1, 0.15	Continuous operation with particle transportation	Fan et al.[46]
IFK	10s	a cone valve (<10 kg/m^2s)	12.4, 0.71	Dual bed hydrodynamics and parameter investigation	Charitos et al.[24,49]
IFK	200	a cone valve	10, 0.22	Stable operation at the pilot scale	Hawthorne et al.[52]
INCAR	30	loop seal (0.5-2.2 kg/m^2s)	6-6.5, 0.1	Continuous operation	Abanades et al.[113,114]
INCAR	1.7 MW_{th}	loop seal (5-10 kg/m^2s)	15, 0.65-0.75	Stable operation at the pre-industrial scale	Sánchez-Biezma et al. 2012[56]

2.3.8.1 Attrition

In the CLP, the circulation of limestone particles between the two fluidized bed reactors might have an influence on the mechanical stability of particles due to attrition. The direct consequence of this phenomenon is an increase in the number of fine particles at the expense of larger particles. The knowledge on this phenomenon could be used for redesigning cement plants, where larger sorbent particles can be used as the sorbent and the fine particles could be used for clinker production. There are many studies on the attrition of limestone in fluidized bed combustors related to SO_2 capture[115-117], but very few studies have been done on the attrition of limestone in the CLP process[42-44,50]. The rate of attrition depends on many factors, such as particle size, porosity, hardness, shape, operating conditions and design. Hawthorne et al.[52] and Charitos et al.[51] investigated attrition in 200 kWth and 10 kWth pilot scale dual fluidized bed reactors, respectively. Their results showed that sorbent loss was less than 5 wt.% and 2 wt.% of the total bed inventory per hour in the 200 kWth and 10 kWth pilot scale plant, respectively. Jia et al.[43] investigated attrition for five types of Canadian limestone in laboratory (quartz) and pilot scale CFB reactors. In the laboratory scale fluidized bed reactor, agglomeration of particles was observed, which might have occurred because of fine particles sticking to the surface of larger particles, whereas this observation was not found in the pilot scale test. The results from the pilot scale CFB reactors showed that the degree of attrition varied considerably for these types of limestone. For most of the limestones tested in the CFB reactor, attrition was significant in the initial few cycles compared to later cycles. Lu et al.[44] investigated attrition in dual fluidized bed reactors using Havelock limestone, which was one type of limestone tested by Jia et al.[43] in a CFB. The attrition behavior for Havelock limestone in a CFB reactor was different compared to a dual fluidized bed reactor. In the dual fluidized bed reactor, attrition was not limited to the initial few cycles, as normally observed in the CFB. So, the attrition of limestone depends not only on the type of limestone, but also

on the system. Furthermore, it was found that a significant amount of material was lost from the bed in the form of fine particles. Understanding the attrition characteristics of limestone in a fluidized bed reactor requires in-depth knowledge of the particle breaking mechanisms to determine the attrition rate constants. As an alternative, an empirical model has been proposed to determine the rate constant. Gonzalez et al.[50] carried out experiments in dual fluidized bed reactor for two types of limestone. The results showed high attrition at the beginning which reduced the size of the particles which remained relatively constant over a long operation period. Different empirical models were used to fit the experimental data from Gonzalez et al.[50] and to estimate the attrition constant. However, the experimental data available to develop a generalized model, which predicts the attrition constant depending on operating conditions, like gas velocity and properties of the sorbent, is still far from adequate.

2.4 Modeling Review

2.4.1 Gas-Solid Particle Model

Understanding the underlying mechanism of CO_2 capture by a calcined limestone is important for developing the carbonate looping process. In any gas-solid reaction, there are a number of basic steps involving external mass transfer, surface reactions, intra-particle diffusion and diffusion through the product layer. These steps might take place simultaneously or successively depending on the particle size, the particle structure and the reaction conditions. In order to describe CO_2 capture according to limestone type, different models have been developed like the spherical grain model[118], the pore model[81,82] and the shrinking core model[111]. Table 2-4 summarizes the list of different particle models proposed in the literature to describe the conversion of calcined limestone particles.

Table 2-4: Different gas-solid particle reaction models developed to explain the carbonation reaction.

Particle rate equation	Parameters	Constants	Ref.
$\frac{dX}{dt} = \frac{k_s S_o C_s (1-X)\sqrt{1-\psi \ln(1-X)}}{(1-\varepsilon_O)\left[1+\frac{\beta Z}{\psi}(\sqrt{1-\psi \ln(1-X)}-1)\right]} \left[\frac{1}{s}\right]$	$\psi = \frac{4\pi L_o (1-\varepsilon_o)}{S_o^2}$ $\beta = \frac{2k_s \rho_{Cao}(1-\varepsilon_o)}{M_{CaO} D S_o}$ $Z = V_{M\_CaCO_3} / V_{M\_CaO}$	$k_s = 5.95 \cdot 10^{-10} \pm 0.18 \left[\frac{m^4}{mol \cdot s}\right]$	Bhatia and Perlmutter[79]
$X = 1 - \exp\left(\frac{1-\left(\frac{\tau}{2}\psi+1\right)^2}{\psi}\right)$ $X = \left(1-\exp\left(\frac{1}{\psi}\right) - \frac{\left(\sqrt{1+\beta Z\tau}-\left(1-\frac{\beta Z}{\psi}\right)\right)^2 \psi}{\beta^2 Z^2}\right)$	$\tau = \frac{ksC_s S_o t}{(1-\varepsilon_o)}$	$k_{so} = 5.59 \cdot 10^{-8} \pm 0.3 \left[\frac{m^4}{mol \cdot s}\right]$ $E_{ak} = 21.3 \pm 1 \left[\frac{kJ}{mol}\right]$	Grasa et al.[82]
$\frac{dX}{dt} = 56 k_s (1-X) C_s^n S_o [1/s]$		$k_{so} = 1.67 \cdot 10^{-3} \left[mol/m^2 s\right]$ $E_a = 29 \pm 4 \left[kJ/mol\right]$	Sun et al.[33]
$\frac{dX}{dt} = \frac{S_o k_s (1-X)^{2/3} C_s}{1+\frac{V_{M\_CaO} k_s}{2D_{pl}} d_{mg} (1-X)^{1/3}\left(1-\sqrt{\frac{1-X}{1-X+XZ}}\right)} \left[\frac{1}{s}\right]$	$D_{pl} = D_{plo} \exp(-aX^b) \left[\frac{m^2}{s}\right]$	$D_{plo} = 2 \cdot 10^{-5} \left[\frac{m^2}{s}\right]$ $a = 12.1, b = 0.9$	Stendardo and Foscolo[118]
$\frac{dX}{dt} = \frac{S_o}{V_{M\_CaO}} \frac{C_s}{\frac{1}{k_s (1-X)^{2/3}} + \frac{S_o R^2 \left(1-(1-X)^{1/3}\right)}{3D(1-X)^{1/3}}} \left[\frac{1}{s}\right]$		$D = 6 \cdot 10^{-7} \left[\frac{m^2}{s}\right]$	Felice et al.[111]

The objectives of these models were different. For example, the spherical grain model[118] and the random pore model[81] were developed to explain the abrupt shift in the reaction rate, and both required numerical simulation. Felice et al.[111] applied a simple shrinking core model to determine the influence of the particle size on the rate of carbonation and for estimating the diffusion coefficient as a fitting parameter. Garsa et al.[82] developed a model to explain both the abrupt shift in the reaction rate and also the effect of the cycle number based on the random pore model developed by Bhatia and Perlmutter[79,119,120]. The model was developed in an analytical form, which was split into two steps: the first step considers only the reaction in the fast reaction regime until the critical conversion limit estimated from product layer thickness, and the second step considers the diffusional resistance added to the reaction. This model requires data to define the initial surface area, pore length and the porosity of the calcined limestone. Along with these data, it also needs information related to the drop in CO_2 capture capacity and residual CO_2 capture capacity. For the carbonate looping process, the expected residence time of a particle in the carbonator is short, which eliminates the importance of the slow reaction regime controlled by diffusion. So, a particle model which predicts the initial fast regime, like the spherical grain model, is more relevant for integration into reactor models compared to complex models.

From the experimental results, it was observed that the conversion rate of the sorbent was rapid at the beginning of the reaction until a certain degree of conversion, and then shifted to a lower rate. This trend was observed for all cycles, with the difference being in the final conversion. So, there is interest in developing the model to predict the decay in the CO_2 capture capacity, which is important for process evaluation. Table 2-5 summarizes the equations used for the estimation of the final CO_2 capture capacity as a function of cycle number.

Table 2-5: Correlation equations developed to explain the final conversion of calcined limestone as a function of cycle number.

Correlation equation	Constants	Ref.
$X_N = f^{N+1} + b$	$f = 0.782; b = 0.174$	Abanades[19]
$X_N = f_m^N (1 - f_w) + f_w$	$f_m = 0.77; f_w = 0.17$	Abanades and Alvarez[27]
$X_N = \frac{1}{1 + kN}$	$k = 0.24$	Wang and Antony[29]
$X_N = \frac{1}{\frac{1}{1 - X_r} + kN} + X_r$	$k = 0.52; X_r = 0.075$	Grasa et al.[31]

Some of the models were developed by Abanades et al.[27], Wang and Antony[29] and Grasa et al.[31]. Among these decay models, the model developed by Grasa et al.[31] predicts more accurately the CO_2 capture capacity with respect to cycle number compared to the other models. Based on the same principles used by Garsa et al.[31], a model was also recently developed by Arias et al. to predict the self-reactivation of highly sintered CaO[121].

2.4.2 Carbonator Reactor Models

Carbonator reactor models were developed to evaluate the performance of the carbonator. Since a fluidized bed reactor is most suitable for the gas-solid carbonation reaction, fluidized bed reactor models were applied. The list of different carbonator models is presented in Table 2-6. Abanades et al.[40] developed a bubbling fluidized bed reactor model based on the KL fluid bed theory[122] to describe their experimental results obtained from a pilot scale (~10 kW) fluidized bed reactor. The model predicted the CO_2 concentration profile in the fluid bed and agreed reasonably well with the experimental data. This model was used to evaluate the influence of active fraction in the bed on CO_2

capture efficiency. However, bubbling fluidized bed reactors are not relevant for industrial application because they require a large cross-sectional area owing to low gas velocities and high throughput.

Table 2-6: Reactor models developed to investigate the influence of parameters.

Reactor model	Parameter investigated	Reaction rate expression	Ref.
Bubbling fluidized bed	Reactor size	$K_r = k_r \left(X_{\max} - X\right)\bar{C}$ $k_r = 0.025[m3/mol \cdot s]$	Shimizu et al.[18]
Bubbling fluidized bed	Active fraction	$k_{ri} = k_s S_o V_{M\_CaO} X_{\max}(1-X)^{2/3}$ $K_r = \frac{1}{\frac{d_p}{6k_g} + \frac{1}{k_{ri}}}$	Abanades et al.[40]
Fluidized bed: particle phase-mixed flow gas phase-plug flow	CO_2 capture efficiency: f(solids inventory, recirculation rate, makeup flow rate)	$K_r = k_s S_{ave} \bar{C}$	Alonso et al.[123]
Circulating fluidized bed	CO_2 capture efficiency: f(recirculation, makeup flow rate, particle distribution, particle fraction in dense bed)	$K_r = \frac{1}{\frac{d_p}{6k_g} + \frac{1}{K_{ri}}}$	Ströhle et al.[23,124]
Circulating fluidized bed	CO_2 capture efficiency: f(recirculation rate, makeup flow rate, solids inventory, reaction rate, gas transfer co-efficient)	$k_{ri,ave} = \frac{\rho_{s,a}}{M_{s,a}} \sum_{N=1}^{\infty} r_{age} \int_0^{\infty} f_t k_s S_N \left(1 - X(t,N,C)\right)^{2/3} dt$	Romano et al.[125]

Ströhle et al.[23] developed a fast fluidized bed reactor model to predict CO_2 capture efficiency. In this model, the particle distribution profile was estimated from the hydrodynamic model in the presented in the fluidization engineering[122]. This model was used to simulate the carbonate looping process for capturing CO_2 from the flue gas from a power plant to estimate the energy penalty. However, there were no experimental data available to validate the model. Alonso et al.[123] developed a simple carbonator model assuming a well-mixed particle phase and plug flow for the gas phase due to the lack sufficient knowledge on the fluid dynamics of the carbonator reactor. This model was used to predict

CO_2 capture efficiency based on the operating conditions and to evaluate the suitable conditions for high capture efficiencies. Fan et al.[107,109] developed KL-based fluidized bed reactor models for 1) the bubbling regime[109] and 2) the fast regime[107]. The bubbling fluidized bed model was used to predict the experimental results from a small (0.0038 m i.d.) fluidized bed reactor by applying reaction rates estimated from a TGA apparatus. The fast regime model was developed to investigate the influence of operating parameters on the CO_2 capture characteristics considering the sorbent circulation, the sorbent activity loss and the average carbonation kinetic rate and to predict the performance of the carbonator simulated in a fast regime. Lasheras et al.[124] used the carbonator model developed by Ströhle et al.[23] to investigate the sensitivity of process parameters and the reactor model parameters on the performance of the carbonator. Felice et al.[111] proposed a simple flow with a reaction model to predict transient behavior using an empirical transfer coefficient estimated from experiments in a small fluidized bed reactor. More recently in 2012, Romano[125] developed a carbonator reactor again based on the Kunii-Levenspiel theory[122,126,127], and the results predicted by the model were compared with the experimental data from pilot scale plants. In all these models, the key parameter, i.e. the particle distribution profile along the height of the reactor, was assumed from the literature. So, a reactor model validated with dedicated experimental data is still not available.

2.4.3 Carbonate Looping Process Simulation

The first process simulation for CO_2 capture from power plants was made by Shimizu[18]. In this study, a comparison was made between oxy-fuel combustion and the carbonate looping process. The preliminary study indicated that the carbonate looping process has a higher net energy efficiency compared to oxy-fuel combustion. Abanades et al.[66,128,129] evaluated the carbonate looping process with the main focus on parameters like the sorbent cost as well as sorbent regeneration options

compared to other CO_2 capture processes, i.e. the oxy-fuel and amine processes. The cost of limestone was much lower (360 times) than the cost of amine to capture 1 mol of CO_2 from the flue gas. The energy efficiency of the carbonate looping process (0.38) was greater compared to the oxy-fuel process (0.33), but lower than reference plants (0.46) without CO_2 capture. Hughes et al.[130] simulated the carbonate looping process using the Aspen simulation tool to evaluate the process. The main conclusion from this study was that that the O_2 requirement for the carbonate looping process is one third of that required for oxy-fuel combustion for a plant of the same size. Ströhle et al.[23] simulated the carbonate looping process for CO_2 capture from a power plant with for two cases: 1) complete conversion of the active fraction and 2) using the carbonator model to determine the conversion. The two methods showed that total energy efficiency dropped by around 3% compared to the reference plant (0.46), without considering CO_2 compression.

In carbonate looping, the CO_2 capture capacity of limestone drops with an increasing number of looping cycles. So, in order to maintain high CO_2 capture capacity of calcined limestone in the carbonator, the spent sorbent has to be replaced with fresh limestone. The consequence of this is that the energy requirements in the calciner are dependent on the flow rate of the recycle stream and the flow rate of fresh limestone. Rodriguez et al.[131] investigated the carbonate looping process with a focus on the heat requirements in a calciner. The model was used to minimize the energy requirements in the calciner by optimizing the flow rate of fresh limestone and the recirculation for a pre-defined CO_2 capture efficiency.

The process model results were used to determine the additional energy penalty and to estimate the cost for CO_2 capture and electricity production. The definitions for the CO_2 capture cost and for electricity production in the literature were adapted from IPCC 2005[5]. Table 2-7 summarizes the cost of

electricity (COE), the additional cost of capturing CO_2 (AC) and the energy efficiency (η) of the integrated process.

Table 2-7: Process simulation models developed for evaluating the carbonate looping process based on COE, AC and overall efficiency (η).

Process	Normal	CLP	Oxy-fuel	Solvent	Ref.
Power plant	COE: \$39/MWh η =0.46	COE: \$49/MWh AC: \$15.5/t CO_2 η =0.39	COE: \$57/MWh AC: \$23.8/t CO_2 η =0.34		Abanades[66,129]
Power plant	COE:N/A η =N/A	COE: \$53/MWh AC: \$23.7/t CO_2 η =0.41		*COE:N/A AC:\$33-80/t CO_2 η =0.28-0.33	MacKenzie[132]
Power plant	COE:N/A η =0.46	COE:N/A AC:N/A η =0.43			Ströhle et al.[23,124]
Power plant	*COE: \$41/MWh η =0.46	*COE: \$57/MWh [1]AC: \$20/t CO_2 η =0.33			Romeo et al.[133]
Power plant	*COE: \$50/MWh η =0.45	*COE: \$63/MWh AC: \$21/t CO_2 η =0.37			Romeo et al.[134]
Power plant	*COE: \$46/MWh η =0.41	COE: \$72/MWh AC: \$39/t CO_2 η =0.35			Yang et al.[135]
Cement Plant	E_{CO2} = 0.8 kg/kg cement	AC:\$19/t CO_2 E_{CO2}=0.36 kg/kg cement			Rodriguez et al.[136]
Cement Plant	E_{CO2} = 0.8 kg/kg cement	AC: \$23/t CO_2 E_{CO2}=0.01 kg/kg cement	AC: \$16/t CO_2 E_{CO2}=0.11 kg/kg cement		Rodriguez et al.[59]

*: converted to \$ from ref.; 1: optimum conditions

Kenzie et al.[132] developed a detailed model from the economic point of view and compared carbonate looping with an amine-based system. The results indicated that the carbonate looping process has the potential for lower costs than the other option. The estimated cost for capturing 1 ton of CO_2 was approximately \$23.7 compared to \$32-80 (2005) for the amine process. Abanades et al.[129] estimated the CO_2 avoided cost at \$15.5/t CO_2 for the carbonate looping process compared to 23.8 \$/t CO_2 for the oxy-fuel process. Romeo et al.[134,137] performed a cost and optimization study on integrating the

carbonate looping process in to existing power plant and concluded that the cost for capturing 1 ton CO_2 was €16 and estimated the cost of electricity production increased from €37.9/MWh to €48.3/MWh. Yang[135] investigated alternative heat integration options and estimated the cost for CO_2 capture at around €29-36/t CO_2, whereas the cost for electricity was €54-60/MWh compared to €35/MWh for the reference plant without CO_2 capture. Romeo et al.[133] performed and optimization study on the makeup flow in the carbonate looping process to minimize the CO_2 avoided cost by purging spent sorbent either from carbonator or calciner. The results show that the CO_2 avoided cost was approximately €15/t CO_2 for both scenarios under optimized makeup flow rates. The cost of electricity production was €43/MWh for the carbonate looping process compared to €31/MWh for the reference plant without CO_2 capture.

There have been few studies related to process modeling applicable to the cement industry. Rodriguez et al.[57,136] investigated the calcination of limestone using hot CaO as the heat carrier particles instead of oxy-fuel combustion; this system was integrated into a cement plant. This method reduced CO_2 emissions by 43% compared to a normal cement plant without the need for an air separation unit; the estimated cost per ton of CO_2 was $19. A more realistic approach for CO_2 capture from a cement plant was later proposed by Rodriguez et al.[59]. In this scenario, the options for CO_2 capture from a cement plant by integrating the carbonate looping process or only an oxy calciner were investigated. The estimated avoided CO_2 cost for capturing CO_2 from the calciner was $16/t CO_2, whereas for the carbonate looping process, this was $23/t CO_2. However, the thermal energy increased from 2.93 GJ/t cement for the reference plant to 4.94 and 5.45 GJ/t cement for the oxy-calciner and the carbonate looping option, respectively.

2.5 Conclusions

The trends in cement production and CO_2 emissions and options for reducing CO_2 emissions from cement production have been presented. The carbonate looping process has the potential to be the best option for the reduction of CO_2 emissions. So, a detailed description of the carbonate looping process was presented along the status of research into industrial application. Based on the literature review, the main focus of developing the carbonate looping process is for fossil fuel-based power plants. The basic principle of the carbonate looping process applied to fossil fuel-based power plants or the cement industry will be the same. The general conclusions from the literature review on the carbonate looping process are:

- The reaction conditions for the calciner and carbonator are well-established.
- The CO_2 capture capacity decreases with an increasing number of looping cycles.
- The decay in CO_2 capture capacity is influenced by many factors, i.e. the number of looping cycles, calcination temperature, type of limestone and sulfation.
- Different methods are being developed to improve the CO_2 capture capacity of limestone.

A summary of different particle models, reactor models and process models was presented to understand the details of the carbonate looping process. However, there are significant differences to be considered for applying the carbonate looping process to fossil fuel-based power plants and the cement industry, such as:

- The number of looping cycles a sorbent particle might undergo,
- Differences in the particle size range,
- Effect of spent limestone on clinker quality,
- Integration of the carbonate looping process into a cement pyro-process.

3. Raw Meal as Sorbent for CO_2 Capture from Cement Production

3.1 Introduction

The carbonate looping process (CLP) for CO_2 capture from power plants has been studied extensively[19,23,35,42,65,66,86,96,105,138,139]. It is shown that the CO_2 capture capacity of the sorbent decreases with an increase in cycle number[27,34], which means that the spent sorbent material has to be replaced with fresh material in order to maintain a high CO_2 capture efficiency. This is one of the main challenges in the application of the carbonate looping process in power plants. However this may not be a serious problem for cement plants, as spent sorbent, i.e. calcined limestone, can be used as feed in clinker production. Thus this process is especially suitable for the cement industry, as the key raw material could be used as a sorbent and with the possibility of producing electricity for internal use.

The cement raw meal may be used directly as a sorbent for the carbonate looping process applied to the cement production process, since the major component in cement raw meal is limestone, which is approximately 70 w/w% together with SiO_2 (S), Al_2O_3 (A) and Fe_2O_3 (F)[140],[141]. The calcined raw meal might serve as both a sorbent for CO_2 capture and as a raw material in clinker production. An energy and cost analysis for integrating an oxy-fuel calciner in cement production was studied by Rodriguez et al.[59], they concluded that high CO_2 capture efficiency was feasible at a relatively low energy penalty. Results from a simple process simulation model showed that the high CO_2 capture capacity of calcined limestone in the cement raw meal will reduce the energy demand of the calciner[142]. Telschow studied the effect of temperature on clinker phase formation, indicating the formation of silicates and aluminates of calcium at 900°C but in minor fractions[140]. It is widely accepted that the formation of dicalcium silicate (C_2S) might start at temperatures as low as 700°C[141]. The temperature in the calciner of the carbonate looping process must be higher than 900°C, due to the

high CO_2 concentration, therefore it is possible that part of the clinkering reaction may commence in the calciner. So under carbonate looping conditions there might be interactions between the lime and other components to form calcium silicates or other intermediate clinker phases, however their effect on the CO_2 capture capacity is not known.

Dean et al.[143] discussed the possible synergy between the carbonate looping process and clinker formation. The synergy effect was observed on the fraction of the tricalcium silicate C_3S phase in final clinker produced from spent limestone used as the sorbent in the carbonate looping process compared with fresh limestone. However, no information on the CO_2 capture capacity of the raw meal is reported, except for the previous study[144]. The results of this study showed that the CO_2 capture capacity was influenced by the type of clay and limestone. The CO_2 capture capacity of different clay and limestone mixtures was lower than limestone when cycle tests were performed under realistic conditions. The observed effect on the CO_2 capture capacity may be partly due to sintering and partly due to the solid-solid interactions between limestone and clay. However the complexity of these interactions makes it difficult to understand the decay mechanism. So, systematic studies are necessary to understand the mechanism of the CO_2 capture capacity of limestone in the raw meal. In the present work, cyclic experiments were carried out in a thermo-gravimetric analyzer to investigate the influence of the main components in the raw meal, i.e. silica, alumina or iron oxide, on the CO_2 capture capacity of limestone.

3.2 Experimental

3.2.1 Materials

Faxe Bryozo limestone obtained from Faxe Kalk A/S, with a particle size of 0.09-0.25 mm was used as the sorbent material. Silica was obtained from quartz sand, with a particle size similar to that of

limestone. Al_2O_3 (purity 99.9%) and Fe_2O_3 (purity 99.9%), with particle sizes <0.045 mm, were obtained from Sigma-Aldrich and Alfa Aesar, respectively. Cement raw meal supplied by FLSmidth A/S, with a particle size 0.045-0.2 mm, was used for comparison. The chemical compositions of limestone and raw meal are summarized in Table 3-1.

Table 3-1: Composition of the limestone and industrial raw used in the cyclic experiments given in w/w%.

w/w%	CO_2	CaO	SiO_2	Al_2O_3	Fe_2O_3	K_2O	MgO	MnO	Na_2O	TiO_2
Faxe Bryozo	43.6	55.1	0.45	0.1	0.08	0.03	0.43	0.02	-	0.01
Raw meal	35.63	43.06	13.94	3.6	2.49	0.13	0.93	-	0.09	0.22

The limestone was mixed with other components in such a way that the fraction of limestone is kept close to 70 w/w % and the rest being single, binary or tertiary mixtures. Since the objective was to evaluate the influence of individual and multiple components, silica, aluminium oxide and iron oxide were included in equal weight fractions.

3.2.2 Experimental Setup and Methods

Cyclic experiments were performed in a thermo-gravimetric analyzer (Netzsch STA 449 F1 Jupiter) with rapid heating (500^{o}C/min) and cooling rates (300^{o}C/min). The amount of the sample used in each experiment was around 20 mg, and the total gas flow rate was 190 Nml/min. In these cyclic experiments, carbonation was carried out at 650^{o}C in 14.7 vol.% of CO_2 in N_2, whilst the calcination conditions were varied. Calcination was performed under mild conditions (850^{o}C in N_2), harsh conditions (950^{o}C in N_2) and realistic conditions (950^{o}C in 84 vol.% CO_2) in order to study the influence of temperature and CO_2 concentration during calcination on the CO_2 capture capacity of the limestone. The time for calcination was 3 min for the first cycle and 2 min for the rest of the cycles under isothermal conditions, which was sufficient for complete calcination. Carbonation was carried

out for 3 min for each cycle under isothermal conditions. The cyclic experiments with limestone and mixtures were repeated three times to examine repeatability, and thus to estimate the standard deviation of the experimental results. Figure 3-1 shows the weight % of the sample from an experiment in thermo-gravimetric analyzer. The degree of carbonation was estimated from the mass change due to calcination and carbonation, based on the following equations. In these equations the weight gain due to CO_2 capture is considered relative to the amount of CO_2 released from the material. Assuming that the total CO_2 released is from calcium carbonate. Thus these equations can not only be used for pure limestone but also any mixture, for the easy comparison of CO_2 capture capacity as a function of cycle number.

$$X_{carb,N} = \frac{n_{CO_2,N}}{n_{CaCO_3,0}} \qquad 3\text{-}1$$

$$n_{CO_2,N} = \frac{\left(m_{sample,N} - m_{CaO,1}\right)}{M_{CO_2}} \qquad 3\text{-}2$$

$$n_{CaCO_3,0} = \frac{\left(m_{sample,0} - m_{CaO,1}\right)}{M_{CO_2}} \qquad 3\text{-}3$$

$X_{carb,N}$ the degree of carbonation in the N^{th} cycle

$n_{CO_2,N}$ the number of moles of CO_2 captured at the end of carbonation in the N^{th} cycle

$n_{CaCO_3,0}$ the initial number of moles of $CaCO_3$

$m_{sample,N}$ the weight of the sample at the end of the N^{th} carbonation cycle

$m_{CaO,1}$ the weight of the sample at the end of the 1^{st} calcination cycle

M_{CO_2} the molecular weight of CO_2

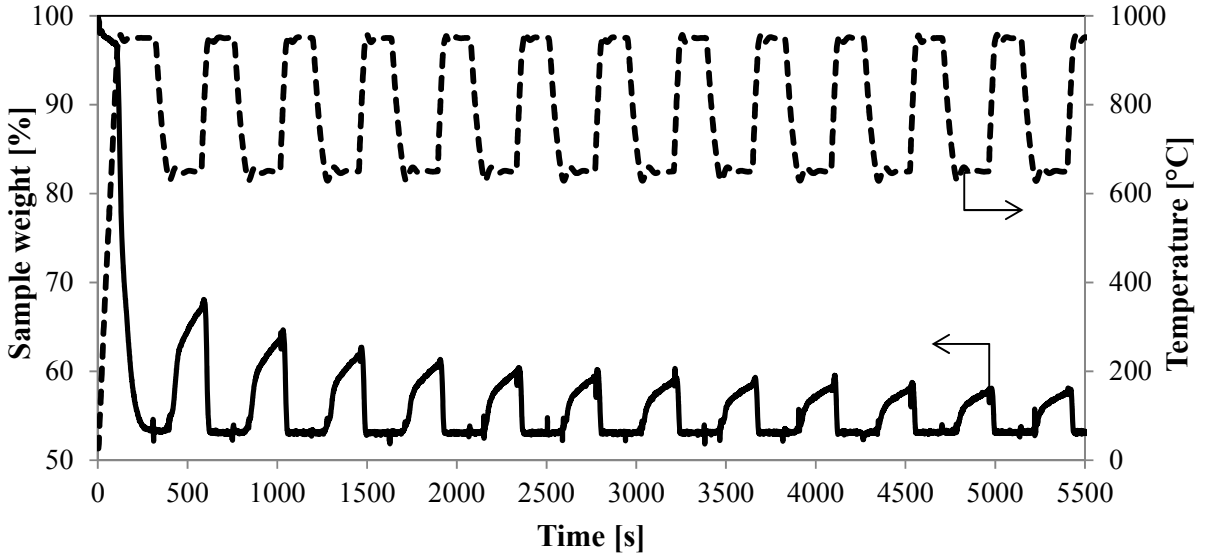

Figure 3-1: Sample weight % of Fake Bryozo limestone from the cyclic experiment in the thermo-gravimetric analyzer, Calcination: 84% CO_2, 950°C; Re-carbonation: 14.7% CO_2 in N_2, 650°C.

In order to understand the mechanism in the CO_2 capture capacity of the sorbent, the calcined particles were characterized by different methods. Scanning Electron Microscopy (SEM) analysis was used to observe changes in the particle morphology after the looping process. The Brunauer-Emmett-Teller (BET) measurement was used to estimate the change in surface area of the sorbent, and X-ray diffraction (XRD) analysis was applied to examine the phase change of the crystalline phases during calcination. Calcination tests were performed in a tubular furnace under a gas flow rate of 1 nL/min under various conditions to obtain the samples of 2 g for BET and XRD measurements.

The surface area of the samples was measured by N_2 physisorption using a Quanta Chrome Autosorb ASIQM002-1 surface area analyzer. The morphology of the sorbent particles exposed to different calcination conditions was examined by SEM (JEOL JSM-5900). The XRD spectrum was obtained from a Huber G670 diffractometer by operating in a transmission mode, in which a sample was placed on a scotch tape. The diffraction spectrum was obtained from 2^o to 100^o using the Cu Kα1 radiation

focused by a quartz monochromator. All the crystalline phases were identified using the International Centre for Diffraction Data (ICDD) files.

3.3 Results and Discussion

The cyclic experiments were first performed with a cement raw meal and with limestone as the reference, under realistic calcination conditions, i.e. at 950°C in a CO_2 rich atmosphere. The number of cycles in these experiments was restricted to 12, as this was more than sufficient when applying the looping process for the cement industry, because the major fraction of the spent sorbent can be continuously fed to clinker production[142]. Figure 3-2 shows the CO_2 capture capacities of limestone as a function of the cycle number.

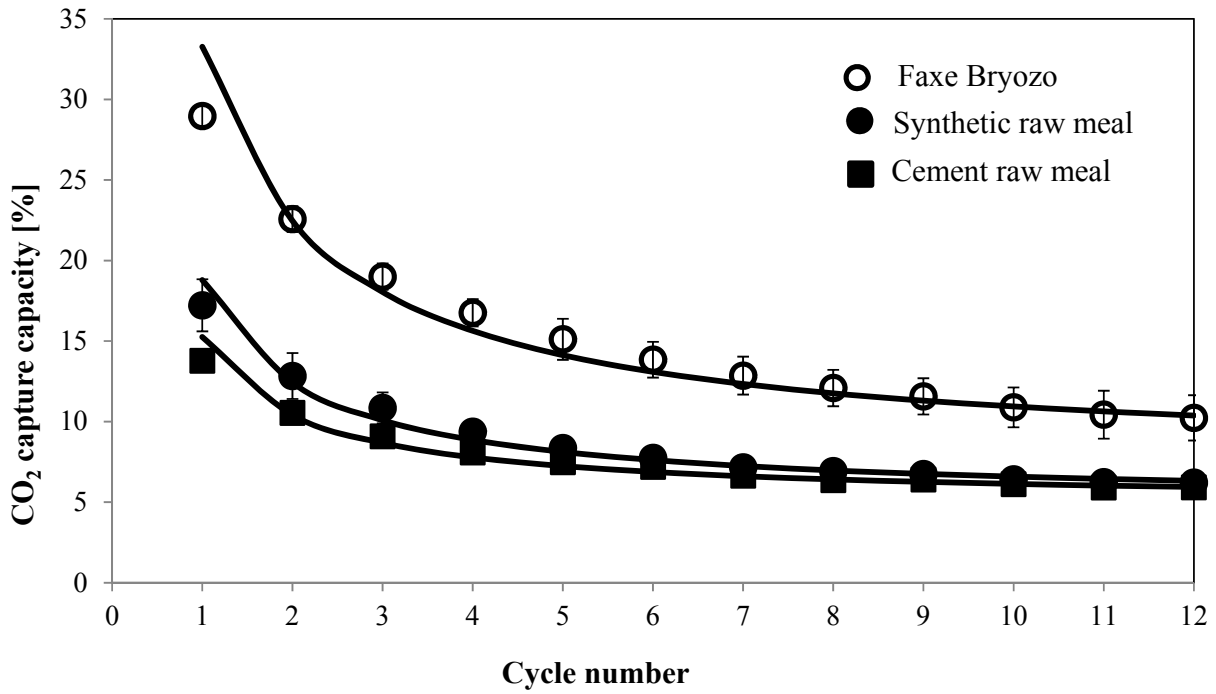

Figure 3-2: CO_2 capture capacity of limestone, synthetic raw meal (70% limestone and 10% each of SiO_2, Al_2O_3 and Fe_2O_3) and cement raw meal as a function of cycle number under realistic calcination conditions; Calcination: 84% CO_2, 950°C; Re-carbonation: 14.7% CO_2 in N_2, 650°C.

The repeatability of the results was good, with standard deviations of ± 1%, which were estimated from three separate experimental results obtained under the same operating conditions. The CO_2 capture capacity decreases with an increasing number of looping cycles, both for the limestone and for the cement raw meal. The trend in the decay of CO_2 capture capacity is similar to the results presented in the literature, i.e. large decay in the initial cycles compared to later cycles[86]. The trend curve representing the experimental data in the figures is derived from the correlation equation presented in the last section of the chapter.

However, by comparing the CO_2 capture capacity of pure limestone with the cement raw meal it is evident that the capture capacity of limestone in the cement raw meal is approximately 50% lower than the pure limestone already in the initial cycles. Experiments were performed with limestone mixed with the other main components (silica, aluminum oxide and iron oxide) present in the cement raw meal, termed "synthetic raw meal". The CO_2 capture capacity of synthetic raw meal was similar to the cement raw meal, as shown in Figure 3-2.

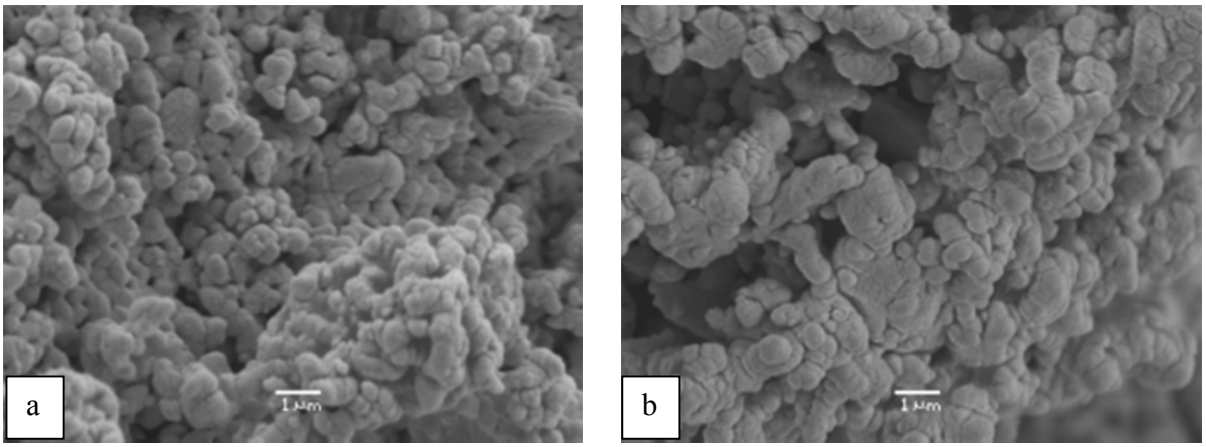

Figure 3-3: SEM images of calcined sorbent material after 12 cycles: a) pure limestone; b) limestone in the synthetic raw meal under realistic calcination conditions.

Samples from the cyclic experiments were examined by SEM after the final calcination cycle in order to visualize the surface morphology of the pure limestone and the limestone in the synthetic raw meal (Figure 3-3). For the limestone, the grain sizes are uniform with clearly visible boundaries, whereas in the limestone from the synthetic raw meal the grain size appears to be larger. It appears that the presence of other main components in the raw meal influences the grain size, which might be one of the reasons for the low CO_2 capture capacity of the limestone in the synthetic raw meal compared to pure limestone.

In order to understand the deviation in the CO_2 capture capacity of the limestone compared to the limestone in the synthetic raw meal, cyclic experiments were performed: 1) under different calcination conditions to investigate the influence of temperature and CO_2 concentration, and 2) with various combinations of the main components of raw meal forming binary and ternary mixtures to evaluate the influence of individual or multiple components present in the mixture.

3.3.1 Influence of Calcination Conditions

Cyclic experiments were performed at 850°C and 950°C in pure N_2, and at 950°C in a CO_2 rich atmosphere. Figure 3-4 shows the CO_2 capture capacity of the limestone and the limestone in the synthetic raw meal. Comparing the CO_2 capture capacity of the limestone under different calcination conditions the capture capacity drops from 62% to 58% when the calcination temperature was increased from 850°C to 950°C in a N_2 atmosphere. The CO_2 capture capacity of the limestone drops significantly at 950°C, when the calcination atmosphere was changed from a N_2 to a CO_2 rich atmosphere, which represents conditions closer to a practical system. Thus, the high concentrations of CO_2 severely enhance the decay in the CO_2 capture capacity of limestone. Comparing the CO_2 capture capacity of the limestone in the synthetic raw meal with pure limestone the following phenomena were

observed: 1) the decaying trend in the CO_2 capture capacity as a function of cycle number for the limestone in the synthetic raw meal was similar to pure limestone under different calcination conditions, and 2) the CO_2 capture capacity of the synthetic raw meal was similar to pure limestone when the calcination was performed at 850°C, whereas at 950°C in a N_2 or CO_2 rich atmosphere the CO_2 capture capacity of the limestone in the synthetic raw meal was significantly lower. The lower CO_2 capture capacity for the limestone under realistic calcination conditions is the cumulative effect of high CO_2 concentration and calcination temperature.

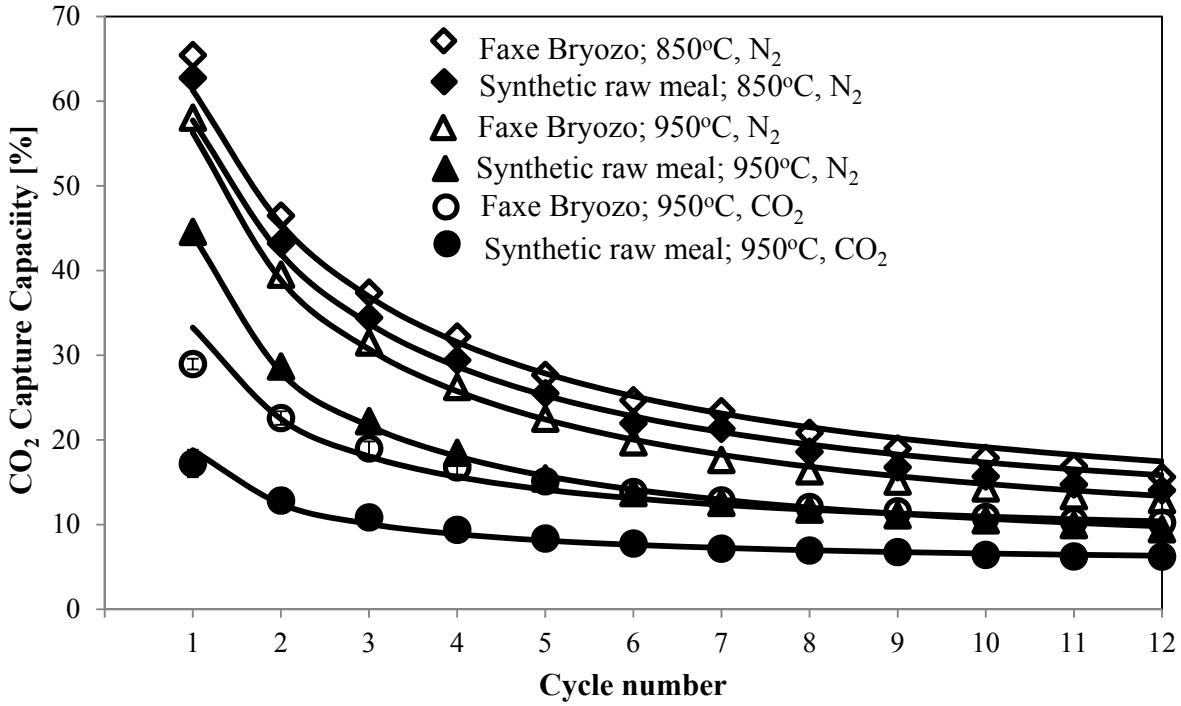

Figure 3-4: CO_2 capture capacity of pure limestone (open) and synthetic raw meal (filled) as a function of cycle number; (◆) under mild calcination conditions; Calcination: N_2, 850°C; Re-carbonation: 14.7% CO_2 in N_2; (●) under realistic calcination conditions; Calcination: 84% CO_2, 950°C; Re-carbonation: 14.7% CO_2 in N_2; (▲) under harsh calcination conditions: N_2, 950°C; Re-carbonation: 14.7% CO_2 in N_2,

In order to study any interaction between the components, XRD analysis was carried out on the synthetic raw meal, calcined in the tubular reactor. Figure 3-5 shows XRD spectra of the synthetic raw meal calcined at 850°C, 950°C and 1050°C in N_2, and at 950°C in a CO_2 rich atmosphere.

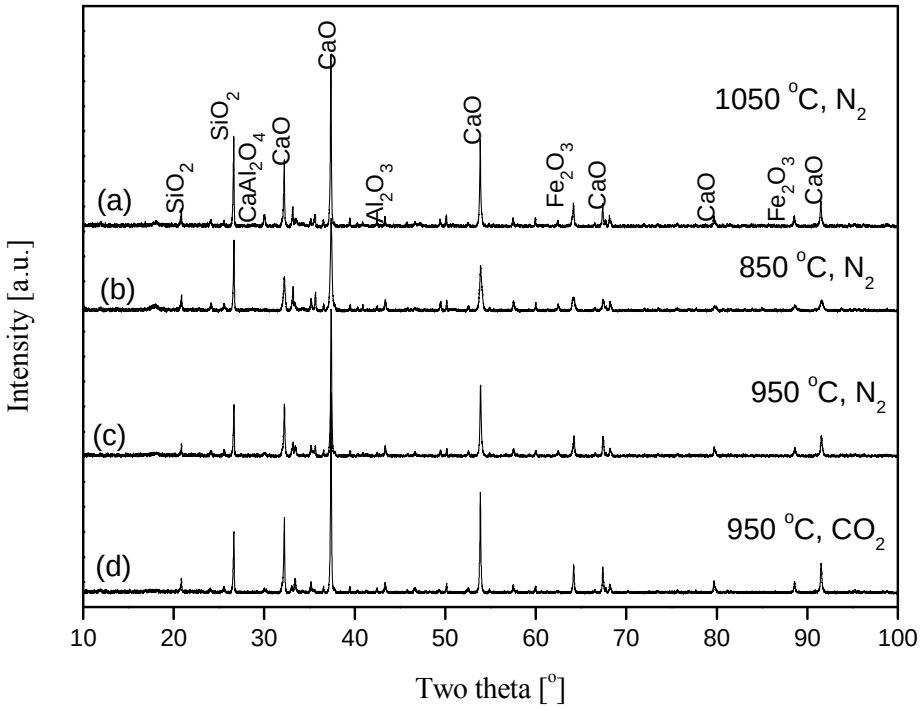

Figure 3-5: XRD spectra of synthetic raw meal under different calcination conditions for 20 min: a): 1050°C, N_2; b): 850°C, N2; c): 950°C, N2; d): 950°C, CO_2 in N_2.

The XRD spectrum data obtained were compared with the International Centre for Diffraction Data (ICDD) database using a search match program to identify the phases. All the main components in the calcined original mixture were identified along with new phases. The calcium aluminate peak has highest intensity for the sample calcined at 1050°C, whereas at 850°C no peak was observed, and at 950°C in CO_2 and in N_2 a small intensity peak was observed. Further, there are many low intensity peaks in the 2-theta range from 30–35° which is characteristic for C_2S peaks[141]. The low intensity

peaks of these new phases might be due to their low fraction in the sample compared to main oxides. The C_2S phase was observed even at a temperature of 850°C, whereas at higher temperature CS was also identified along with C_2S. Based on the XRD spectrum and the Crystallographic Search-Match (CSM) program, the confidence threshold for the peak search match results is estimated as 90%. Since the possibility of forming C_2S is large compared to other clinker phases, XRD analysis was carried out for the mixture containing limestone and silica. For comparison the XRD spectrum were also obtained for single components of limestone and silica, as well as the mixture of limestone and silica with a weight fraction of 30% silica calcined under similar conditions. The XRD spectra for these samples are presented in Figure 3-6.

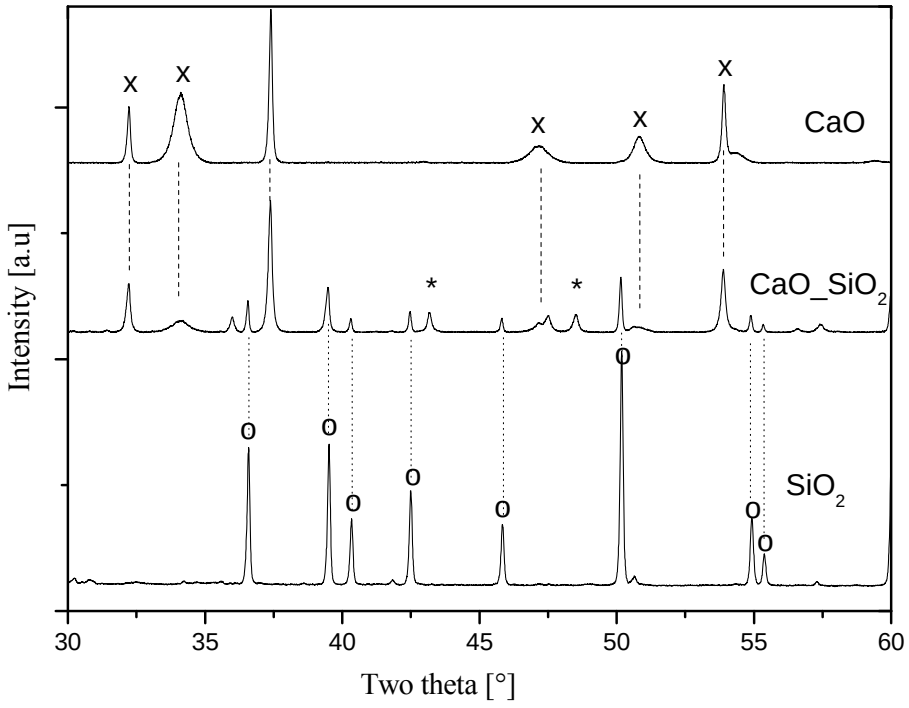

Figure 3-6: XRD spectra of calcined limestone (x), silica (o) and a mixture of limestone and silica calcined for 20 min under realistic calcination conditions: 950°C, 84 vol.% CO_2 in N_2.

From Figure 3-6, the new peaks were observed for the sample containing the mixture of limestone and silica compared to data from the individual components of limestone and silica. The identified new phase peaks matched the peaks positions of calcium silicate (CS) and C_2S[141]. Even though a new phase like C_2S could be identified by the search-match program, it is difficult to quantify the phases due to a low intensity of the peaks compared to the other phases. Similar experiments were performed by Telschow in a lab scale rotary kiln simulator, which showed the formation of C_2S, C_4AF and C_3A at 900°C, and their fraction increasing with temperature[140].

However, the expected amount of the new phase under the present experimental condition is low due to bad contact efficiency in the tubular furnace. So the phase formed may not be the only reason for the decay in CO_2 capture capacity. In order to identify other possible reasons for the drop in the CO_2 capture capacity, the crystallite size of CaO under different calcination conditions for the synthetic raw meal was estimated from the diffraction data presented in Figure 3-5. The crystallite size of CaO was calculated according to the Debye-Scherrer equation[145], which uses the full width at half maximum intensity (FWHM).

$$D = \frac{K\lambda}{\beta \cos\theta} \qquad 3\text{-}4$$

where D = Crystallite size, nm

K = Crystallite-shape factor = 0.9

λ = X-ray wavelength, 0.15418 nm

θ = Observed peak angle, radians

β = X-ray diffraction broadening (FWHM), radians

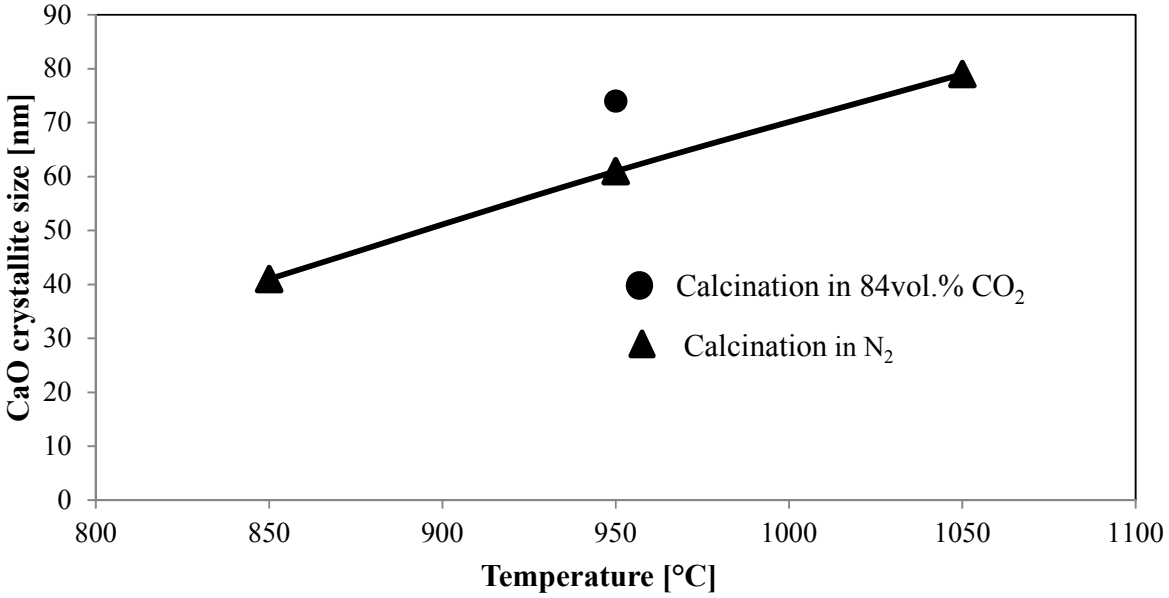

Figure 3-7: CaO crystallite size in synthetic raw meal determined from XRD peak broadening analysis with respect to temperature under different calcination conditions.

According to this equation, the crystallite size was estimated and presented in Figure 3-7, for the CaO peak corresponding to $2\theta = 37.4°$, which had the highest intensity. The trend observed, i.e. increase in the crystallite size of the CaO in the synthetic raw meal with an increase in calcination temperature, is similar to the results for calcined limestone in the literature[146,147]. The influence of a high concentration of CO_2 on the CaO crystallite size in the synthetic raw meal during calcination was also studied. It appears that a higher CO_2 concentration increases the size of the crystallite, which is in agreement with the results of Chen et al.[67] from their study on the calcination of limestone under oxy-fuel conditions. In order to observe the change in the particle morphology of the limestone due to presence of the other main components in the cement raw meal, SEM analysis was carried out for the pure limestone and the synthetic raw meal. The samples were calcined in a tubular furnace under different calcination conditions. Figure 3-8 shows the particle surface morphology of the limestone

calcined at 850°C (a), 950°C (b) and 1050°C (c) in N_2 and at 950°C (d) in a CO_2 rich atmospheres. At 850°C the individual grains are clearly visible, but by increasing the temperature the grains coalesce together and grow in size. The effect of CO_2 concentration during calcination at 950°C is visible in the form of large pores compared to limestone calcined in N_2.

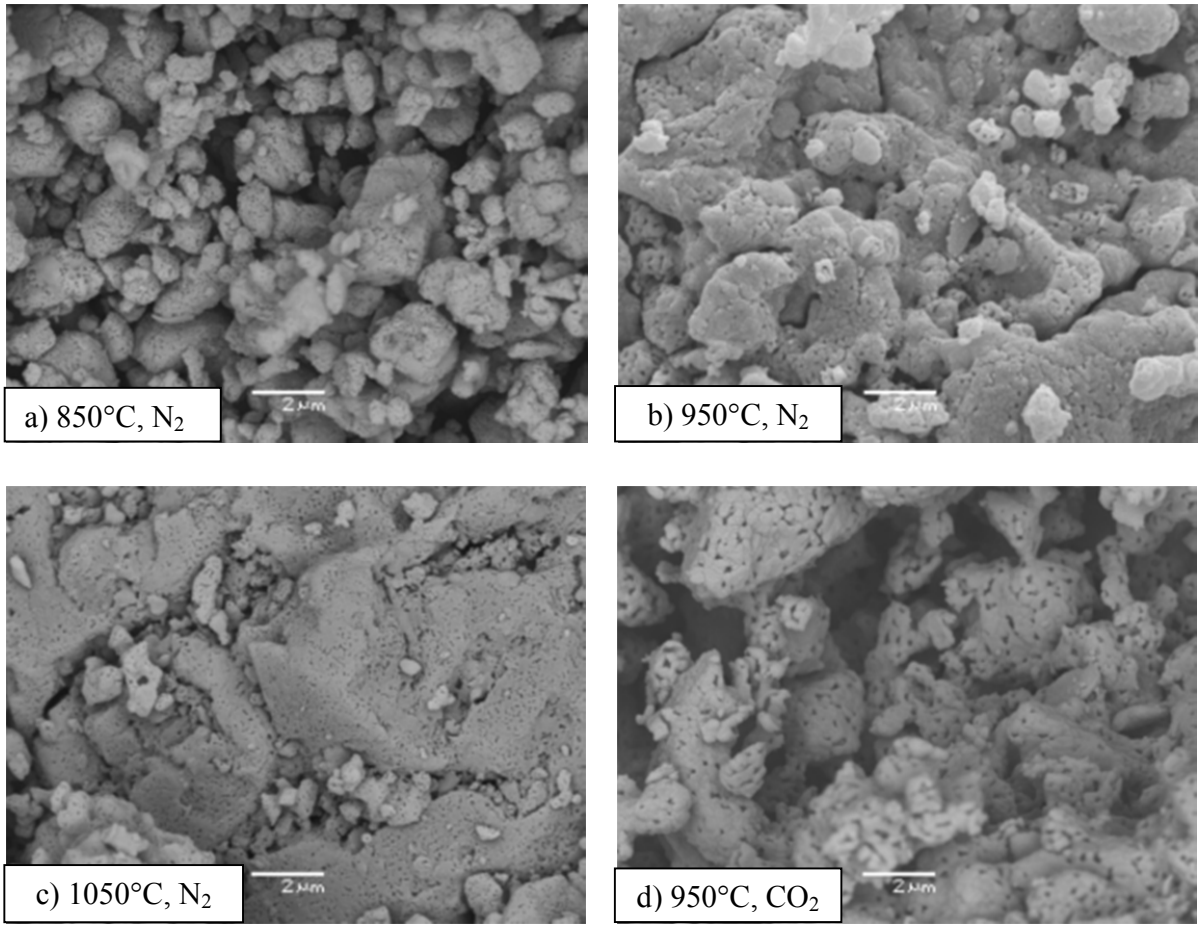

Figure 3-8: SEM images of pure limestone: a) calcined at 850°C in N_2, b) calcined at 950°C in N_2, c) calcined at 1050°C in N_2, and d) calcined at 950°C in 84 vol.% CO_2 in N_2.

SEM images of the synthetic raw meal calcined under different conditions are shown in Figure 3-9. At 850°C the grains are clearly visible, similar to limestone, but with an increase in temperature to 950°C and 1050°C the grains coalesce together at the contacted surfaces and grow in size. The synthetic raw

meal calcined at 950°C in a CO_2 rich gas has a surface morphology which appears to be similar to that calcined at 950°C in N_2, which might be due to the similar interaction between the limestone and other components on the surface. However, at the nanometer scale a difference was observed in the CaO crystal size estimated from the XRD peak widening technique as shown in Figure 3-7. In general, an increase in temperature or CO_2 concentration resulted in larger grains in the particles.

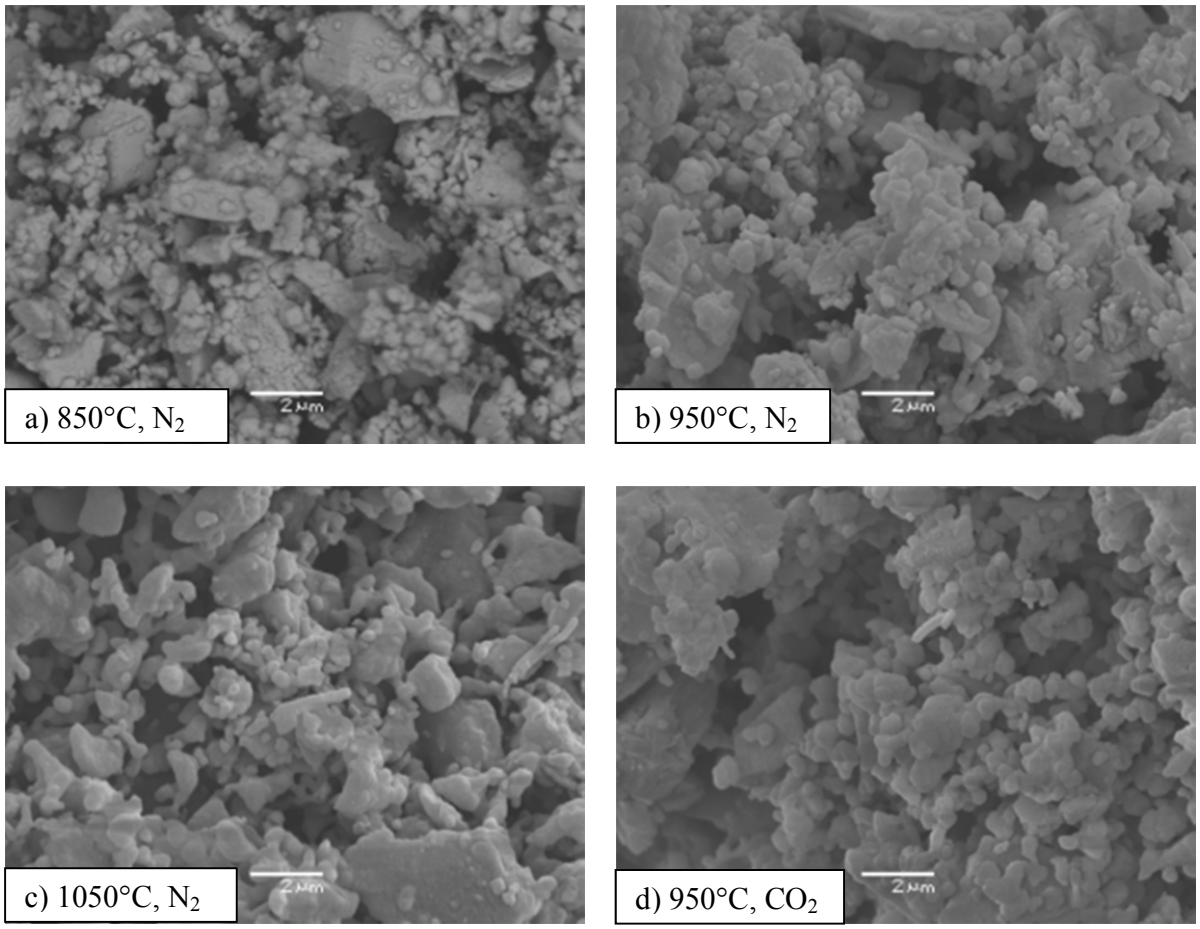

Figure 3-9: SEM images of limestone in the synthetic raw meal calcined for 20 mins at: a) at 850°C in N_2; b) at 950°C in N_2; c) at 1050°C in N_2; and d) at 950°C in 84 vol.% CO_2 in N_2.

The SEM images presented here indicate the sintering phenomenon of the synthetic raw meal and the limestone qualitatively. In order to obtain quantitative information regarding the sintering phenomenon,

BET measurements were carried out for the original materials and for the material calcined under different calcination conditions in a tubular furnace. First, BET measurements were performed for each component at 950°C in a CO_2 rich atmosphere. The surface area measurement for each component before and after calcination is summarized in Table 3-2. The limestone surface area increased due to the release of CO_2 under calcination conditions. For the other components: aluminum oxide sintered with the surface area decreasing from 10 to 1 m^2/g, iron oxide decreased from 6 to 2 m^2/g, and for silica no change in the surface area was expected due to very low initial surface area. The measured BET surface area of the pure components is used for estimating the BET surface area of mixture considering no interactions compared to real measurement.

Table 3-2: BET measurements of main components of cement raw meal under atmospheric conditions and calcined at 950°C in a CO_2 rich atmosphere.

Material	Original	Calcined
	m^2/g	m^2/g
Faxe Bryozo	1.08	4.04
Al_2O_3	10.4	0.94
Fe_2O_3	6.08	1.82
SiO_2	0.23	-

If there are no interactions between the components in the synthetic raw meal, the surface area can be estimated from the surface area of each component and its respective weight fraction. The surface area of the Faxe Bryozo calcined under realistic calcination conditions was measured to be 4.04 m^2/(g of calcined synthetic raw meal). Since the weight fraction of the limestone was maintained at 70 w/w% in the synthetic raw meal, on calcination this reduces to 56 w/w% in the calcined sample. Estimating the surface area of the calcined synthetic raw meal based on the assumption that there are no interactions

between the components it is expected to be 2.7 m^2/(g of calcined synthetic raw meal), but the surface area measured is 2 m^2/(g of calcined synthetic raw meal). If the surface area is only contributed to by the calcined limestone in the synthetic raw meal it should be 2.26 m^2/(g of calcined synthetic raw meal), e.g. 4.04 m^2/g times 0.56 g/(g of calcined synthetic raw meal), which is higher than the measured cumulative surface area. This indicates that there may be interactions between the limestone and other components, resulting in the reduced surface area of the synthetic raw meal. Comparing the CO_2 capture capacity of limestone in the synthetic raw meal and the pure limestone the capture capacity was lower for the raw meal, which might be because of the interaction between the components along with sintering enhanced by calcination conditions.

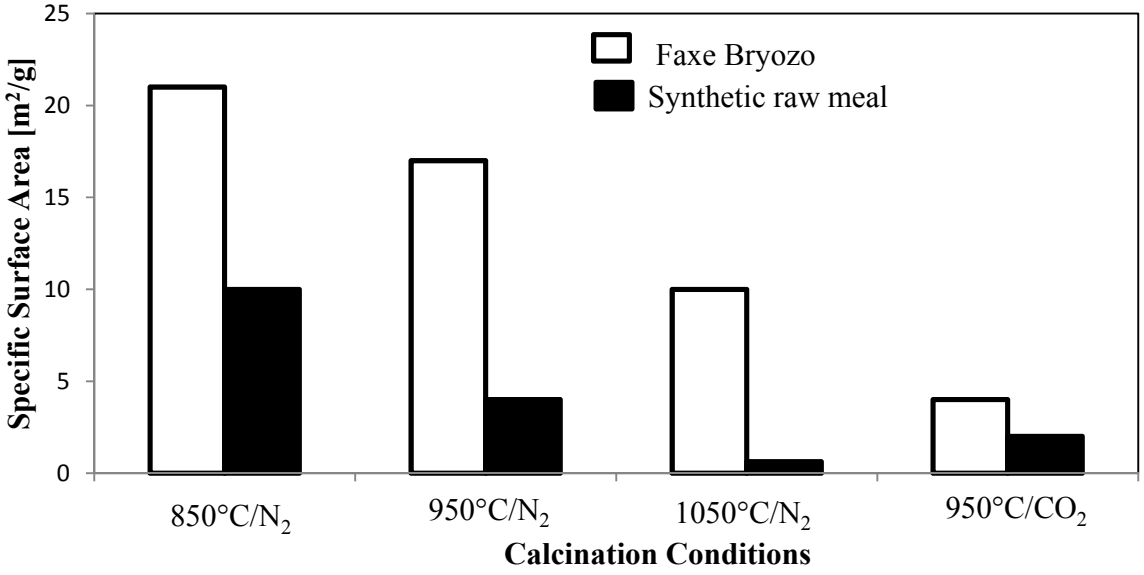

Figure 3-10: BET surface areas of limestone and synthetic raw meal at 850°C, 950°C and 1050°C in a pure N_2 atmosphere and a high CO_2 concentration atmosphere for 20 min.

To verify the influence of calcination conditions on the surface area of the synthetic raw meal, BET measurements of the samples under different calcination conditions were carried out. The results from

these measurements are summarized in Figure 3-10. For comparison, the BET measurements for the pure limestone were also carried out under similar calcination conditions.

The surface area of the synthetic raw meal calcined at 850°C, 950°C and 1050°C under aN_2 atmosphere was 11, 3.9 and 0.69 m^2/(g of calcined synthetic raw meal), respectively. The surface area of the calcined limestone was 21, 17 and 10 m^2/(g of calcined limestone) under similar calcination conditions, respectively. The decreasing trend in the surface area of limestone with an increase in temperature is due to sintering[73], which reduces the CO_2 capture capacity of the limestone[66]. Comparing the surface area of limestone and synthetic raw meal it is obvious that the surface area of the synthetic raw meal is lower than the area contributed by the limestone alone in the synthetic raw meal, were there no interactions between the components then the measured surface area must be equal to the estimated surface area, under respective calcination conditions as presented in Table 3-3.

Table 3-3: The measured surface area of the calcined limestone, synthetic raw meal (SRM) and estimated surface area of SRM assuming no interaction between components.

Temperature [°C]	Calcined limestone [m^2/g]	SRM measured [m^2/g]	SRM estimated* [m^2/g]
850	21	11	12
950	17	3.9	10
1050	10	0.69	6

*based on the assumption of no interaction between components

For all calcination temperatures, the measured surface area of the calcined synthetic raw meal is lower than that estimated. The difference between the estimated and measured surface areas increases with temperature. The surface area results under mild calcination conditions appear to correlate with only a small difference in the CO_2 capture capacity. At 950°C there is a significant difference in the expected

and estimated surface areas, similar to the difference in the CO_2 capture capacity results in Figure 3-2. This shows that the interaction between limestone and the other main components of the synthetic raw meal increases with temperature, which results in the formation of new phases along with a decrease in the surface area of the limestone.

Based on the observation from the crystallite size estimation, SEM images and BET surface area measurements, the mechanisms of the sintering phenomena and their effect on the CO_2 capture capacity of limestone is observed. With increasing temperature, the SEM images show the grains coalescing together, the BET surface area decreasing and the crystallite size increasing, which confirms the sintering process. It is well known that the main parameter that influences sintering is temperature. An increase in temperature results in an increase in the vibrational energy of the atoms which facilitates mobilization for a reduction in free surface energy. Sintering advances in different stages, increasing with time, by the initiation of neck growth between grains as observed in the SEM images, and the elimination of small pores resulting in a lower surface area as observed in the BET measurements. Along with temperature and time, atmosphere is another parameter which influences sintering. It was claimed[73] that CO_2 concentration has a catalytic effect on the sintering of CaO crystallites, but no mechanism was explained. The CO_2 partial pressure during the calcination of limestone influences the calcination temperature due to thermodynamic equilibrium. There might be a dynamic equilibrium, which enhances the movements of atoms in the crystal structure form from calcium oxide to calcium carbonate resulting in enhanced sintering. Thus under realistic calcination conditions sintering reduces the porosity of the calcined limestone, which has an effect on the carbonation due to the increase in the molar volume of the carbonate from oxide (36.9 from16.9 cm^3/mol).

CaO crystallite sizes in pure limestone and in the synthetic raw meal were estimated under realistic calcination conditions and were estimated to be 63 nm and 74 nm. This indicates that the crystallite size of CaO was not only influenced by temperature, time and atmosphere, but also by the components present in the synthetic raw meal, an effect which needs to be further investigated.

3.3.2 Influence of Components

A comparison of the surface area and corresponding CO_2 capture capacity of the limestone and synthetic raw meal under different calcination conditions indicates the complex nature of solid-solid particle interaction.

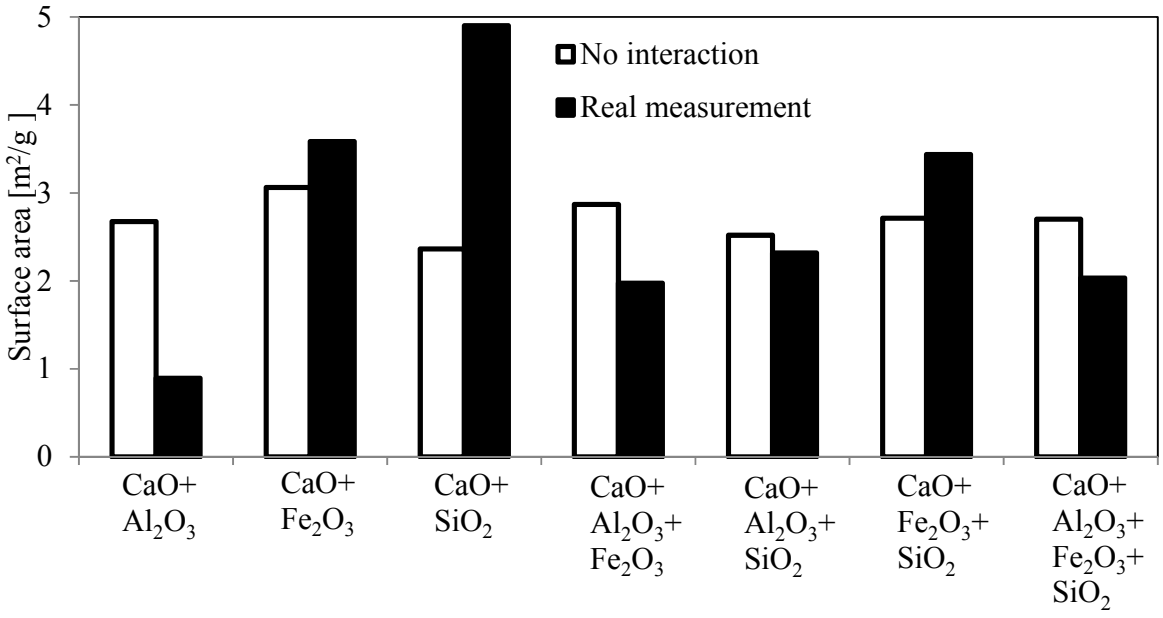

Figure 3-11: Comparison of measured and estimated surface areas of mixtures containing limestone and other main components of raw meal calcined under realistic calcination conditions.

In order to further elucidate the influence of each main component in the cement raw meal, cyclic experiments were carried out under realistic calcination conditions. Since the surface area of the

material appears to be the controlling parameter in the CO_2 capture capacity, BET measurements were carried out for the calcined material. The surface areas estimated by BET measurements are presented in Figure 3-11 for all the possible combinations of limestone and the other main components of the cement raw meal, and compared with the surface area estimated assuming no interaction between components.

According to the results obtained, the surface area of each mixture is different from the expected surface area of the mixture without any interactions between the components. The degree of interaction at 950°C appears to depend on the components present along with limestone.

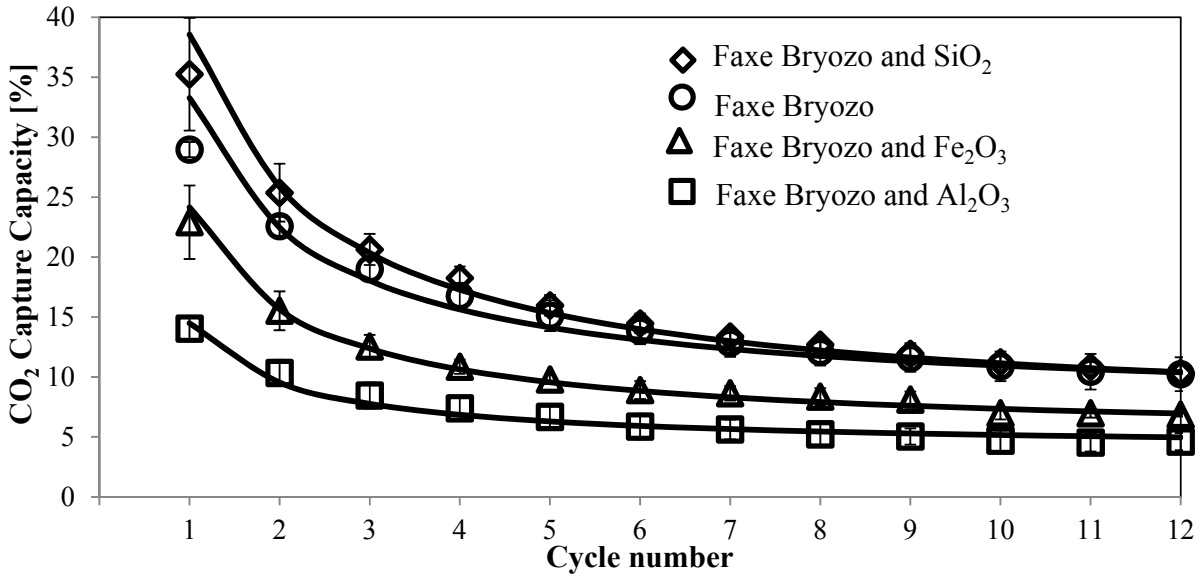

Figure 3-12: CO_2 capture capacity of binary components as a function of cycle number under realistic calcination conditions; Calcination: 84% CO_2, 950°C; Re-carbonation: 14.7% CO_2 in N_2.

Considering the binary components of the synthetic raw meal, limestone with aluminum oxide has the lowest surface area and the combination of limestone with silica has the highest surface area. To verify its effect on CO_2 capture capacity, cyclic experiments were performed. Figure 3-12 shows the CO_2

capture capacity of limestone and limestone with the other main component of the raw meal. The limestone with aluminum oxide has the lowest CO_2 capture capacity, similar to its measured surface area. Likewise limestone with silica has the highest CO_2 capture capacity among the binary combinations, as expected from the surface area measured.

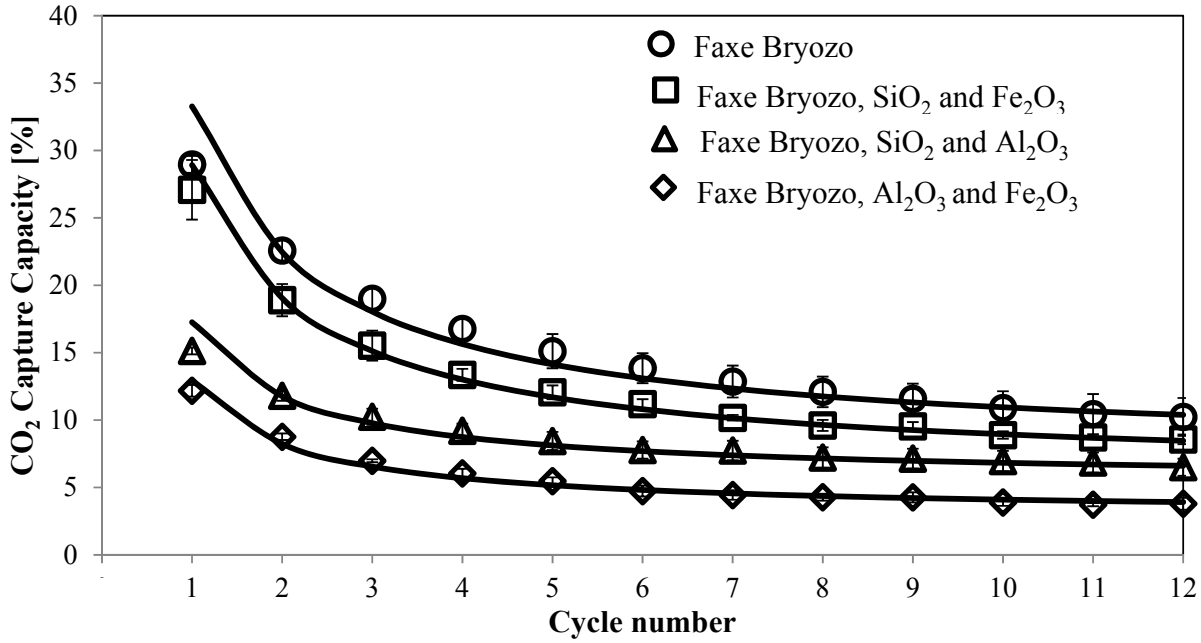

Figure 3-13: CO_2 capture capacity of ternary components as a function of cycle number cycle number under realistic calcination conditions; Calcination: 84% CO_2, 950°C; Re-carbonation: 14.7% CO_2 in N_2.

Cyclic experiments were performed with the ternary mixtures to verify any relationship between the surface area measured and their respective CO_2 capture capacity. The CO_2 capture capacity of limestone mixed with the other two components are summarized in Figure 3-13. The ternary mixture containing limestone, silica and iron oxide has a higher CO_2 capture capacity compared to the other tertiary mixtures, whereas limestone mixed with aluminum oxide and iron oxide has the lowest CO_2 capture capacity. The observed trend in CO_2 capture capacity also matched the measured surface areas of the mixtures.

From a detail analysis of the experimental results from the cyclic experiments and the BET surface area measurements of the mixture, it is possible to correlate the surface area of the mixture with the CO_2 capture capacity of the calcined limestone. Figure 3-14 summarizes the correlation between CO_2 capture capacity and surface area of the mixture calcined at 950^oC and in a CO_2 rich atmosphere. In the cement raw meal the main component after limestone is SiO_2, which did not show any negative effect on the CO_2 capture capacity but the addition of Al_2O_3 or Fe_2O_3 or both decreased the CO_2 capture capacity.

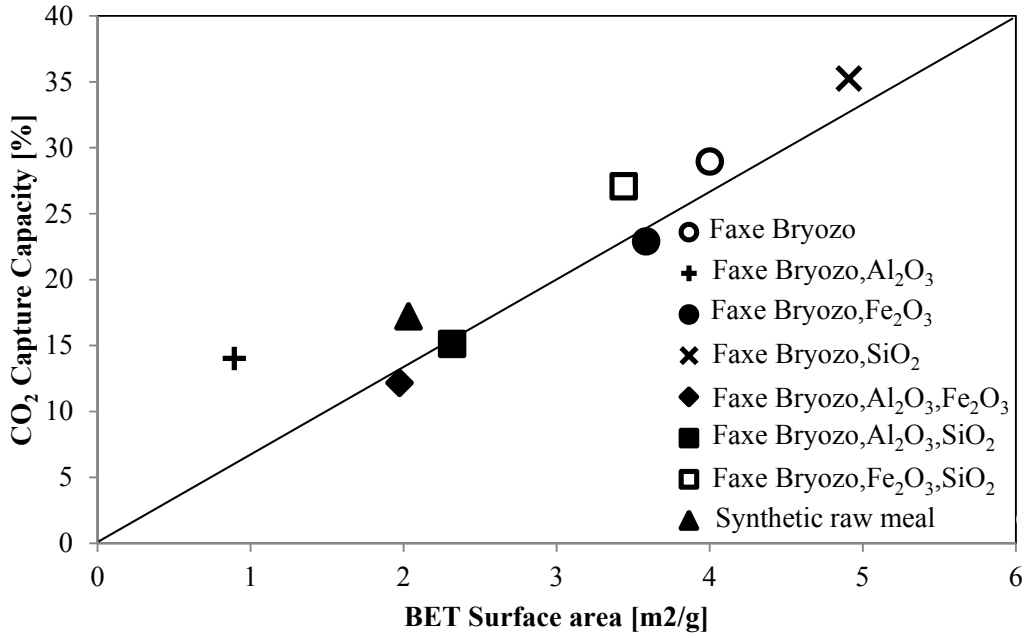

Figure 3-14: CO_2 capture capacity after the first cycle in the TGA apparatus as a function of the measured BET surface area for the mixtures under realistic calcination conditions; 950°C, 84 vol.% CO_2.

The surface area of the mixture containing limestone and silica was slightly higher than the pure limestone, and no decay in the CO_2 capacity compared to pure limestone is observed. The surface area of the mixture containing aluminum oxide was lowest and also resulted in the lowest capacity, whereas

the mixture containing iron oxide was slightly superior. Thus a direct correlation between the CO_2 capture capacity and the measured surface area seems to exist. Similarly in the tertiary mixtures a higher capture capacity was obtained for the sample with the highest surface area. The presence of Al_2O_3 in the mixture has a significant effect on the surface area, followed by Fe_2O_3, whereas SiO_2 showed no effect.

Different calcination conditions showed a correlation between the CO_2 capture capacities, the BET surface measured and the estimated crystallite size of the CaO in the synthetic raw meal. To verify the mechanism for decay in CO_2 capture capacity influenced by the components, the CaO crystallite size was also estimated by the XRD technique and the results are summarized in Table 3-4.

Table 3-4: CaO crystallite size estimated by the XRD technique under realistic calcination conditions.

CaO Crystallite	CaO	$CaO+SiO_2$	$CaO+Fe_2O_3+SiO_2$	$CaO+Al_2O_3+SiO_2$	$CaO+Al_2O_3+Fe_2O_3+SiO_2$
Size [nm]	63	53	51	68	74

The results also indicate that the size of the CaO crystallite was influenced by the components present. The probable explanation for this can be drawn from the sintering of the pure components. The components which sintered most may have induced additional movement in the adjacent atoms, along with its natural tendency to move depending on the sintering temperature and atmosphere. This might have resulted in a high degree of sintering of CaO in the presence of Al_2O_3 and Fe_2O_3, contrary to the presence of SiO_2. However there is an exception for the case with the mixture containing CaO, SiO_2 and Fe_2O_3, which was expected to have a crystal size larger than CaO and SiO_2. This indicates the complex nature of the components, which need to be further investigated.

3.4 Decay in CO_2 Capture Capacity

The CO_2 capture capacity of limestone decreases with an increase in the number of cycles. The detailed analysis by SEM and BET measurements show the textural changes in the particles. It can be concluded that the main mechanism in limestone capacity decay is sintering, and a correlation can be observed from Figure 3-14 between the surface area and CO_2 capture capacity. Similar decay mechanisms were observed by Abanades[27], and Wang and Anthony[29]. They formulated simple correlations to describe the decay in CO_2 capture capacity. However these correlations were developed for natural limestone (>95w/w% is $CaCO_3$) unlike the complex material (raw meal) considered in this study. The main observation from the CO_2 capture capacities as a function of cycle numbers was a fast decay in the initial cycles followed by slow decay, reaching an asymptotic value which is independent of the cycle number.

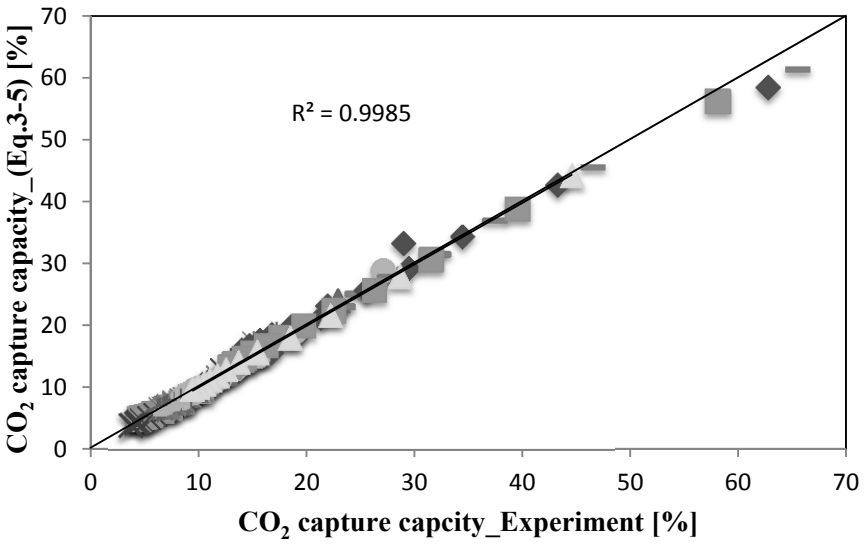

Figure 3-15: CO_2 capture capacity of limestone from the cyclic experiments in TGA apparatus compared with CO_2 capture capacity estimated using the equation 3-5.

In order to formulate this trend of decay in the CO_2 capture for application in the process simulation studies it is important to consider two parameters: 1) the degree of decay, and 2) the final CO_2 capture capacity. The correlation proposed by Grasa and Abanades[148] is used to quantify the degree of decay and residual CO_2 capture capacity shown by the following equation:

$$X_N = \frac{1}{\frac{1}{1-X_r} + kN} + X_r \qquad 3\text{-}5$$

The decay constant (k) and residual capture capacity (X_r) were determined from curve fitting. The results of this fitting exercise are compiled in Table 3-5. The correlation between the experimental and predicted CO_2 capture capacities is good as presented in Figure 3-15.

Table 3-5: CO_2 capture decay constant (k) and residual CO_2 capture capacity (X_r) of limestone mixed with the main components of the raw meal.

Solids	T (calcination) [°C]	CO_2 conc. [vol.%]	k	X_r
Faxe Bryozo	850	0	0.79	0.08
Faxe Bryozo	950	0	0.97	0.075
Faxe Bryozo	950	84	2.8	0.075
Synthetic raw meal	850	0	0.91	0.075
Synthetic raw meal	950	0	1.5	0.05
Synthetic raw meal	950	84	6.2	0.05
Cement raw meal	950	84	8.7	0.05
Faxe Bryozo, Al_2O_3	950	84	8.5	0.04
Faxe Bryozo, Fe_2O3	950	84	4.17	0.05
Faxe Bryozo, SiO_2	950	84	2.05	0.065
Faxe Bryozo, Al_2O_3, Fe_2O_3	950	84	9.05	0.03
Faxe Bryozo, Fe_2O_3, SiO_2	950	84	3.3	0.06
Faxe Bryozo, Al_2O_3, SiO_2	950	84	7.45	0.055

The results show that for pure limestone and for the limestone in the raw meal under the tested conditions, the calcination temperature influences the residual CO_2 capacity of the limestone, whereas the CO_2 concentration has a profound effect on the decay constant with no influence on the residual CO_2 capture capacity. These observations were similar to the results obtained by Garsa[31], but the effect of the main components of the raw meal was complex, and both the residual CO_2 capture capacity and decay constant were affected.

3.5 Conclusions

Based on the experimental work the main conclusions are summarized as follows:

1. Raw meal could be used as the sorbent even though there are interactions between the lime and other components, especially under realistic calcination conditions.
2. SEM, XRD and BET analyses indicated that sintering is the main reason for the observed decrease in CO_2 capture capacity. A correlation was established between the surface area of the mixtures and the CO_2 capture capacity of the limestone in the mixture under realistic conditions.
3. XRD results show that the CaO crystallite size was not only influenced by the calcination conditions but also by the components of the cement raw meal.
4. The decay in CO_2 capture capacity of the limestone in the raw meal is due to sintering, resulting in a change in particle morphology and a larger CaO crystal size
5. The CO_2 capture capacity as a function of cycle number can be described by a two parameter correlation, which can used for process simulation studies using raw meal sorbent.

4. Cyclic Experiments in a Fluidized Bed Reactor

In the previous chapter, detailed investigations into the application of raw meal for CO_2 capture were presented, where experiments were carried out in a TGA apparatus. However, a fluidized bed reactor is suitable for gas-solid particle reactions at industrial scale. So, in this chapter, the cyclic experiments performed in a fluidized bed reactor are presented. The objective was to simulate the looping process to investigate parameters in a fluidized bed reactor. The different parameters investigated were: the bed composition (only limestone, limestone with sand and raw meal as the sorbent (30% clay in limestone)), attrition, carbonation temperature and simultaneous SO_2 and CO_2 capture. Along with these parameters, the conversion of calcined limestone in the fluidized bed reactor was compared with the conversion of particles in a TGA apparatus and the rate constant was determined.

A reactor model was developed based on the principles of the Kunii-Levenspiel fluidized bed reactor model. The model predicted results were compared with the experimental results. The validated model was used for a sensitivity analysis of the model parameters of the fluidized bed reactor.

4.1 Experimental

4.1.1 Setup

To study the carbonate looping process, cycle experiments were carried out in a laboratory scale fluidized bed reactor. A schematic drawing of the setup is shown in Figure 4-1. The setup included a gas mixing system, four mass flow controllers, an electric gas pre-heater, a reactor, a cyclone, a container, a heat exchanger, a gas conditioning system, gas analyzers, thermocouples, pressure transducers and a data acquisition system.

The reactor was made from a steel tube with an inner diameter of 60 mm; the total height of the reactor was 2.5 m. A perforated steel plate used as a gas distributor with 1 mm holes was located at the bottom of the reactor. The reactor was electrically heated by five independently controlled heating elements. The temperature and pressure in the reactor were measured at three locations: 1) just above the distributor plate (T1, P1), 2) 0.8 m above the distributor plate (T2, P2) and 3) at the top of the reactor close to the exit (T3, P3).

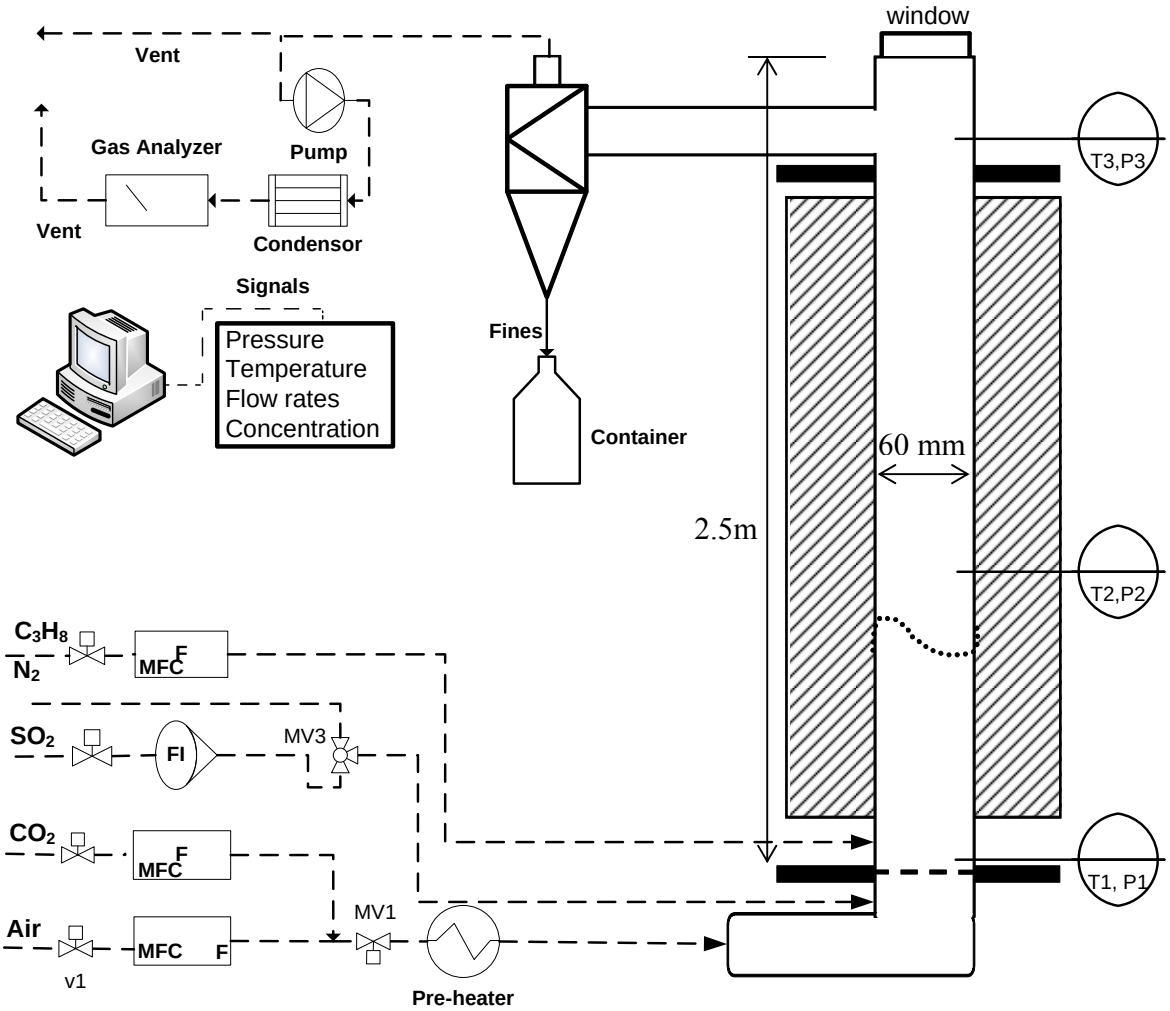

Figure 4-1: Schematic of the experimental setup used for cyclic experiments.

Solid particles are fed from the top of the reactor by opening a window flange. Compressed fluidizing gases, controlled by precision mass flow controllers, were fed at the bottom of the reactor through the gas pre-heater. Propane gas was injected directly in to the hot bed, at the bottom of the reactor above the distributor plate, to supply additional energy for the endothermic reaction. The elutriated fine particles in the exit gas were separated from the gas by a cyclone and collected in a container. A small fraction of the exit gas was induced by a pump to the centralized gas analyzer section to monitor the concentrations of gases like CO_2, O_2 and SO_2. Temperature, pressure, inlet gas flow rate and exit gas concentrations were continuously logged to the system with a time step of 1s.

4.1.2 Materials

Faxe Bryozo limestone (0.71-1.0 mm) from Faxe Kalk A/S was used as the sorbent material. Quartz sand was used as bed a material with a particle size range of 0.4-0.8 mm. Sandy clay (0.71-1.0 mm) was supplied by FLSmidth A/S; its composition is presented in Table 4-1. To simulate raw meal as the sorbent, the clay was mixed with limestone for the cycle experiments. The composition of Faxe Bryozo is same as that presented in Chapter 3.

Table 4-1: Composition of Faxe Bryozo and sandy clay in wt%.

wt.%	CO_2	CaO	SiO_2	Al_2O_3	Fe_2O_3	K_2O	MgO	MnO	P_2O_5	TiO_2
Faxe Bryozo	43.6	55.1	0.45	0.1	0.08	0.03	0.43	0.02	-	0.01
Sandy clay	-	3.53	52.39	15.53	10.17	-	2.13	0.16	0.22	1.87

4.1.3 Pre-experimental Considerations

In order to perform experiments under controlled conditions, it is important to determine the experimental operating conditions and procedures suitable to achieve the objective when a new experimental setup is established. The most important parameters to consider are the particle size, the gas velocity and the bed inventory. The velocity of the gas is a function of flow rate and temperature.

Since the maximum temperature in the reactor is 850°C, the only other parameter that can be controlled is the gas flow rate. A gas flow rate 60 NL/min was selected for the experiment, which resulted in a maximum gas velocity equal to 1.3 m/s at 850°C in the reactor. The minimum size of particles in the bed should have terminal velocity higher than 1.3 m/s, so that the bed particles are not elutriated from the reactor during the experiment. The particle size range of 0.71-1.0 mm was selected such that the bed was fluidized without being entrained with gas flow. The next parameter that is important for stable operating conditions during the experiments is the bed inventory. The optimum bed inventory was estimated by experiments, and a bed inventory of 1 kg was selected for these experiments.

Before each experiment, the gas analyzer were calibrated with zero gas (N_2) and calibration gas to make sure that the concentrations of the gas analyzed during the experiments is accurate. The verification of inlet gas composition is presented in Figure 4-3.

For the calcination reaction, energy has to be supplied to maintain favorable thermodynamic conditions. So, during the calcination process, propane was injected into the bed to supply additional energy for fast calcination. During carbonation, the energy released due to the reaction has to be dissipated, so quartz sand was mixed with limestone such that the energy released was distributed throughout the whole bed, thereby controlling the rise in bed temperature.

4.1.4 Experimental Procedure

The general procedure for the cyclic experiments is presented here for the reference experiment conditions (Looping 1 see: Table 4-3). The reactor was heated by setting the temperature of heating elements to 800°C with air flowing at a rate of 60 NL/min. 750 g of quartz sand was fed into the reactor from the top window of the reactor, when temperature T2 (Figure 4-1) was above 400°C. A temperature above 400°C was selected to increase the bed temperature quickly and the gas velocity was

high enough for proper fluidization of the bed and to avoid bleeding of bed material through the gas distributor plate. The gas pre-heater was set to 400°C to heat the fluidizing gas and reduce the temperature difference of the fluidizing gas above and below the distributor plate.

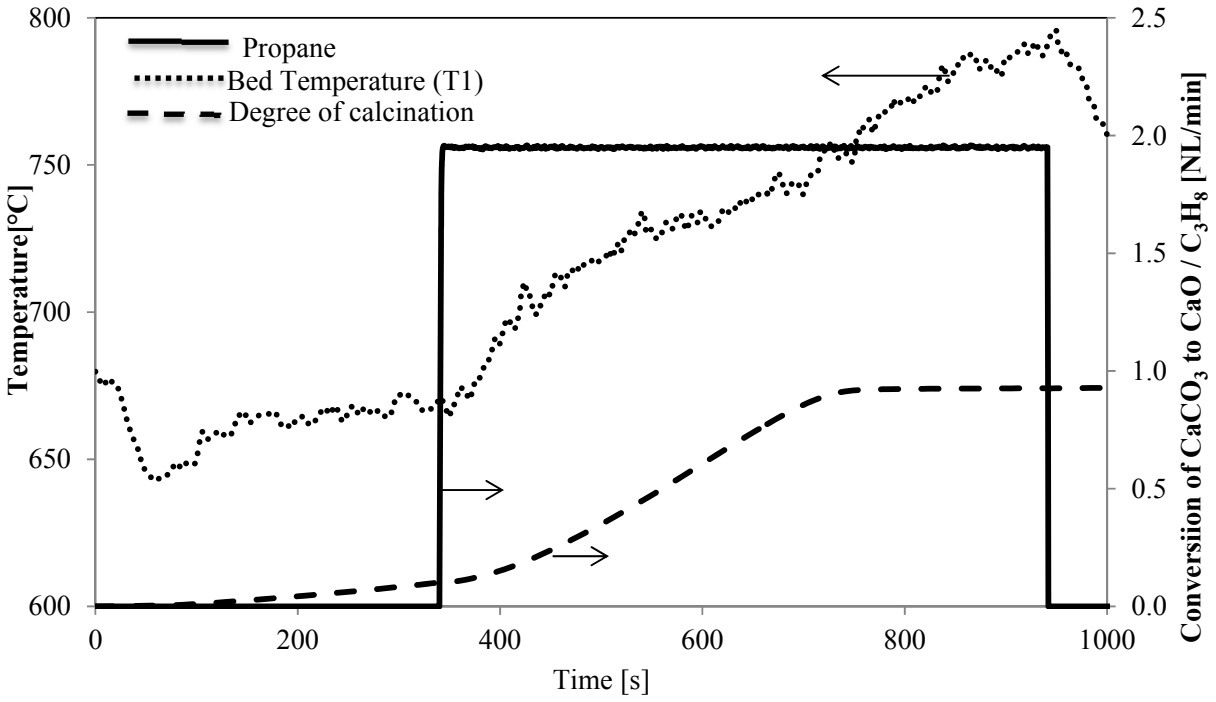

Figure 4-2: Calcination of limestone under propane combustion for the first cycle in the fluidized bed reactor.

In this experiment, 250 g of limestone were added to the bed when the temperature of the bed at T1 (Figure 4-1) was above 700°C. The temperature of the bed dropped due to the addition of cold limestone and the calcination reaction of bed took place at a very low rate. So, a propane flow of 2 NL/min was injected directly into the hot bed to supply additional energy for fast calcination. The temperature of the bed increased slowly until the complete calcination of limestone, after which the temperature rose rapidly. A small portion of the exit gas from the reactor was sampled and pumped to the centralized gas analyzer to measure the CO_2 gas concentration. Thus, the calcination reaction could

be monitored by the bed temperature along with online gas concentration measurements. When the calcination of the bed was complete, the concentration of CO_2 was constant and equivalent to the amount released by propane combustion. Calcination of limestone in the fluidized bed reactor under propane combustion is summarized in Figure 4-2. The degree of calcination was based on the CO_2 balance according to equation 4-9. After calcination, the propane flow was stopped and the temperature of the heating elements was lowered such that the bed temperature (T1) dropped to 600°C. During the carbonation step, the fluidizing gas was changed to 15 vol.% CO_2 in air, keeping the total gas flow rate constant. The concentration of CO_2 gas in the exit gas was monitored. Carbonation was carried out for 10 min, and the fluidizing gas was later changed to air. The temperature of the bed was increased again by increasing the set point temperature of the heating elements for the next calcination cycle along with the injection of propane gas.

Figure 4-3 summarizes the cyclic experiment process in four steps: 1) inlet CO_2 concentration measurement, 2) calcination (first cycle) 3) carbonation (first cycle) and 4) calcination (second cycle), by measuring the CO_2 concentration in the exit gas, the inlet CO_2 flow rate and the propane flow rate. The first plateau curve (1, Figure 4-3) indicates the CO_2 concentration in the inlet gas during the carbonation step measured before the beginning of the cyclic experiment. The second curve (2, Figure 4-3) indicates the first calcination cycle where the CO_2 concentration increased to maximum and dropped to a stable value corresponding to the CO_2 concentration released from propane combustion, excluding the water content in the exit gas. The third curve (3, Figure 4-3) represents the carbonation step where the CO_2 concentration increased with time for a constant inlet CO_2 flow rate. The fourth curve (4, Figure 4-3) shows the second calcination cycle, which has a smaller area compared to the first cycle due to the lower amount of CO_2 released, equivalent to the CO_2 captured in the first cycle.

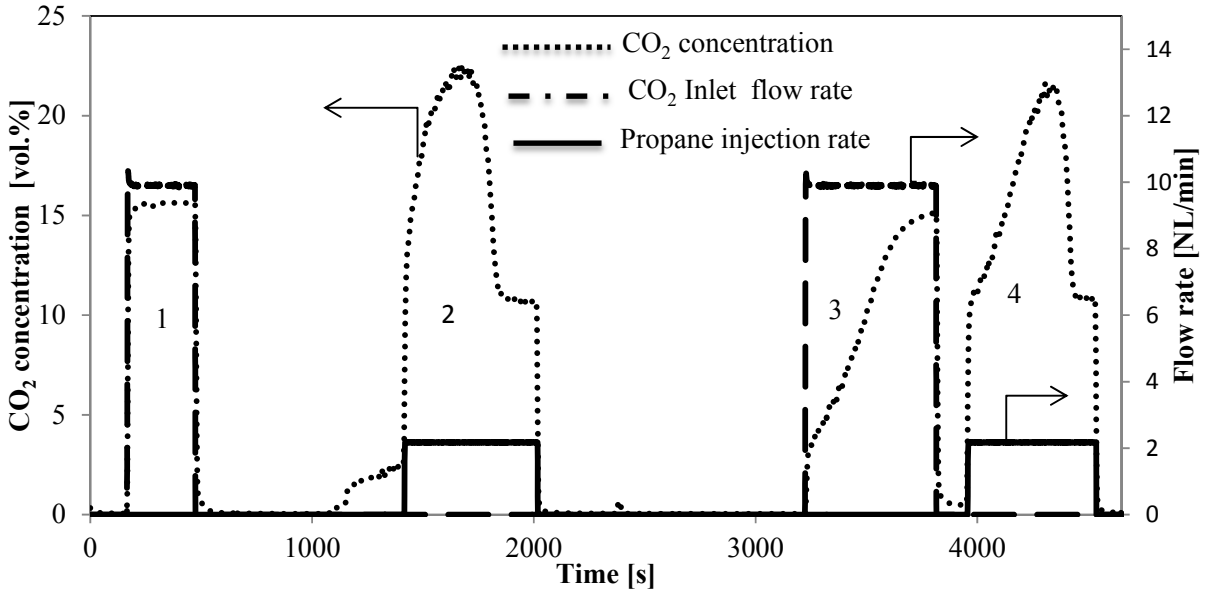

Figure 4-3: Cycle experiment: (1) inlet CO_2 flow rate and CO_2 concentration, measurement through the sand bed, (2) CO_2 concentration in the exit gas due to calcination and propane combustion along with the propane flow rate during the first calcinations step, (3) CO_2 concentration and inlet CO_2 flow rate during the first carbonation step and (4) CO_2 concentration and propane flow rate during the second calcination step.

Thus, by alternating the calcination and the carbonation conditions, cyclic experiments were performed. The operating conditions for the reference case are summarized in Table 4-2.

Table 4-2: Operating conditions in the fluidized bed reactor.

Parameter	Calcination	Carbonation
Temperature [^oC]	650 to 800	600 to 650
Time [min]	30	10
Atmosphere	10% CO_2 in air (propane combustion)	15% CO_2 in air
Gas flow rate [NL/min(m/s)]	60 (1.1-1.3)	60 (1-1.1)

Table 4-3 summarizes the list of main cyclic experiments performed in the fluidized bed reactor. Based on the parameters investigated in the cyclic experiments, a few modifications were made in the

experimental procedure described for the experiment (Looping 1). During these experiments, one parameter was changed and compared to Looping 1.

The objective of the experiment (Looping 0) was performed to estimate the loss of bed material as fines. In this experiment, 1 kg of limestone was added to bed instead of quartz sand, as mentioned in the procedure above. In this experiment, samples were taken from the bed through the top window after each carbonation cycle to evaluate the degree of carbonation of calcined limestone. Further fines entrained with the gas were collected below the cyclone after each calcination cycle.

The objective of the experiment Looping 2 was to evaluate the influence of high temperature during carbonation. In the experiment Looping 1, the carbonation temperature measured by (T1) was in the range of 600 to 650°C, whereas in this experiment T1 was above 700-730°C.

The objective of the experiment Looping 4 was to simulate raw meal as a sorbent in the cyclic experiment. Thus, 30 wt.% of sandy clay mixed with limestone was added to the reactor instead of 250 g of limestone alone as used the experiment Looping 1.

The objective of experiment Looping 5 was to investigate the influence of SO_2 during the carbonation of limestone. Thus, SO_2 was injected into the bed at a flow rate of 30 mL/min only during the carbonation stage, which corresponds to 500 ppmv in the inlet gas.

Table 4-3: List of looping experiments.

Experiment no.	Cycles	Parameter changed wrt. Looping 1
1. Looping 0	9	Inventory 1 kg limestone and no sand
2. Looping 1	10	Reference
3. Looping 2	8	Carbonation temperature 700^{o}C
4. Looping 4	5	30% clay in limestone
5. Looping 5	5	Simultaneous SO_2 and CO_2 capture

4.2 Data Analysis

Except for the experiment Looping 0, the other experiments were analyzed by exit gas analysis to estimate the degree of conversion of the bed due to carbonation or conversion of SO_2. In the experiment Looping 0, samples were taken after each carbonation cycle and samples were analyzed in a TGA apparatus to estimate the weight loss due to CO_2 release and evaluate the degree of carbonation.

4.2.1 Solid Particle Analysis:

The sampled limestone particles from the bed after the carbonation step were placed in a desiccator to cool down before being stored in an airtight 50 mL glass bottle. The cooled samples were analyzed by measuring the weight loss of the sample by heating the particles up to 900°C in a TGA apparatus in an N_2 atmosphere.

The degree of carbonation (X_{carb}) of limestone particles was determined by the weight loss of the sample:

$$X_{carb,N} = \frac{\left(\left(w_{in,N} - w_{f,N}\right)/44\right)}{\left(x_{CaO} \cdot w_{f,N}/56\right)} \qquad 4\text{-}1$$

Here, $w_{in,N}$ is the weight of the sample before analysis and $w_{f,N}$ is the final weight of the sample; the weight fraction of CaO in the calcined sample was $x_{Cao} = 0.98$, estimated from Table 4-1. N is the cycle number.

4.2.2 Gas Analysis

The degree of calcination and carbonation was determined by the CO_2 mass balance, which was determined from the exit gas concentrations and inlet gas flow rates. The volume of CO_2 released

during the calcination of fresh limestone was taken as the basis for the total CO_2 capture capacity of fed limestone.

$$V_{CO_2,total} = \frac{w_{CaCO_3} M_{CO_2}}{M_{CaCO_3}} \frac{1}{\rho_{CO_2}} [NL] \quad \text{4-2}$$

During the calcination reaction, CO_2 gas is released from the combustion of propane and the calcination of limestone. So, to estimate the degree of calcination, it is important to determine the CO_2 gas flow in the exit gas from propane combustion. The gas balance for propane combustion and simultaneous calcination is as follows:

Total flow rate of inlet gas into the reactor:

$$\phi_{t,in} = \phi_{air,in} + \phi_{C_3H_8,in} \quad \text{4-3}$$

Total flow rate of gas out of the reactor, excluding H_2O as the sample is dried before analyzing the gas concentration:

$$\phi_{t,out} = \phi_{air,out} + \phi_{CO_2,out} \quad \text{4-4}$$

Flow rate of air out of the reactor after complete propane combustion:

$$\phi_{air,out} = \phi_{air,in} - 4.9 \cdot \phi_{C_3H_8,in} \quad \text{4-5}$$

Flow rate of CO_2 in the exit gas which includes both combustion and calcination processes:

$$\phi_{CO_2,out} = 3 \cdot \phi_{C_3H_8,in} + \phi_{CO_2,cal} \quad \text{4-6}$$

Volume fraction of CO_2 gas in the exit gas:

$$x_{CO_2,out} = \frac{100\phi_{CO_2,out}}{\phi_{CO_2,out} + \phi_{air,out}} \quad \text{4-7}$$

Release rate of CO_2 gas from the calcination of limestone:

$$\phi_{CO_2,cal} = \phi_{CO_2,out} - 3 \cdot \phi_{C_3H_8,in} \quad \text{4-8}$$

The degree of calcination can be estimated by the equation:

$$X_{cal} = \frac{\int_0^t \left(\left(\frac{x_{CO_2,out}\phi_{air,out}}{100 - x_{CO_2,out}} \right) - 3\phi_{C_3H_8,in} \right) dt}{V_{CO_2,total,N}} \quad \text{4-9}$$

Similarly, the CO_2 balance is used for estimating the degree of carbonation based on the inlet and outlet flow rate of CO_2 gas. The inlet concentration is controlled using mass flow controllers and verified by gas analyzers. The degree of carbonation can be estimated by the equation:

$$X_{carb} = \frac{\int \phi_{in} \cdot \frac{\left(x_{CO_2,inlet} - x_{CO_2,outlet} \right)}{(100 - x_{CO_2,outlet})} dt}{V_{CO_2,total}} \quad \text{4-10}$$

Conversion of SO_2 gas is estimated based on the SO_2 concentration (measured in ppmv) in the exit gas according to the equation:

$$X_{SO_2} = \frac{\frac{\left(\phi_{air,in} + \phi_{CO_2,out} \right) x_{SO_2,out}}{\left(1e^6 - x_{SO_2,out} \right)}}{\phi_{SO_2,in}} \quad \text{4-11}$$

here, $V_{CO_2,total}$, the volume of CO_2 in the fed fresh limestone [NL]

w_{CaCO_3} , the weight of limestone fed in to the reactor [g]

ρ_{CO_2} , the density of CO_2 gas [1.97 g/NL]

M_{CaCO_3} , Molecular weight of $CaCO_3$ [g-mol]

ϕ_{in} , the volumetric flow rate of the fluidizing gas [NL/min]

$x_{CO_2,inlet}$, the inlet volume fraction of CO_2 in the fluidizing gas [vol.%]

$x_{CO_2,outlet}$, the outlet volume fraction of CO_2 in the exit gas [vol.%]

X_{carb}, the conversion of CaO to $CaCO_3$ by carbonation [-]

x_{SO_2}, the concentration of SO_2 in the exit gas in [ppmv]

X_{SO_2}, the conversion of SO_2 gas

$\phi_{SO_2,in}$, the inlet flow rate of SO_2 gas [NL/min]

4.3 Repeatability Test

In order to verify the repeatability of the results in the present experimental setup, two experiments were performed. The experimental conditions were similar to the Looping 1 experiment operating conditions mentioned in Table 4-2. In these experiments, two looping cycles were performed to check the conversion of CaO in the bed. Figure 4-4 shows the conversion of calcined limestone in the bed with respect to time for two experiments in the first two carbonation cycles. The conversion profiles obtained for the two cycles in two separate experiments overlapped closely, meaning that the repeatability of the results was quite good. Thus, the experimental procedure applied for performing the experiments is reliable in the present experimental setup.

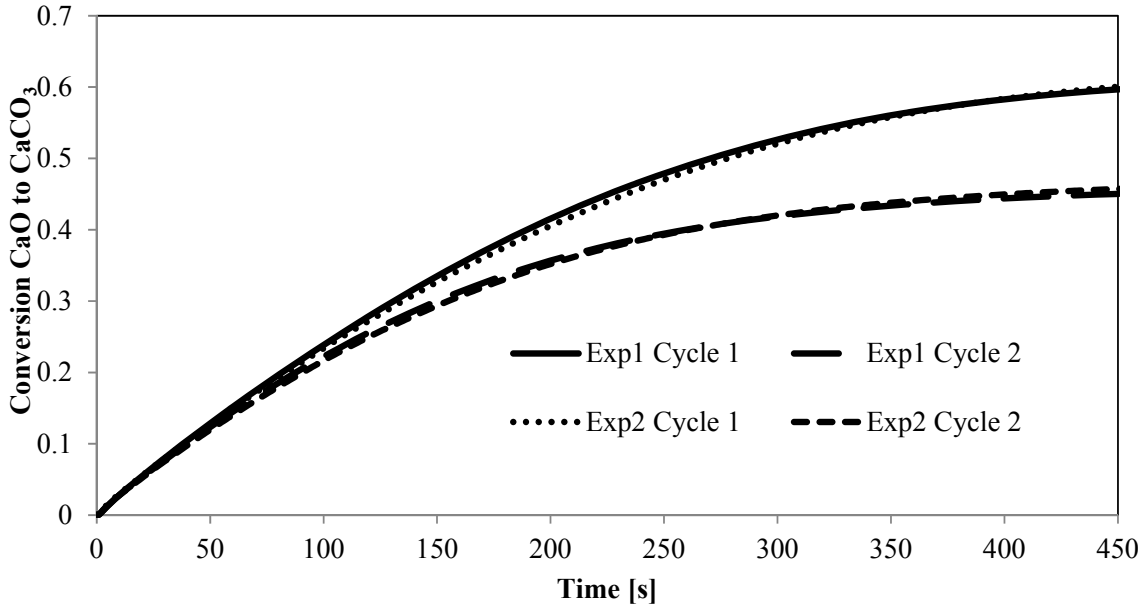

Figure 4-4: Degree of conversion of limestone obtained for first two looping cycles from two different experiments under similar operating conditions.

4.4 Results and Discussion

4.4.1 Cycle Experiments

The degree of conversion of calcined limestone to calcium carbonate with respect to cycle number is summarized in Figure 4-5 from the cyclic experiments. The general trend in the average conversion of the bed is similar for the all experiments. Comparing the experiment Looping 4 (30% clay in limestone) with the Looping 1 experiment, the presence of clay had no significant influence on the bed conversion in the fluidized bed reactor under the present operating conditions. Similar results were also obtain from the TGA apparatus, where under mild calcination conditions, there was no significant different in the conversion of Cao to $CaCO_3$.

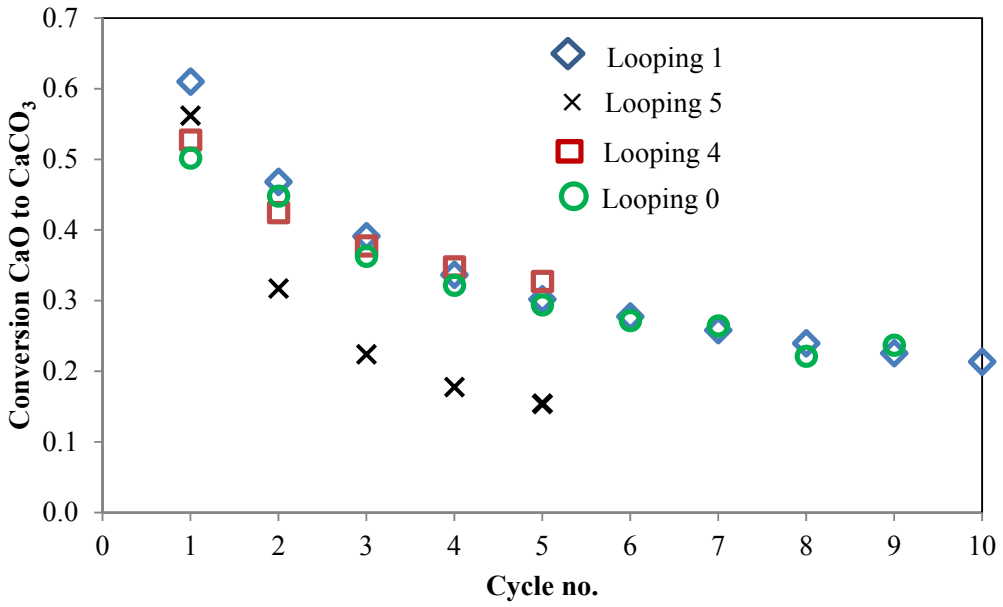

Figure 4-5: Final conversion of calcined limestone with respect to cycle number for different looping experiments in the fluidized bed reactor.

Figure 4-5 shows the degree of conversion of CaO to $CaCO_3$ for the Looping 1 and Looping 5 (simultaneous SO_2 and CO_2 capture) experiments. In the first carbonation cycle, the difference in the conversion of CaO to $CaCO_3$ was very low. However, the conversion of CaO to $CaCO_3$ decreased significantly with increasing cycle number. The significant drop in the CO_2 capture capacity was due to the permanent retention of SO_2 by limestone, which accumulates with increasing cycle number and reduces the limestone available for CO_2 capture.

Comparing the conversion of CaO in the experiment Looping 1 with the experiment Looping 0 (only limestone), in the first cycle, there was a large difference in the final conversion, but the difference was reduced with increasing cycle number. In these two experiments, the main difference, apart from the bed composition, was the initial loading of limestone. So, in the experiment Looping 1, the conversion of calcined limestone reached its maximum capacity in 10 min, whereas in Looping 0, the conversion of the bed did not reach its maximum capacity in the first cycle due to the high initial loading. However, with increasing cycle number, the maximum conversion capacity decreased so the limestone could reach its maximum capacity, similar to the Looping 1 experiment.

The detailed investigation of each experiment is discussed in the following sections.

4.4.2 Conversion of Calcined Limestone in a Fluidized Bed Reactor

In Figure 4-6, the degree of conversion of CaO with respect to time is presented from the first cycle to the tenth cycle. The main features that can be observed from the experiment are:1) the deviation in the rate of the reaction during the first 1 min was not significant for cycles 1-10; 2) the time to shift the reaction rate from fast to slow decreased from one cycle to the next cycle; 3) the final degree of re-carbonation decreased from 60% to 20% from the first cycle to the tenth cycle; 4) the decrease in the

final degree of conversion of calcined limestone during carbonation was large in the first three cycles compared to the later cycles.

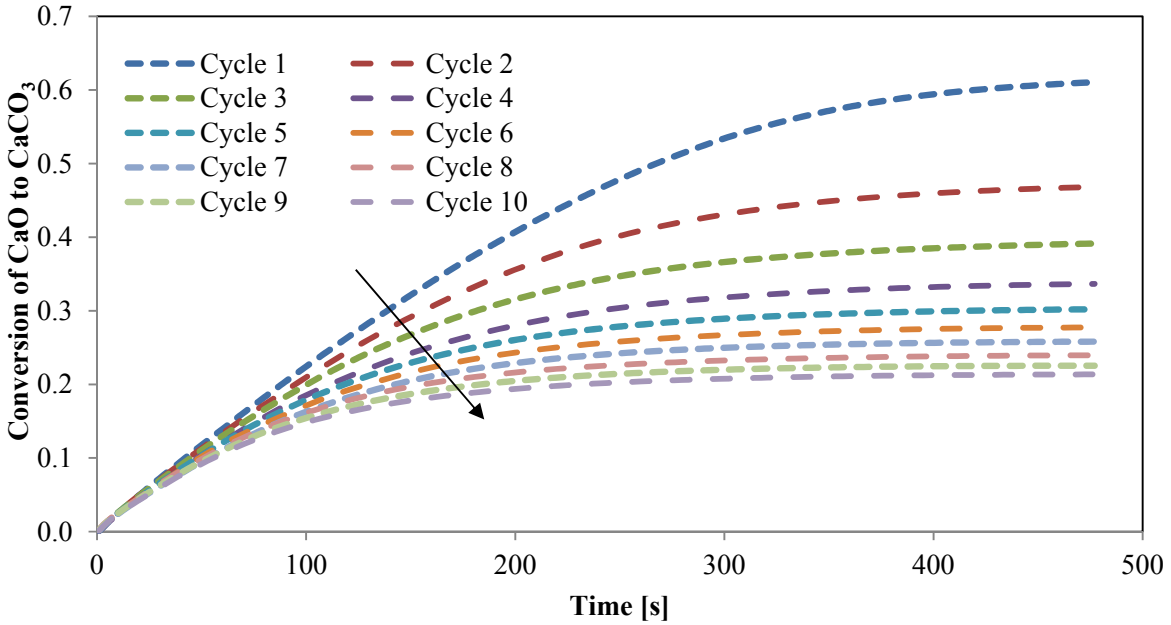

Figure 4-6: Degree of carbonation with respect to time for cycles 1-10. Calcination (mild conditions): temperature 650-800°C, under propane combustion (2 NL/min) in air, gas flow rate of 60 NL/min; Carbonation: 15 vol.% CO_2 in air, temperature 600- 650°C.

The observed features from the looping process by alternating the looping conditions were similar to the trend observed in the TGA apparatus. However, there was a difference in the observed rate of conversion, which can be observed by comparing the conversion profile in the fluidized reactor and the TGA apparatus, as shown in Figure 4-7. Figure 4-7 shows the degree of conversion of calcined limestone to calcium carbonate in the first carbonation cycle. In the TGA apparatus, the apparent rate of conversion was estimated as 0.0053 [1/s] whereas for in the fluid bed reactor, it is 0.0017 [1/s] before the shift in the reaction regime, indicated by slope measurements in Figure 4-7 .

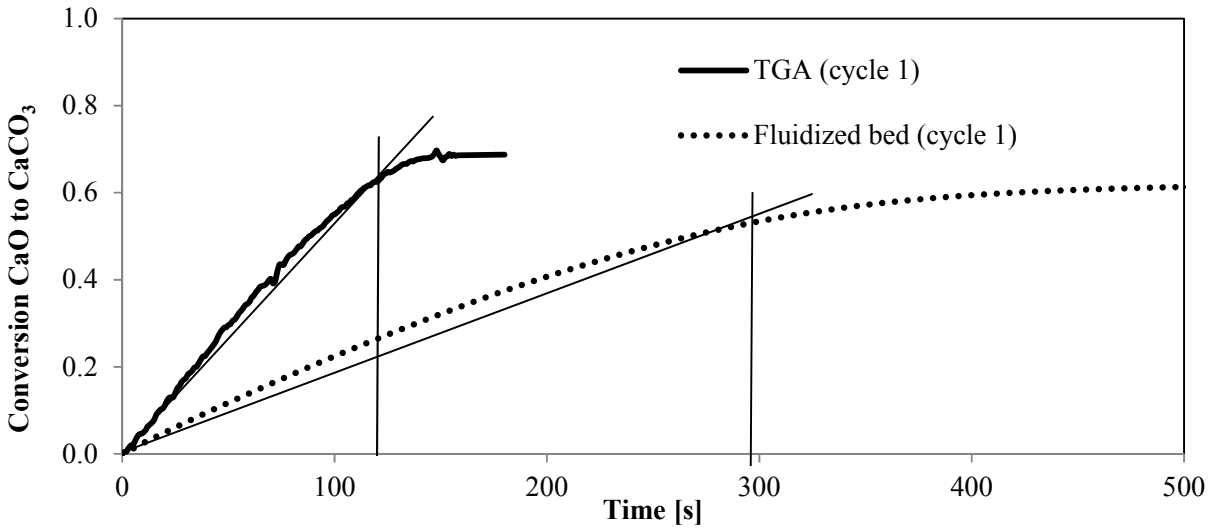

Figure 4-7: Comparing the conversion of calcined limestone in the TGA apparatus and fluid bed for the first cycle under mild calcination conditions (< 850°C).

The difference in the rate of conversion was due the concentration of CO_2 in the reaction zone. In the TGA apparatus, the change in the CO_2 concentration due to CO_2 sorption by calcined limestone was less than 0.1%, estimated from the gas flow rate and rate of degree of particle conversion, whereas in the fluidized bed, the CO_2 concentration changed continuously with time, as shown in Figure 4-8.

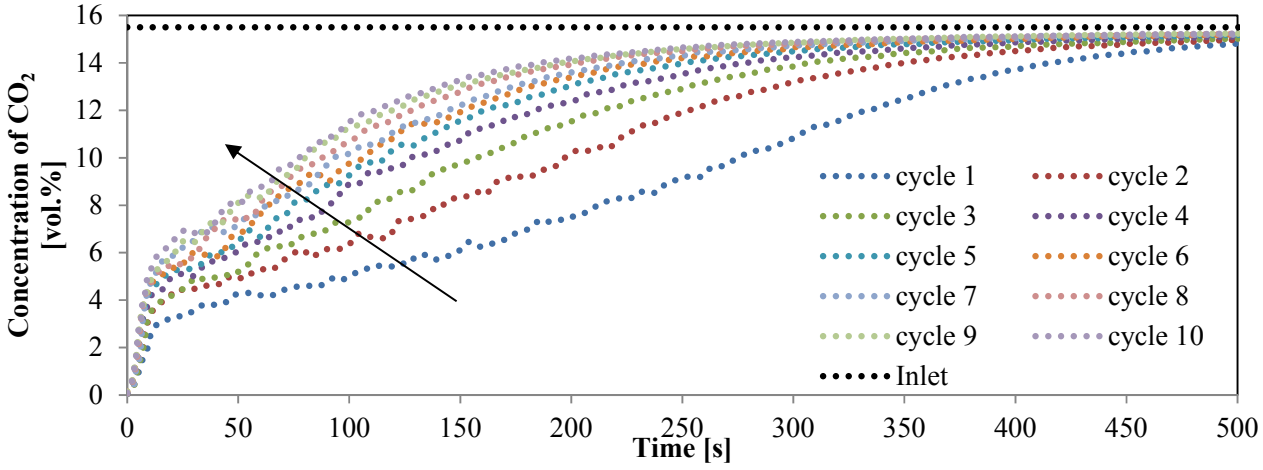

Figure 4-8: The concentration profile of CO_2 gas in the exit gas stream with respect to time for 1-10 carbonation cycles along with the inlet CO_2 concentration.

Using the spherical grain model expression, the rate of constant for the carbonation reaction was estimated according to equation 4-17. In this equation, the concentration of CO_2 in the TGA apparatus was assumed to be constant as the difference in the inlet and the out CO_2 concentration was very small, whereas for the fluidized bed reactor, the average of inlet and outlet CO_2 concentrations were selected. The experimental results show a kinetically controlled reaction regime where the slope of the estimated rate constant is zero, followed by a transition regime where the reaction shifts from kinetically controlled to diffusion controlled and a third diffusion controlled regime where the reaction rate drops rapidly. The estimated rate constant in the kinetically controlled reaction regime is 3 [m^3/kmol.s].

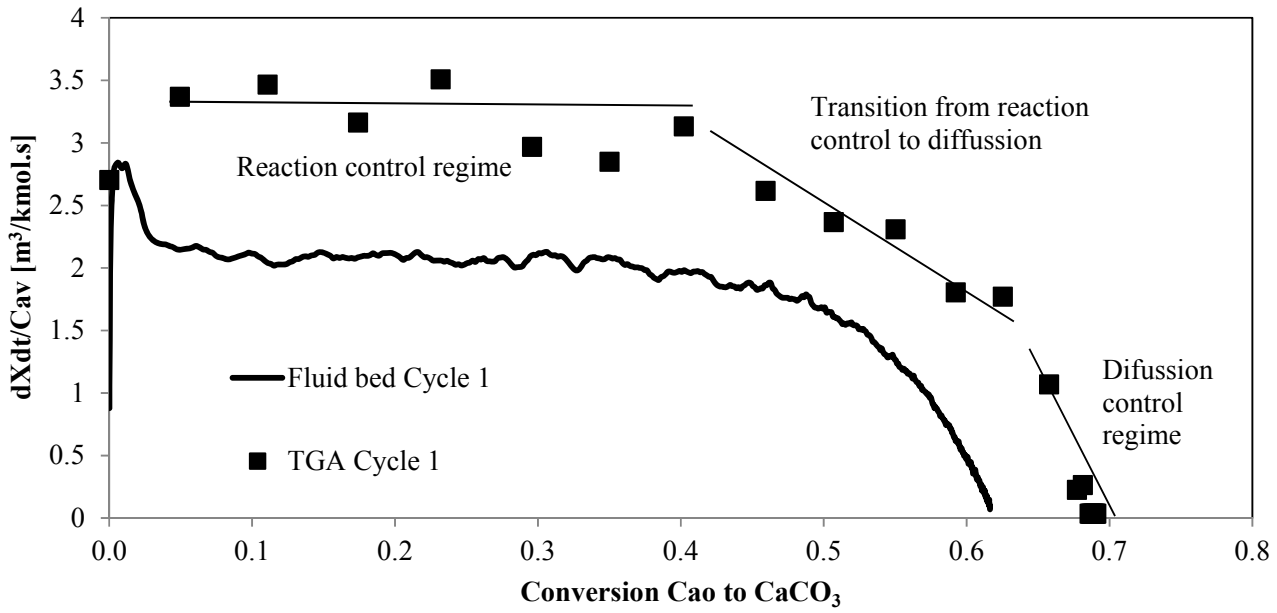

Figure 4-9: Rate constant estimated for the carbonation of limestone in the TGA apparatus and in the fluidized bed reactor.

4.4.3 Attrition

Attrition is an important factor to consider in the fluidized bed reactors as a high attrition rate might result in the loss of bed material. So, a cyclic experiment (Looping 0) in the fluidized bed reactor was

carried out to estimate the loss of bed material due to attrition. Figure 4-10 below indicates the weight fraction of the sample collected below the cyclone after each calcination cycle. It is clearly shown that most of the elutriation took place in the initial cycles, which might be due to breakage of sharp edges on the surface of the particles due to inter-particle collision or collision with the reactor wall. Once the particles attain a smooth surface, then the loss of bed material decreases. The fines collected below the cyclone decreased from 2 wt.% in the first calcination cycle to nearly 0 wt.% in the ninth cycle based on the initial weight of the bed.

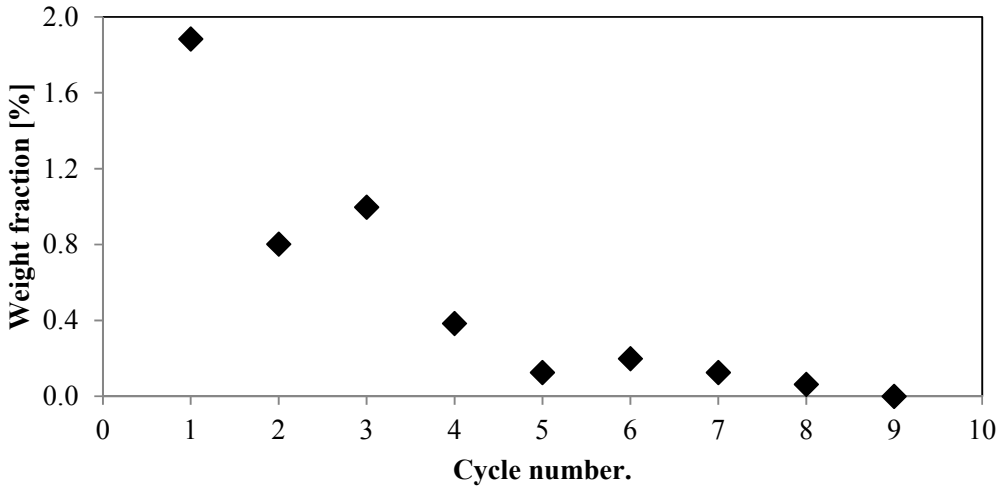

Figure 4-10: Weight fraction [%] of limestone fines collected below the cyclone after respective calcination cycle. The gas velocity was 1.45 m/s and the initial weight of the limestone (particle size range of 0.71-1 mm) was 1 kg.

The initial bed weight was 1 kg, which upon calcination will theoretically reduce to around 560 g. This weight was estimated roughly from the bed average pressure monitored after the first calcination cycle (19 mbar ±2 as 1 mbar = 28.8 g in this reactor). The amount of material collected after the experiment was 388 g. The total fines collected below the cyclone sum up to 45 g. Along with the fines collected

below the cyclone, samples were also taken from the bed for particle analysis to estimate the degree of carbonation. The total amount of sample collected from the bed was 51 g after the calcination cycles and 67 g after the carbonation cycles. The total material balance is summarized in Table 4-4.

Table 4-4: Summary of limestone particle material mass balance in g.

Fresh limestone [g]	Calcined limestone [g]	Fines [g]	*Carbonated samples [g]	Calcined samples [g]	*Final bed material (CO_2) [g]
1008	564	45	67	52	388 (41)

*includes calcium carbonate and calcium oxide

The final bed material retrieved is after the ninth carbonation cycle, and contains both calcium oxide and calcium carbonate. The degree of carbonation was estimated from samples collected after the carbonation cycle. Figure 4-11 shows the degree of conversion of limestone with respect to cycle number. The thermal analysis showed that conversion of the bed decreased from 50% in the first cycle to 23% in the ninth cycle.

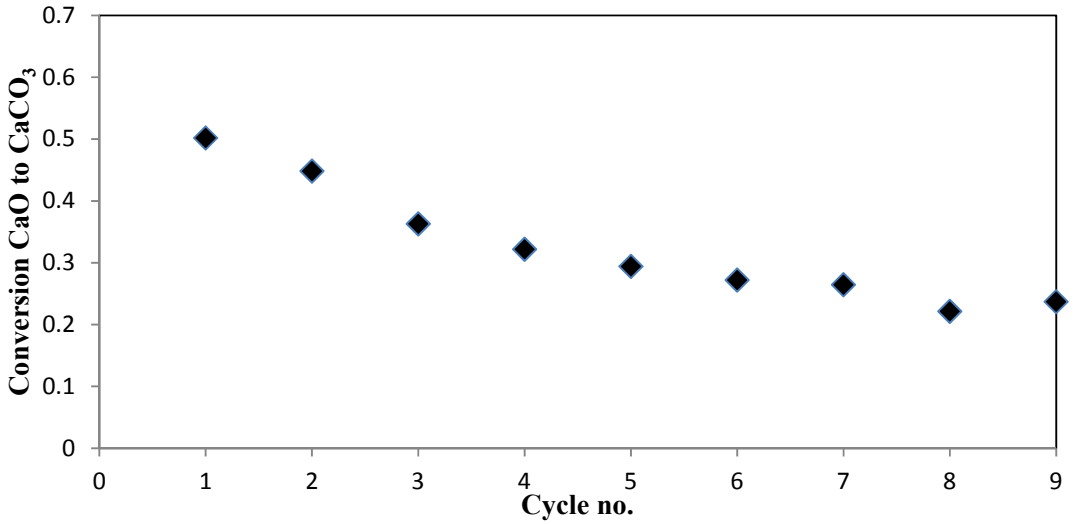

Figure 4-11: Degree of carbonation with respect to cycle number. The flow of gas was 1.3 m/s, the temperature in the bed was 600-640°C and the CO_2 concentration in the inlet was 15 vol.%.

The amount of calcium carbonate in the bed material was 23%, which means that 92 g of the bed material was calcium carbonate. So, the weight of CO_2 capture by the bed was approximately 41 g. According to the material mass balance, the amount of fines elutriated from the system with the exit gas was around 3.6 wt.% based on the initial loading after nine cycles and 6 h of operation.

The weight of the bed after the first and the last calcination was used to estimate the attrition rate constant for the limestone. The final bed weight (341 g) after the ninth calcination cycle was estimated from the average bed pressure (12 mbar±1.5). Since the weight fraction of the fines generated after the ninth calcination cycle was 0, it was assumed that the bed weight would not decrease further due to attrition. Based on this assumption, the attrition rate constant of the limestone was estimated based on the equation (4-12) by Lee et al[149]:

$$\frac{dW}{dt} = -k_a(W - W_{\min}) \qquad 4\text{-}12$$

where $w = 560g$ for the weight of limestone after the first calcination and $w_{\min} = 341g$ after the ninth calcination cycle. So, the attrition rate constant was estimated to be $2.3e^{-5}$ [1/s], which is comparable with the attrition rate constant estimated by Gonzalez et al.[50], which was $1.8e^{-5}$ [1/s] and $5.09e^{-5}$ [1/s] for two different types of limestone used in those experiments.

4.4.4 Influence of Sorbent Inventory

Figure 4-12 shows the influence of the sorbent inventory on the conversion of calcined limestone. The conversion of limestone in the experiment Looping 1 (cycle 1) clearly showed a gradual shift in the conversion rate from the fast to the slow reaction regime, whereas for the sorbent in the experiment Looping 0, where the sorbent inventory was 1 kg, the observed conversion rate was linear. This can be attributed to the sorbent particles that had not reached the maximum conversion limit under the present

carbonation time limit of 10 min. The difference in the exit CO_2 concentration for the two experiments clearly indicates the influence of space time ($n_{Ca,0}/\dot{n}_{CO_2}$), as the inlet CO_2 concentration in the fluidizing gas was the same for both experiments (15 vol.%). The differences between the two experiments are summarized in Table 4-5.

Table 4-5: Summary of differences in the two looping experiments.

Parameter	Looping 0	Looping 1
Sorbent inventory [g-mol]	10	2.5
CO_2 flow rate [g-mol/min]	0.45	0.39
Space time [min]	22.06	6.43

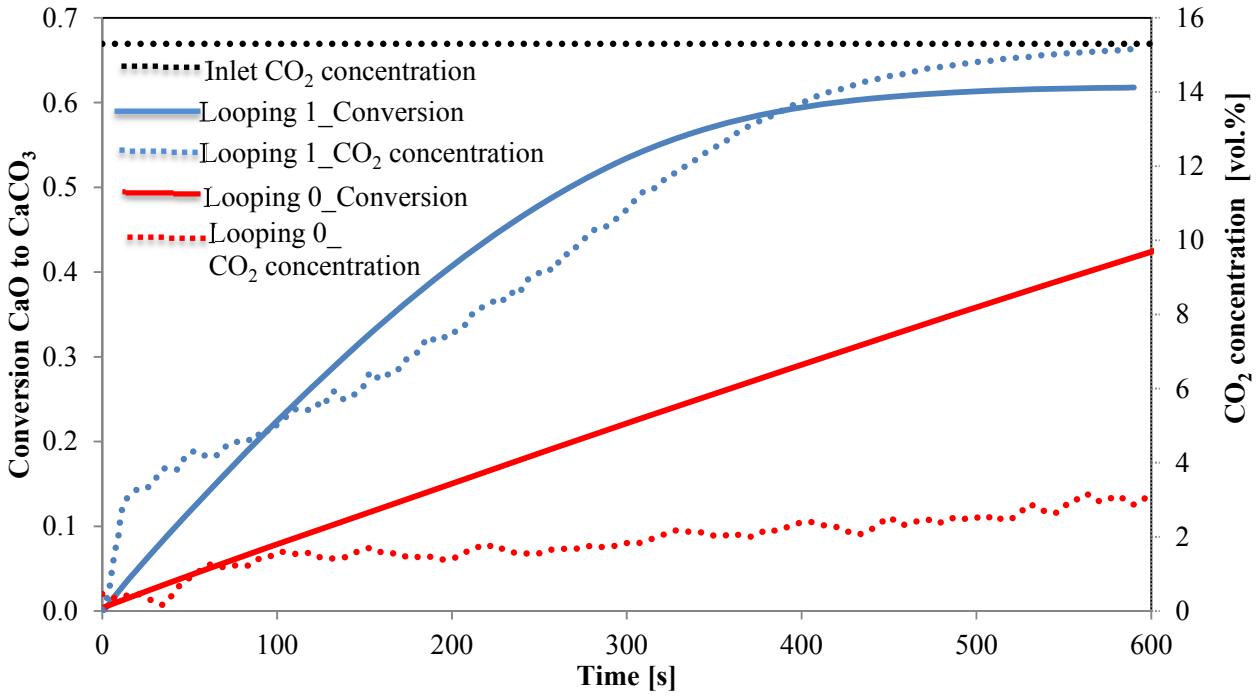

Figure 4-12: Conversion of calcined limestone and concentration of CO_2 in the exit gas for the first cycle and for different sorbent inventories of 1 kg (Looping 0) and 250 g (Looping 1).

The CO_2 concentration in the exit gas with respect to time depends on the sorbent inventory. This difference can be observed in Figure 4-12. Thus, increasing the space time from 6 min to 22 min resulted in higher CO_2 capture efficiency ($Ecarb$) for a longer period (see Figure 4-13) under the present operating conditions.

$$Ecarb = \left(\phi_{CO_2,in} - \phi_{CO_2,out}\right) \Big/ \phi_{CO_2,in} \qquad 4\text{-}13$$

The optimum sorbent inventory in the carbonator is essential both for high CO_2 capture efficiency, but in continuous operation there is another parameter that influences the CO_2 capture efficiency, i.e. the circulation rate of calcined limestone. However, a minimum sorbent inventory is essential for good gas-solid contact in the fluidized bed reactor. So, there has to be a balance between sorbent inventory, CO_2 capture efficiency and residence time of the sorbent in the reactor.

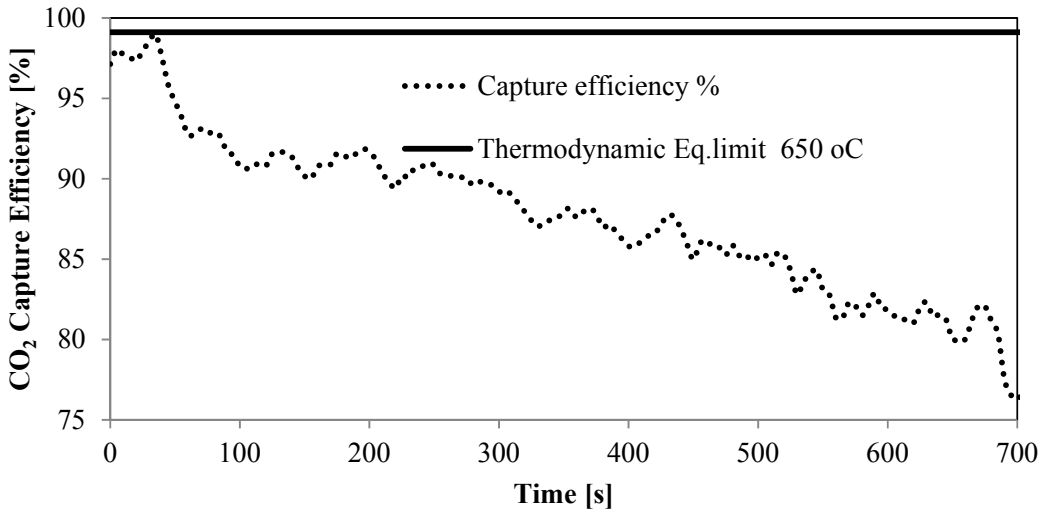

Figure 4-13: CO_2 capture efficiency with respect to time in the first re-carbonation cycle with a sorbent inventory of 1 kg (Looping 0), temperature of 600-650°C and fluidizing gas flow rate of 70 NL/min containing 15.5 vol.% CO_2.

4.4.5 Influence of Carbonation Temperature

The influence of a carbonation temperature above 700°C was investigated in the fluidized bed reactor. The objective of this experiment was to investigate the carbonation behavior at a higher bed temperature compared to the Looping 1 experiment. Figure 4-14 shows the degree of conversion of the limestone bed with respect to time for cycles 1-8. At a higher temperature, the drop in the final degree of conversion was not significant, even for the eighth cycle compared to the first cycle, which was only 10%. Furthermore, the rate of conversion was similar for all cycles.

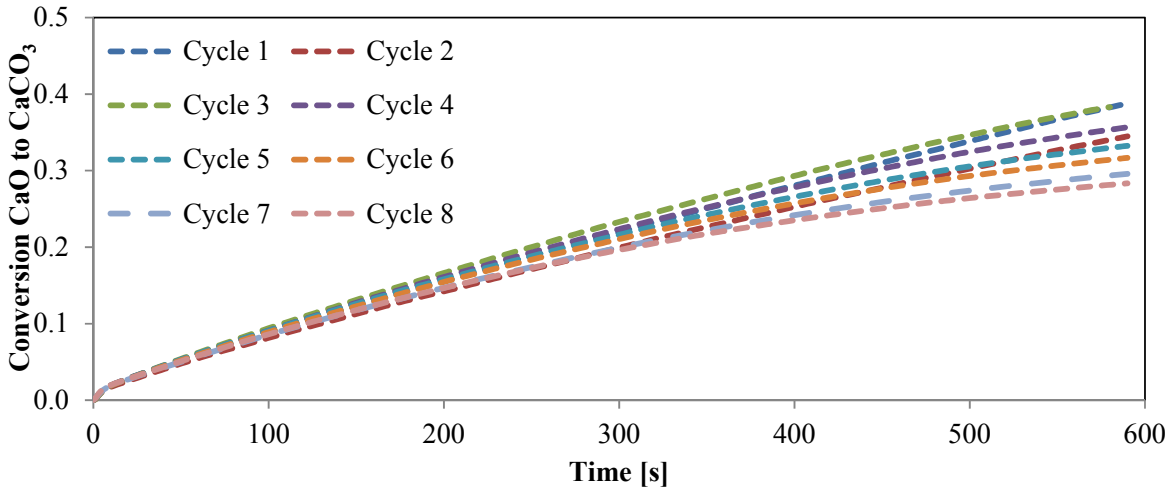

Figure 4-14: Degree of re-carbonation with respect to time for cycles 1-8. Calcination (mild conditions): temperature 650-800°C, under propane combustion (2 NL/min) in air, gas flow rate of 60 NL/min. Carbonation: 15 vol.% CO_2 in air, temperature 700-730°C.

Comparing the degree of carbonation with respect to time for carbonation at these two temperatures, the difference in the rate of conversion can be seen from Figure 4-15. Carbonation at the lower temperature had a faster rate in the beginning and shifted to a slower rate, but with carbonation at the higher temperature, there was no significant change in the rate of conversion. The lower rate of

conversion at the higher carbonation temperature was due to a rise in the equilibrium partial pressure of CO_2, which reduced the rate of the reaction.

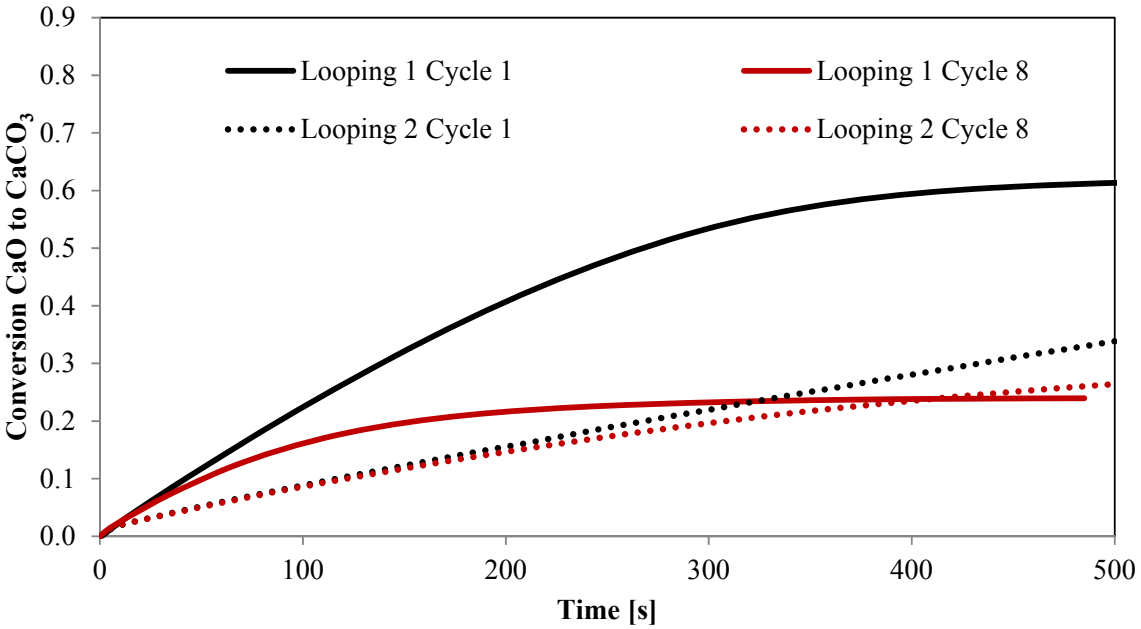

Figure 4-15: Degree of carbonation with respect to time for cycles 1 and 8; for reference see case (looping 1) and for the experiment where carbonation was performed at 700°C (looping 2). Calcination (mild conditions): temperature 650-800°C, under propane combustion (2 NL/min) in air, gas flow rate of 60 NL/min.

The linear rate of conversion at the higher temperature was due to the fraction of active calcined limestone compared to the reference experiment. The shift in the reaction rate might become significant when the conversion of sorbent particles approaches the ultimate conversion limit. So, if the reaction had continued for a longer period of time, then it might be possible to see the shift in the reaction rate.

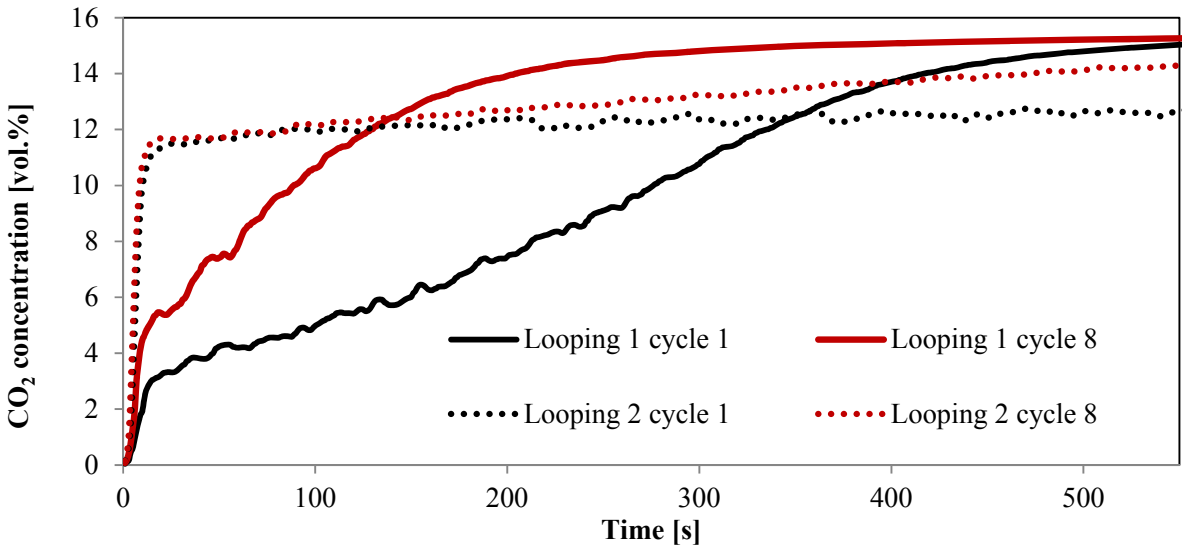

Figure 4-16: CO_2 concentration in the exit gas for two different experiments, looping 1 (reference) with a carbonation temperature of 600-650°C and looping 2 with a carbonation temperature of 700-730°C.

The significant difference in the observed rate of conversion can be attributed to: 1) the equilibrium concentration of CO_2 varied from 2.7 to 5.1% as the temperature changed from 700°C to 730°C during this experiment compared to 0.2 to 0.8% during the experiments in the reference case. Figure 4-16 shows that the exit CO_2 concentration in the looping 2 experiment had a linear change in the concentration, barring the initial period, whereas for the looping 1 experiment, the CO_2 concentration profile had an S-shaped profile, with gradual rise in the concentration with time, which increased at a faster rate once the conversion of the particles reached the maximum conversion limit. So, the optimum temperature in the reactor should be below 650°C to attain higher capture efficiencies for a longer period of time.

4.4.6 Influence of Clay on the Degree of Carbonation

In this experiment, 75 g of sandy clay was added to 250 g of limestone to keep the initial number of moles of limestone equal to that in the Looping 1 experiment. Figure 4-17 shows the degree of

carbonation of calcined limestone with respect to time for the experiment Looping 1 compared to Looping 4 (limestone mixed with sandy clay).

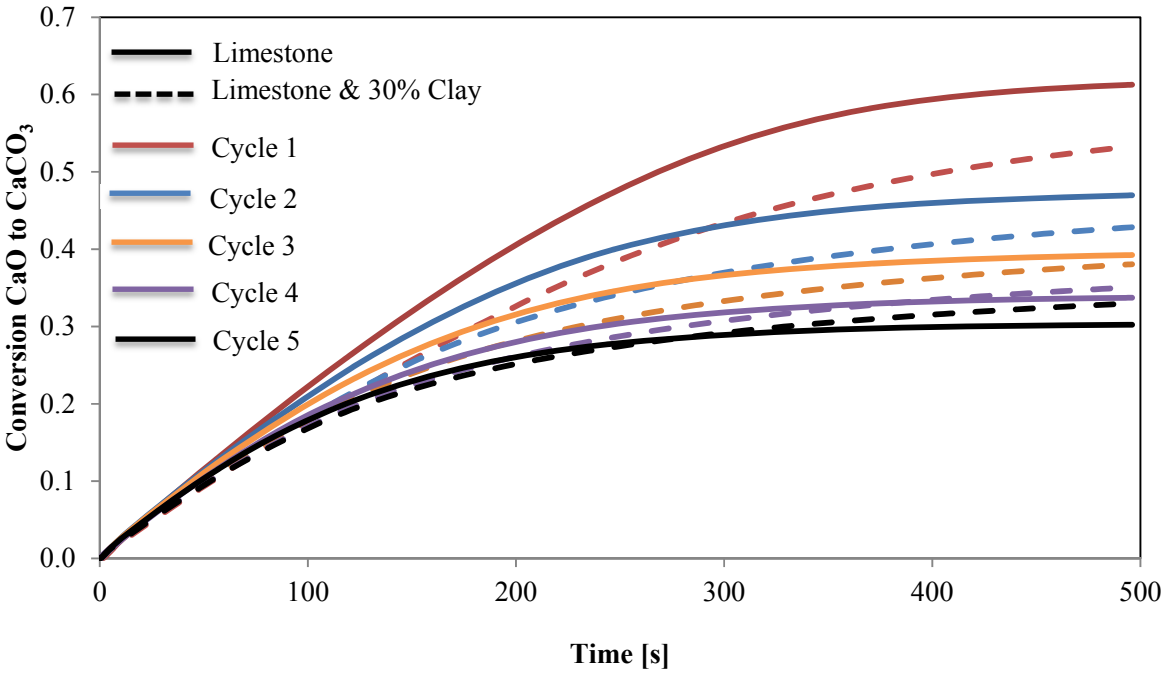

Figure 4-17: Comparison of degree of carbonation with respect to time for cycles 1-5 for limestone in the reference case and a mixture of 30% clay in limestone. Calcination (mild conditions): temperature 650-800°C, under propane combustion (2 NL/min) in air, gas flow rate 60 NL/min. Carbonation: 15 vol.% CO_2 in air, temperature 600-650°C.

There was no difference in the trend of carbonation with respect to time and cycle number. Under the present operating conditions, there were no major differences between limestone and limestone mixed with clay. Similar results were also obtained from the cyclic experiments from the TGA apparatus under mild calcination conditions. However, under realistic conditions, there was significant difference in the CO_2 capture capacity of the limestone.

4.4.7 Simultaneous SO_2 and CO_2 Capture

The effect of SO_2 on the CO_2 capture capacity of limestone is another important factor in the carbonate looping process because SO_2 is also captured by the limestone under carbonate looping conditions. So, experiments were performed to investigate the influence of simultaneous SO_2 and CO_2 capture during carbonation. In this experiment, SO_2 gas (30 mL/min) was injected into the fluidizing gas [500 ppmv] only during the carbonation stage. Figure 4-18 shows the conversion of CaO to $CaCO_3$ and the conversion of SO_2 gas (capture of SO_2) during the carbonation cycle.

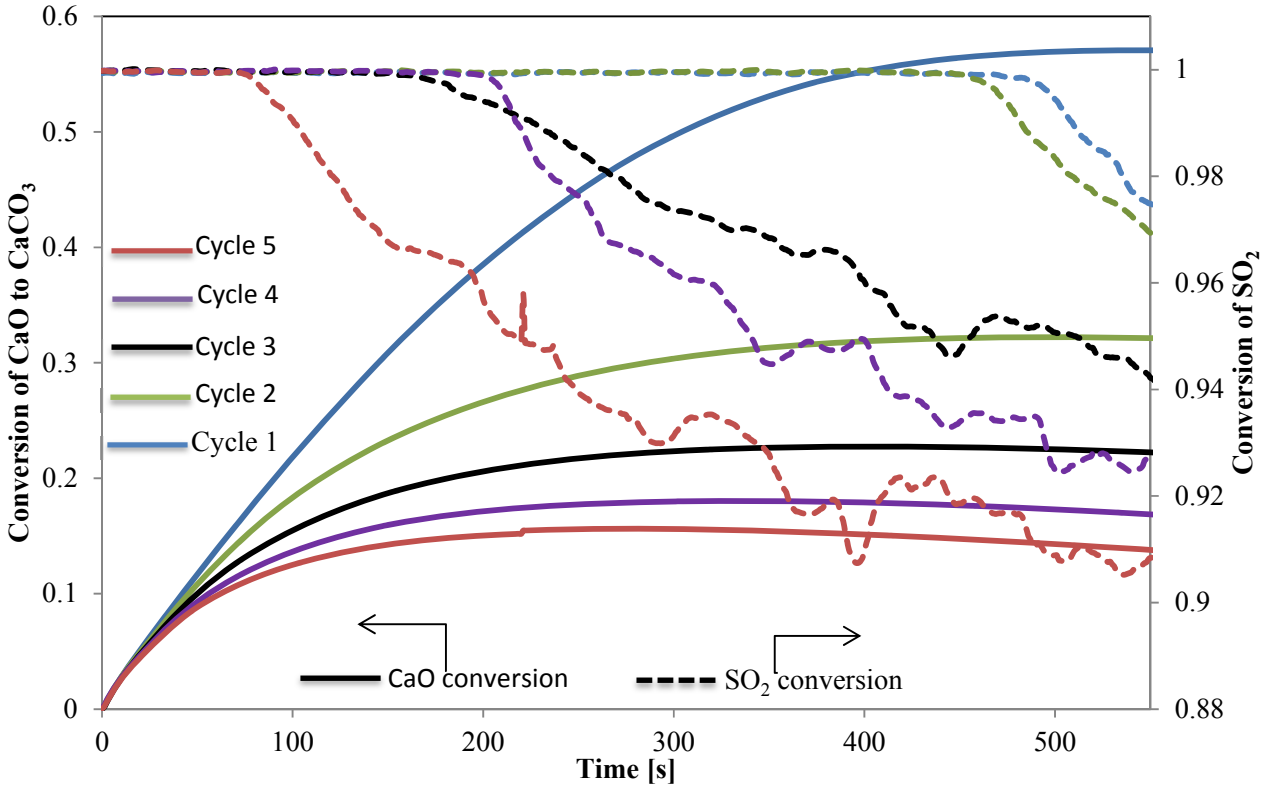

Figure 4-18: Degree of carbonation with respect to time for cycles 1-5, during the simultaneous re-carbonation and sulfation of lime.

Due to the high space time ($n_{Ca,0}/\dot{n}_{SO_2} = 1950$), complete conversion of SO_2 gas was observed at 500 s in the first carbonation cycle. In the subsequent cycles, the conversion of SO_2 dropped quickly compared to the earlier cycles. This phenomenon is due to the retention of SO_2 in the limestone, which accumulates from cycle to cycle, thereby lowering the CO_2 capture capacity from cycle to cycle. The presence of SO_2 had no significant effect on the CO_2 capture capacity of limestone in the first cycle. An important factor that can be observed with simultaneous capture is the release of CO_2 from $CaCO_3$ occurred after a certain time, and this effect was more pronounced with increasing cycle number. The negative conversion of CaO to $CaCO_3$ was due to direct sulfation according to the reaction:

$$CaCO_3 + SO_2 + 0.5O_2 \rightarrow CaSO_4 + CO_2 \qquad \text{4-14}$$

and with indirect sulfation of calcined limestone at the beginning of the cycle according to the reaction:

$$CaO + SO_2 + 0.5O_2 \rightarrow CaSO_4 \qquad \text{4-15}$$

So, the concentration of CO_2 in the exit gas increased due to the release of CO_2 by direct sulfation.

If the spent sorbent is continuously replaced by the fresh limestone, then it is possible to capture both SO_2 and CO_2 from the flue gas.

4.5 Modeling of the Carbonator in the Bubbling Fluidized Bed Reactor

The main objective of the fluidized bed reactor model is to describe the cyclic experimental results in the fluidized bed reactor and to investigate the parameters which cannot be studied in the small TGA apparatus, such as bed inventory and the time required for CO_2 breakthrough. The Kunii-Levenspiel model[122] was adapted to describe the experimental conditions. The model was formulated to describe the transient conversion of calcined limestone in the bed and the CO_2 concentration profile along the height of the bed. The critical information necessary to predict the experimental results are the conversion of limestone particles and the gas-solid contact pattern in the reactor.

4.5.1 Particle Conversion

The conversion of limestone is defined by the reaction rate term, which is assumed to be first order with respect to CO_2 concentration. The carbonation reaction at the surface of the particle is described by the semi-empirical equation based on the spherical grain model[79]:

$$\frac{dX}{dt} = k_x (1-X)^{2/3} \left(C_{CO_2} - C_{CO_2,eq}\right) \quad \text{4-16}$$

where $k_x \left[\frac{m^3}{mol \cdot s}\right]$ is the effective rate constant. This equation is slightly modified to represent the carbonation of limestone under the fast reaction regime for each cycle as:

$$\frac{dX_N}{dt} = k_f \left(1 - \frac{X}{X_{\max,N}}\right)^{2/3} \left(C_{CO_2} - C_{CO_2,eq}\right) \quad \text{4-17}$$

under each cycle where $X_{\max,N}$ is the maximum conversion attained by calcined limestone particles in the fast reaction regime of the carbonation cycle "N", $k_f \left[\frac{m^3}{mol \cdot s}\right]$ is the function of surface area $s_o \left[\frac{m^2}{m^3}\right]$ and initial porosity e_o of particles and the surface rate constant $k_s \left[\frac{m^4}{mol \cdot s}\right]$, given by the equation:

$$k_f = \frac{k_s s_o}{(1-e_o)} \quad \text{4-18}$$

$$k_s = k_{so} e^{(-E_{ak}/RT)} \quad \text{4-19}$$

$E_{ak}\left[\frac{kJ}{mol}\right]$ is the activation energy and $k_{so}\left[\frac{m^4}{mol \cdot s}\right]$ is the pre-exponential constant. The activation energy in the kinetically controlled regime was reported to be zero by Bhatia and Perlmutter[79], whereas Kyaw et al[150] estimated the value to be 78 kJ/mol. Grasa et al.[82] and Sun et al.[33] estimated the activation energy around 20 and 29 kJ/mol, respectively. The reason for the difference activation in energies might be because of the limestone structure, which is influenced by the limestone composition and calcination conditions. For any reaction to occur, there are two barriers: the first one is chemical energy and the second one is mechanical energy related to structure, which might also have a significant effect as observed by the difference in activation energies for different limestones[33]. The reaction rate constant estimated from the TGA and the fluidized bed reactor k_f is 2-3.5$\left[\frac{m^3}{kmol \cdot s}\right]$. The rate constant estimated by Bhatia and Perlmutter[79] and Grasa et al.[82] is based on the surface area of the particle, which depends on the calcination conditions. Converting the kinetic surface rate constant estimated by Grasa et al.[82], $k_s = 0.559e-5\left[m^4/kmol \cdot s\right]$ to $k_f = 27\left[m^3/kmol \cdot s\right]$, using the given surface area of the particle per unit volume at 650°C, the estimated rate constant is one order of magnitude higher compared to the estimated value for the limestone used in the TGA and fluidized bed reactor. The main factor that contributes to this difference is the surface area of the particle per unit volume or the activation energy for the type of limestone used. Since the surface area of the calcined limestone varies with calcination conditions, it is not easy to compare reaction rate constants. Figure 4-19 shows the conversion profile of calcined limestone using equation 4-17 with the experimentally determined rate constant compared with experimental conversion.

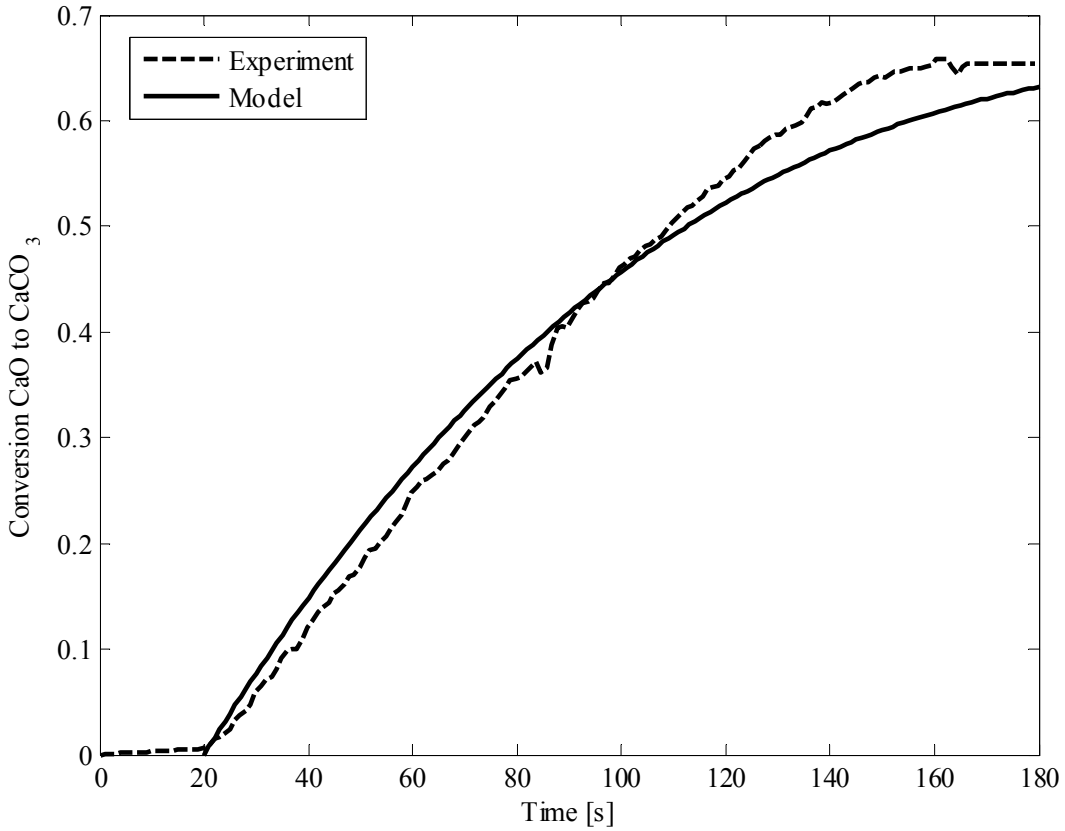

Figure 4-19: Carbonation of limestone calcined under mild calcination conditions with respect to time in a TGA apparatus: the dashed line is the experimental conversion and the solid line is the predicted conversion applying equation 4-17.

The maximum conversion of calcined limestone particles is given by:

$$X_{\max,N} = \frac{1}{\left(\frac{1}{1-X_r}\right) + k \cdot N} + X_r \qquad 4\text{-}20$$

where $X_r = 0.13$ is the residual conversion of limestone and $k = 0.9$ is the decay constant. Cyclic experimental results were used to determine these parameters.

4.5.2 Flow Profile in a Bubbling Fluidized Bed Reactor

The bubbling fluidized bed carbonator reactor model was adapted from the general model defined by Kunii and Levenspiel. The fluidizing gas entering the bed is considered to split into two phases: 1) an emulsion and 2) a bubble phase. The flow of gas through the bed is assumed to be in plug flow and the bed material is assumed to be well-mixed.

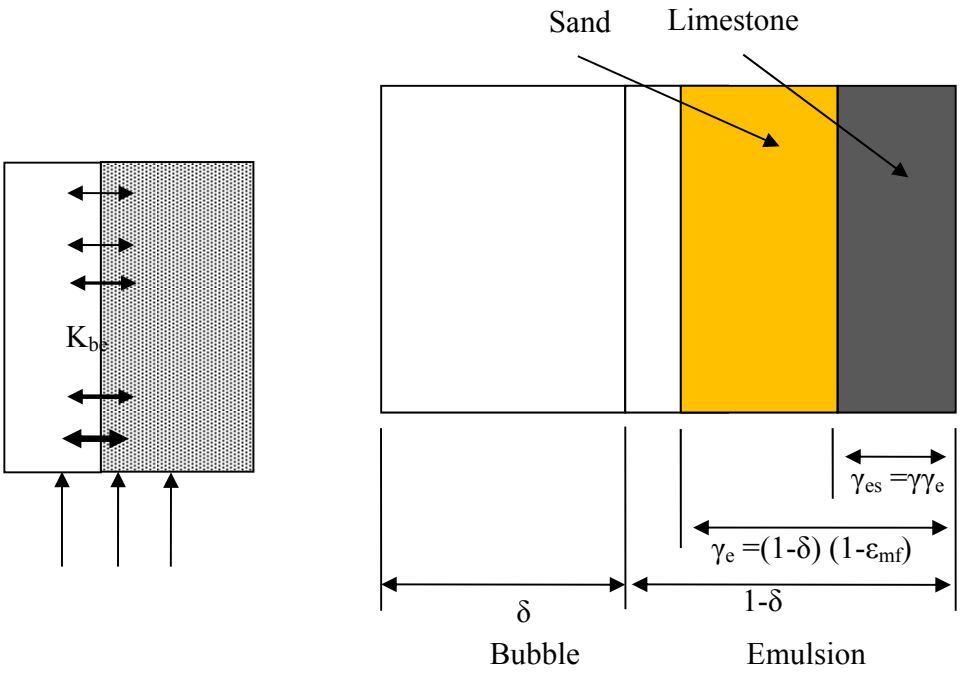

Figure 4-20: Gas flow pattern in the bubbling fluidized bed reactor with intermediate sized particles.

The emulsion region is assumed to be under minimum fluidization conditions, meaning that the void fraction in the emulsion phase is equivalent to the conditions at the minimum fluidization velocity. CO_2 gas in the emulsion phase reacts with calcined limestone particles along the length of the bed. In the emulsion region, particles are considered to be well-mixed. Further CO_2 gas transfer from bubbles to the emulsion is defined as a function of the gas concentration in the bubble region where the gas is

assumed to flow as a plug flow. The bubble fraction in the bed is defined by the following equation for intermediate sized particles[151] :

$$\delta = \frac{u_o - u_{mf}}{u_o + \frac{5u_o - u_b\varepsilon_{mf}}{4}} \quad for\ 1 < \frac{u_b\varepsilon_{mf}}{u_{mf}} < 5 \qquad \text{4-21}$$

The fraction of the emulsion region in the bed is $(1-\delta)$, further assuming that the minimum fluidization condition in the bubble region void fraction of the bed is ε_{mf}. Thus, the fraction of particles in the emulsion region is $\gamma_e = (1-\varepsilon_{mf})\cdot(1-\delta)$. The fraction of bed material in the bubble region is assumed to be negligible. In the bubbling fluidized bed reactor experiments, the bed consisted of both sand and limestone particles. So, the fraction of limestone particles in the bubble and emulsion region depended on the weight fraction of the limestone particles in the bed. The initial weight of the bed was 1 kg, of which 750 g was sand the rest was 250 g of limestone particles. The initial weight fraction of the sorbent (calcined limestone) in the bed was $\gamma = 0.25$.

So, the estimated fraction of sorbent in the emulsion region, considering a uniform distribution of sand and sorbent, in this case is given by:

$$\gamma_{es} = \gamma \cdot \gamma_e \qquad \text{4-22}$$

The transfer of gas from bubbles to the emulsion given by[122]:

$$K_{be} = 4.5\left(\frac{u_{mf}}{d_b}\right) \qquad \text{4-23}$$

The transfer of gas from the emulsion to bubbles or vice versa depends on the concentration difference between these two phases, i.e. $(C_b - C_e)$. So, finally, the mass balance for CO_2 gas along the length of the reactor in the bubble and emulsion phases is:

In bubble: disappearance in bubble = transfer to emulsion

In emulsion: disappearance in emulsion = reaction in emulsion + transfer to bubble

$$\frac{dC_b}{dz} = \frac{-K_{be}(C_b - C_e)}{u_b^*} \qquad \text{4-24}$$

$$\frac{dC_e}{dz} = \frac{\left(-(1-\delta)(1-\varepsilon_{mf}) f_a \gamma_{es} K_r (C_e - C_{eq}) + \delta K_{be}(C_b - C_e)\right)}{(1-\delta)u_{mf}} \qquad \text{4-25}$$

The velocity of bubble gas depends on the flow rate of fluidizing gas and is defined by:

$$u_b^* = \frac{u_o - (1-\delta)u_{mf}}{\delta} \qquad \text{4-26}$$

The rate of reaction in the fluidized bed reactor is obtained according to the equation to measure the molar volume of CO_2 captured per molar volume of calcium oxide:

$$K_r = k_f \left(1 - \frac{X}{X_{\max,N}}\right)^{2/3} \frac{\rho_{CaO}}{M_{CaO}} \qquad \text{4-27}$$

In order to describe the transient behavior, the conversion of the bed has to be considered with respect to time. This will result in a change in the exit concentration of CO_2 and the concentration profile along the height of the bed with respect to time. The transient behavior is taken into account by discretizing the model over time. The discretization time step is estimated by dividing the height of the bed by the gas velocity. The model is solved for each time step by guessing the limestone conversion and estimating the CO_2 capture, which is used for calculating back the limestone conversion using the iterative code developed in Matlab. The sequence of steps carried out in the program to predict the

experimental result is presented in the flow sheet. In order to solve the model, the initial conversion of the bed was estimated and used to estimate the average reaction rate of the bed. This average reaction rate was used to estimate the CO_2 concentration along the height of the reactor. The number of moles of CO_2 captured was estimated based on the exit CO_2 concentration. Since the number of moles of CO_2 captured must be equal to the number of moles of converted limestone, the average conversion of the bed was calculated again. This value was compared with the initial estimated value, and if the absolute difference in error was less than 0.0007, then the solutions converged. If the error was higher than the given criteria, then a new estimated value was provided and the procedure was repeated. The concentration of CO_2 at the exit of the bubbling bed was obtained by adding the concentration estimated from each phase. Table **4-6** lists model parameters used for the simulaion.

$$C_{CO_{2\_exit}} = \delta C_{b,exit} + (1-\delta) C_{e,exit} \qquad \textbf{4-28}$$

The volume of fraction of CO_2 in the exit gas was estimated according to:

$$x_{CO_2} = C_{CO_{2,exit}} \left(\frac{RT}{P} \right) \qquad \textbf{4-29}$$

The fraction of CO_2 captured in the carbonator was estimated based on the volume fraction at the inlet and outlet gas streams:

$$X_{CO_2} = \frac{\phi_{g,in} x_{CO_2,in} - \phi_{CO_2,out}}{\phi_{g,in} x_{CO_2,in}} \qquad \textbf{4-30}$$

In this equation, the flow rate of CO_2 in the exit gas was determined according to:

$$\phi_{CO_2,out} = \frac{\phi_{g,in}(1 - x_{CO_2,in}) x_{CO_2,exit}}{(1 - x_{CO_2,exit})} \qquad \textbf{4-31}$$

The change in the average conversion of the bed is given as:

$$X(t) = \frac{\sum_{t=1}^{t=t_{end}} \phi_{CO_2,in} C_{CO_2,in} - \phi_{CO_2,out(t)} C_{CO_2,out(t)}}{n_{CaO,0}} \quad \text{4-32}$$

Table 4-6: Values of different parameters used in the model.

Parameter	Value	units
d_p	800	mm
u_{mf}	0.14	m/s
K_{be}	11.04	1/s
δ	0.64	-
u_b^*	1.09	m/s
γ	0.25,1[a]	-
d_b	0.06	m

[a]total bed material is limestone

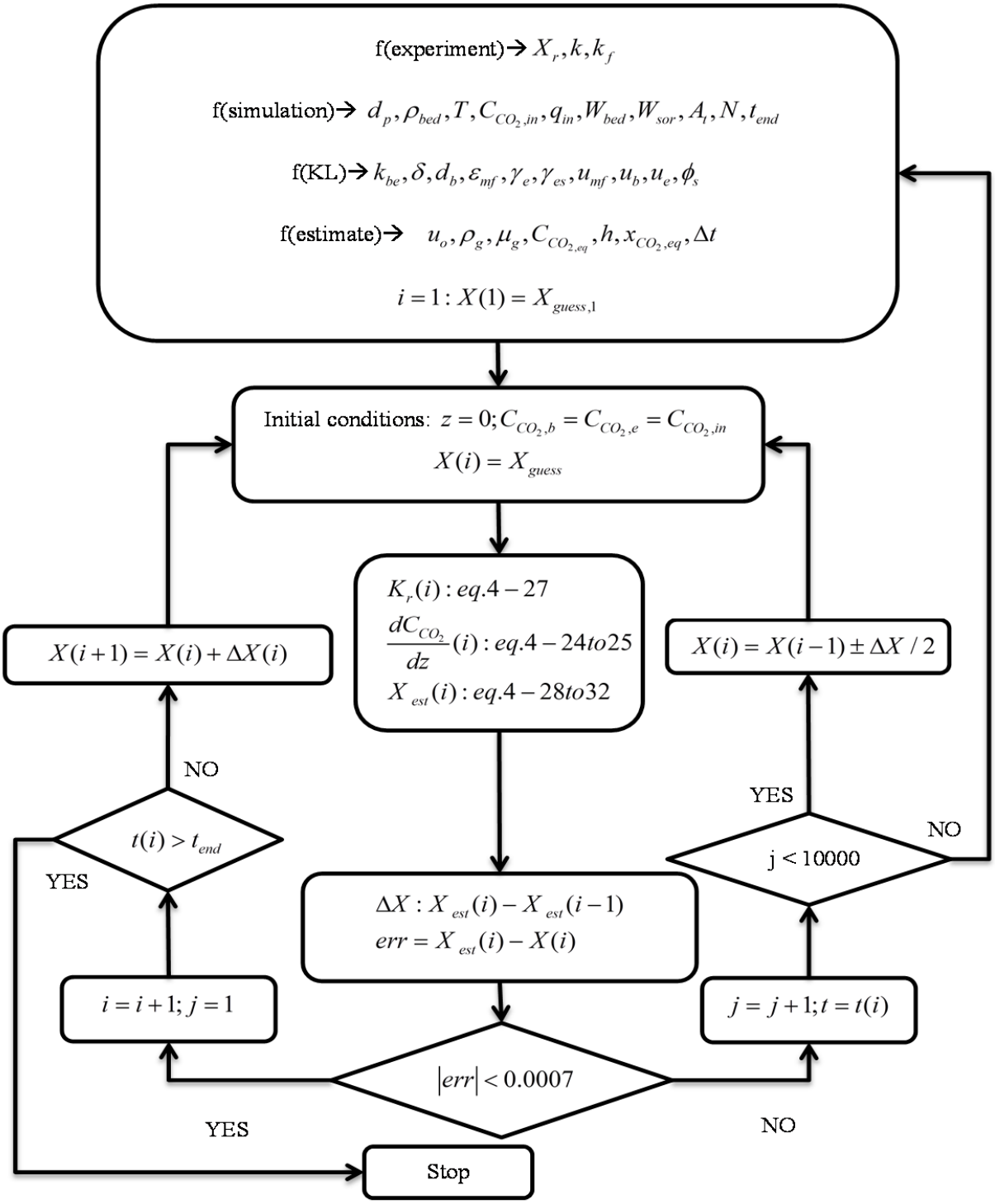

Figure 4-21: Flow sheet for the sequence of calculations used to solve the proposed model.

4.5.3 Model Validation

In Figure 4-22, the conversion of calcined limestone in the bed predicted by the model was compared with the reference experiment for cycles 1 and 10. The model predicted fairly well the conversion of calcined limestone in the bed for the first cycle and the tenth cycle.

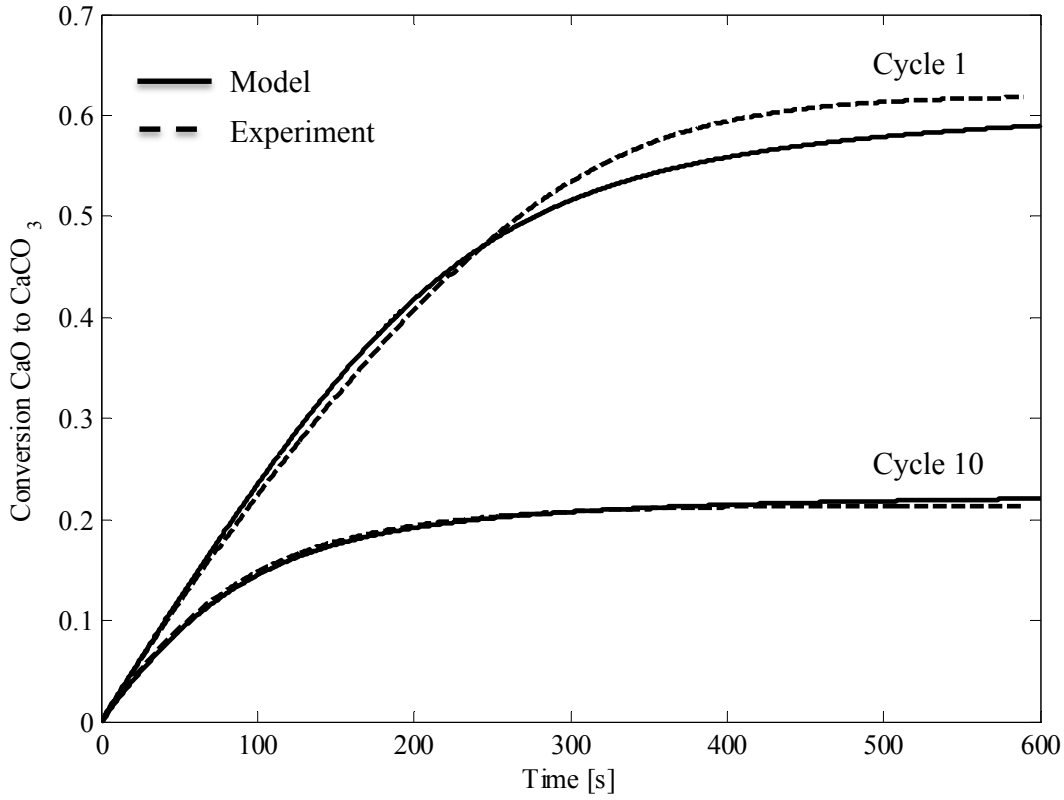

Figure 4-22: Comparing the conversion of calcined limestone in the bed for the first cycle and the tenth cycle with the model predicted results.

Similarly, the concentration of CO_2 in the exit gas from the experiment was compared with the model predicted CO_2 concentration in Figure 4-23. There were some deviations in the predicted values which are reasonable based on the simplification assumed to solve the model. The CO_2 concentration in the

exit gas showed a sharp increase in the beginning, which corresponds to the equilibrium concentration of CO_2 gas and gas escaped the bed in the form of bubbles without interacting with the calcined limestone in the bed. The rise in the CO_2 concentration in the exit gas from the initial level was due to the change in active fraction of calcium oxide available for CO_2 capture until the exit concentration of CO_2 gas was equal to the inlet concentration.

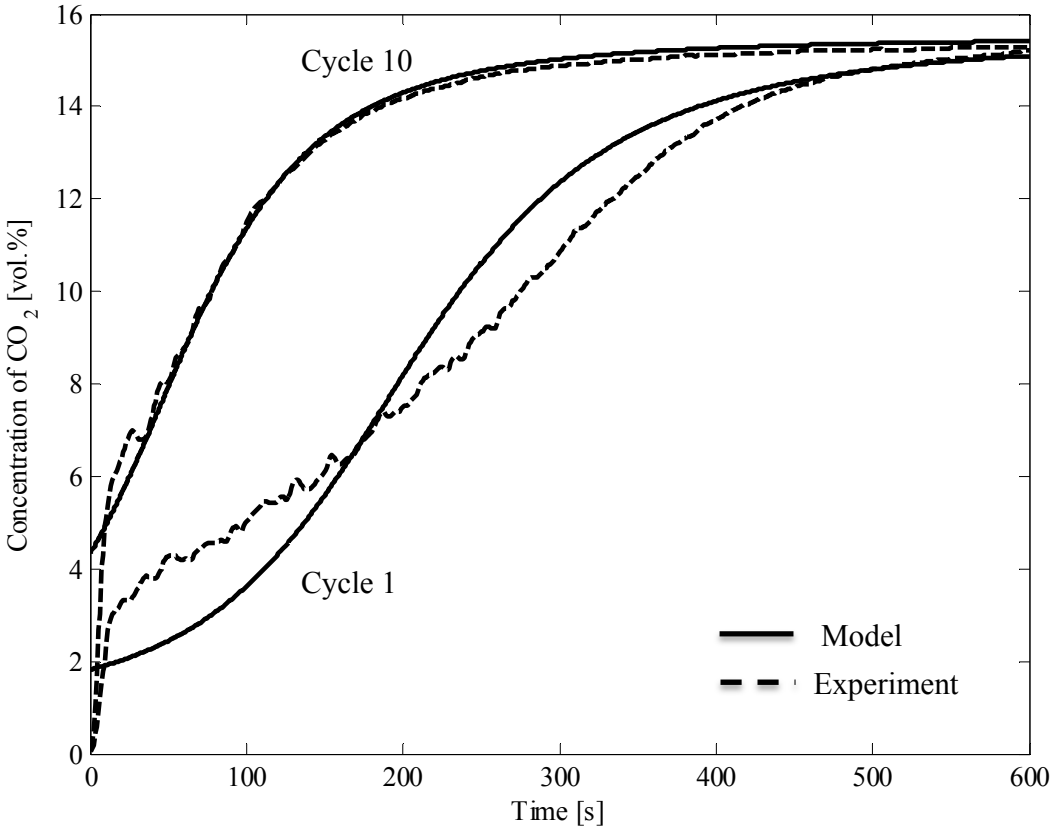

Figure 4-23: Comparing CO_2 concentration in the exit gas with respect to time for the first cycle and the tenth cycle with the model predicted results.

In the fluidized bed reactor, the concentration of CO_2 at the fluidizing gas inlet was equal to the inlet concentration. The change in the concentration of CO_2 along the height of reactor changed over time

and with the conversion of the bed. Figure 4-24 shows the model predicted results for the CO_2 concentration profile along the height of the bed with respect to time. At the bottom of the bed, the concentration of CO_2 dropped sharply along the height of the reactor in the beginning of the reaction, but the drop in the CO_2 concentration decreased with time, as expected. So, for a low CO_2 concentration in the exit gas, fresh calcined limestone has to continuously replace the partially carbonated limestone in the bed.

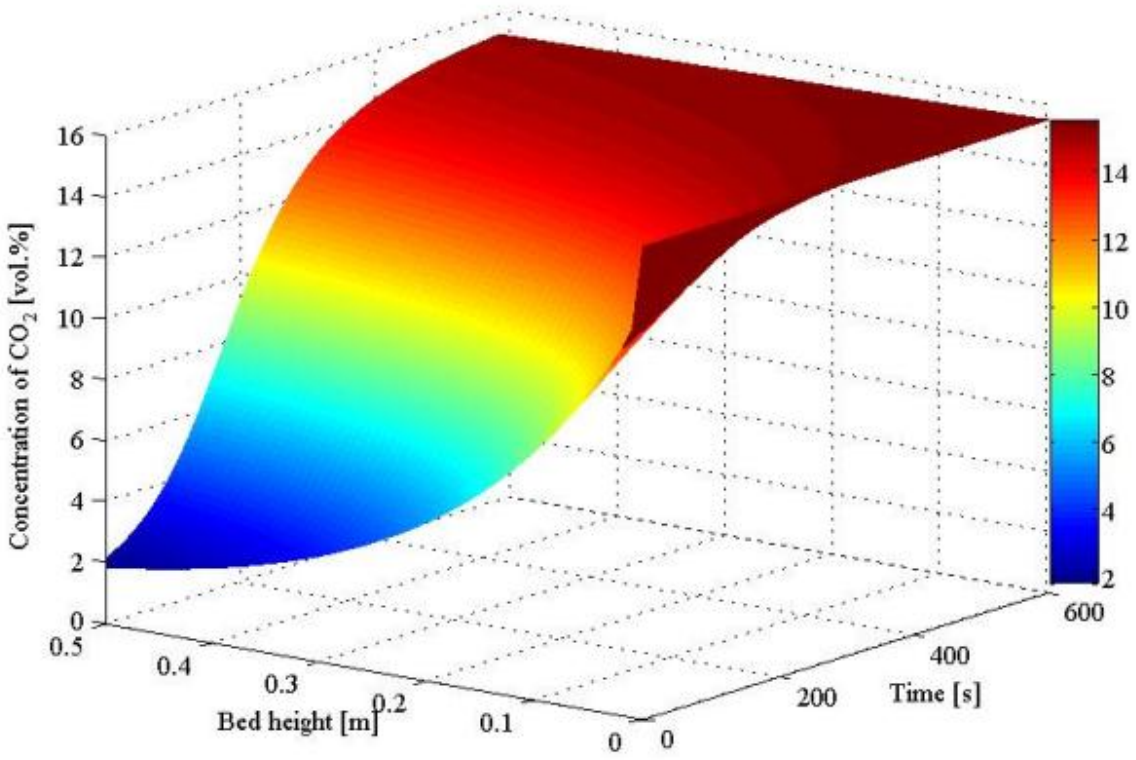

Figure 4-24: CO_2 concentration along the height of the reactor as a function of time for the first carbonation cycle.

4.5.4 Influence of Sorbent Inventory

The sorbent inventory is an important operating parameter. Cycle experiments were carried out with 1 kg and 250 g of limestone. The main difference observed was the concentration of CO_2 in the exit gas (see Figure 4-12). The bubbling fluidized bed reactor model was simulated with different fractions of limestone and sand to investigate its influence on the exit CO_2 concentration. The results show the exit CO_2 concentration not only depends on the calcined limestone conversion but also on the sorbent inventory. For 50% conversion of the calcined limestone, the concentration of CO_2 was 9 vol.%, 4.5 vol.% and 1 vol.% for a limestone inventory of 100 g, 250 g and 1000 g, respectively, as observed in Figure 4-25.

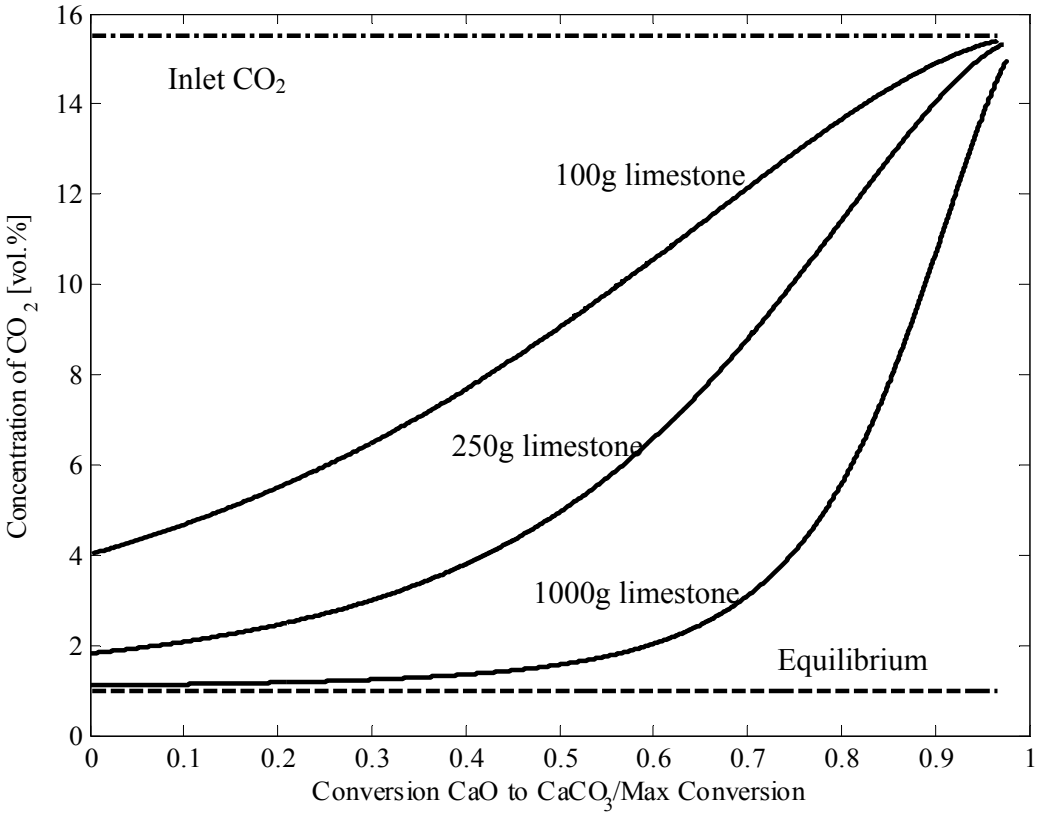

Figure 4-25: CO_2 concentration in the exit gas with respect of different conversions for different sorbent inventories in the bubbling fluidized bed model.

4.5.5 Sensitivity Analysis of the Model

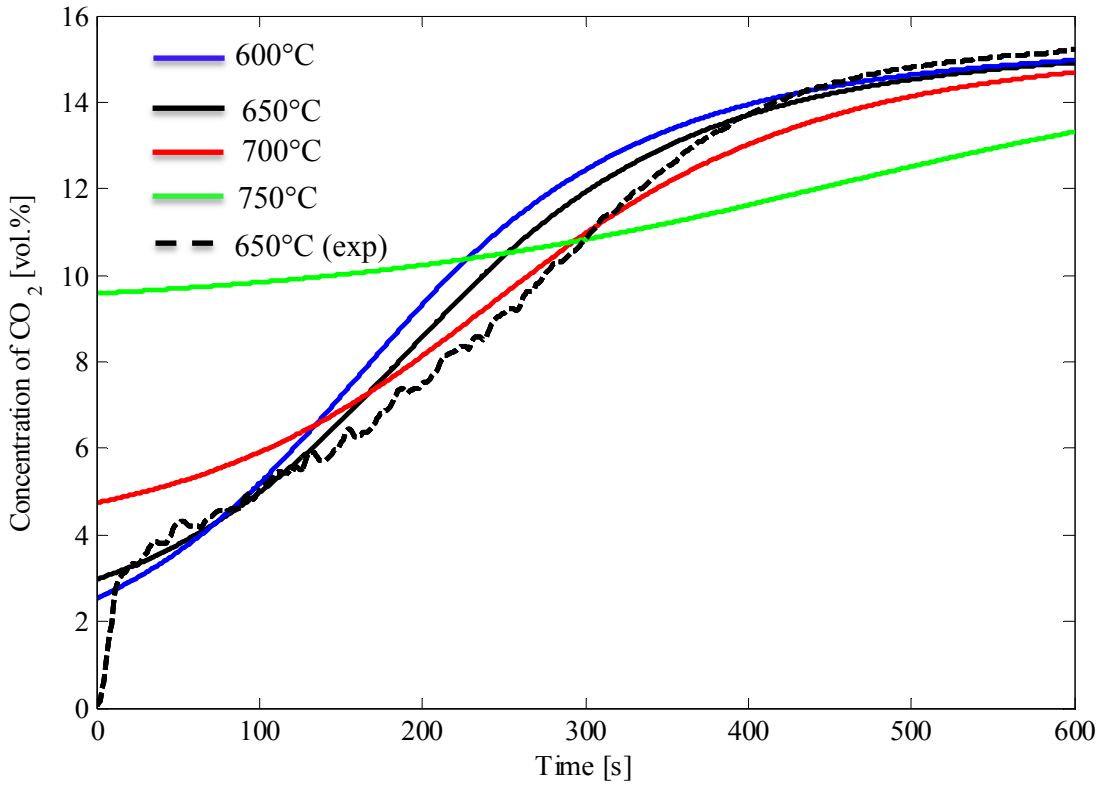

Figure 4-26: Sensitivity of bed temperature on the exit CO_2 concentration evaluated for temperatures of 600°C-750°C; the inlet CO_2 concentration was 15.5 vol.%, and the weight of limestone in the bed was 250g.

The model was simulated by varying parameters and the exit CO_2 concentration was compared with the experimental results. The sensitivity of the bed temperature was investigated by simulating the model for different temperatures, i.e. 600-750°C, which is important to control the bed temperature as the energy released from the exothermic reaction should be extracted. Figure 4-26 shows the model predicted results, and a temperature below 700°C is important for high capture efficiency. The CO_2 concentration in the exit gas matched with the simulation results at 600/650°C in the initial period, in the intermediate period it was closer to the CO_2 concentration predicted at 700°C and in the lower end,

the temperature results were close to the experimental results. The observed deviation in the model and experiment results might be due the change in the temperature profile in the bed during the carbonation period.

The influence of gas-transfer between the bubble and emulsion phase was evaluated by varying the transfer co-efficient: 5.7 to 22.8 [1/s]. The results presented in Figure 4-27 indicate that the sensitivity of the gas transfer co-efficient was very high in the beginning when the conversion of the bed was very low, which resulted in a large difference in the CO_2 concentration. The sensitivity of this parameter decreased as the active fraction in the bed decreased over time.

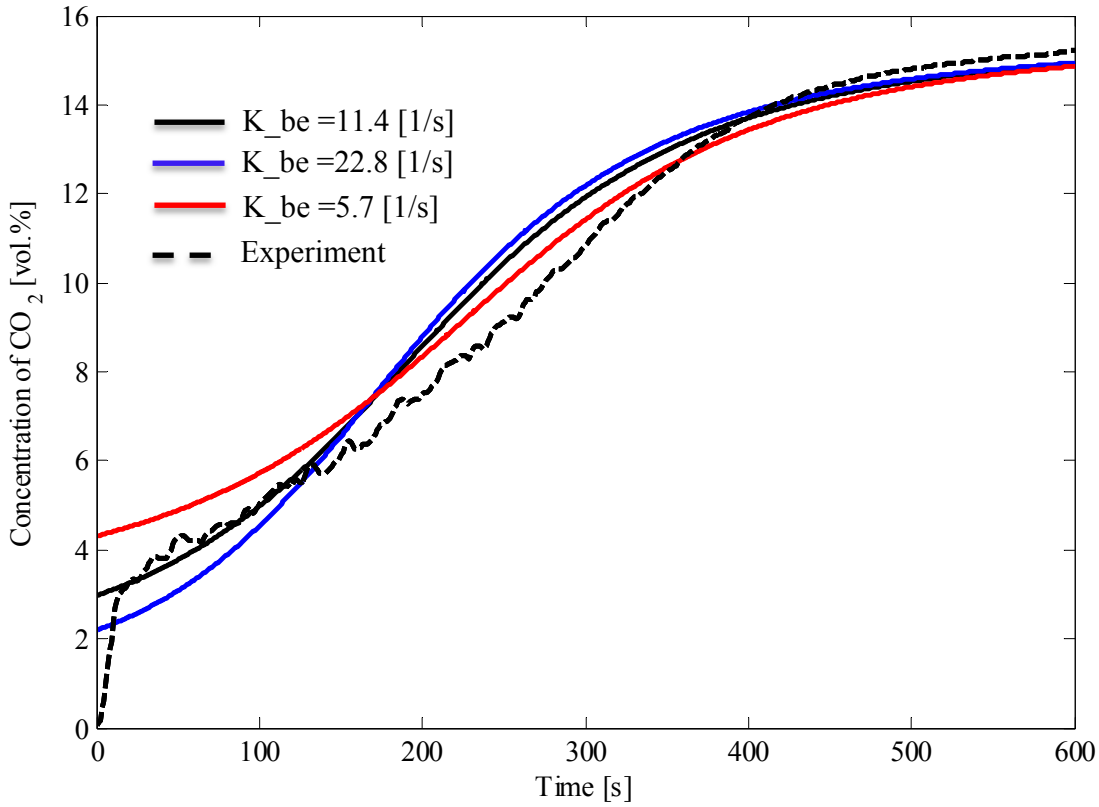

Figure 4-27: Sensitivity of gas transfer between bubbles and the emulsion evaluated for three values: the reference gas–transfer (11.4 [1/s]) was taken from the literature, along with double the reference value and half of the reference value.

The bubble fraction in the bed is another parameter for which the sensitivity was investigated as this parameter is difficult to study experimentally. The value was estimated based on the literature correlation equation and sensitivity was investigated by varying the estimated parameter by ± 20%. Figure 4-28 presents the results for the three values; a lower bubble fraction in the bed resulted in high CO_2 capture efficiency when the bed had a high active fraction and dropped sharply with to a lower capture efficiency due to high bed conversion. However, the value estimated from the literature better fits the experimental results compared to the other two values.

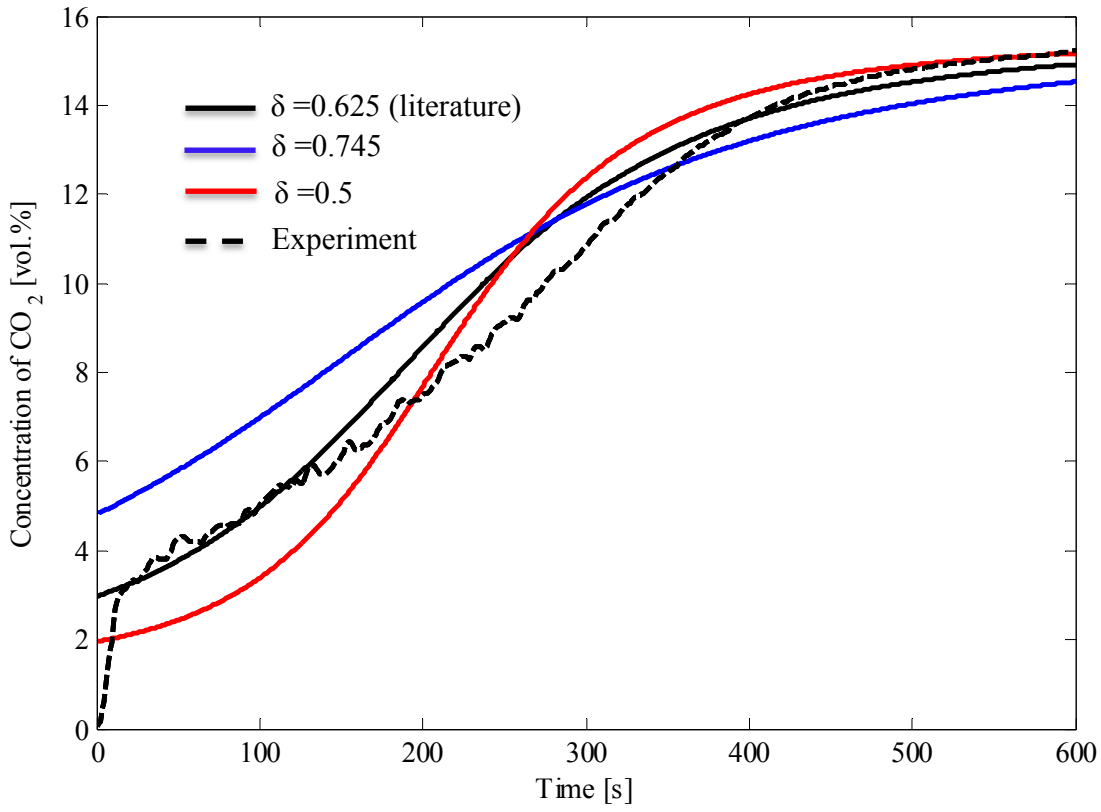

Figure 4-28: Sensitivity of the bubble fraction on the exit CO_2 concentration evaluated for three values: 0.625 is the reference value taken from the literature, 0.745 is 20% higher than the reference value and 0.5 is 20% lower than the literature value.

The sensitivity of the rate constant was investigated for two values: 1) the rate constant estimated by Grasa et al.[82] and 2) the rate constant estimated using the spherical grain model with the TGA experimental results under similar conditions as the fluidized bed reactor. The result predicted using the rate constant obtained by Grasa et al.[82] was very optimistic compared to the experimental results, as observed in Figure 4-29.

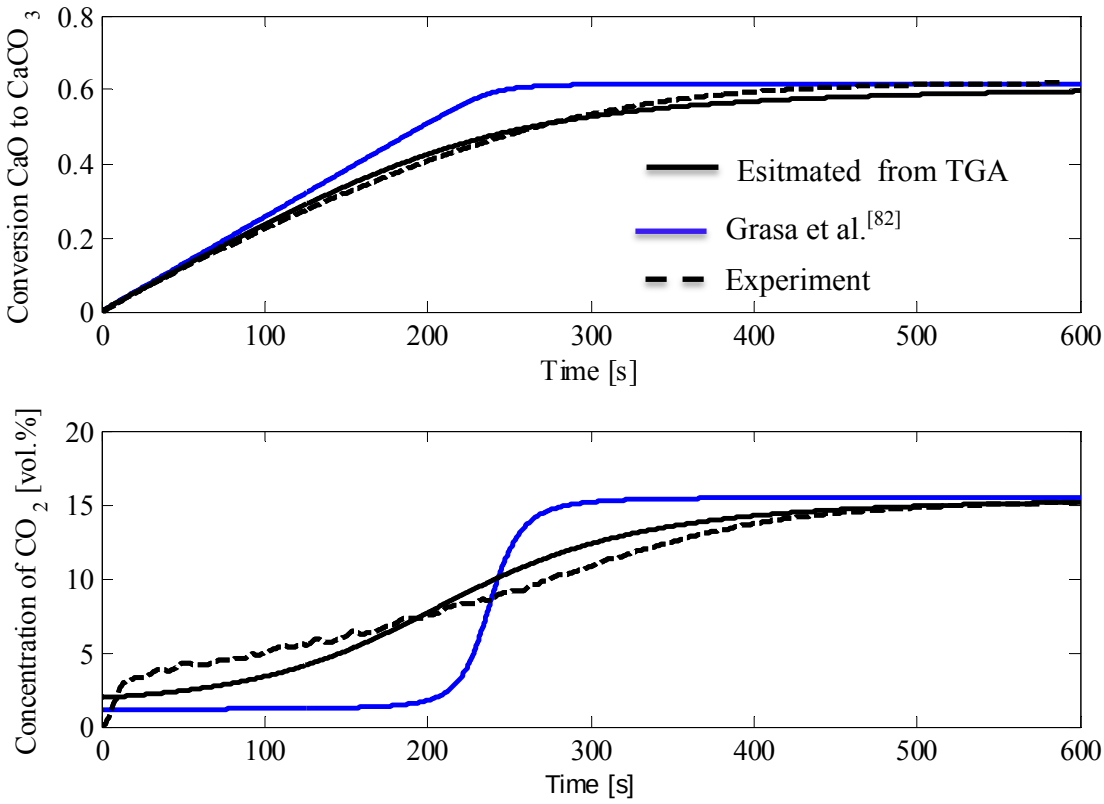

Figure 4-29: Comparison the rate constant: 1) determined from limestone in the TGA apparatus $k_f = 3[m^3 / kmol \cdot s]$ and 2) $k_f = 27[m^3 / kmol \cdot s]$[82].

4.6 Conclusions

Cyclic experiments were performed in the fluidized bed reactor and a fluidized bed reactor model was developed to explain the experimental results, which was later used for a sensitivity analysis. Based on the cyclic fluidized bed experimental results and the fluidized bed reactor model, the following conclusions were made:

- The general trend in the CO_2 capture capacity (conversion of CaO to $CaCO_3$) as a function of cycle number was similar to the TGA cycle experiments.
- The performance of the fluidized bed reactor using clay mixed with limestone was similar to using limestone alone.
- The shift in the rate constant from the kinetically controlled reaction regime to the diffusion control regime was observed in the TGA and fluidized bed reactor. The estimated kinetically controlled reaction rate constant was 3 [m^3/kmol·s].
- The rate of attrition constant was estimated for limestone, $3.01e^{-5}$ [1/s], was comparable to the attrition constant value found in the literature.
- A high sorbent inventory will result in a high CO_2 capture efficiency for a longer period of time, but the rate of conversion of calcined limestone will be lower. So, the optimum inventory should be a balance between the CO_2 capture efficiency and the average conversion of the bed.
- SO_2 in the gas can be captured along with CO_2, but the capacity to capture CO_2 dropped significantly from cycle to cycle.
- The fluidized bed reactor model predicted the experimental results using the rate constant estimated from the TGA apparatus. Although this model is not suitable for industrial application, it can be used to study the influence of some parameters which cannot be measured directly.

- The sensitivity of the model parameters was investigated:
  - The results indicate that the temperature of the bed during carbonation should be below 700°C for high CO_2 capture efficiency.
  - The influence of the gas-transfer co-efficient between bubbles and the emulsion was also investigated and the bubble fraction was investigated. The results show that values estimated from the literature fit the experimental results.
  - The estimated carbonation rate constant for the limestone was lower than rate constant presented in the literature.

5. Carbonation of Calcined Limestone in a Circulating Fluidized Bed Reactor

In Chapters 3 and 4, cycle experiments were carried out in a TGA and in a fluidized bed reactor to investigate the carbonate looping process. The qualitative results concerning the CO_2 capture capacity of the sorbent as a function of cycle number were similar. However, for industrial application, continuous operation of the fluidized bed reactor is necessary. The most suitable reactor for continuous operation is a circulating fluidized bed reactor. So, in this chapter, the performance of the carbonator for continuous carbonation of calcined limestone was investigated in a circulating fluidized bed reactor. The objective of the experimental work was to evaluate the most sensitive parameter that controls the performance of the carbonator, defined by the CO_2 capture efficiency.

The other objective of this chapter was to develop a carbonator model using the experimental data to simulate important parameters. A circulating fluidized bed reactor model consisting of a dense bed and a lean region was proposed. The most important parameters in the simulation of the CFB reactor are the particle distribution profile along the height of the reactor and the rate of the reaction. The particle distribution along the height of reactor was estimated from experiments and the carbonation reaction rate constant was fitted to experimental data.

5.1 Experimental

5.1.1 Setup

To study the carbonation of calcined limestone in the CFB reactor, experiments were carried out in a laboratory scale fluidized bed reactor. The schematic drawing of the experimental setup used for the carbonation experiments is presented in Figure 5-1. This experimental setup is the same as that used for

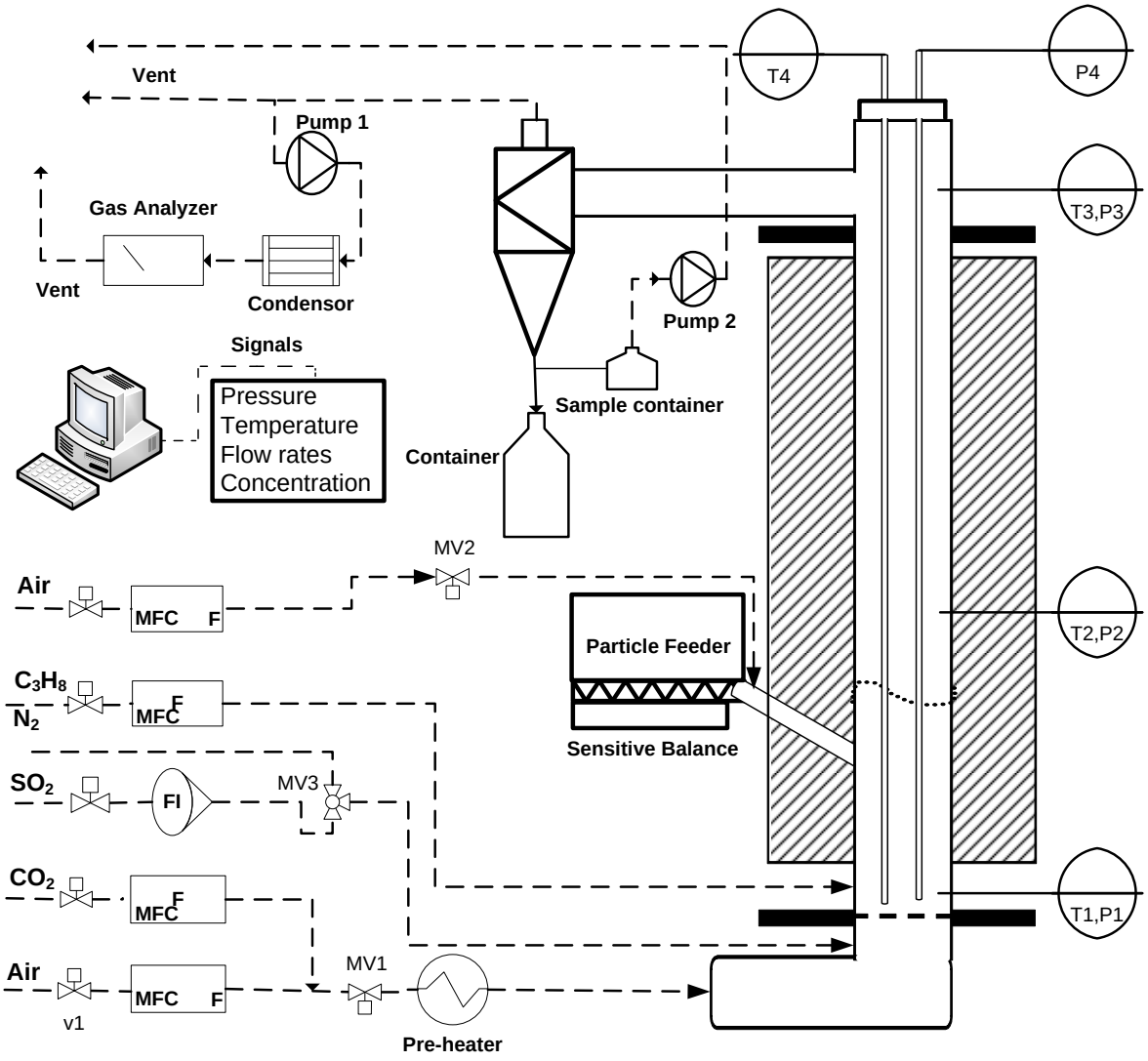

Figure 5-1: Schematic drawing of the experimental setup used for the carbonation experiments.

the cyclic experiments in Chapter 4, but with additional probes and equipment. In order to operate the reactor as a CFB, a particle feeder was installed (to simulate recirculation) which can feed particles at a controlled rate into the reactor. However, it has the limitation of a maximum feeding rate of 1.1 kg/m^{2}s. The feeder was placed on a sensitive balance which measures the weight of feeder. A particle sampling system was installed to sample particles during the experiments. This system consists of a probe, a small vacuum pump (Pump 2) and a gas-solid particle separator/collector. The probe is a 0.25" tube

with a wide opening (2.54 cm by 0.67 cm) along the length of probe which can be inserted in to the downer below the cyclone. The small vacuum pump was used to direct the particles through the probe into the gas-solid particle separator where particles were collected in small container at the bottom; gas flowed to the vent line. Along with a fixed thermocouple (T1-3) and pressure transducers (P1-3), there were additional temperature (T4) and pressure (P4) probes (3 m long) installed vertically from the top of the reactor. These probes were mobile and could be used to measure the temperature and pressure along the length of the reactor during the experiments. The data from the pressure transducers, the thermocouples, the gas analyzers, the feeder weighing balance and the mass flow controllers was logged continuously to the system using the Lab-view software with a time intervals of 1 s.

5.1.2 Materials

Calcined Faxe (coral) limestone (0-2 mm) delivered by Faxe Kalk A/S was used for the experiments. The calcined limestone was sieved to obtain three different particle size ranges: 0.5-1 mm, 0.25-0.5 mm and 0.09-0.25 mm. Quartz sand (0.50-0.71 mm) was used as bed material, during the experiments with calcined limestone particles in the size range of 0.09-0.25 mm, to improve the fluidization properties. The calcined limestone particles were characterized in terms of the degree of calcination, the degree of hydration and the maximum CO_2 capture capacity. The degree of hydration and the degree of calcination were estimated by weight loss of a sample in N_2 by: 1) heating to 450°C, 2) maintaining 450°C for 3 min, 3) heating 450°C to 900°C, and 4) maintaining 900°C for 3 min. The maximum CO_2 capture capacity was estimated by heating the sample to 650°C for 10 min in 15 vol. % CO_2. A summary of particle characterization is presented in Table 5-1.

Table 5-1: Degree of calcination, hydration and CO_2 capture capacity of calcined limestone for different particle size range (PSR) in mol/mol% and the BET surface area measurements from 3 samples each.

PSR [mm]	Deg. of Calcination	Deg. of Hydration	CO_2 capture capacity in 10 min	BET [m^2/g]
0.09-0.25	99.3±0.2	1.6±0.3	9.6±2.2	0.94±0.01
0.25-0.50	99.0±0.1	1.7±0.2	11.5±0.2	1.65±0.18
0.50-1.00	97.0±2.3	2.0±0.3	12.6±1.6	1.95±0.01

5.1.3 Experimental Procedure

The main objective of the continuous carbonation experiments was to determine the most sensitive parameter that controls the performance of the carbonator. Experiments were performed with three particle size ranges, as mentioned in Table 5-1. The influence of temperature was assessed by varying the reactor temperature, and the effect of the particle recirculation rate was investigated by controlling the particle feeder. The particle recirculation tested in the carbonate looping process in the dual fluidized bed reactors was in the range of 1-4 kg/m^2s[113] and 10-20 kg/m^2s[24], but in the present experiments, the maximum particle feed rate was only 1.1 kg/m^2s. The influence of particle recirculation rate was not straightforward, as varying the particle recirculation rate changes the inlet Ca/C ratio and also influences the average CO_2 concentration experienced by the particles in the reactor. So, it is important to understand the influence of each parameter: the particle recirculation rate and the CO_2 concentration with a focus on the inlet Ca/C ratio. So, experiments were performed by: 1) varying only the particle recirculation rate at a constant inlet CO_2 concentration, 2) varying the inlet CO_2 concentration at a constant particle circulation rate and 3) varying both the inlet CO_2 concentration and particle feed rate to keep the inlet Ca/C ratio constant. Additional experiments were also performed to investigate the influence of simultaneous SO_2 and CO_2 capture by injecting SO_2 into the fluidizing gas. A list of the main experiments performed in the fluidized bed reactor is presented Table 5-2. The experiment identity mentioned in the table explains the parameters varied, for example in Exp_T_1, “T” indicates temperature as the study parameter.

Before each experiment, the particle feeder was filled with calcined limestone particles and closed tightly. The weight of the feeder placed on the sensitive balance was noted. Feeder air was set to 10 NL/min such that air flowed continuously through the feeding line, avoiding back pressure into the feeder.

Table 5-2: Summary of the main experiments performed in the fluidized bed reactor.

Experiment Identity	Particle Size mm	T[1] °C	Feeder_Air NL/min	Air NL/min	CO_2 NL/min	CO_{2_in} Vol.%	SO_2 NmL/min	Feeding rate kg/min
Exp_0	0.25-0.50	631	5.51	93.15	0.00	0.00	0	0.19
Exp_T_1	0.25-0.50	608	5.51	74.11	17.32	17.86	0	0.19
Exp_T_2	0.25-0.50	705	5.51	74.09	17.32	17.87	0	0.19
Exp_T_3	0.25-0.50	660	5.51	74.11	17.32	17.87	0	0.19
Exp_G_s_1	0.50-1.00	660	10.69	207.72	20.49	8.58	0	0.09
Exp_G_s_2	0.50-1.00	660	10.69	211.61	20.49	8.44	0	0.11
Exp_G_s_3	0.50-1.00	660	10.69	211.60	20.48	8.44	0	0.19
Exp_Ca/C_1	0.25-0.50	670	10.69	67.76	17.31	18.08	0	0.81
Exp_Ca/C_2	0.25-0.50	650	10.69	80.54	5.43	5.62	0	0.06
Exp_Ca/C_3	0.25-0.50	660	12.76	76.22	8.84	9.04	0	0.09
Exp_CO_2_1	0.25-0.50	650	10.69	76.22	8.84	9.23	0	0.18
Exp_CO_2_2	0.25-0.50	650	10.69	67.77	17.32	18.08	0	0.18
Exp_CO_2_3	0.25-0.50	650	10.69	80.46	5.66	5.85	0	0.18
Exp_SO_2_1	0.25-0.50	650	10.69	76.22	8.84	9.23	0	0.18
Exp_SO_2_2	0.25-0.50	650	10.69	76.22	8.84	9.23	61	0.18
Exp_SO_2_3	0.25-0.50	650	10.69	76.22	8.84	9.23	115	0.18
Exp_dp_1	0.09-0.25	660	10.69	76.22	8.84	9.23	0	0.13
Exp_dp_2	0.09-0.25	660	10.69	76.22	5.66	6.12	0	0.13
Exp_dp_3	0.09-0.25	660	10.69	76.22	5.66	6.12	115	0.13

The reactor was heated by external heating elements under a flow of air to attain a stable temperature in the reactor, measured by four thermocouples (T1-T4) as shown in Figure 5-1. The flow rate of air was predetermined based on the gas velocity for the particle size range used for the experiment (see Table 5-3). The cold air was heated using the gas pre-heater to 400°C in order to reduce the temperature difference in the fluidizing gas around the air distributor plate.

Table 5-3: Main operating parameters for the three particle size ranges.

Particle size range [mm]	0.09-0.25	0.25-0.5	0.5-1.0
Uo [m/s]	1.8	1.95	4.8
Wo[kg]	1.1*	1.2	0.7

*mixture of sand and limestone

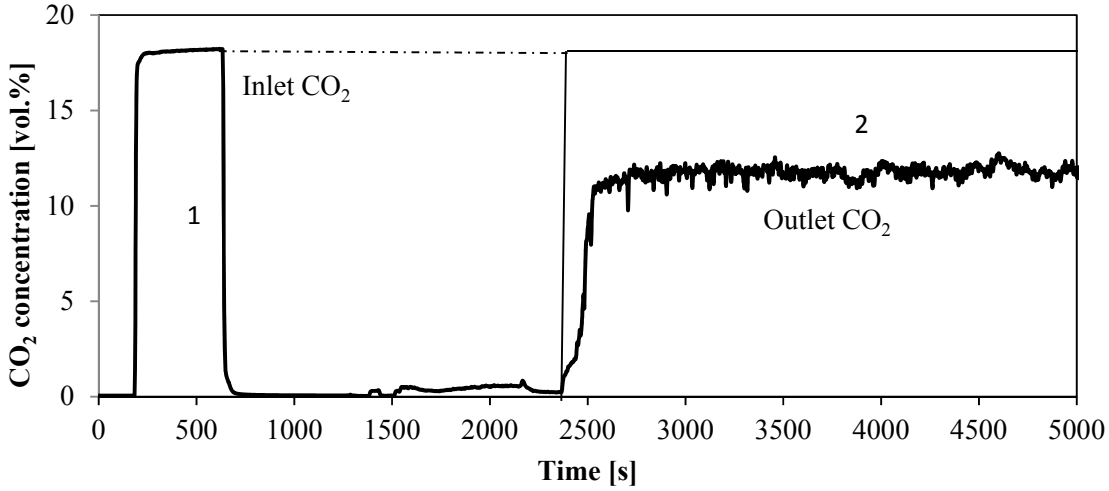

Figure 5-2: CO_2 concentration in the gas measured before adding calcined limestone and during continuous feeding of calcined limestone (Exp_Ca/C_1).

During the heating process, the fluidizing gas was changed from air to a mixture of CO_2 and air, where the concentration of CO_2 gas was equal to the inlet CO_2 concentration during the carbonation experiment. The CO_2 gas concentration was measured using calibrated gas analyzers (1, Figure 5-2) in order to verify the CO_2 concentration estimated from the inlet gas flow rates. The fluidizing gas was

again changed to air after verification. The flow rate of the fluidizing gas was reduced before loading limestone through the top of reactor by opening the flange. After loading the limestone, the top of the reactor was closed tightly, then the temperature of the bed was increased and a small fraction CO_2 in the exit gas was observed (Figure 5-2) at 1500 s due to the calcination of calcium carbonate present in the limestone. When the temperature in the reactor had stabilized in the range of 630-660°C, then the particle feeder was turned on and immediately the gas flow rate and composition changed to match the experimental conditions. The difference in the inlet and the exit CO_2 concentration during the experiment is presented in Figure 5-2 (2, in the figure).

The bed inventory, the temperature and the exit CO_2 concentration settled in a stable range indicating steady operating conditions as shown in Figure 5-3. The steady operating conditions during the experiment (Exp_Ca/C_3) were a temperature of 640 (±10) °C at the bottom of reactor, a bed pressure indicating 42 mbar (± 4.5) equivalent to 1.2 kg of bed material in the reactor, an inlet CO_2 concentration of 9 vol.% and an exit CO_2 concentration of 5.8 (±0.2) vol.%. During steady operating conditions, the temperature and the pressure along the height of the reactor were measured using the mobile temperature (T4, Figure 5-1) and pressure (P4, Figure 5-1) probes. The measurements were taken by lowering the probes in small steps (15 cm) from the top of the reactor. The probes were lowered and fixed in the position for 2-3 min and the time average (2 min) measurement from the system was noted. The temperature and the pressure profile along the height of the reactor is presented in Figure 5-4. In the experiments with a particle size range of 0.09-0.250 mm, the initial bed material loaded in the reactor was quartz sand particles (0.5-0.71mm) instead of calcined limestone. Quartz sand was used as a bed material in these experiments to enhance the fluidization properties along with maintaining stable operating conditions.

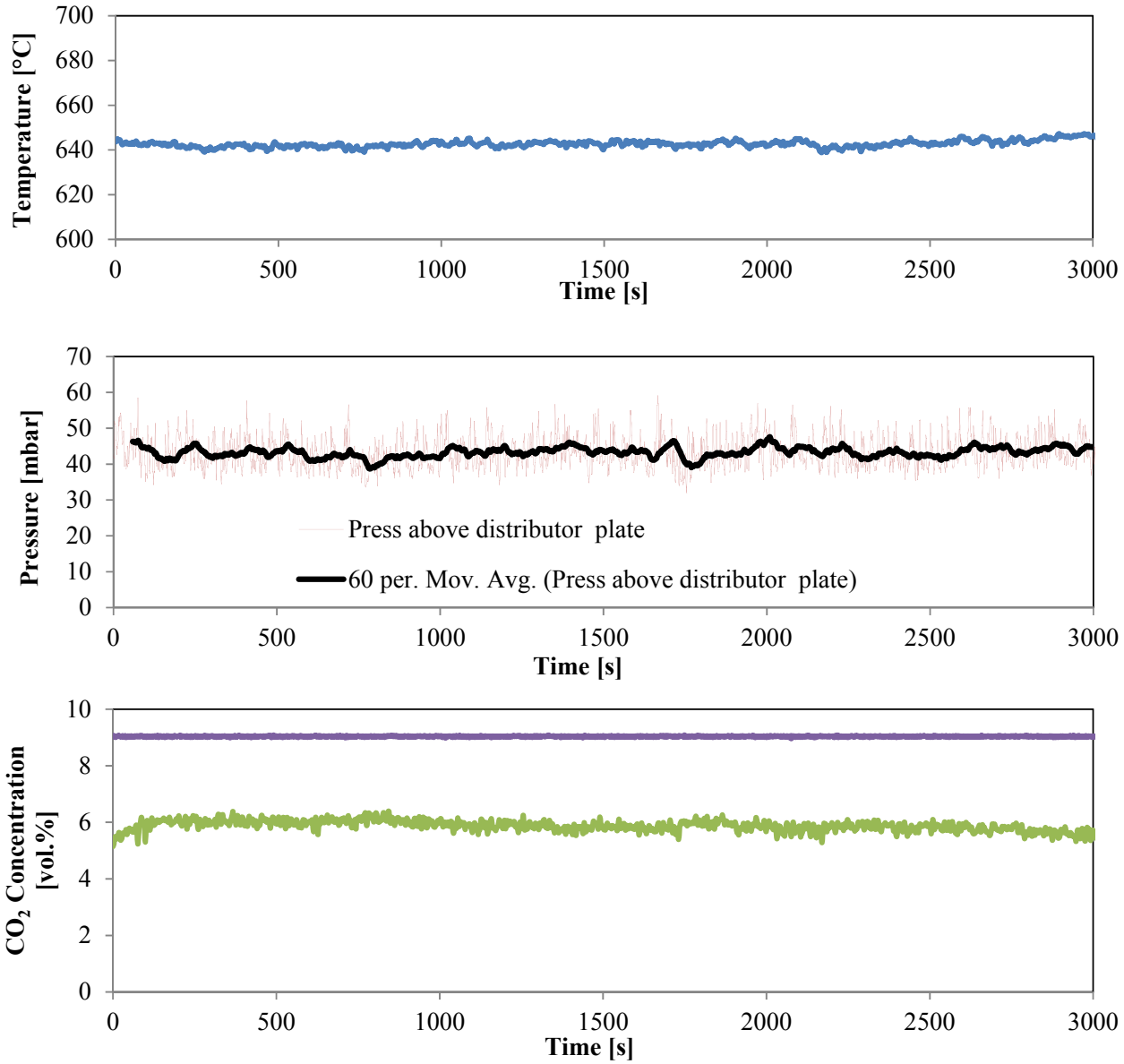

Figure 5-3: Pressure due to sorbent inventory, average bed temperature and CO_2 concentration in the inlet and the exit gas in a typical experiment (Exp_Ca/C_3) under stable operating conditions.

The pressure profile is presented for three particles size ranges in Figure 5-4. The pressure dropped rapidly above the distributor plate due to the dense bed region, and further up along the reactor height, the pressure dropped at a lower rate due to the lean particle phase distribution. The pressure profile measurement was used to estimate the particle distribution along the reactor height. The temperature

profile is presented for the particle size range of 0.25-0.5 mm for experiments with and without CO_2 capture. The temperature along the height of the reactor was constant, barring the bottom and top zones of the reactor mainly due to cold gas entering the system and heat loss from the top of the reactor, respectively.

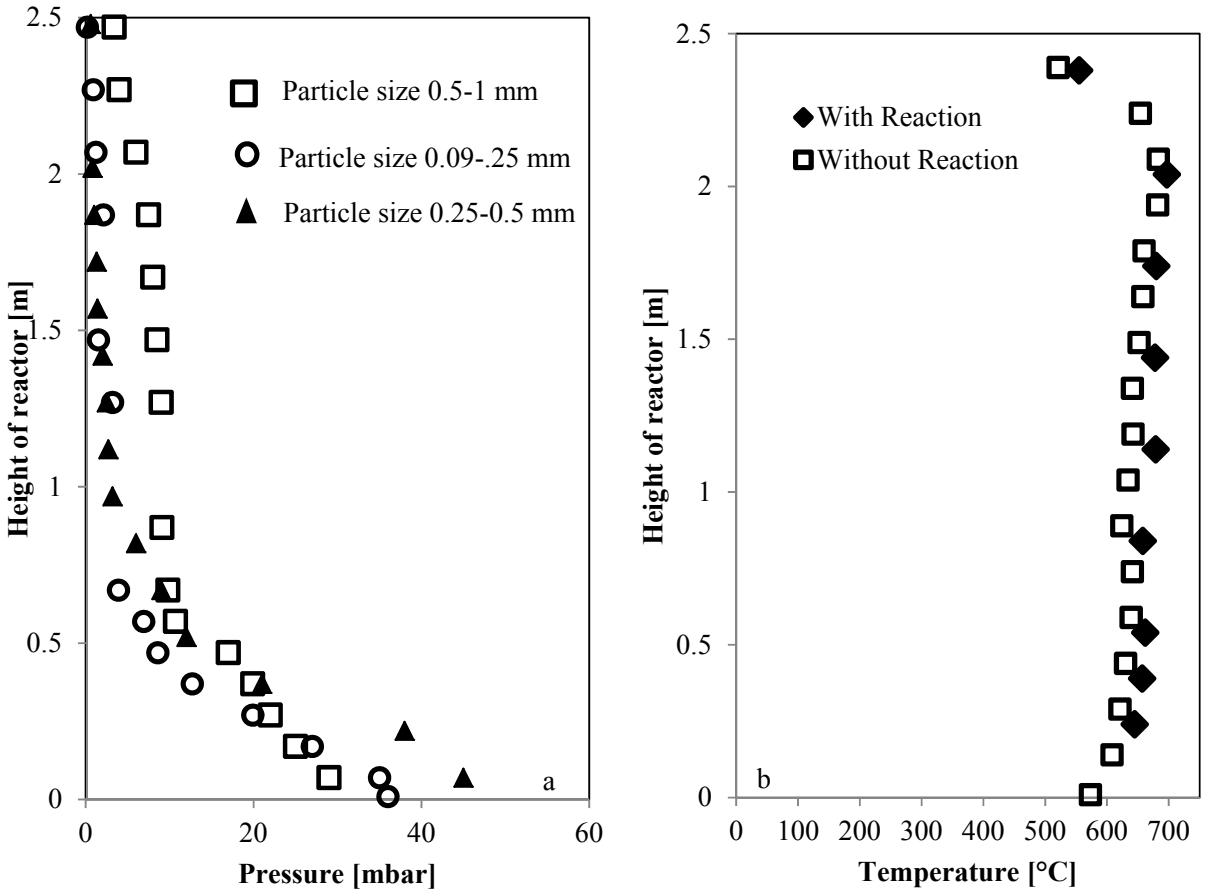

Figure 5-4: Pressure (a) and temperature (b) profile in the reactor under stable conditions. The pressure profile is presented for three particle size ranges; the gas flow rate for the particle size range 0.5-1.0 mm was 250 NL/min and for the others it was 97 NL/min. The temperature profile is presented for specific operating conditions with the gas flow rate (97 NL/min ~2 m/s), particle recirculation rate (1.08 kg/m^2.s) and bed inventory (~1 kg) for particles sized 250-500 μm; without reaction (Exp_0) and with reaction (Exp_Ca/C_1).

Under stable conditions, the particles separated from the gas need to be sampled for analysis. In order to sample the particles, without influencing the operating conditions in the reactor, a simple particle sampling system was installed which was turned on to take representative samples. The limestone particles sampled below the cyclone were cooled in a desiccator before storage in a 50 mL airtight container. The conversion of the sampled particles was estimated in a TGA apparatus and compared with the gas conversion data obtained from the inlet and exit gas concentrations.

5.2 Data Analysis

The experimental results were analyzed based on two methods: 1) particle analysis and 2) gas analysis. Particles sampled during the experiments were used to estimate the average degree of carbonation. The gas analysis was used to estimate the difference in the inlet and outlet gas compositions, since the amount of CO_2 captured from the fluidizing gas in the carbonator should reflect in the average degree of carbonation of the solid particles. Thus, the closure of mass balance estimated from the gas analysis and the particle analysis will represent the accuracy of the results.

5.2.1 Gas Analysis

Under steady operating conditions, the concentration of CO_2 in the exit gas will be constant. Thus, it can be used to evaluate the performance of the CFB carbonator with respect to the operating parameters. The performance was evaluated based on the CO_2 capture efficiency (E_{carb}), which is defined as:

$$E_{carb} = \frac{\phi_{CO_2,in} - \phi_{CO_2,out}}{\phi_{CO_2,in}} \qquad 5\text{-}1$$

In this equation, the flow rate of CO_2 in the exit gas is estimated based on the concentration of CO_2 in the exit gas ($x_{CO_2,outlet}[vol.\%]$) according to the following equation:

$$\phi_{CO_2,out} = \frac{x_{CO_2,outlet} \cdot (\phi_{t,in} - \phi_{CO_2,in})}{(100 - x_{CO_2,outlet})} \quad \text{5-2}$$

where

$\phi_{t,in}$, the volumetric flow rate of the fluidizing gas [NL/min]

$\phi_{CO_2,in}$, the volumetric flow rate of CO_2 in the fluidizing gas [NL/min]

5.2.2 Solid Particle Analysis

The collected samples were analyzed in a TGA apparatus to estimate the degree of carbonation (X_{carb}).The assumption during the analysis was that the weight loss measured from the TGA is due to CO_2 release.

$$X_{carb} = \frac{\left(\left(w_{in} - w_f\right)/44\right)}{\left(w_f/56\right)} - X_{carb,in} \quad \text{5-3}$$

where w_{in} is the weight of the sample before analysis, w_f is the final weight of the sample and $X_{carb,in}$ is the initial degree of carbonation.

Based on the gas analysis (E_{carb}), particle analysis (X_{carb}) and the respective molar flows rates, the mass balance for the capture system was evaluated according to the following equation:

$$F_{CaO} \cdot X_{carb} = \phi_{CO_2,in}\left(\rho_{CO_2}/44\right) \cdot E_{carb} \quad \text{5-4}$$

where $F_{CaO}[gmol/s]$ is the molar flow rate of calcined limestone estimated from the feeder set point, $\phi_{CO_2,in}[NL/s]$ is the flow rate of CO_2 in the fluidizing gas and ρ_{CO_2} is the density of CO_2 under normal conditions.

5.3 Sensitivity of Experimental Results

Table 5-4 summarizes the list of experiments performed with the stated operating parameters along with gas and particle analysis results. The mass balance closure was evaluated for most of the experiments listed in Table 5-4 except for a few experiments performed before installing the particle sampling system (Exp_Gs.). Figure 5-5 summarizes the experimental results where the number of moles of converted lime is compared with the number of moles of CO_2 captured according to equation 5-4. The mass balance results from the experiments, with a correlation coefficient of 0.96, indicate good reliability of the experimental results.

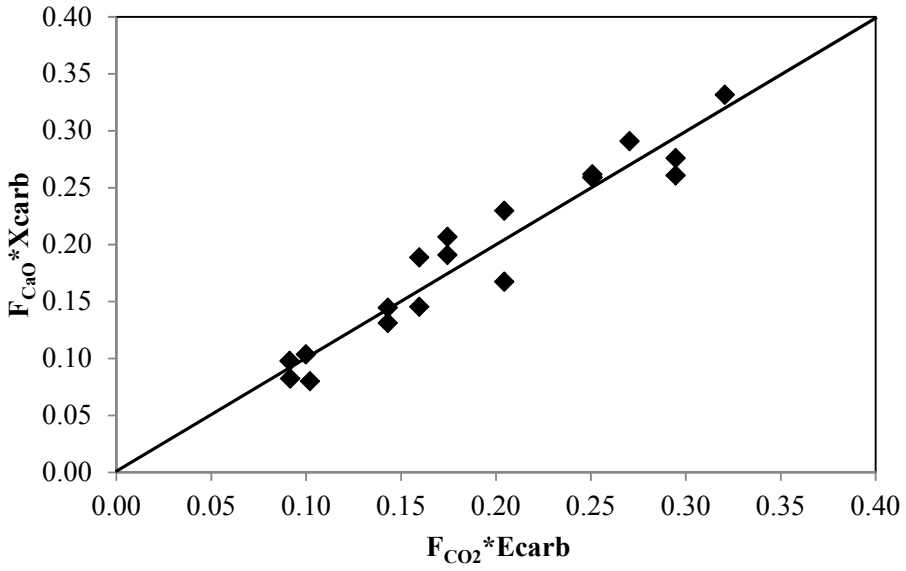

Figure 5-5: Mass balance closure for all the experiments in the circulation fluidized bed carbonator under steady state operating conditions.

Table 5-4: List of the main experiments performed in the fluidized bed reactor.

Experiment Identity	T[1] °C	V_{FG} NL/min	CO_2_in Vol.%	SO_2 ppmv	U m/s	Wo kg	Gs $kg/m^2.s$	tau min	CO_2_out %	Ca/CO_2 -	X_{carb} -	E_{carb} -	$F_{CaO}.X_{carb}$ -	$F_{CO2}.E_{carb}$ -	X_{carb}/X_{max} -
Exp_0	631	98.7	0.00	0	1.9	1.1	1.09	6.3	0.04	-	-	-	-	-	
Exp_T_1	608	96.9	17.86	0	1.8	1.	1.09	5.6	12.55	4.4	0.07	0.34	**0.23**	**0.25**	0.61
Exp_T_2	705	96.9	17.87	0	2.0	1.	1.09	6.0	11.53	4.4	0.10	0.40	**0.33**	**0.30**	0.87
Exp_T_3	660	96.9	17.87	0	2.0	1.4	1.09	7.8	12.03	4.4	0.09	0.37	**0.30**	**0.28**	0.75
Exp_Gs_1	660	238.9	8.58	0	4.8	0.7	0.54	7.5	8.37	1.8	0.01[3]	0.03	**0.02**	**0.02**	0.1[3]
Exp_Gs_2	660	242.8	8.44	0	4.9	0.7	0.65	6.7	7.57	2.2	0.05[3]	0.11	**0.10**	**0.10**	0.38[3]
Exp_Gs_3	660	242.8	8.44	0	4.9	0.7	1.09	4.1	6.82	3.7	0.06[3]	0.21	**0.18**	**0.18**	0.42[3]
Exp_Ca/C_1	670	95.8	18.08	0	2.0	1.3	1.07	7.3	11.80	4.3	0.08	0.39	**0.26**	**0.29**	0.70
Exp_Ca/C 2	650	96.7	5.62	0	1.9	1	0.35	17.3	3.51	4.6	0.09	0.39	**0.10**	**0.09**	0.79
Exp_Ca/C_3	660	97.8	9.04	0	2.0	1.2	0.53	13.9	5.85	4.2	0.08	0.37	**0.13**	**0.14**	0.71
Exp_CO_2_1	650	95.7	9.23	0	1.9	1.5	1.07	8.5	2.88	8.5	0.09	0.71	**0.29**	**0.27**	0.78
Exp_CO_2_2	650	95.8	18.08	0	1.9	1.5	1.07	8.3	11.20	4.3	0.10	0.43	**0.33**	**0.32**	0.89
Exp_CO_2_3	650	96.8	5.85	0	1.9	1.4	1.07	7.7	1.01	13.2	0.07	0.84	**0.23**	**0.20**	0.62
Exp_SO_2_1	650	95.7	9.23	0	1.9	1.4	1.07	7.9	3.37	8.5	0.08	0.66	**0.26**	**0.25**	0.70
Exp_SO_2_2	650	95.7	9.23	600	1.9	1.4	1.07	7.9	3.37	8.5	0.08	0.66	**0.26**	**0.25**	0.70
Exp_SO_2_3	650	95.7	9.23	1200	1.9	1.4	1.07	7.9	3.37	8.5	0.08	0.66	**0.26**	**0.25**	0.70
Exp_dp_1	660	95.8	9.23	0	1.9	0.2[2]	0.78	1.6	6.98	6.2	0.04	0.26	**0.10**	**0.10**	0.46
Exp_dp_2	660	92.6	6.12	0	1.9	0.25[2]	0.78	1.9	3.66	9.6	0.03	0.42	**0.08**	**0.10**	0.35
Exp_dp_3	660	92.6	6.12	1200	1.9	0.25[2]	0.78	1.7	3.92	9.6	0.04	0.37	**0.08**	**0.09**	0.36

1: Average temperature in the reactor along the reactor height under stable operation with a maximum standard deviation of ± 30°C;

2: Only sorbent inventory excluding a sand bed of 1.1 kg;

3: Estimated from Ecarb.

5.3.1 Material Balance

Along with mass balance from the gas and particle analysis, the other important parameter to evaluate the control in the experiments was the material balance. So, after each experiment listed in Table 5-5, the material balance was evaluated to check the amount of material entrained from the system in the exit gas. The material balance was evaluated based on the total input: initial loading of the calcined limestone, the feed rate of the calcined limestone times the total feeding time, the total CO_2 captured based on the CO_2 capture efficiency estimated from the experiment and the total output, i.e. the total weight of the particles collected in the container after the experiment. The difference between the input and the output gives the weight of fines entrained from the system or the coating of fine particles on the inner walls of the system. However, two experiments listed in Table 5-5 showed an excess of material, which may have been due to the release of particles from the inner reactor surface.

Table 5-5: Material mass balance for different experiments including gas captured and particle conversion.

Experiment	Initial Loading	Time	Total fed	CO_2 capture	Total Material expected	Measured after experiment	Difference
	kg	min	kg	kg	kg	kg	kg
Exp_0	1.10	60.00	10.86	0.00	11.96	11.39	-0.57
Exp_Ca/C_1-2	1.10	52.50	9.50	0.63	11.23	11.62	0.39
Exp_Ca/C_3	1.30	110.00	8.95	0.56	10.81	10.30	-0.51
Exp_CO2_1-3	1.20	83.00	15.02	0.83	17.05	17.48	0.43
Exp_Gs_1*	0.65	46.00	8.33	0.32	9.30	9.06	-0.24
Exp_Gs_2*	0.74	47.00	8.51	0.35	9.59	9.52	-0.07
Exp_SO2_1-3	1.10	56.00	10.14	0.48	11.72	11.17	-0.55
Exp_dp_1-3	1.00	66.00	8.71	0.28	9.99	9.38	-0.61

The material balance results indicate that the difference in the bed material for each experiment was on average 4%, estimated based on the expected bed weight. The material balance results and gas/particle analysis results show that the results obtained from the set of experiments have low uncertainty.

5.4 Results and Discussion

5.4.1 Influence of Temperature

The influence of temperature was investigated by performing experiments at three different temperatures: 600°C (Exp_T_1), 650°C (Exp_T_3) and 700°C (Exp_T_2). The experiments were performed with the particle size in the range of 0.25-0.5 mm, with a particle circulation rate (feed rate) of 1 [kg/m^2.s] and at a constant inlet CO_2 concentration of 18 [vol.%]. Figure 5-6 summarizes the effect of reactor temperature on the performance of the carbonator.

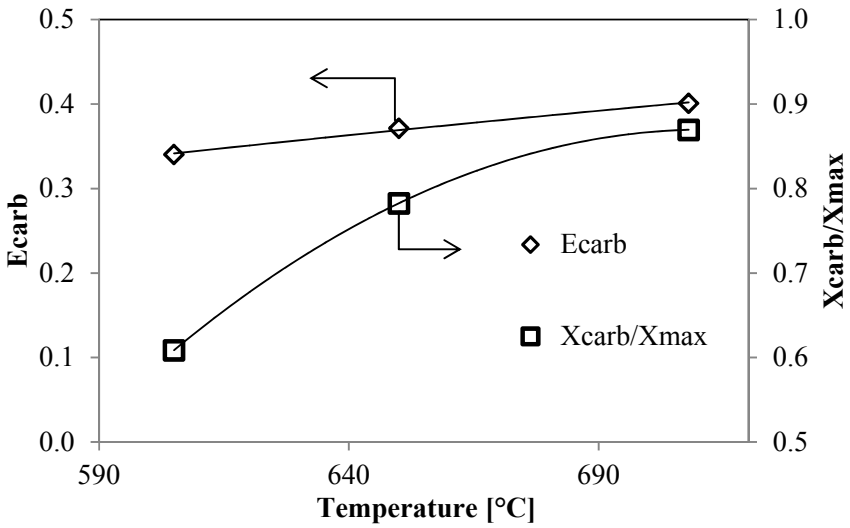

Figure 5-6: Influence of carbonation temperature on the carbonator performance with an inlet CO_2 concentration of 18 vol.%, for particle size range of 250-500 µm, with maximum CO_2 capture capacity of 11.5% at constant inlet Ca/C ratio 4.4.

Increasing the temperature from 600-700°C resulted in increased CO_2 capture efficiency. Since the maximum CO_2 capture capacity of calcined limestone is only 11.5% (Table 5-1), the CO_2 capture efficiency of the carbonator was relatively low i.e. 0.3-0.4 with an inlet Ca/C ratio of 4.4. Comparing the conversion of calcined limestone to carbonate, the effect of temperature in the range of 600-700°C was clearly visible with an increase from 0.6 to 0.85 normalized to its maximum conversion. The obtained results in the fluidized bed reactor under steady state agree with the results obtained by the Bhatia and Perlmutter[79]. The observed trend is due to the low particle re-circulation rate during experiments where the maximum CO_2 capture efficiency limit of the carbonator is only 0.5. The maximum CO_2 capture efficiency limit is estimated as $Ca/C \cdot X_{max}$ (4.4x0.115). This value is well below the thermodynamic equilibrium limit which ranges from 0.99 to 0.96 for the carbonation temperature from 600°C to 700°C, respectively.

For the rest of the experiments, the temperature of the reactor was set according to this experiment (Exp_T_3), such that the bed average temperature was close to 650°C, which resulted in an equilibrium CO_2 concentration of 0.9 vol.%. This temperature was selected because a higher temperature should increase the equilibrium CO_2 concentration limit exponentially for the carbonation reaction and might influence the final results in the experiments performed with a low inlet CO_2 concentration.

5.4.2 Influence of Inlet Ca/C Ratio

In the CFB, the particle recirculation rate is an important parameter, but the accurate measurement of this parameter is not easy. The uncertainty over the measurement of this parameter was eliminated by using a controlled particle feeder to simulate recirculation. The performance of the carbonator was evaluated under controlled conditions to investigate the influence of inlet Ca/C. The experiments were performed to evaluate this parameter by: 1) changing only the CO_2 concentration at a constant particle

circulation rate, 2) changing only the particle circulation rate at a constant inlet CO_2 concentration and 3) by changing both the inlet CO_2 concentration and the particle circulation rate to keep the Ca/C ratio constant. Thus, it was possible to reveal the influence of the inlet Ca/C ratio on the performance of the carbonator.

5.4.2.1 Varying the CO_2 Concentration

The influence of the CO_2 concentration was investigated by changing the inlet CO_2 concentration, i.e. 5.8 vol.% (Exp_CO2_3), 9.2 vol.% (Exp_CO2_1) and 18 vol.% (Exp_CO2_1). The experiments were performed with a particle size range of 0.25-0.5 mm at a constant particle recirculation rate of 1 $kg/m^2.s$. Figure 5-7 summarizes the effect of changing the inlet CO_2 concentration on the performance of the carbonate at a constant particle recirculation rate. The degree of limestone conversion increased with an increasing inlet concentration, as expected, since the exit CO_2 concentration in the reactor was 1, 3 and 11 vol.%. A similar observation was observed from the in the literature when where the CO_2 concentration was directly proportional when it was less than 10 vol.% [33,79,81,82]. The inlet Ca/C ratio decreased with an increase in the inlet CO_2 concentration from 13 to 4, respectively, which might have been a reason for the poor performance of the carbonator. Charitos et al.[152] investigated the influence of the inlet Ca/C ratio in a dual fluidized bed reactor where the carbonator was operated as a bubbling fluidized bed reactor. In their investigation, increasing the inlet Ca/C ratio from 4 to 17 improved the CO_2 capture efficiency from 50% to 95% indicating the similar trend compared to current experimental results.

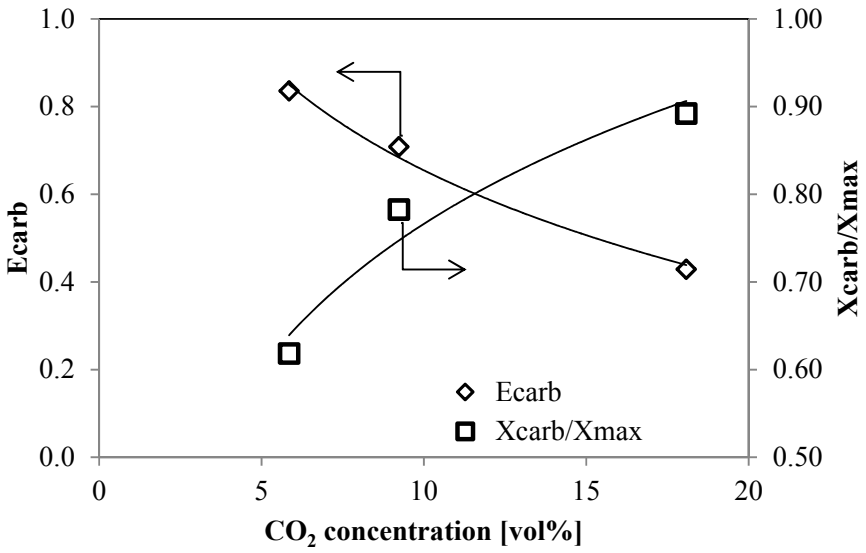

Figure 5-7: Influence of inlet CO_2 concentration on the performance of carbonator at a constant particle recirculation rate of 1.08 [kg/m^2.s] for a particle size range of 0.25-0.50 mm.

5.4.2.2 Varying the Particle Circulation Rate

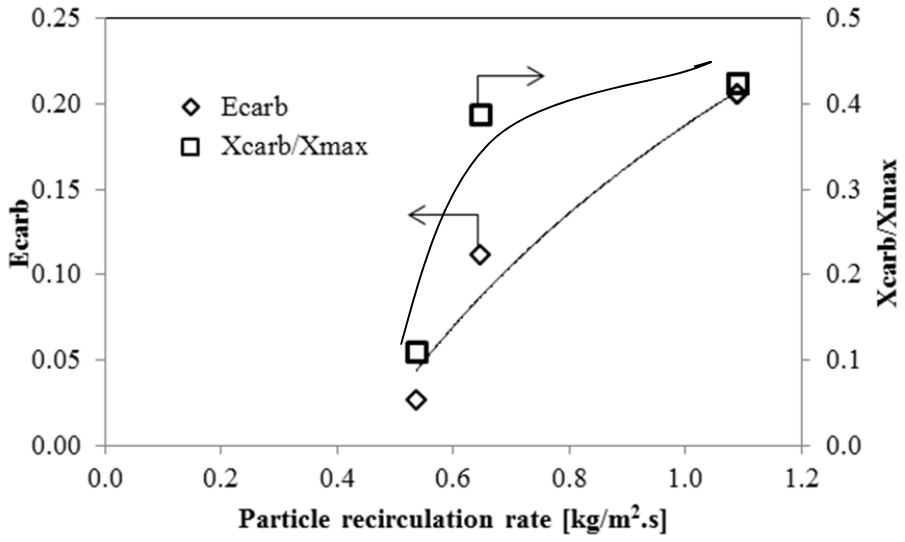

Figure 5-8: Influence of particle recirculation rate on the performance of carbonator at a constant inlet CO_2 concentration (8.5 vol.%) for a particle size range of 0.5-1.0 mm.

The influence of the particle circulation rate was investigated by varying the particle feed rate, i.e. 0.54 kg/m^2.s (Exp_Gs_1), 0.65 kg/m^2.s (Exp_Gs_2) and 1.1 kg/m^2.s (Exp_Gs_3). The experiments were performed with a particle size range of 0.5-1.0 mm at a constant inlet CO_2 concentration of 8.5 vol.%. Figure 5-8 shows the influence of the particle recirculation rate on the performance of the carbonator. A higher CO_2 capture efficiency resulted in an increase in the particle recirculation rate. However, the inlet Ca/C ratio also increased with an increased particle circulation rate, i.e. from 1.8 to 4. Comparing the results with the results from Charitos et al.[152], there are two observations: 1) the trend in the CO_2 capture efficiency is similar with respect to the increase in the inlet Ca/C ratio and 2) the trend in the conversion of calcined limestone particles is contradictory, i.e. in the current experiments, particle conversion increased with an increase in the particle recirculation rate, but the literature results indicated the opposite trend. Based on the detailed observations regarding the CO_2 capture efficiency and the range of the inlet Ca/C ratio, it can be concluded that the average conversion of the calcined limestone particle increases with increasing the inlet Ca/C ratio, but this achieves a maximum and then drops again according to the mass balance equation 5-4. So, the present experiment represents the lower range of the inlet Ca/C ratio (1.8-4) and the literature results include the upper range of 4-17[152]. The increase in the CO_2 capture efficiency in the current experiments could be either due to an increase in the particle recirculation rate or due to an increase in the inlet Ca/C ratio under a constant inlet CO_2 concentration.

5.4.2.3 *Varying both the CO_2 Concentration and Particle Circulation Rate*

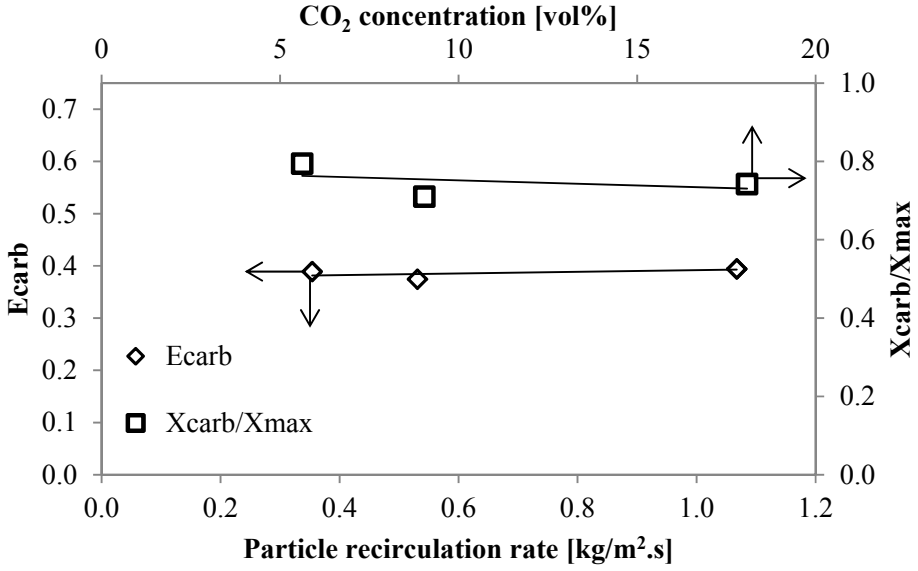

Figure 5-9: Influence of a simultaneous change in the particle recirculation rate and the inlet CO_2 concentration on the performance of carbonator at a constant inlet Ca/C = 4 for a particle size range of 0.25-0.50 mm.

Varying either the CO_2 flow or the particle flow resulted in a change in the inlet Ca/C ratio, which produced similar results regarding the performance of the carbonator. So, both the inlet CO_2 concentration and the particle circulation rate were varied such that the inlet Ca/C ratio was held constant at 4. The particle recirculation rate was varied from 0. 35 kg/m^{2}s to 1.1 kg/m^{2}s, whereas the inlet CO_2 concentration changed from 5.6 vol.% to 18 vol.%, respectively. Figure 5-9 summarizes the performance of the carbonator and bed conversion with respect to varying these parameters at a constant Ca/C ratio. The results clearly indicate that the inlet Ca/C ratio is the controlling parameter for the performance of the carbonator.

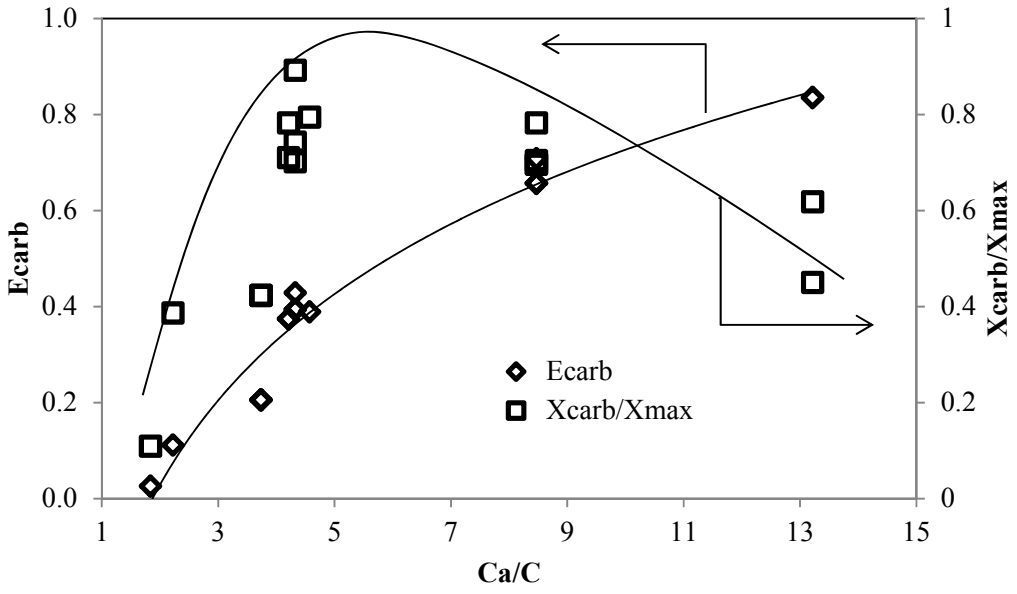

Figure 5-10: Influence of the inlet Ca/C ratio on the CO_2 capture efficiency and on the conversion of the bed in the carbonator.

A summary of the experimental results from the study of the inlet Ca/C ratio is presented in Figure 5-10. It is evident that increasing the inlet Ca/C ratio increases the performance of the carbonator. Furthermore, the average conversion of the calcined limestone particle increases with an increase in the inlet Ca/C ratio in the lower range up to 4 and decreases with a further increase in the ratio. Charitos et al.[152] presented only the upper range of the inlet Ca/C ratio, i.e. > 4. So, based on the experiment results, it can be concluded that if the inlet CO_2 concentration is defined, then the performance of the carbonator can be controlled by the inlet calcined limestone flow rate.

5.4.3 Influence of SO_2

Experiments were performed to investigate the influence of the SO_2 concentration on the performance of the carbonator. The SO_2 concentration was varied from 600 ppmv (Exp_SO_2_2) to 1200 ppmv

(Exp_SO_2_3) and the results were compared with the performance of the carbonator without SO_2 (Exp_SO_2_1) injection into the system. The particle size range used for these experiments was 0.25-0.5 mm at a constant inlet Ca/C =8.5 with 9 vol.% CO_2 and 1.1 kg/m^2.s as the particle circulation rate. Figure 5-11 summarizes the performance of the carbonator and the average bed conversion with respect to the SO_2 concentration.

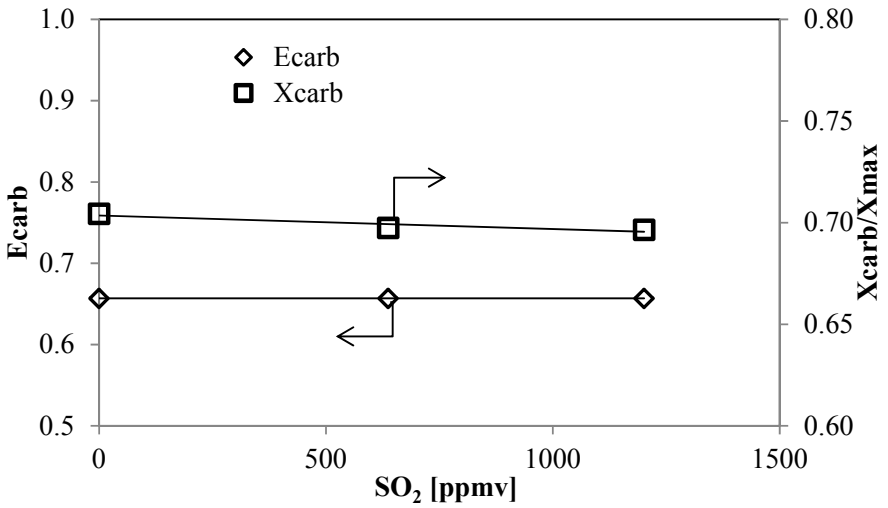

Figure 5-11: Influence of the SO_2 concentration on the CO_2 capture efficiency for the particle size range of 0.25-0.50 mm.

The results indicate that the effect of SO_2 on the performance of carbonator was negligible. Similarly, the bed conversion was not significantly affected by an increase in the SO_2 concentration. The concentration of SO_2 in the exit gas was less than 10 ppmv. From the cycle experiments results, the effect of SO_2 on the conversion of the bed was insignificant in the first cycle; however, with increasing cycle number, the CO_2 capture capacity decreased due to permanent retention of SO_2. In the current experiment, under steady state operation with fresh calcined limestone fed continuously, there was no effect on the performance of the carbonator. The inlet Ca/S ratio for these experiments was found to be

very high, with values of 1224 (Exp_SO_2_2) and 650 (Exp_SO_2_3). A high Ca/S ratio might be the reason for the complete capture of SO_2. Sulfation had no significant effect on CO_2 capture because the degree of sulfation under steady conditions was very low (< 0.1 mol%).

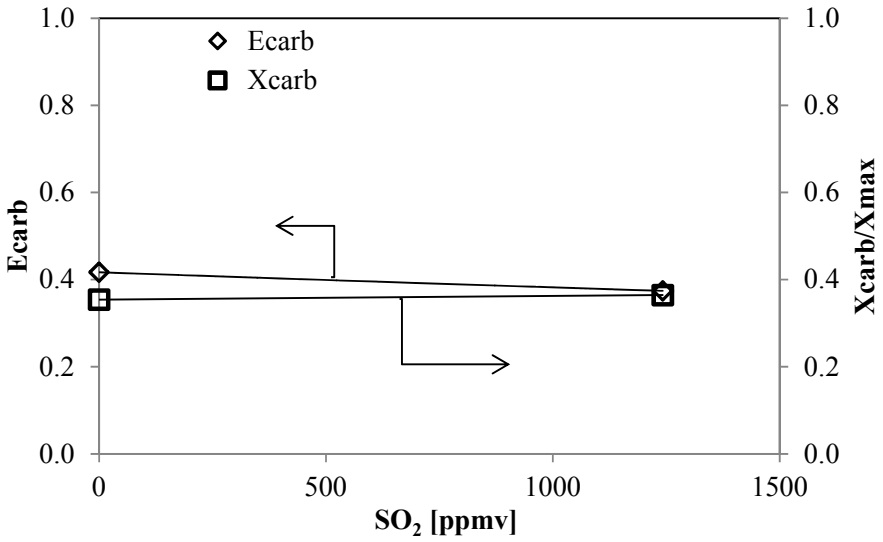

Figure 5-12: Influence of the SO_2 concentration on the CO_2 capture efficiency for the particle size range of 0.09-0.25 mm.

Simultaneous SO_2 and CO_2 capture experiments were also carried with the smaller particle size range of 0.09-0.25 mm (Exp_dp_2-3); the results are summarized in Figure 5-12. The main difference in the operating conditions in this experiment compared to the larger particle size range is the composition of the dense bed. The major fraction of bed inventory for the experiment with the limestone particle size range of 0.09-0.25 mm was sand, which was used for stable operation along with improving fluidization properties, whereas for the experiment with limestone particles sized 0.25-0.5 mm, no sand was used as the bed material. Injection of 1200 ppmv of SO_2 into the carbonator had no significant effect on the CO_2 capture efficiency of the carbonator, similar to the experimental results with larger

limestone particles. The exit SO_2 concentration was also less than 10 ppmv because of the high inlet Ca/S ratio, which was 470. As with the experimental results with a larger particle size, the difference in the CO_2 capture efficiency was due to the difference in the inlet Ca/C ratio. The inlet Ca/C ratio was 8.5 (Exp_SO2_1) for the larger particle size range whereas it was 6 (Exp_dp_1) for the smaller particle size under the same inlet CO_2 concentration (see Table 5-4).

5.5 Modeling the Carbonator as a Fast Fluidized Bed Reactor

A carbonator reactor model has been proposed based on the Kunii-Levenspiel (K-L) model for a circulating fluidized-bed reactor[126,127,153]. The performance of carbonator is defined by the fraction of CO_2 captured (E_{carb}) by the calcined limestone particles, which depends on the particle distribution along the height of the reactor and rate of CO_2 capture by the particles. The particle distribution parameter is determined by bed pressure measurements during the experiment, as presented in Figure 5-4 (a) and the CO_2 capture rate is the fitting parameter.

5.5.1 Assumptions

The K-L reactor model to simulate the CO_2 capture from the flue gas is developed based on the following assumptions:

- Uniform temperature along the height of the reactor, which was verified by temperature profile measurement during the experiment.
- No change in the bed inventory meaning that the particle feeding rate is constant and equal to entrainment rate from the reactor.

The velocity of gas is assumed to be constant throughout the system as it did not has any significant influence on the evaluation of performance of the carbonator[125].

- The change in particle density is not considered due to fractional conversion of calcined limestone.
- The particle conversion was modeled using the work by Bhatia and Perlmutter[79] with minor modification to limit the reaction to the experimentally determined maximum CO_2 capture capacity of the calcined limestone used.
- The sorbent decay with respect to cycle number is not considered as the cycle number is limited to one.
- The single fluidized bed reactor is operated in the "lower dense bed and lean freeboard" regime. Further the particle distribution profile was determined experimentally to validate the hydrodynamic model.
- Further, the hydrodynamics data was obtained from the experiments which eliminate the use of correlations depending on particle size.
- The main control parameter is the particle recirculation rate.

5.5.2 Particle conversion

The particle conversion of calcined limestone to carbonate in the initial fast stage was described according to the semi-empirical function given by equation 5-5:

$$\frac{dX_N}{dt} = k_f \left(1 - \frac{X}{X_{\max}}\right)^{2/3} \left(C_{CO_2} - C_{CO_2,eq}\right) \qquad 5\text{-}5$$

The rate of reaction in the fluidized bed reactor was obtained according to equation 5-6 to measure the molar volume of CO_2 captured per molar volume of calcium oxide, where $k_f \left[m^3/kmol \cdot s \right]$ was fitted to match the experimental results.

$$K_r = k_f \left(1 - \frac{X}{X_{\max}} \right)^{2/3} \frac{\rho_{CaO}}{M_{CaO}} \qquad 5\text{-}6$$

5.5.3 Particle Distribution

In a circulating fluidized bed, the particle distribution along the length of the reactor is divided into two distinct regions i) a lower dense region and ii) a lean freeboard region. Under steady operating conditions the hydrodynamics in the reactor control the particle distribution ε_s and the gas-particle contact efficiency η. First considering the particle distribution, the CFB carbonator reactor of height H_t is divided into two regions: a lower dense bed of height H_d and a upper lean region H_l. In the dense bed, the volume fraction of particles is constant represented by "ε_{sd}". There are two phases in the dense bed: 1) gas rich phase (core/bubble) and particle rich phase (wall/emulsion). The fraction of core/bubble region (δ_{cd}) in the dense bed is assumed to have no particles and in the particle rich phase ε_{mf} is void fraction under minimum fluidization conditions and the fraction of solids in the wall region is given by $\left(1-\varepsilon_{mf}\right)\left(1-\delta_{cd}\right)$. Based on the above simplifications the fraction of core or bubble region in the dense bed can be estimated by equation[127]:

$$\delta_{cd} = \frac{(1-\varepsilon_{mf}) - \varepsilon_{sd}}{(1-\varepsilon_{mf})} \qquad 5\text{-}7$$

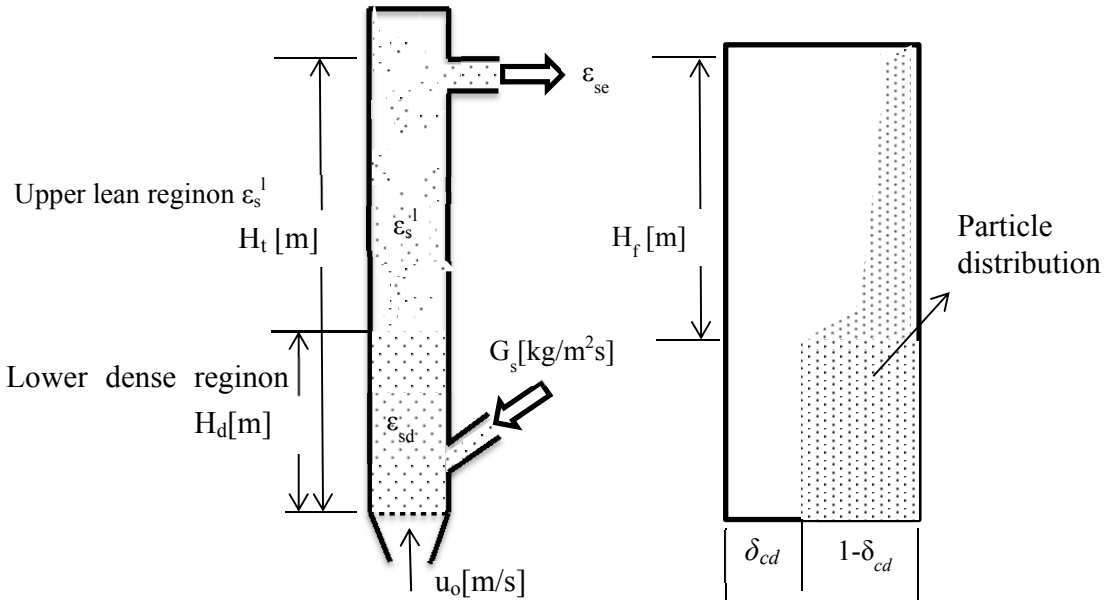

Figure 5-13: Illustration of the fast fluidized bed reactor model used to describe the experimental results.

The main parameters which control these regions are the gas velocity, particle size and particle circulation rate. In general, with a constant particle circulation rate and particle size distribution, an increase in the gas velocity reduces the length of the lower dense region and increases the freeboard region. However, an accurate prediction of the particle distribution is difficult using the correlation presented in the literature, which depends on the dimensions of the fluidized bed reactor. So, the particle distribution profile along the height of the reactor was measured using the pressure probe under stable operating conditions, as shown in Figure 5-4. The difference in the pressure from one location to the next was used to estimate the particle distribution. The conversion of bed pressure into the particle volume fraction was estimated with 1 mbar equivalent to 28.8 g, taken from the experiments. The experimental data (Figure 5-14) was used to estimate the decay constant '*a*' according to the equation:

$$\varepsilon_s^l = \varepsilon_s^* + \left(\varepsilon_{sd} - \varepsilon_s^*\right) e^{-ah_l} \qquad 5\text{-}8$$

where ε_s^l is the volume fraction of solids in the freeboard region at location h_l, which varies from 0 at H_d to H_f at the top of the reactor. ε_s^* is the particle fraction independent of height of reactor, taken from the literature as 0.001[122]. ε_{sd} is the dense bed volume fraction of particles measured during the experiments. The height of the freeboard region above the dense bed region is given by the difference in the total height of the reactor and height of the dense bed (H_t-H_d). The height of the dense bed was estimated by solving equation 5-9.

$$\frac{W}{A_t \rho_s} = \frac{\varepsilon_{sd} - \varepsilon_{se}}{a} + H_t \varepsilon_{sd} - H_f (\varepsilon_{sd} - \varepsilon_s^*) \qquad 5\text{-}9$$

where W is the inventory of solids in the reactor, A_t is the cross-sectional area of the reactor, ρ_s is the bulk density of the particles and ε_{se} is the fraction of solids at the exit of the reactor estimated from equation 5-8. Substituting all known values, H_f was estimated by solving equations 5-8 and 5-9 simultaneously in Matlab using the function "fsolve", where H_f and ε_{se} were guessed to find out the solution that satisfied equations 5-8 and 5-9. A summary of the experimental values and estimated values is presented in Table 5-6.

Table 5-6: Summary of hydrodynamic parameters such as volume fraction in the dense bed, the decay constant and height of the freeboard region estimated to represent experimental data for the two particle size ranges.

dp range [µm]	u_o [m/s]	au_o [1/s]	H_f	ε_{sd}	ε_s^*
250-500	1.8	6	2	0.3	0.001
500-1000	4.5	16	2.25	0.2	0.001

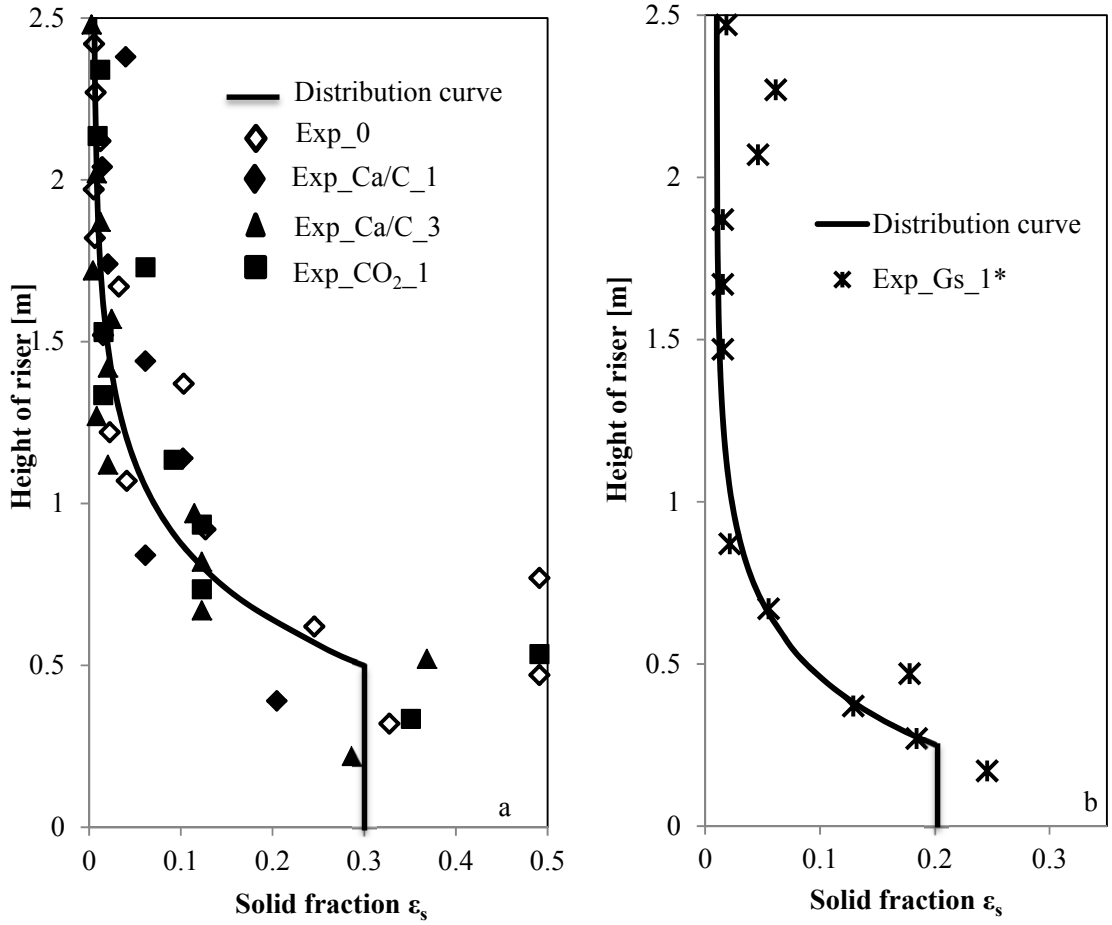

Figure 5-14**:** Solid particle distribution in the riser for different experiments in the circulating fluidized bed reactor for lime particles in the size range of 0.25-0.5 mm (a) and 0.5-1 mm (b).

5.5.4 Carbonator Reactor Model

In the CFB, the concentration of CO_2 gas along the height of reactor can be described by the general equation under steady state[126]:

$$u_o \frac{dC_{CO_2,z}}{dz} = -\varepsilon_s \eta K_r \left(C_{CO_2,z} - C_{CO_2,eq} \right) \qquad 5\text{-}10$$

here ε is particle volume fraction, η is the contact efficiency between the gas and particle which depends on the particle distribution, K_r is the average rate constant and C_{CO_2} is the concentration of CO_2, u_o is the superficial gas velocity and z is the height of the reactor. There are two expressions for estimating the CO_2 concentration: one for the dense bed region and the other for the lean region based on the general equation 5-10. The concentration of CO_2 at the top of the dense region, $C_{CO_{2,d}}$, is given by an equation:

$$\ln\left(\frac{C_{CO_2,in}-C_{CO_2,eq}}{C_{CO_2,d}-C_{CO_2,eq}}\right)=\frac{\eta_d\varepsilon_{sd}K_rH_d}{u_o} \qquad 5\text{-}11$$

where η_d is the contact efficiency in the dense bed region described by the equation[126]:

$$\eta_d=\frac{1}{\left(K_r\big/\delta_{cd}k_{cw}+1\big/(1-\varepsilon_{mf})(1-\delta_{cd})\right)(1-\varepsilon_{mf})(1-\delta_{cd})} \qquad 5\text{-}12$$

Substituting equation 5-12 in 5-11 gives the CO_2 concentration at the end of the dense bed region.

$$C_{CO_{2,d}}=C_{CO_{2,eq}}+(C_{CO_{2,in}}-C_{CO_{2,eq}})\exp\left(-1/\left((1/\delta_{cd}k_{cw})+(1/(1-\varepsilon_{mf})(1-\delta_{cd})K_r)\right)\right)\frac{H_d}{u_o} \qquad 5\text{-}13$$

The CO_2 concentration in the lean region $H_f=H_t-H_d$ is calculated according to the equation:

$$\ln\left(\frac{C_{CO_2,d}-C_{CO_2,eq}}{C_{CO_2,h_l}-C_{CO_2,eq}}\right)=\frac{\eta_l\varepsilon_s^lK_rh_l}{u_o} \qquad 5\text{-}14$$

where η_l is the contact efficiency in the lean region, which varies along the height of the reactor, i.e. $\eta_l=\eta_d$ at the top of dense bed H_d and increases along the height of the reactor according to η_l by the equation[154]:

$$\eta_l = 1-(1-\eta_d)e^{-bh_l} \qquad 5\text{-}15$$

where b is the decay contact for gas-solid contact inefficiency in the lead region of a CFB. This constant is similar to the decay constant estimated to describe the particle distribution, which decreases along height of the reactor and the particles have high contact efficiency with gas along the height of the reactor. So, the constant b is assumed to be equal to a, which was estimated from the experimental data. Substitution of equation 5-8 and 5-15 into equation 5-14 gives the CO_2 concentration along the height of the reactor in the lean region:

$$C_{CO_{2,h_l}} = C_{CO_{2,eq}} + (C_{CO_{2,d}} - C_{CO_{2,eq}})\exp\left[\frac{K_r}{u_o}\left(\varepsilon_s^*\left(h_l - \frac{1-\eta_d}{a}(1-e^{-ah_l})\right) + (\varepsilon_{sd}-\varepsilon^*)\left(\frac{1-e^{-ah_l}}{a} - \frac{1-\eta_d}{2a}(1-e^{-(2a)h_l})\right)\right)\right] \qquad 5\text{-}16$$

5.5.5 Model Description

The steady state carbonator CFB model is formulated in Matlab. The input parameters include the height of the reactor, cross sectional area, bed inventory under steady state, inlet gas flow rate, CO_2 concentration at the inlet, carbonator temperature, reactor pressure, particle re-circulation rate, decay constant, dense bed particle fraction, maximum CO_2 capture capacity of calcined limestone. Considering the simplifying assumptions, the model was solved according to the flow sheet shown in Figure 5-15. The average conversion of the bed X_{carb} is guessed and reaction rate constant is evaluated according to equation 8. Then based on the estimated reaction rate constant, inlet CO_2 concentration and the particle fraction in the denser region along with volumetric fraction of core/bubble and wall/emulsion region, and the gas transfer co-efficient between two regions, the CO_2 concentration at the end of the dense region is estimated according to equation 5-13. The CO_2 concentration at the end of dense bed region is used as the initial value and the CO_2 concentration along the reactor height is estimated according to equation 5-16. The exit CO_2 concentration is used to estimate the CO_2 capture

efficiency of carbonator based on the CO_2 absorbed and compared with the carbonator performance based on sorbent conversion with initial guessed value using following equations.

$$E_{carb,g} = \frac{\phi_{CO_2,in} - \phi_{CO_2,out}}{\phi_{CO_2,in}} \quad \text{5-17}$$

$$E_{carb,s} = \frac{F_R X_{ave}}{F_{CO_2,in}} \quad \text{5-18}$$

If the difference between the CO_2 capture efficiency estimated from gas phase conversion and solid phase conversion, i.e. $\left|E_{carb,s} - E_{carb,g}\right| / E_{carb,g} < 0.01$, the model is assumed to converge; if not average conversion is initiated with a new guess value and the process reiterates with a sequence of steps until the solution converges. The simulation parameters for the steady state carbonator model are summarized in Table 5-7 for two particle size ranges.

Table 5-7: Parameters used in the reactor model simulation (a: 0.25-0.5 mm ; b: 0.5-1.0 mm)

Parameter	Value
Height [m]	2.5
Diameter [m]	0.06
Gas velocity [m^2/s]	1.8[a];4.5[b]
Inlet CO_2 concentration [vol.%]	5.6-18
Temperature [°C]	600-700
Solid Inventory [kg/m^2]	245-530
Solid density [kg/m^3]	1655
Solid fraction in dense bed [-]	0.3[a];0.2[b]
Particle decay constant [1/m]	2.7[a];3.5[b]
Reaction rate constant k_r_fit [m^3/kmol·s]	2

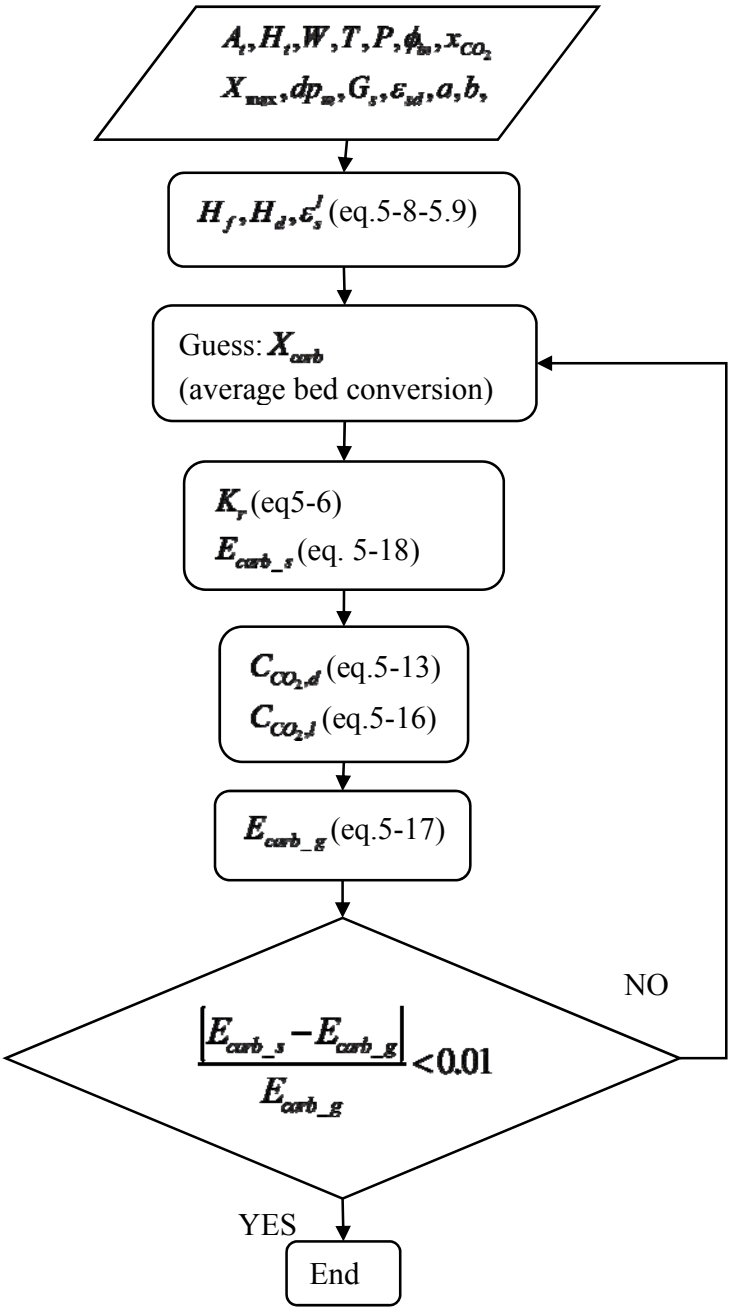

Figure 5-15: Flow description of CFB model solution and the iterative procedure used to find the steady state conversion, reaction rate and CO_2 concentration profile along the length of the reactor.

5.5.6 Model Validation

Figure 5-16 summarizes the model predicted CO_2 capture efficiency of the carbonator with the experimental results. The degree of accuracy of the model is reasonable (R^2 = 0.8). The summary of important model parameters used for simulating the carbonator reactor is presented in Table 5-7. In the listed parameters, the rate of reaction $\left(k_r\left[m^3 / kmol \cdot s\right]\right)$ is the fitted to match the experimental results. Comparing the fitted reaction rate with the value presented in the literature $\left(25\left[m^3 / kmol \cdot s\right]\right)$ [18,82], it is lower by one magnitude order. The observed difference in the reaction rate might be because of the type of the limestone and the calcination conditions which influence the structure of the particles.

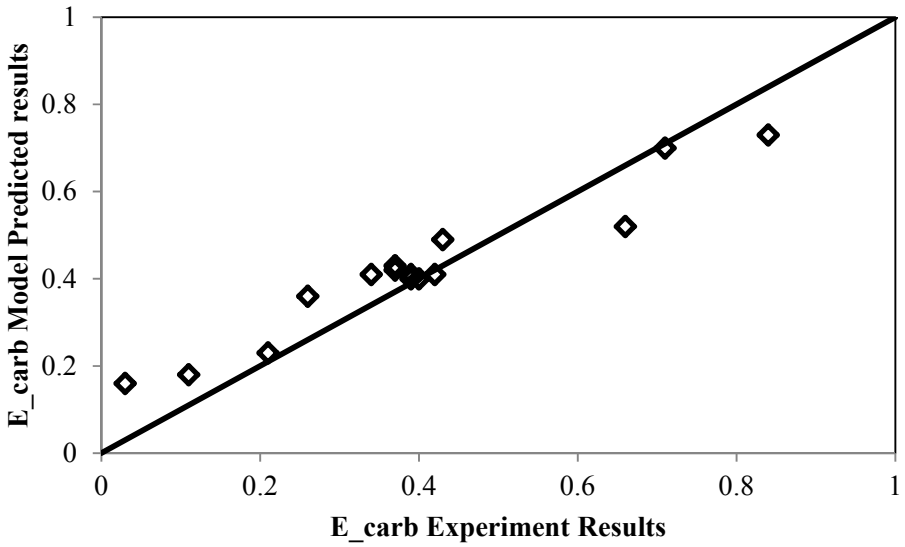

Figure 5-16: Comparison of the experimental values with the model predicted values for both solid and gas conversions at different temperatures.

5.5.7 Model simulation of Carbonator Operation

The model is used to study the effect of changing carbonator operating parameters: 1) the carbonator temperature, 2) inlet CO_2 concentration, in the range 14-28 vol.% as typically found in the flue gas from power plants and cement plants, respectively 3) CO_2 capture capacity of sorbent limestone or cement raw meal and, 4) Increasing cycling number. The CO_2 capture efficiency of the carbonator was simulated with respect to the particle re-circulation rate having constant CO_2 capture capacity, for defined inlet CO_2 concentration, which is the controlling parameter.

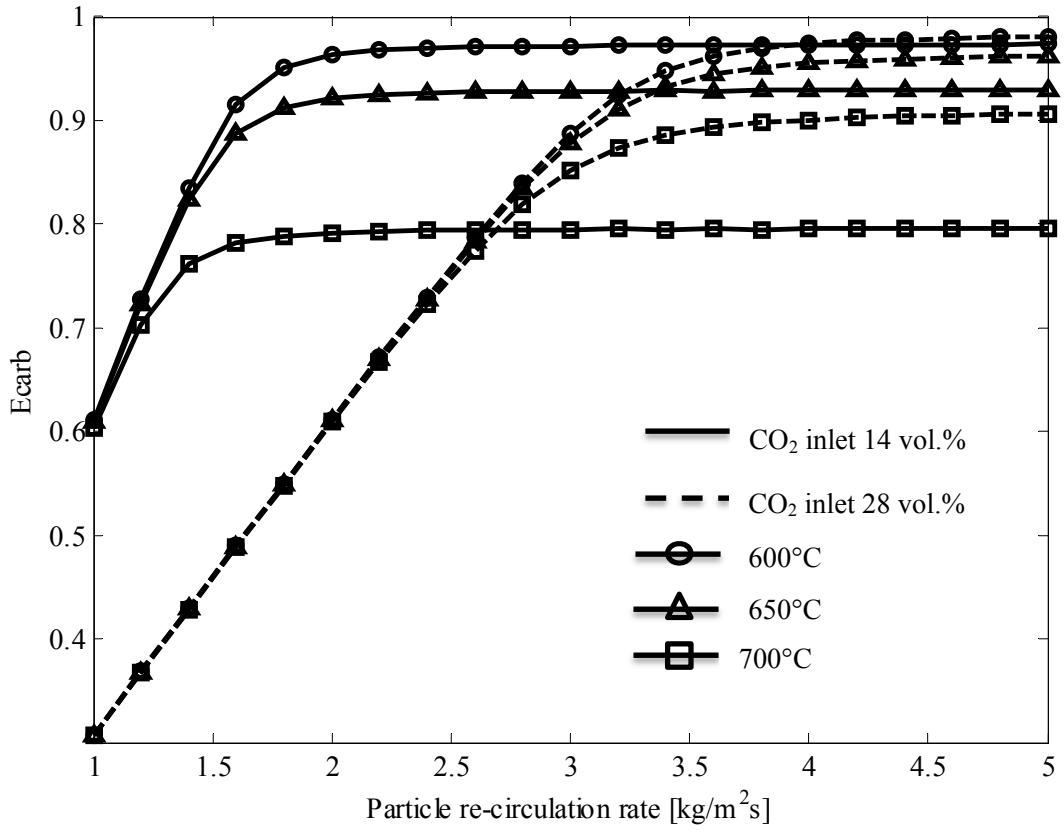

Figure 5-17: Influence of carbonation temperature (600, 650, and 700°C) and inlet CO_2 concentration (14 and 28 vol.%) on the performance of carbonator. The maximum CO_2 capture capacity of CaO is 11.5%.

The influence of the carbonator temperature is presented in Figure 5-17. The results show that at low particle recirculation rates, there is little difference in the CO_2 capture efficiency, whereas with increasing particle re-circulation rate the effect of temperature is clearly observed. This is similar to the experimental results presented by Charitos et al.[152].

The influence of the inlet CO_2 concentration is also shown in Figure 5-17. The inlet Ca to C ratio, ranges from 5 to 28 and 3 to 13 for an inlet CO_2 concentration of 14 and 28 vol%, respectively. However, a CO_2 capture efficiency of about 90% was obtained for inlet Ca to C ratios around 10 for the both cases.

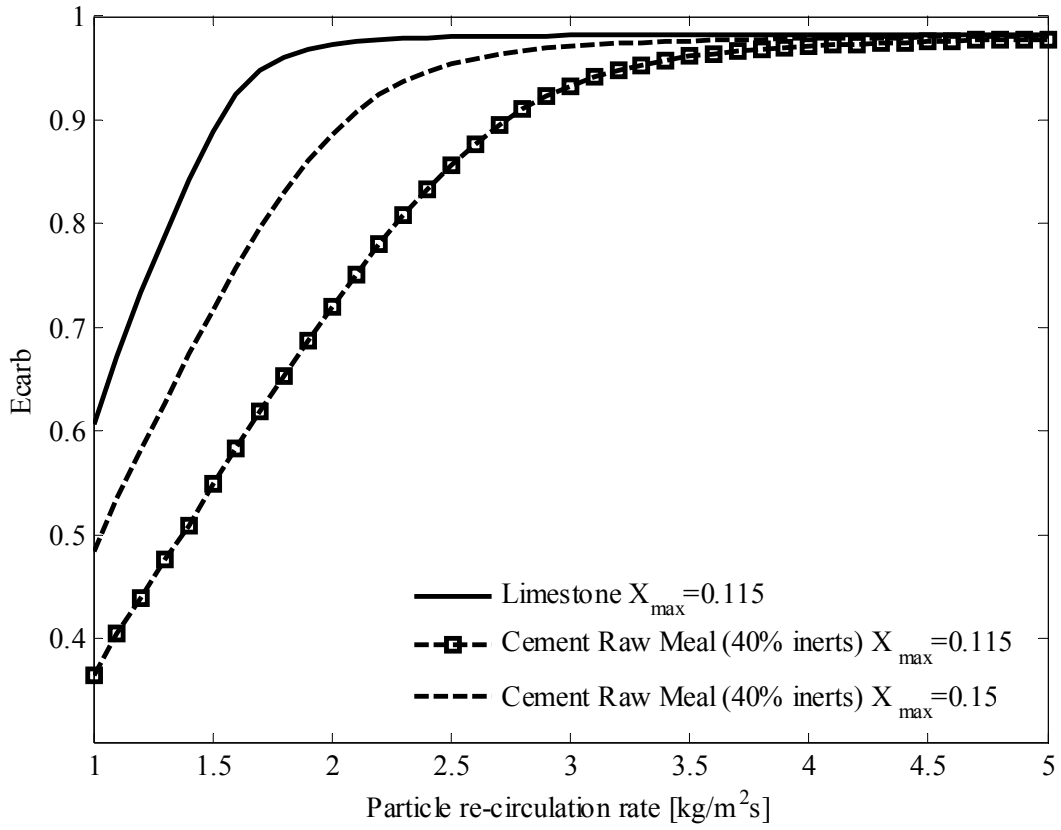

Figure 5-18: Influence of calcined limestone and calcined raw meal on the performance of carbonator. The carbonator temperature was 600°C and inlet CO_2 concentration is 14 vol.%.

Finally, the CO_2 capture efficiency of cement raw meal is compared with limestone in Figure 5-18. For raw meal, the calculated CO_2 capture efficiency increases from about 40% at a particle recirculation rate of 1 kg/m^{2}s to more than 90% above 3 kg/m^{2}s. As expected, raw meal has lower efficiency than limestone due to its content of inert material of about 40%. Figure 5-18 also present the performance of a carbonator applying industrial raw meal that has a maximum CO_2 capture capacity of 0.15 in the first cycle estimated using the two parameter correlation equation with $X_r = 0.05$ and $k = 8.7$.

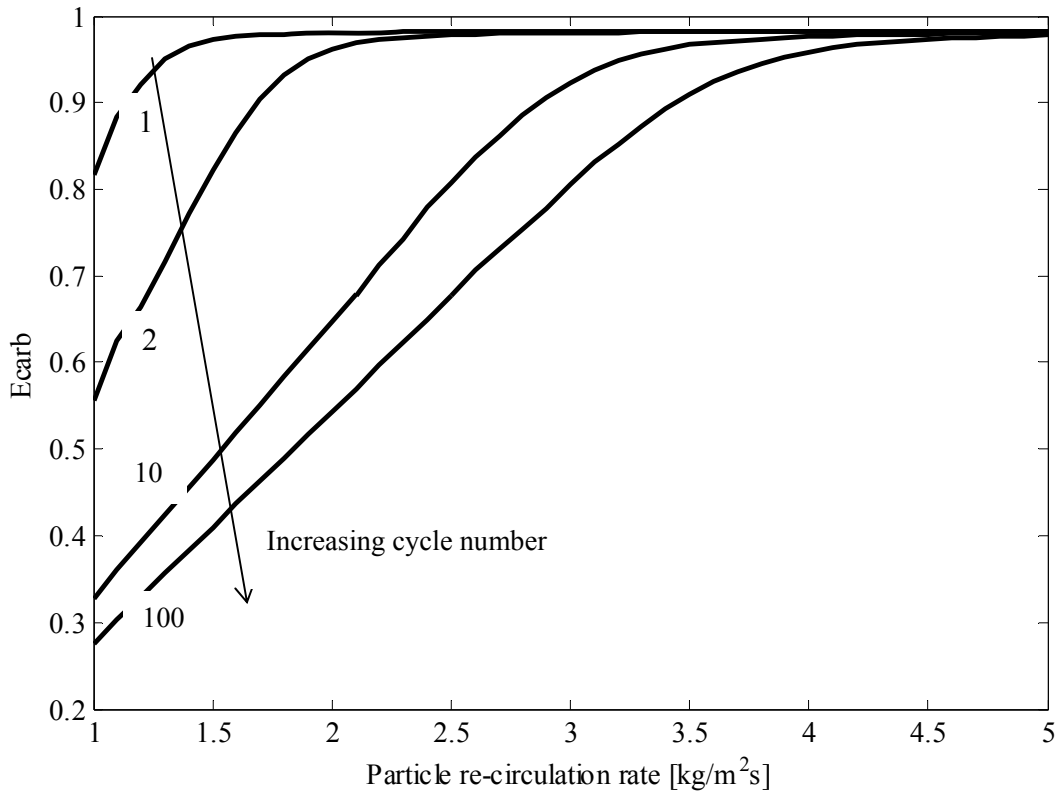

Figure 5-19: Influence of cycle number on the performance of carbonator using the limestone whose residual CO_2 capture capacity ($X_r = 0.05$) and decay constant ($k = 8.7$). The carbonator temperature was 600°C and inlet CO_2 concentration is 14 vol.%.

Figure 5-19 shows the influence of increasing cycling number on the performance of a carbonator as a function of particle recirculation rate. In order to maintain high CO_2 capture efficiency in the carbonator the particle recirculation rate has to be increased to compensate the decay in CO_2 capture capacity of sorbent with increase in looping cycle number. Further, it can be observed that the difference in particle recirculation rate for same CO_2 capture efficiency is higher in the initial cycle compared to later cycles.

Based on the experimental results and model predicted results, the inlet Ca/C ratio is the most sensitive parameter which controls the performance of the carbonator. This parameter can be used to obtain the desired CO_2 capture efficiency by controlling the particle recirculation rate. For example, by fixing the CO_2 capture efficiency E_{carb}, the particle recirculation G_s [kg/m^{2}s] can be estimated by the following equation:

$$G_s = F_{CO_2}\left(E_{carb}/X_{ave}\right)\left(M_{CaO}/x_{CaO}\right)\left(1/A_t\right) \qquad \text{5-19}$$

where $F_{CO_2}[mol/s]$ is the molar flow rate of CO_2 into the carbonator, $M_{CaO}[g/mol]$ is the molar weight of CaO, x_{CaO} is the weight fraction of CaO in the particle recirculation stream, E_{carb} is the desired CO_2 capture efficiency, X_{ave} is the average conversion of the sorbent estimated by the model converged solution and $A_t[m^2]$ is the surface area of the reactor.

5.6 Conclusions

Continuous carbonation experiments were carried out in a fast fluidized bed reactor where particle feeder was used to simulate the particle recirculation with accurate measurement. On the basis of the experiments and modeling of the carbonator reactor the following conclusions are obtained.

- High CO_2 capture efficiency can be obtained in the carbonator even with sorbent material having low CO_2 capture capacity.
- The most influencing parameter on the performance of carbonator is the inlet calcium to carbon ratio.
- The carbonator model was used to simulate different operating conditions relevant for industrial process.
- The modeling results show that a particle recirculation rate (feed rate) of 2-5 kg/m^2s is sufficient to achieve about 90% CO_2 capture efficiency.
- Carbonation experiments with a smaller particle size (0.09-0.25 mm) were carried out using large sand particles as the bed material, which enhanced the fluidization properties. So, cement raw meal, which has fine particles, can also be used in the fluidized bed reactor as a sorbent. This facilitates easy integration of the carbonator into the cement production process.
- The experimental results for simultaneous SO_2 and CO_2 capture show that the presence of SO_2 up to 1200 ppmv had no significant effect on the CO_2 capture efficiency.

More work is required to include the effect of SO_2 capture simultaneously with CO_2 in presence of H_2O. Further, more work is also required to evaluate the detailed effect of particle size, which will influence both the hydrodynamics and the particle conversion in the carbonator.

6. Process Simulation of a Cement Plant Integrated with the Carbonate Looping Process

6.1 Introduction

Two options for reducing CO_2 emissions from cement production were investigated by the ECRA[15]: 1) full oxy-fuel technology and 2) partial oxy-fuel technology. Full oxy-fuel technology is suitable for a new plant due to changes in the kiln operating conditions. In partial oxy-fuel technology, where only a part of the total CO_2 emissions is captured, two scenarios have been investigated: 1) two string pre-heater towers and 2) a single pre-heater tower where the flue gas from the kiln is let off, capturing only CO_2 from the calcination step. Partial oxy-fuel technology has been shown to be applicable for retrofitting, but with constrains; one of the main constraints is the recirculation of CO_2 gas to match the gas-to-solid ratio in the pre-heater section of the normal plant as the kiln flue gas is not directed to pre-heater tower. However, even with partial oxy-fuel technology, it is expected that the operating conditions will change significantly, which might have severe effects on the efficiency of the process. So, CO_2 capture from a new plant is relatively easier compared to the retrofitting option.

A third alternative was investigated in this chapter for a new plant to capture maximum CO_2 from the flue gas by integrating the carbonate looping process with the cement pyro-process. For easy integration, calcined cement raw meal can be used as the sorbent, according to the results from the cycle experiments described in Chapter 3. The new integrated process system consists of a dual fluidized bed reactor integrated with a rotary kiln for clinker production along with CO_2 capture. The dual fluidized bed reactor will be the oxy-calciner and the carbonator. The CO_2 capture capacity of clay mixed with limestone in fluid bed (Chapter 4) was similar to the TGA cycle experiment results

(Chapter 3). However, the particle size used in these experiments was much larger compared to cement raw meal. In Chapter 5, the performance of the carbonator was evaluated; a particle size of 0.09-0.25 mm was used, which is close to the cement raw meal particle size range. So, it is assumed that cement raw meal can be used in the fluidized bed reactor without fluidization problems.

The objective of this chapter was to determine: 1) the energy penalty for CO_2 capture and 2) the stream flow rates for the integrated process. The carbonate looping process integrated into a cement plant was simulated using the process simulation software PRO/II. Process modeling was carried out to simulate a cement plant without CO_2 capture as a reference case for comparison with the integrated process. In the simulation of the integrated system, the average conversion of calcined raw meal in the carbonator was dependent on the maximum CO_2 capture capacity as a function of the looping cycle number, which was estimated from the TGA experiments, and the inlet Ca/C ratio into the carbonator was estimated from previous experiments in the CFB reactor. The effect of the scale of the cement plant was investigated along with a sensitivity analysis of the important parameters that influence the cement plant with full CO_2 capture.

6.2 Process Simulation Tool

PRO/II is a process simulation program[155]. In this program, a process flow sheet consisting of different unit operations can be simulated to evaluate the mass and energy balance. This program has an inbuilt data bank component useful for process simulation. The components selected from the data bank load all the thermo-physical properties required for the simulation. The program needs the following inputs: stream flow rates and composition, inlet conditions, reaction stoichiometry and the desired unit operations. It calculates the mass and the energy balance for each unit operation following the sequence in accordance with the defined process flow scheme.

6.3 Assumptions for System Boundary and Inputs

There are many assumptions made to simplify the process simulation compared to the real process without compromising the final objective. In order to simulate the process model system, the system temperature boundary conditions for the reference case are defined in Table 6-1.

Table 6-1: Temperatures defined for the reference system.

	Value	Units
Inlet stream	25	°C
Flue gas outlet	300	°C
Clinker outlet	100	°C
Pre-calciner	900	°C
Kiln	1400	°C

The main inputs to the system are the fuel and the raw material composition. Pet coke was used as the fuel as it is one of the most common fuels used to provide energy in the cement industry[156]. The composition of the fuel used in this simulation is presented in Table 6-2 with ash being 0.3 wt.%, which has lower heating value (LHV) of 30 MJ/kg fuel (ash-free). The composition of the fuel presented here excludes the ash content. It is assumed that ash in the fuel ends up in the final product. Furthermore, the composition of cement raw meal is controlled by taking into account of the fuel ash content to maintain the desired quality.

Table 6-2: Composition of pet coke in weight % (ash-free basis).

Fuel	Carbon	Hydrogen	Oxygen	Sulfur	Nitrogen	Moisture
Wt.%	82.23	3.09	0.5	5.5	1.9	6.78

Complete combustion of pet coke with 10% excess air results in flue gas, as summarized in Table 6-3. The composition of flue gas is given before desulfurization and deNO_x according to the stoichiometric[157].

Table 6-3: Composition of flue gas from the combustion of pet coke.

	CO_2	N_2	O_2	SO_2	NO	H_2O	Total
Wet mol.%	16.07	76.71	1.97	0.40	0.32	4.53	100.00
kg/kg fuel	3.01	9.16	0.27	0.11	0.04	0.35	12.94

The other input to the simulation is the composition of the raw meal. In this simulation, only four main components of the cement raw meal were used, as the other components are present in minor fractions and it is assumed that these minor components have no significant effects on the simulation results. The composition of the assumed cement raw meal and clinker, based on the main components, is summarized in Table 6-4.

Table 6-4: Composition of cement raw meal and clinker in weight %.

Components	CaO	SiO_2	Al_2O_3	Fe_2O_3	CO_2
Raw meal [wt.%]	42.3	15.64	4.91	3.91	33.24
Clinker [wt.%]	63.36	23.43	7.35	5.86	0

In the process simulation, the calciner, the carbonator and the kiln were simulated as an isothermal conversion reactor. In these reactors, the conversion of input streams is defined at a fixed reactor temperature. The reactor evaluates the product stream composition based on the defined conversion, and the energy balance is evaluated based on the inlet stream temperature and reactor temperature. The heat of the reaction is evaluated based on the degree of conversion. The reactor energy balance is estimated as reactor duty, which is the result of energy consumed/released to heat/cool input flow streams to the reactor temperature and the heat of the reaction released or consumed by the reactions. Negative reactor duty means energy is released from the system and positive reactor duty means energy

has to be supplied for defined reactions to be carried out. The reactions defined in the process simulation tool are listed below as equations 6-2 to 6-8. The combustion of fuel includes following reactions. The heat of reaction was estimated by the process simulation tool and was verified by the standard reference[158].

$$C_cH_hS_sN_nO_o \cdot (H2O)_w + 1.1(c + h/4 + s + n/2 - O/2)O_2 \rightarrow cCO_2 + (H/2 + w)H_2O + sSO_2 + nNO \quad \text{6-1}$$

This reaction was defined in the reaction data for the simulation as the following reactions.

$$C + O_2 \rightarrow CO_2 \ \Delta H_r = -32MJ/kgC \quad \text{6-2}$$

$$H_2 + 0.5O_2 \rightarrow H_2O \ \Delta \mathrm{H}_r = -120MJ/kgH_2 \quad \text{6-3}$$

$$S + O_2 \rightarrow SO_2 \ \Delta \mathrm{H}_r = -17.5MJ/kgS \quad \text{6-4}$$

$$N_2 + O_2 \rightarrow 2NO \ \Delta H_r = 6.4MJ/kgN_2 \quad \text{6-5}$$

Along with combustion, the following reactions were defined for the calcination, carbonation and sulfation reactions, respectively, as:

$$CaCO_3 \rightarrow CaO + CO_2 \ \mathrm{H}_r = 1.77MJ/kgCaCO_3 \quad \text{6-6}$$

$$CaO + CO_2 \rightarrow CaCO_3 \ \mathrm{H}_r = -1.77MJ/kgCaCO_3 \quad \text{6-7}$$

$$CaO + 0.5O_2 + SO_2 \rightarrow CaSO_4 \ \mathrm{H}_r = -3.68MJ/kgCaSO_4 \quad \text{6-8}$$

6.4 Normal Cement Plant Process Description

In the modern dry cement pyro-process with a pre-heater and pre-calciner, the energy consumption is in the range of 2.9-3.4 MJ/kg cl[9,156]. The reference system considered here is the modern dry process with a pre-heater and pre-calciner. Figure 6-1 shows the main components: a pre-heater, a pre-calciner, a kiln and a cooler with the mass and the energy balance on the basis of 1 kg of clinker. The pre-heater is simulated as a simple heat exchanger where the hot flue gases from the pre-calciner are used to pre-

heat the cold raw meal. The pre-heated raw meal, fuel, tertiary air and hot gases from the kiln enter the pre-calciner. In the calciner, combustion of fuel in 10% excess air is carried out along with calcination of raw meal. An isothermal (900°C) conversion reactor is used to simulate this process, where the 100% conversion of fuel, 90% of limestone in the raw meal is calcined and SO_2 released from the fuel and present in the hot flue gas from the kiln is captured by the calcined raw meal, resulting in 1.4 wt% of SO_3. The value is below the defined limit required in the clinker for Portland cement, which is 3 wt.%[9]. The reference cement plant operating parameters are summarized in Table 6-5 on the basis of 1 kg of clinker produced.

Table 6-5: Main operating parameters of the reference plant on the basis of 1 kg of clinker

Main parameters of simulated reference plant		
Raw material	1.5	kg/kg cl
Limestone	1.13	kg/kg cl
Air flow to kiln (secondary air)	0.49	kg/kg cl
Air flow to pre-calciner (tertiary air)	0.73	kg/kg cl
Thermal energy	2.9	MJ/kg cl
Flue gas	1.81	kg/kg cl
CO_2 emissions	0.81	kg/kg cl

In the calciner conversion reactor, the reaction set is defined, which includes equation 6-2 to 6-6 and 6-8. The calcined raw meal from the pre-calciner is heated with the hot flue gases from the kiln and the hot raw meal enters the kiln operated as an isothermal reactor at 1400°C. The kiln is simulated as a conversion reactor where complete combustion of fuel in 10% excess air and calcination of the rest of the limestone is carried out. It is assumed that the hot raw meal undergoes a series of reactions[159] to form clinker in the kiln. The hot clinker is cooled to 100°C using cold air, and the resulting hot air is used for combustion in the kiln and in the pre-calciner.

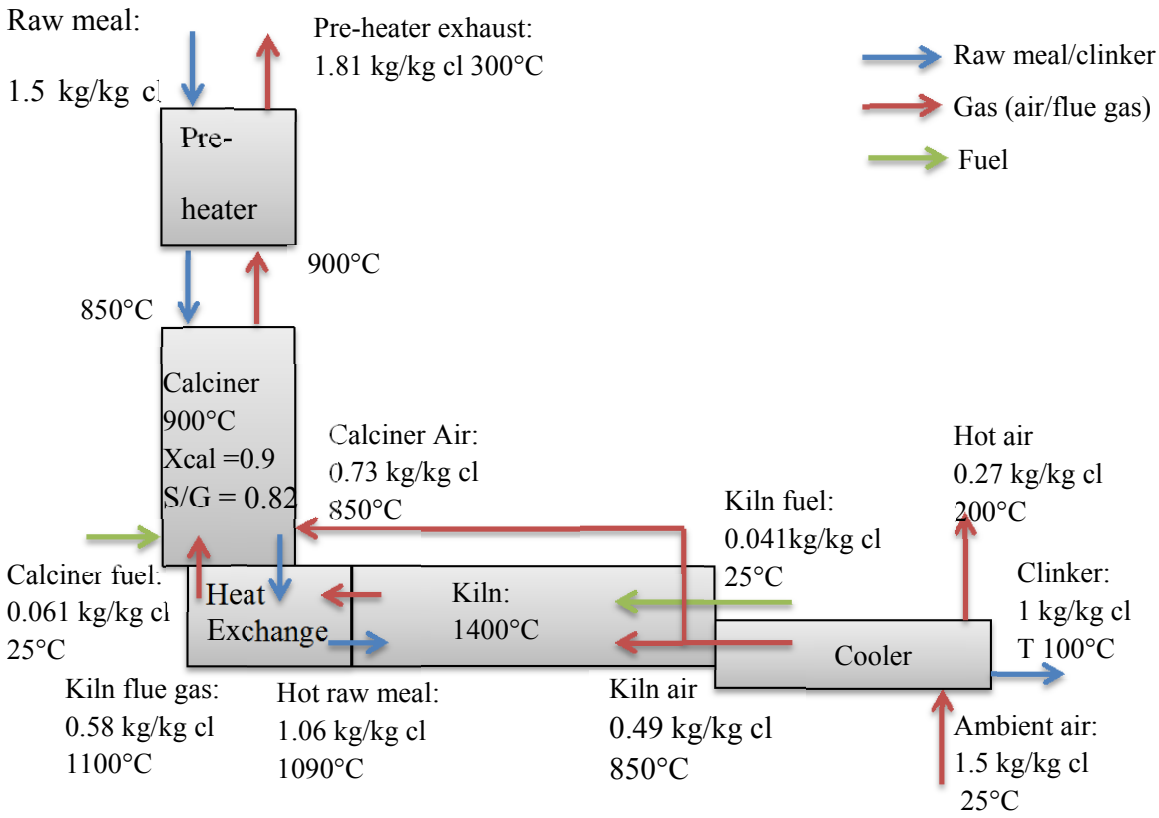

Figure 6-1: Reference pyro-process model system on the basis of 1 kg of clinker.

6.4.1 Mass Balance

In order to produce 1 kg of clinker, the amount of raw meal required is 1.5 kg; the composition of the raw meal used in the simulation is presented in Table 6-4. The cold raw meal enters the system at 25°C, then is heated in the pre-heater section using hot flue gases from the pre-calciner. The hot raw meal enters the calciner operated as an isothermal reactor at 900°C. The energy required for the calcination reaction is supplied by the combustion of fuel (0.061 kg/kg cl) using tertiary air (0.73 kg/kg cl). The calcined raw meal enters the rotary kiln operated at 1400°C, which is also an isothermal reactor. The energy for heating the raw meal to 1400°C is supplied by the combustion of fuel (0.041 kg/kg cl) with

secondary air (0.49 kg/kg cl). The hot raw meal is assumed to be converted to clinker in the kiln and the hot clinker is cooled to 100°C using cold air, which is used as secondary and tertiary air while the rest can be sent to a heat recovery system. The composition of flue gas from the kiln and from the cement pyro-process is summarized in Table 6-6.

Table 6-6: Flue gas composition from the reference pyro-process model system on the basis of 1 kg/kg cl.

	Flue gas from pyro-process		Kiln flue gas	
Components	Mol [%]	Flow rate [kg/kg cl]	Mol [%]	Flow rate [kg/kg cl]
O_2	1.50	0.03	2.03	0.01
N_2	61.28	0.94	72.20	0.38
CO_2	33.45	0.81	21.16	0.17
SO_2	0.00	0.00	0.38	0.00
H_2O	3.60	0.04	4.23	0.01
NO	0.18	0.00	0.21	0.00
Total	100	1.81	100	0.58

6.4.2 Energy Balance

The enthalpy balance of the system was estimated by defining the reference enthalpy to be 0 kJ/kg at 0°C and 1 atm. The specific heat capacity of each stream was obtained from the simulation tool and compared with reference data[5]. The overall energy balance is summarized in Table 6-7. The main energy input is from the combustion of fuel, which is 2.9 MJ/kg cl. The other considered input is the energy released from the clinkering reaction in kiln and the sulfation reaction (6-8), which accounts for 318 kJ/kg cl and 87 kJ/kg cl by capturing SO_2 (0.0045 kg/kg cl from the kiln and 0.0068 kg/kg cl from the calciner), respectively.

Table 6-7: Enthalpy balance for the reference system on the basis of 1 kg of clinker.

Input	Total Mass Rate	Temperature	Total C_p	Total Specific Enthalpy
	kg / kg cl	°C	kJ/kg°C	kJ / kg cl
Air in	1.5	25	1.01	18
Fuel to pre-calciner	0.06	25	1.35	2
Raw meal	1.5	25	0.79	29
Fuel to kiln	0.04	25	1.35	1
Energy input	-	-	-	2850
Energy from sulfation of CaO	-	-	-	87
Energy from clinker formation	-	-	-	318
Total input				3316
Output	Total Mass Rate	Temperature	Total C_p	Total Specific Enthalpy
	kg / kg cl	°C	kJ/kg°C	kJ / kg cl
Clinker	1	100	0.88	88
Exhaust gas	1.81	300	1.08	586
Hot Air	0.28	200	1	56
Calcination	-	-	-	2013
Energy losses	-	-	-	469
Total out				3212

The energy requirement for producing 1 kg of clinker, as estimated from the simulation results, is 2.9 MJ/kg cl. This estimated value lies in the expected range, indicating the accuracy of the process model, considering many simplifying assumptions to simulate the process. It can be seen that the major fraction of the fuel (60 w/w%) is consumed in the calciner due to the endothermic calcination reaction. The remaining fuel is consumed in the kiln for the clinker reaction at a higher temperature. The total energy loss from this process was assumed to be around 15% of the total energy input, which was

estimated for a plant with capacity of 3000 tons/day[160]. In a cement plant, low quality thermal energy can be recovered from the hot gases leaving the system using waste heat recovery systems. Thus, from the reference simulation model, the energy required for 1 kg of clinker is 2.9 MJ, with 0.8 kg CO_2 released and around 0.6 MJ/kg cl (exit flue gas and hot air from clinker cooler) of heat is available as the low quality thermal energy, which is difficult to recover. These values will be compared with the integrated process model for an evaluation of the carbonate looping process.

6.5 Integrated Process System

In order to reduce CO_2 emissions from the cement production process, the carbonate looping process has to be integrated into the cement pyro-process. In this process, cement raw meal is used as a sorbent for easy integration; its behavior as a sorbent was presented in Chapter 3.

The integration can be performed by connecting the dual fluidized bed reactors with the kiln. The integrated process is outlined in Figure 6-2. In this system, a separate oxy-fuel calciner is used instead of an in-line calciner in the normal cement plant. The heat recovery from the hot kiln flue gases is carried out by heating the fresh raw meal before directing the flue gases into the carbonator. In the oxy-calciner, the raw meal is calcined in a CO_2-rich atmosphere and the CO_2-rich flue gas at 950°C is directed for heat recovery before it can be sent to storage. The calcined raw meal from the calciner is used for both clinker production and for the CO_2 capture from the kiln flue gas. In the carbonator, CaO in the calcined raw meal reacts with CO_2 in the flue gas from the kiln and CO_2 lean flue gas is released into the atmosphere. The carbonated raw meal is recycled back to the oxy-calciner along with fresh raw meal. The CO_2 lean flue gas at 650°C is cooled by extracting energy before letting it off into the atmosphere.

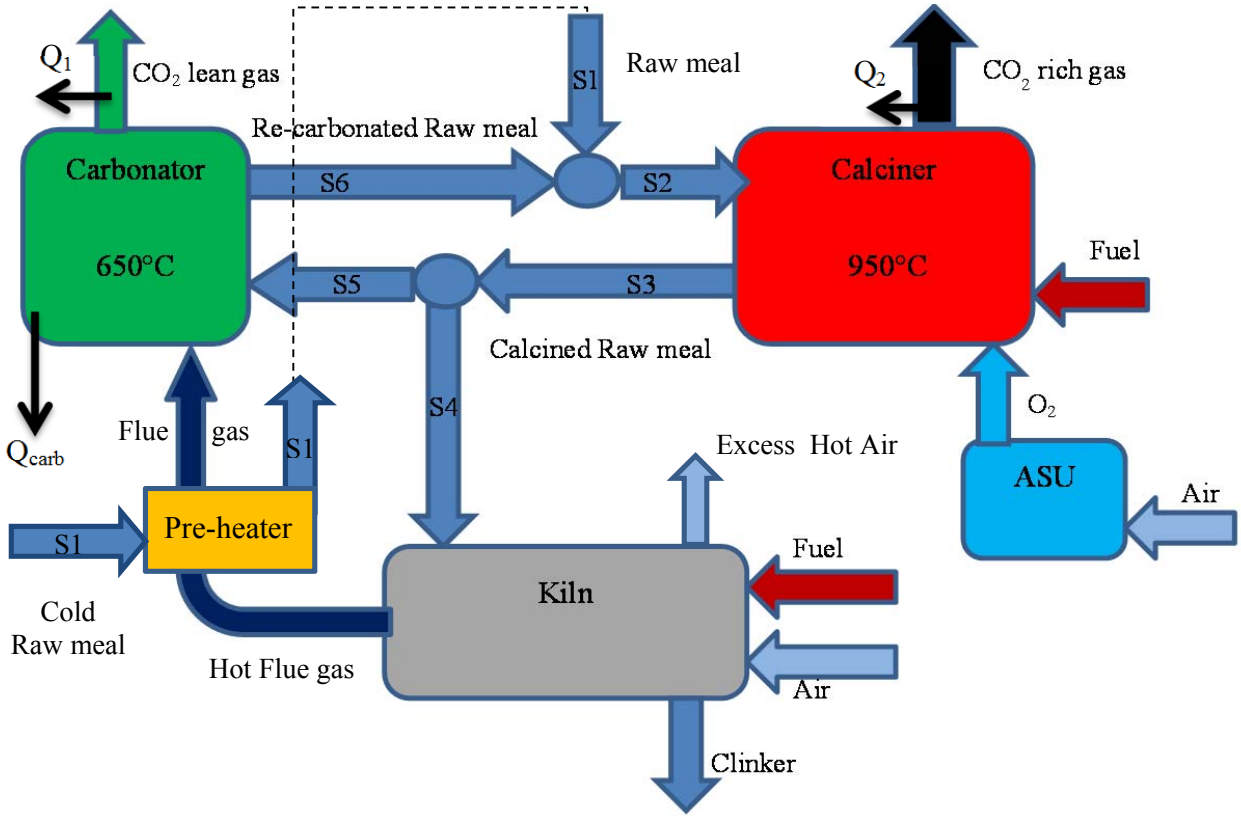

Figure 6-2: Schematic of the carbonate looping process integrated into the kiln.

Further the carbonation is an exothermic reaction, so energy from the carbonator has to be extracted for maintaining a constant temperature in the reactor. Since the whole process is carried out at a high temperature (650-950°C), the high quality energy from the carbonator (Q_{carb}) as well as the exit flue gases from the calciner (Q_2) and the carbonator (Q_1) can be used for generating electricity. The energy recovery potential from the carbonate looping process is the main advantage of this process compared to other alternatives such as the partial oxy-fuel, the full oxy-fuel or the amine processes. In setting up this model in PRO II, the reference pyro-process model was modified by changing the in-line pre-calciner in to a separate line oxy-calciner and directing flue gas from the kiln into a separate reactor (carbonator) where CO_2 from the flue gas reacts with calcined limestone in the raw meal. The

description of the main unit processes and the solution for this model was achieved in the following sequence: the kiln, the carbonator and the oxy-calciner due to the recirculation stream from the carbonator to the oxy-calciner.

Kiln

The first mass balance for the kiln was performed where 90% calcined raw meal was the input with a stream flow equivalent to the production capacity. For the initial run, the fuel into the kiln was similar to the reference case where the temperature of the kiln was set to 1400°C. The complete combustion of fuel in 10% excess air was assumed. The flue gas composition and the flow rate were estimated based on inlet stream flow rates to the kiln. The flue gas stream from the kiln was directed to the carbonator for CO_2 capture by CaO in the calcined raw meal.

Carbonator

The carbonator is an isothermal reactor operated at 650°C, where the carbonation and sulfation reactions take place according to equations 6-6 and 6-7. In the carbonator, the CO_2 capture efficiency of the system is defined as 90%, which was estimated from the performance of the carbonator in Chapter 5. Complete capture of SO_2 occurred due to the high calcium to sulfur ratio, as observed in the experimental results in Chapter 5. The performance of the carbonator was mainly dependent on the inlet Ca/C ratio, as presented in Chapter 5 (Figure 5-10), where the CO_2 capture efficiency of the carbonator increased with an increasing inlet Ca/C ratio, but the conversion of CaO peaked with an increasing inlet Ca/C ratio and subsequently dropped to a lower value. Figure 6-3 summarizes the performance of the carbonator using raw meal as the sorbent, estimated from the experimental data. In this figure, the normalized conversion of the CaO in the raw meal as a function of the inlet Ca/C ratio

was derived from the CFB experiments, whereas the performance of the carbonator was estimated according to equation 6-14, where $X_{\max,raw\ meal} = 0.15$ from the TGA experiments.

$$Ecarb = (Ca/C) \cdot \left(X_{Carb}/X_{\max}\right)_{\exp} \cdot X_{\max,raw\ meal} \qquad 6\text{-}9$$

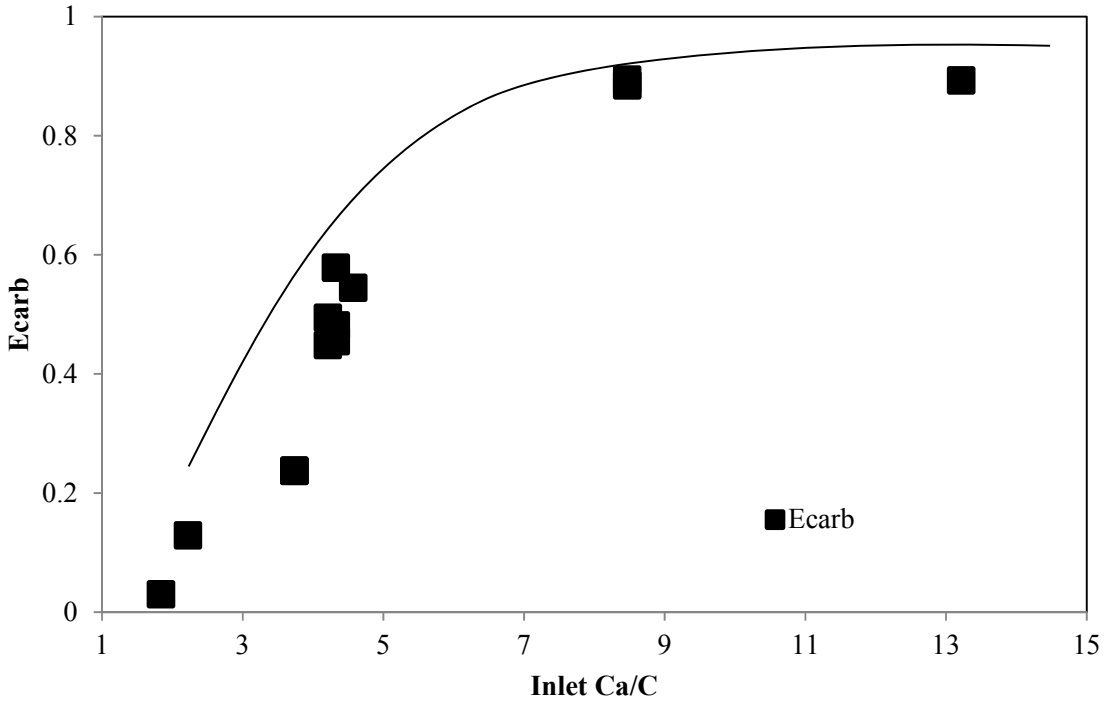

Figure 6-3: Influence of the inlet Ca/C ratio on the performance of the carbonator and the normalized average conversion of CaO in the cement raw meal.

Thus, based on the experimental results (average conversion of the bed as a function of the inlet Ca/C ratio) from the CFB reactor and the maximum CO_2 capture capacity of cement raw meal from the first TGA cycle experiments, the required inlet Ca/C ratio can be determined for 90% CO_2 capture efficiency, i.e. 8.5. In the above mentioned procedure, the optimum inlet Ca/C ratio was estimated assuming that the maximum CO_2 capture capacity was 15% for the particles, but in reality, this

decreases with an increasing number of cycles. However, it was not possible to determine the cycle number of individual particles that circulated between the calciner and the carbonator. So, a second procedure was used to determine the inlet Ca/C ratio using a mathematical formulation employing a "sum of series", which was also applied by Abanades[19]. The optimum flow rate of the calcined raw meal into the carbonator was estimated as it is dependent on the flow rate of CO_2 into the carbonator and the CO_2 capture capacity of the raw meal, which decreases with an increasing number of looping cycles. The cycle experimental results for the cement raw meal (presented in Chapter 3) can be formulated using the following equation 6-10:

$$X_N = \frac{1}{\left(\frac{1}{1-X_r}\right) + kN} + X_r \qquad \text{6-10}$$

The two parameters were estimated using the correlation equation 6-10 and the TGA experimental data from chapter 3 (pg. 79) as: $X_r = 0.055$ and $k = 8.7$.

The CO_2 capture capacity of the raw meal in the carbonator is a function of the flow rate of fresh limestone in stream S1 ($F_o = S1 x_{CaCO_3,1} / M_{CaCO_3}$) and that of calcined limestone in the re-circulated stream S3 into the carbonator ($F_r = S3 x_{CaO,3} / M_{CaO}$). These two stream flow rates determine the fraction of material recycled in the Nth cycle according to the following equation[19]:

$$r_N = \left(\frac{F_r / F_o}{F_r / F_o + 1} \right)^N \cdot \left(\frac{F_o}{F_r} \right) \qquad \text{6-11}$$

where r_N is the fraction of calcined limestone experiencing the Nth cycle. The average CO_2 capture capacity in the carbonator is a function of the CO_2 capture capacity in the Nth cycle (X_N) and the fraction of material recycled for the N^{th} time, according to following equation:

$$X_{ave} = \sum_{N=1}^{\infty} X_N \cdot r_N \qquad \text{6-12}$$

The average conversion of calcined limestone in the carbonator was estimated using an iterative procedure programmed in Matlab. The inputs for this procedure to determine the average conversion of the carbonator were the molar flow rate of CO_2 (F_{CO_2}), the molar flow rate of calcined limestone in the purged raw meal (F_o), the residual CO_2 capture capacity of CaO in the cement raw meal (X_r), the decay constant (k), the CO_2 capture efficiency ($Ecarb$) and the looping cycle number (N), which can be a large number according to the infinite sum series. However, the fraction of raw meal cycling more than 10 times is insignificant according to the results presented in Figure 6-5. The initial average conversion of the carbonator was guessed to estimate the molar flow rate of calcined limestone into the carbonator (F_r), thereby re-evaluating the average conversion according to equations 6-10 to 6-12. If the difference between the average conversion and the guessed value is less 0.001, then the estimated F_r is considered to be the optimum value. Otherwise, a new guessed value is used and the process is repeated until the convergence criteria are met. The flow sheet in Figure 6-4 illustrates the calculation procedure.

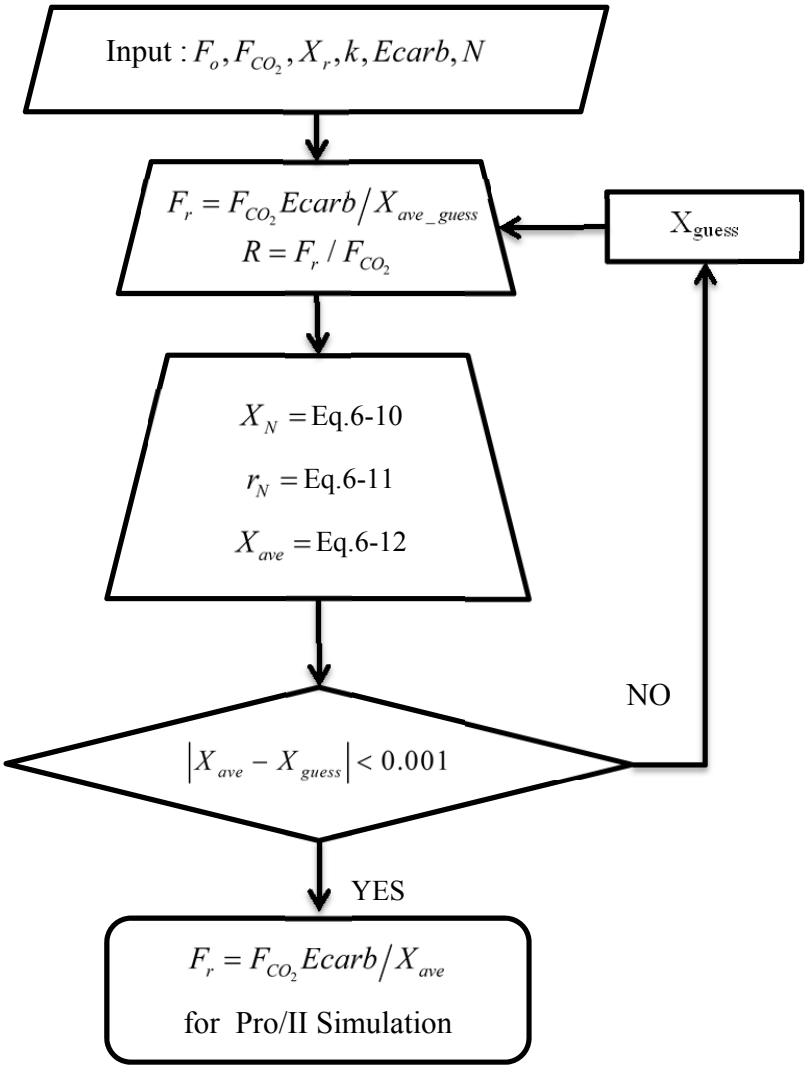

Figure 6-4: Flow sheet for the optimum flow rate of recycled calcined limestone in the integrated process.

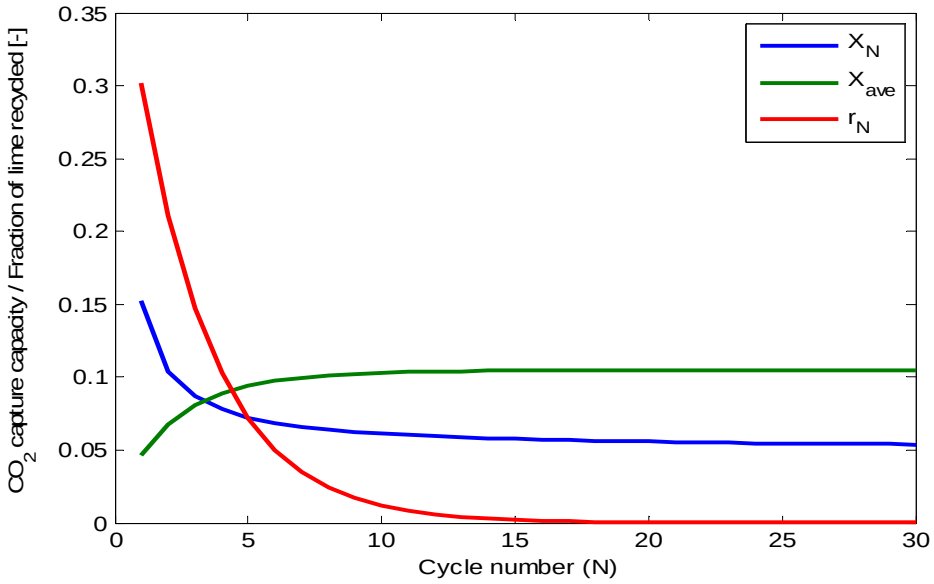

Figure 6-5: Estimation of average conversion of calcined raw meal in the carbonator with 90% capture efficiency.

Using the above procedure, the optimum value for (F_r) is estimated for the CO_2 flow rate ($2.8e^{-3}$ kg-mol/kg cl) from the kiln into the carbonator. Based on this procedure, the estimated inlet Ca/C ratio is 9. Thus, the two different procedures used for estimating the inlet Ca/C ratio and the average conversion of CaO in the carbonator match for the desired carbonator performance, which serves as a cross-verification of the results. The optimum value for F_r is the inlet stream flow rate to the carbonator and with a defined capture efficiency, the composition and flow rate of the exit solid stream and gas can be estimated.

Oxy-calciner

The solid stream from the carbonator is separated from the gas stream and mixed with a fresh raw meal stream. This stream flows into the oxy-calciner, operated as an isothermal reactor at 950°C, where 90% calcination of limestone was assumed to match the conditions of the reference case. The energy

required for the calcination of limestone and for heating the inlet stream to 950°C was estimated and the required energy was supplied by the combustion of fuel using pure O_2. The complete combustion of fuel was carried out in 10% excess O_2. Subsequently, the calcined raw meal stream from the oxy-calciner was split into two streams to match the stream flow rate to the kiln and the carbonator.

In the next step, the inlet into the kiln and carbonator were replaced with the outlet stream from the calciner using a controller to vary the flow rate of fresh raw meal and recalculating the mass balance for the oxy-calciner, kiln and carbonator. The converged process model was verified to check the energy balance for the kiln, the carbonator and the oxy-calciner. The fuel input for the kiln and oxy-calciner were verified such that the reactor duty was close to the reference model. After a fuel input change, the conversion of the calcined limestone in the raw meal in the carbonator was checked, and if necessary, the stream flow rate was optimized. The process had to be repeated after any changes to the process simulation conditions.

6.5.1 Mass Balance

The integrated system shown in Figure 6-6 is based on the necessity to extract high quality thermal energy for captive power generation. Table 6-8 summarizes the flow rates of the main streams in the integrated system on the basis of 1 kg cl produced. Considering the mass balance of raw materials and the final product of the system, 1.5 kg of fresh raw meal was required for 1 kg of clinker produced, similar to the reference case. The composition of raw meal was similar to the reference case, whereas the final clinker composition showed a small deviation in the fraction of calcium sulfate. The high sulfate content (SO_3 w/w% is 2.4) was due to the capture of SO_2 generated from fuel combustion, which was relatively high compared to the reference system (1.4 wt.%). In the oxy-calciner, along with 1.5 kg/kg cl of fresh raw meal, 2.56 kg/kg cl of partially re-carbonated raw meal entered the calciner. In

the calciner, 90% of $CaCO_3$ was calcined and 100% of SO_2 generated (0.0165 kg/kg cl) from the fuel combustion was captured by the calcined limestone.

Table 6-8: Flow rate and composition of main streams from the integrated process system model for 1 kg of clinker.

Components [molar fraction]	Fresh raw meal	Final product clinker	Carbonated raw meal from carbonator	Fresh and carbonated raw meal to oxy-calciner	Calcined raw meal to carbonator	Calcined raw meal to kiln
$CaCO_3$	0.69	0.00	0.09	0.28	0.03	0.03
CaO	0.00	0.67	0.57	0.40	0.65	0.65
SiO_2	0.24	0.24	0.24	0.24	0.24	0.24
Al_2O_3	0.04	0.04	0.04	0.44	0.04	0.04
Fe_2O_3	0.02	0.02	0.02	0.02	0.02	0.02
$CaSO_4$	0.00	0.02	0.02	0.02	0.02	0.02
Total[kg-mol/kg cl]	0.016	0.016	0.04	0.05	0.04	0.02
Total [kg /kg cl]	1.50	1.00	2.55	4.06	2.43	1.04

The combustion of 0.15 kg fuel/kg cl was carried out utilizing 0.43 kg of O_2/kg cl, resulting in 1.15 kg/kg cl flue gas, which included CO_2 released from the calcination of the limestone. The flow rate of the calcined raw meal stream from the oxy-calciner was 3.45 kg/kg cl, which was split into two streams: 1) 1.04 kg/kg cl for clinker production and 2) 2.43 kg/kg cl into the carbonator to capture CO_2 in the flue gas from the kiln. In the kiln, 1 kg cl was produced by complete calcination $CaCO_3$ in the raw meal; 1.05 kg/kg cl and 0.46 kg/kg cl flue gas was released containing 26 w/w% CO_2. The flue gas was generated from the complete combustion of fuel and the calcination of remaining un-calcined limestone in the raw meal. The flue gas from the kiln entered the carbonator and 90% of the CO_2 and 100% of the SO_2 in the flue gas was captured. The flue gas from the carbonator (0.35 kg/kg cl) was

released, containing 2 vol.% CO_2. The overall mass balance of the integrated system is summarized in Figure 6-6, and the flow rates of flue gas from the oxy-calciner, the carbonator and the kiln are presented in Table 6-9.

Table 6-9: Flue gas composition from the integrated model system for 1 kg of clinker.

Components	Carbonator	Calciner	Kiln
O_2	0.19	0.04	0.02
N_2	0.90	0.00	0.75
CO_2	0.02	0.85	0.19
SO_2	0.00	0.00	0.00
H_2O	0.05	0.10	0.04
NO	0.00	0.01	0.00
Total [kg mol/kg cl]	0.01	0.03	0.02
Total [kg /kg cl]	0.35	1.15	0.46

6.5.2 Energy Balance

The detailed energy balance of the overall system is summarized in Table 6-10. The total enthalpy input to system was estimated to be 6.5 MJ/kg cl. Of this, 5.6 MJ/kg cl was from the fuel, while around 0.6 MJ/kg cl was from the exothermic carbonation and sulfation reactions. The enthalpy output from the system was estimated to be 6.5 MJ/kg. Of this, around 2.5 MJ/kg cl was consumed for the endothermic calcination reaction. However, 2.7 MJ/kg cl (from the WHRS) was available as high quality energy for electricity production, along with 0.8 MJ/kg cl as low quality energy similar to the energy available in a normal cement plant.

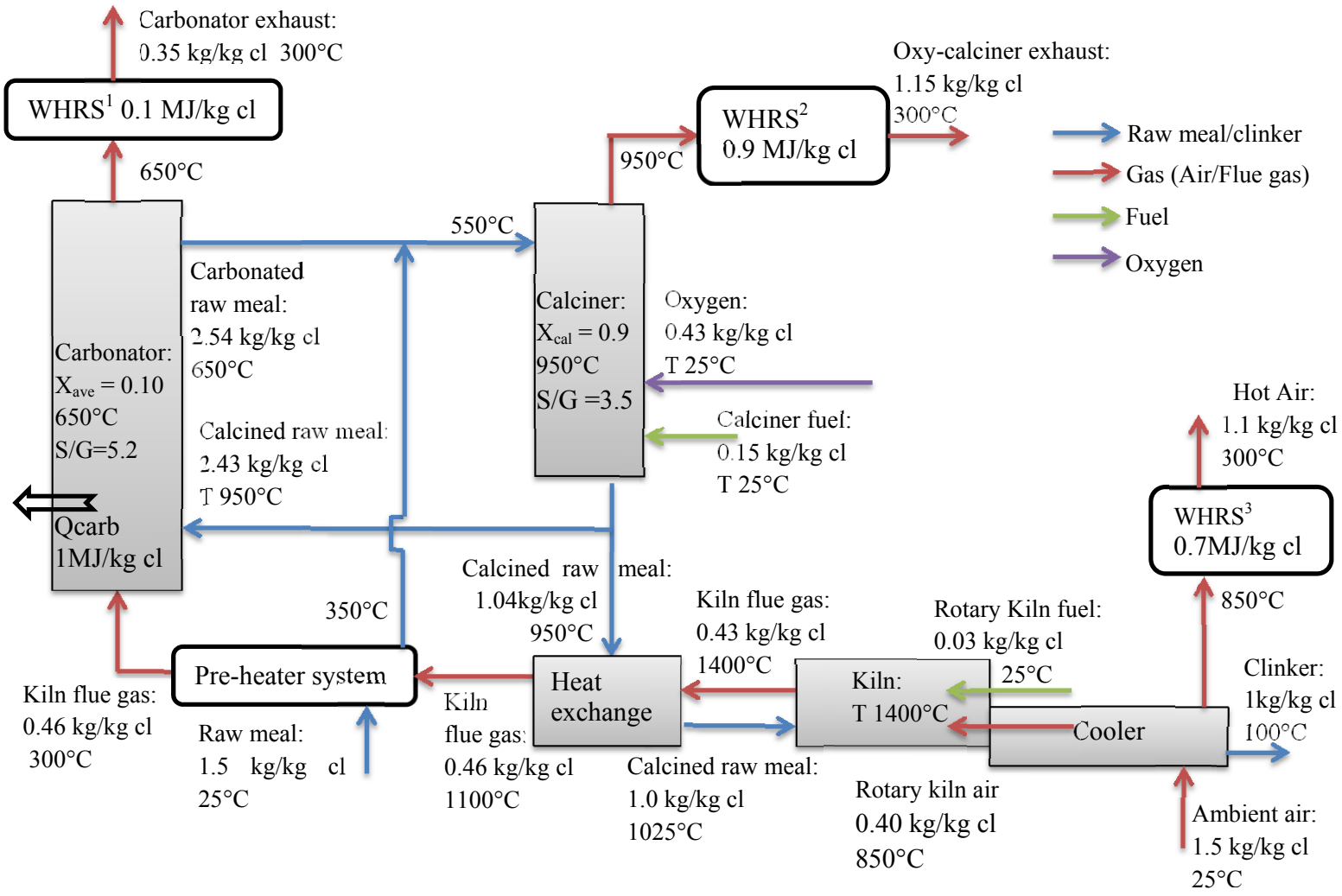

Figure 6-6: Integrated process model of carbonate looping into pyro-process system for producing 1 kg of clinker.

Table 6-10: Enthalpy balance for the integrated system for 1 kg clinker.

Input	Total mass rate	Temperature	Total C_p	Total specific enthalpy
	kg/kg cl	°C	kJ/kg°C	kJ/kg cl
Oxygen to oxy-calciner	0.43	25	0.9	10
Fuel to pre-calciner	0.155	25	1.3	5
Fresh raw meal	1.5	25	0.79	30
Air to kiln	0.4	25	1.01	10
Fuel to kiln	0.031	25	1.3	1
Additional air	1.1	25	1.01	28
Energy input	-	-	-	5541
Energy from carbonation	-	-	-	452
Energy from sulfation	-	-	-	163
Energy from clinker formation	-	-	-	318
Total input				6557
Output	Total mass rate	Temperature	Total C_p	Total specific enthalpy
	kg/kg cl	°C	kJ/kg°C	kJ/kg cl
Clinker	1	100	0.88	88
Flue gas from calciner[2]	1.15	300	1.09	376
Flue gas from Carbonator[1]	0.35	300	1	105
Additional air from cooler[3]	1.1	300	1	330
Energy for calcination	-	-	-	2403
Energy loss	-	-	-	469
Energy for calcination in kiln	-	-	-	80
Energy from WHRS[1]	-	-	-	130
Energy from WHRS[2]	-	-	-	920
Energy from WHRS[3]	-	-	-	690
Energy form carbonator	-	-	-	1000
Total output				6591

Based on the mass flow stream from the process simulation of the integrated system, the flow rates of the streams are different from a normal cement plant. So, for CO_2 capture from the cement production process, applying the carbonate looping process requires significant changes. The major modification will be in the pre-heater section of the normal cement plant as it needs to be modified with the main objective of extracting energy from the hot kiln gas using fresh raw meal, thereby reducing the temperature of the flue gas to one suitable for pumping into the carbonator. Furthermore, the new pre-heater section might provide an opportunity to reduce the construction cost by using a more compact heater, as the flow rate of the gas is reduced by one quarter compared to the normal reference plant. For the calcination of raw meal and for CO_2 capture from the flue gas, a dual fluidized bed reactor is suitable with operating solid to gas (S/G) ratios (presented in Figure 6-6) at the lower end of large scale CFB reactors[136]. In these reactors, the carbonator can be operated in the fast fluidization regime and the calciner can be operated in the bubbling regime. Operating the calciner as the bubbling fluidized bed reactor will eliminate the high gas flow rate as a fluidizing gas, meaning that only O_2 can be used. However, in the oxy-fuel technology, the CO_2 recirculation flow rate is essential for controlling the temperature, but this might not be a problem in the carbonate looping process integrated into a cement plant due to the recirculation of raw meal. The energy required for the endothermic calcination reaction and for heating the raw meal to 950°C eliminates the requirement for CO_2 recirculation to control the temperature. The raw meal particle size range falls within the Geldart A or C[161] classification, which are difficult fluidize, but this challenge can be overcome by using inert particles to improve the bed fluidization properties, as demonstrated in the experiments (in Chapter 5) on 90-250 μm limestone particles using larger quartz sand particles.

Along with these units, the other new components are the interconnecting piping between the units, an air separation unit, a CO_2 processing unit and a waste heat recovery system to recover energy from different locations.

6.6 Comparison of Normal Cement Production and the Integrated Process

A major challenge of the integrated system is the electricity consumption of: 1) cryogenic oxygen generation (ASU), 2) CO_2 compression and purification (CPU), and 3) material (sorbent) recirculation. On the other hand, the integrated system has the potential to be self-sufficient in terms of electricity. Notice that the following analysis is simplified for the sake of comparison.

The power required for O_2 separation from air depends very much on scale and purity requirements. Since the production capacity of the ASU will be lower compared to a large power plant, a correlation was found to estimate the electricity for 97% O_2 purity from data presented by Palfreyman et al.[162] as:

$$El_{O_2} = -62.81\ln(x) + 728.91 \qquad 6\text{-}13$$

where x is the O_2 capacity (tons/day) and El_{O_2} the electricity consumption (kWhe/ton).

The electricity consumption of the CPU depends among other on the purity of CO_2 in the flue gas, which in turn depends on the O_2 purity and the amount of false air entering the process. For CO_2 concentrations in the range 72-93%, an electricity consumption of 120-95 kWhe/ton CO_2, respectively, has been reported.[163] In practice it is not possible to avoid air ingress, which on cement plants typically amounts to 8 vol-% of the exhaust gas. This results in a higher thermal energy demand, but, on the other hand, more energy is available for electricity production. With 97% O_2 purity and 8% air ingress, the flue gas CO_2 concentration reduces to 88 % (dry basis). In this case the CO_2 capture efficiency of CPU is about 95%[164] (the remaining 5% being lost with the vent gas stream) and the specific power requirement about 100 kWhe/ton CO_2 (compression to 15 MPa).[163,165]

The energy required for circulating the raw meal between the calciner and the carbonator was estimated from the energy consumed by material and gas transport in the standard cement pyro-process. This constitutes about 10% of the total electric energy consumed in the pyro-process.[166] Assuming the energy required for material transport proportional to flow rate, the energy demand for material transport in the integrated plant increases by a factor of 4/1.5=2.6 compared to the standard case. The sensitivity of this parameter is analyzed in the later section.

The self-sufficiency in terms of power requirement depends on the conversion efficiency of available thermal energy into electricity. This again depends on scale, e.g. the efficiency is only 20% on the scale of several MW, but increases to 45% on the several hundreds of MW scale.[167] A correlation was used to estimate the conversion efficiency based on the data provided by Spliethoff[167]:

$$\eta_p = 0.0434 \ln\left(Q_{th\_el}\right) + 0.15 \qquad \text{6-14}$$

where η_p is the efficiency and $Q_{th\_el}[MW]$ the thermal energy available for electricity generation.

Based on the above assumptions the additional electricity requirement of the integrated system, including ASU, CPU and material transport, can be calculated as function of plant capacity.

Figure 6-7 summarizes the results that clearly demonstrate the effects of scale. The electricity demand and production capacity seem to be balanced at scales from about 3400 ton per day. If the conversion efficiency was lower compared the estimated value using the equation 9 by 10 and 20%, then the electricity demand and production capacity appears to be balanced at scale from about 5900 and 11000 ton per day, respectively.

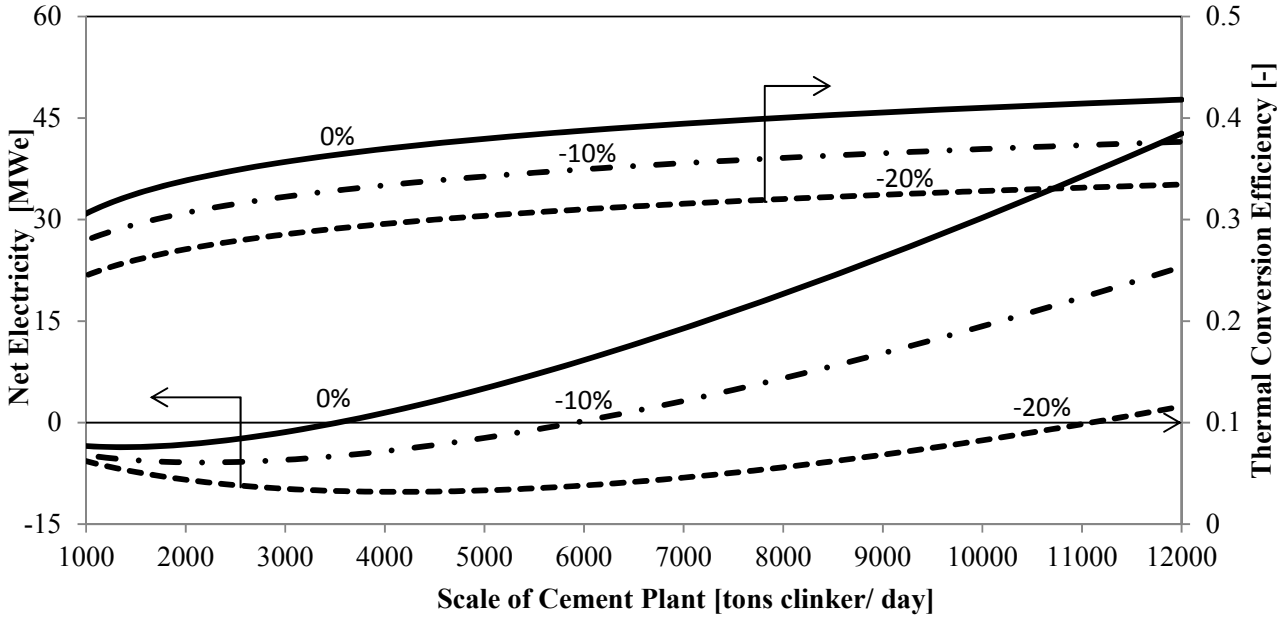

Figure 6-7: Net electricity production or demand versus clinker capacity of the integrated system for three different electricity generation efficiencies.

The overall thermal performance (η) of the two systems can be evaluated by:

$$\eta = \frac{Q_R}{Q_{th}}, \qquad 6\text{-}15$$

where Q_R is the energy consumed by reactions and Q_{th} the thermal energy supplied for 1 kg of clinker production. Table 6-11 summarizes the performance data of both systems. The CO_2 emission from the integrated plant includes 0.06 kg CO_2/kg cl from the CPU (vent gas). The additional energy demand for the integrated plant for CO_2 capture is 2.0 MJ/kg CO_2 captured. This value is however very dependent on the energy conversion efficiency.

Table 6-11: Comparison of the thermal efficiency of a standard and integrated system (basis: 1 kg of clinker), production capacity 3400 ton per day (energy conversion efficiency 0.36 for electricity production).

	Q_{th}	Q_r	η	CO_2 Emissions	Capture Energy
	MJ/kg cl	MJ/kg cl	-	kg/kg cl	MJ/kg CO_2
Reference system	3.9	2.0	0.51	0.9	-
Integrated system	5.6	2.4	0.42	0.07	2.0

6.7 Sensitivity Analysis

A sensitivity analysis was performed for a plant with a capacity of 3400 tons of clinker/day by varying the parameters to investigate the respective effects on the electricity power surplus or deficiency. A summary of the parameter sensitivity analysis is presented in Figure 6-8. Each parameter was varied by ± 50% to evaluate its effect on the electricity generation or consumption. The most sensitive parameter is the efficiency in converting thermal energy into electricity and the least sensitive parameter is the power for particle recirculation in the looping process. The sensitivity analysis of the power for operating the ASU and the CPU was similar. The electricity conversion efficiency was varied from 0.18 to 0.54, with the rest of the parameters held constant. The integrated plant was barely self-sufficient in this scenario with a base efficiency of 0.36. The assumed electricity demand for ASU was 276 kWhe/ton of O_2; this value is higher than the value present in the literature, which is only 200 kWhe/ton of O_2, in which case the integrated plant has room for lower conversion efficiency. Similarly, the electrical power for CO_2 compression was assumed to be 100 kWhe/ton of CO_2 for the base case. This value was varied from 150 to 50 kWhe/ton of CO_2. The integrated plant might need more power with a positive deviation in the power for compression. If the scale of the plant increases from 3100

tons of clinker/day to 12000 tons of clinker/day, then the room for lower efficiency increases from 0 to -23% compared to the base case. The relative room for power self-sufficiency increases even with a positive deviation in the parameters with an increase in the scale of the plant.

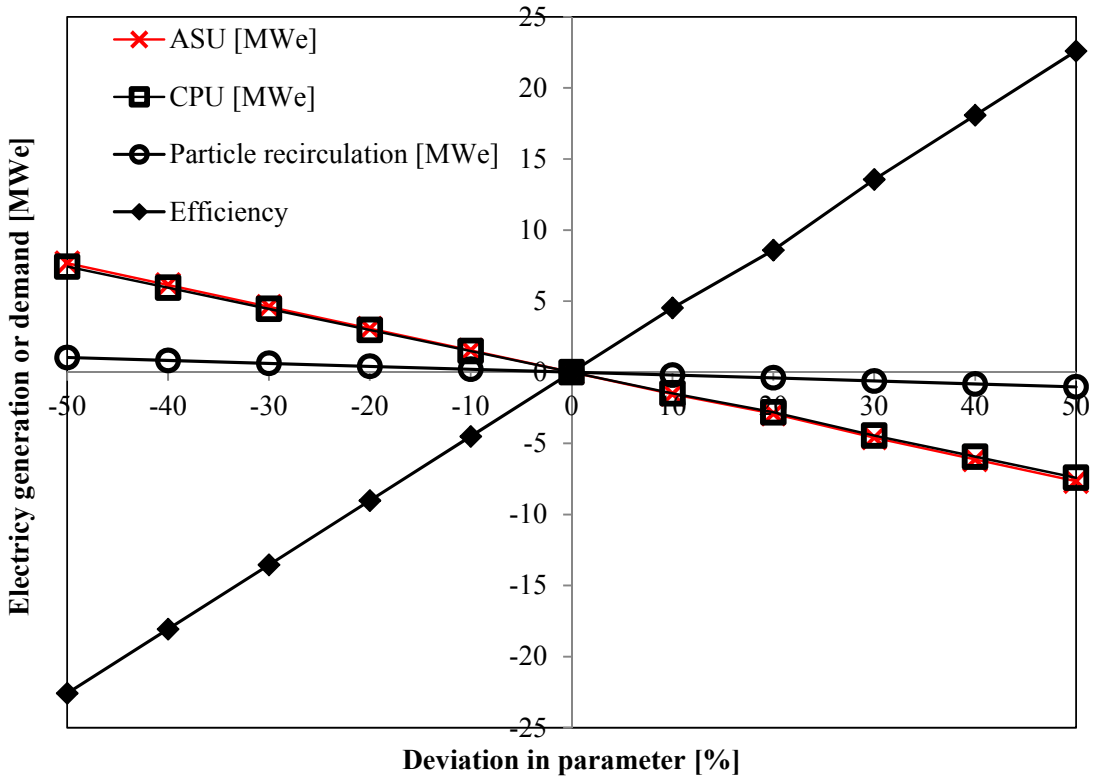

Figure 6-8: Sensitivity analysis of the integrated process for the assumed parameters by varying in the range of +/- 50% from the selected base case.

The results show that the carbonate looping process has the potential to reduce CO_2 emissions by more than 90% compared to a normal cement plant. Comparing the total energy demand for a normal cement plant with the carbonate looping integrated plant, this increases from 3.9 MJ/kg cl to 5.6 MJ/kg cl, which is 30% more energy required; these values include the thermal energy required for electricity generation. Thus, the carbonate looping process reduces CO_2 emissions from cement production with a

energy penalty of 2 MJ/kg CO_2, which is lower than wet post-combustion processes. Furthermore, this process is more efficient in a large scale plant than in low-capacity plants.

6.8 Conclusions

Based on the comparison of the reference cement pyro-process system and the integrated system, the following conclusions can be drawn:

- Integrating the carbonate looping process in to cement plant only reduces CO_2 emissions but also provides surplus energy for cogeneration to meets electricity demand of the whole process.
- The specific energy required for 1 kg of clinker increases from 3.9 MJ to 5.6 MJ, including thermal energy for electricity utilization.
- The scale of cement plant is critical for implementing the carbonate looping process with minimum capacity being in above 3400 tons of clinker per day.
- The efficiency of the WHRS is the most sensitive parameter affecting the self-sufficiency of the integrated system.
- The energy penalty for CO_2 capture is 2 MJ/kg CO_2.
- A comparison with the full oxy-fuel and partial oxy-fuel shows that each technology has its own drawbacks and advantages. Full oxy-fuel technology has high CO_2 capture efficiency but it has challenges in terms of additional electricity demand and sealing the entire system to avoid air exposure. Partial oxy-fuel technology can capture only part of the total CO_2 emissions along with higher electricity demand, but the implementation of this technology is relatively easy compared to the other options. The new alternative i.e. the carbonate looping

process provides an improvement over partial oxy-fuel technology in terms of CO_2 capture efficiency and over full oxy-fuel technology with no change in kiln operation along with avoiding CO_2 recirculation for temperature control due to large recirculation of raw meal. Moreover, the surplus energy spent can be recovered for cogenerating the necessary power.

7. General Conclusions and suggestions for future work

7.1 Conclusions

The main objective of this thesis was to provide scientifically-based knowledge regarding the carbonate looping process for reducing CO_2 emissions in the cement industry. In order to achieve the objective studies were carried out at different scales to understand the CO_2 reduction process systematically. The three scales are: 1) at particle scale, 2) at reactor scale and 3) at process scale. The particle scale investigations were carried out to understand the fundamentals in the carbonate looping process using cement raw meal as sorbent. The results from the particle scale formed the basis for investigating cyclic and continuous carbonation in a fluidized bed reactor for obtaining results applicable for scale up studies. The experimental results from the particle scale and the reactor scale were used in the process modeling and simulation to investigate the carbonate looping process for integrating into cement pyro-process.

Based on the systematic investigations, the main conclusions are summarized as follows:

- Raw meal can be used as the sorbent even though there are interactions between the lime and other components, especially under realistic calcination conditions. SEM, XRD and BET analyses indicated that sintering is the main reason for the observed decrease in the CO_2 capture capacity. A correlation was established between the surface area of the calcined mixture and the CO_2 capture capacity of the limestone in the mixture under realistic conditions. The XRD results show that the CaO crystallite size was not only influenced by the calcination conditions but, also by the components of the cement raw meal. The decay in the CO_2 capture capacity of the limestone in the raw meal was due to sintering, resulting in a change in particle morphology

and a larger CaO crystal size. The CO_2 capture capacity as a function of cycle number can be described by a two-parameter correlation, which was used for process simulation studies.

- In the fluidized bed reactor, different parameters were investigated such as the behavior of bed conversion compared to the TGA apparatus, the behavior of cement raw meal as the sorbent and the attrition of limestone particles. The rate of attrition for the Faxe Bryozo limestone was not severe under the current investigated experimental conditions. The loss of bed material due entrainment of fines was 2 wt% after the first calcination and diminished to close 0 wt.% after the ninth calcination cycle; the attrition rate constant was estimated to be $2.3e^{-5}$ [1/s] after 6 hours of batch operation. The conversion of calcined limestone in the TGA apparatus and in the fluidized bed reactor was investigated. The main difference between these two systems was the CO_2 concentration profile during the carbonation reaction. After considering the CO_2 concentration in the reaction zone, the reaction rate constant estimated from these two systems was in the rage of 2-3.5 [m^3/kmol·s] during the initial fast reaction regime, which decreased with an increase in conversion due to the change in reaction regime. The difference in the CO_2 capture capacity of the simulated raw meal and the Faxe Bryozo limestone was not significant in the fluidized bed reactor, since the calcination conditions during the cycle experiments were mild, similar to the experimental results from the TGA apparatus.
- In the carbonate looping process, the performance of the carbonator, which was operated as a circulating fluidized bed reactor, is very important. Experiments in the circulating fluidized bed reactor were performed to investigate the important parameters that control the performance of the carbonator. Experiments were performed under a controlled particle recirculation rate to evaluate the influence of the carbonator temperature, the CO_2 concentration, the particle

recirculation rate and the inlet Ca/C ratio. The results show that the most sensitive parameter on the performance of carbonator is the inlet Ca/C ratio. In the experiment, more than 80% of the inlet CO_2 was captured by highly deactivated limestone, which had a maximum CO_2 capture capacity of 11.5%, with an inlet Ca/C ratio of 13. So, the performance of the carbonator can be defined by the inlet Ca/C ratio, which can be estimated if the maximum capture capacity of limestone is known using the normalized bed conversion obtained from experiments as a function of the inlet Ca/C ratio.

- Finally based on the main experimental results, i.e. the CO_2 capture capacity of raw meal as a function of raw meal and the main parameters influencing the performance of the carbonator, a process model integrating the carbonate looping process with the cement pyro-process was simulated. The process simulation results indicate that the specific thermal energy, including electricity utilization, for producing 1 kg of clinker increased from 3.9 MJ in a normal cement plant to 5.6 MJ/kg cl in the integrated process system. Comparing the CO_2 emission, for 1 kg cl this was 0.9 kg in a normal cement plant, whereas in the integrated plant it was only 0.07 kg. The energy penalty for CO_2 capture by carbonate looping is 2 MJ/kg CO_2. The main outcome of the carbonate looping process is the potential to generate electricity sufficient to meet the needs of the cement plant, including the CO_2 capture units. This self-sufficiency in power demand increases with the size of the cement plant employing co-generation, with the lower limit being at least 3400 tons of clinker per day.

7.2 Future work

In the current study, the focus was mainly on a few fundamental points, as described above. However, more studies need to be carried out as listed below:

- Raw meal can be used as the sorbent for CO_2 capture, but its CO_2 capture capacity is much lower compared to limestone. One of the reasons for this is sintering, but the effect of different components present with the limestone has a unique effect and the exact mechanism for this behavior is still not clear. Further work on this could reveal the reason for this observation and provide the possibility to improve the CO_2 capture capacity of raw meal.
- The CO_2 capture capacity of raw meal was tested under ideal conditions, which has to be subject to realistic flue gas, which has three reactive components (CO_2, SO_2 and H_2O) with CaO and also the effect of ash components. As was observed, the each inorganic raw meal component has a unique effect on the CO_2 capture capacity.
- An engineering solution is needed to handle large flow streams between an oxy-calciner, a carbonator and a kiln with separate gas streams consisting of CO_2 lean and rich gases.
- Since the efficiency of energy recovery in the carbonator is critical for the carbonate looping process. A new system for extracting energy is needed to develop where the main challenge will to avoid coating of raw meal on the heat exchangers which might reduce the heat transfer efficiency.
- The main focus in this thesis was on CO_2 capture, but as oxy-fuel calcination is the first step in the carbonate looping process, a detailed investigation into the calcination process has be carried out to determine the optimum operating conditions in the calciner 1) so that the

maximum CO_2 capture capacity of limestone can be improved and 2) to ensure stable operation of the calciner as a fluidized bed reactor under oxy-fuel conditions by investigating the effect of reactor operating conditions on the fluidization of cement raw meal.

8. References

[1] Worrell E, Price L, Martin N, Hendriks C, Meida LO. *Carbon dioxide emissions from the global cement industry 1*. Annual Review Energy Environment **2001**;26:303-29.

[2] Olivier JG, Peters JA, Janssens-Maenhout G. *Trends in global CO_2 emissions 2012 report*. : PBL Netherlands Environmental Assessment Agency, **2012**.

[3] Qian Zhu. *CO_2 Abatement in the Cement Industry*. London: IEA, **2011**.

[4] Herzog T. *World greenhouse gas emissions in 2005*. World Resources Institute, Washington DC **2009**.

[5] Metz B, Davidson O, De Coninck H, Loos M, Meyer L. *Special Report on Carbon dioxide Capture and Storage*. IPCC special report on carbon dioxide capture and storage **2005**.

[6] Bosoaga A, Masek O, Oakey JE. *CO_2 Capture Technologies for Cement Industry*. Energy Procedia **2009**;1:133-40.

[7] Cembureau. *Activity Report 2011*. Rue d' Arlon 55-BE-1040, Brussels: Cembureau, *2012*.

[8] VDZ. *Enivorinmental Data of the German cement Industry*. Düsseldorf: Verein Deutscher Zementwerke, **2010**.

[9] Larsen MB. *Alternative Fuels in Cement Production. Alternative Fuels in Cement Production*, Technical University of Denmark, Department of Chemical Engineering **2007**.

[10] GHG I. CO_2 Capture in the Cement Industry.International Energy Agency Greenhouse Gas R&D Programme, Technical Study **2008**.

[11] Taylor HFW. Cement Chemistry. London: Thomas Telford, **1997**.

[12] FLSmidth A/S. *Dry process kiln systems*, **2013**.

[13] New Energy and Industrial Technology Development (NEDO). J*apanese Technologies for Energy Saving/GHG Emissions Reduction*, Kawasaki, Japan, **2008**.

[14] FLSmidth A/s. *Brouchure for kilns and firing, Rotax-2 development*.

[15] Gauthier D, Schneider M. *ECRA Technical Report CCS _Phase III*. Duesseldorf: European Cement Research Academy GmbH, **2012**.

[16] Lide DR, Bruno TJ. *CRC handbook of chemistry and physics*, CRC PressI Llc, **2012**.

[17] Silcox GD, Kramlich JC, Pershing DW. *A mathematical model for the flash calcination of dispersed calcium carbonate and calcium hydroxide particles*. Industrial Engineering Chemistry Research **1989**, 28:155-60.

[18] Shimizu T, Hirama T, Hosoda H, Kitano K, Inagaki M, Tejima K. *A twin fluid-bed reactor for removal of CO_2 from combustion processes*. Chemical Engineering Research & Design, **1999**,77:62-8.

[19] Abanades JC. *The maximum capture efficiency of CO_2 using a carbonation/calcination cycle of $CaO/CaCO_3$*. Chem Eng J , **2002**;90:303-6.

[20] Gupta H, Fan LS. *Carbonation-calcination cycle using high reactivity calcium oxide for carbon dioxide separation from flue gas,* Industrial Engineering Chemistry Research **2002**, 41:4035-42.

[21] Salvador C, Lu D, Anthony EJ, Abanades JC. *Enhancement of CaO for CO_2 capture in an FBC environment,* Chemical Engineering Journal 2003;96:187-95.

[22] Li Z, Fang F, Cai N. *Experiment and modeling of CO_2 capture from flue gases in a fluidized bed with limestone and dolomite sorbents*, **2007**.

[23] Ströhle J, Lasheras A, Galloy A, Epple B. *Simulation of the Carbonate Looping Process for Post-Combustion CO_2 Capture from a Coal-Fired Power Plant*. Chemical Engineering Technology **2009,** 32:435-42.

[24] Charitos A, Hawthorne C, Bidwe A, Korovesis L, Schuster A, Scheffknecht G. *Hydrodynamic analysis of a $10kW_{th}$ Calcium Looping Dual Fluidized Bed for post-combustion CO_2 capture*, Powder Technology **2010**;200:117-27.

[25] Johnsen K, Ryu HJ, Grace JR, Lim CJ. *Sorption-enhanced steam reforming of methane in a fluidized bed reactor with dolomite as CO_2-acceptor*, Chemical Engineering Science **2006**,1:1195-202.

[26] Huang C, Hsu H, Liu W, Cheng J, Chen W, Wen T et al. *Development of post-combustion CO_2 capture with $CaO/CaCO_3$ looping in a bench scale plant*, Energy Procedia **2011**;4:1268-75.

[27] Abanades JC, Alvarez D. *Conversion limits in the reaction of CO_2 with lime*, Energy Fuels **2003**;17:308-15.

[28] Alvarez D, Abanades JC. *Determination of the critical product layer thickness in the reaction of CaO with CO_2*. Industrial Engineering Chemistry Research **2005**;44:5608-15.

[29] Wang J, Anthony EJ. *On the decay behavior of the CO_2 absorption capacity of CaO-based sorbents*, Industrial Engineering Chemistry Research **2005**;44:627-9.

[30] Alvarez D, Abanades JC. *Pore-size and shape effects on the recarbonation performance of calcium oxide submitted to repeated calcination/recarbonation cycles*, Energy Fuels **2005**,19:270-8.

[31] Grasa GS, Abanades JC. *CO_2 capture capacity of CaO in long series of carbonation/calcination cycles*, Industrial Engineering Chemistry Research **2006,** 45:8846-51.

[32] Grasa G, Gonzalez B, Alonso M, Abanades JC. *Comparison of CaO-Based SyntheticCO(2) sorbents under realistic calcination conditions*, Energy Fuels **2007**, 21:3560-2.

[33] Sun P, Grace JR, Lim CJCJ, Anthony EJ. *Determination of intrinsic rate constants of the CaO and CO_2 reaction,* Chemical Engineering Science **2008**;63:47-56.

[34] Grasa GS, Abanades JC, Alonso M, Gonzalez B. *Reactivity of highly cycled particles of CaO in a carbonation/calcination loop*, Chemical Engineering Journal **2008**;137:561-7.

[35] Sun P, Grace JR, Lim CJ, Anthony EJ. *Sequential capture of CO_2 and SO_2 in a pressurized TGA simulating FBC conditions*, Environmental Science Technology **2007**;41:2943-9.

[36] Manovic V, Anthony EJ. *CO_2 carrying behavior of calcium aluminate pellets under high-temperature/high-CO2 concentration calcination conditions*, Industrial Engineering Chemistry Research **2010**, 49:6916-22.

[37] Koirala R, Reddy GK, Smirniotis PG. *Single Nozzle Flame-Made Highly Durable Metal Doped Ca-Based Sorbents for CO_2 Capture at High Temperature*, Energy Fuels **2012**, 26:3103-9.

[38] Manovic V, Anthony EJ, Grasa G, Abanades JC. *CO_2 looping cycle performance of a high-purity limestone after thermal activation/doping,* Energy Fuels **2008**, 22:3258-64.

[39] Manovic V, Wu Y, He I, Anthony EJ. *Spray Water Reactivation/Pelletization of Spent CaO-based Sorbent from Calcium Looping Cycles,* Environmental Science Technology **2012**.

[40] Abanades JC, Anthony EJ, Lu DY, Salvador C, Alvarez D. *Capture of CO_2 from combustion gases in a fluidized bed of CaO*, AICHE J **2004**, 50:1614-22.

[41] Ryu H, Grace JR, Lim CJ. *Simultaneous CO_2/SO_2 capture characteristics of three limestones in a fluidized-bed reactor*, Energy Fuels **2006**, 20:1621-8.

[42] Fennell PS, Pacciani R, Dennis JS, Davidson JF, Hayhurst AN. *The effects of repeated cycles of calcination and carbonation on a variety of different limestones, as measured in a hot fluidized bed of sand*, Energy Fuels **2007**, 21:2072-81.

[43] Jia L, Hughes R, Lu D, Anthony E, Lau I. *Attrition of calcining limestones in circulating fluidized-bed systems*, Industrial Engineering Chemistry Research **2007**;46:5199-209.

[44] Lu DY, Hughes RW, Anthony EJ. *Ca-based sorbent looping combustion for CO_2 capture in pilot-scale dual fluidized beds*, Fuel Process Technology **2008,** 89:1386-95.

[45] Ryu H, Park Y, Jo S, Park M. *Development of novel two-interconnected fluidized bed system*, Korean Journal of Chemical Engineering **2008**,25:1178-83.

[46] Fang F, Li Z, Cai N. *Continuous CO_2 Capture from Flue Gases Using a Dual Fluidized Bed Reactor with Calcium-Based Sorbent*. Industrial Engineering Chemistry Research **2009**, 48:11140-7.

[47] Proell T, Kolbitsch P, Bolhar-Nordenkampf J, Hofbauer H. *A Novel Dual Circulating Fluidized Bed System for Chemical Looping Processes,* AICHE J **2009**, 55:3255-66.

[48] Fang F, Li Z, Cai N. *Design and cold mode experiment of dual bubbling fluidized bed reactors for multiple CCR cycles*, **2010**:533-9.

[49] Charitos A, Rodríguez N, Hawthorne C, Alonso M, Zieba M, Arias B. *Experimental validation of the calcium looping CO_2 capture process with two circulating fluidized bed carbonator reactors,*. Industrial Engineering Chemistry Research **2011**;50:9685-95.

[50] González B, Alonso M, Abanades JC. *Sorbent attrition in a carbonation/calcination pilot plant for capturing CO_2 from flue gases*, Fuel **2010**;89:2918-24.

[51] Hawthorne C, Bidwe A, Holz H, Pfeifer T, Schulze A, Schlegel D. *Parametric Study on the CO_2 Capture Efficiency of The Carbonate Looping Process in a 10 kW Dual Fluidized Bed*, **2010**, 583-9.

[52] Hawthorne C, Dieter H, Bidwe A, Schuster A, Scheffknecht G, Unterberger S. *CO_2 capture with CaO in a 200 kWth dual fluidized bed pilot plant,* Energy Procedia **2011**, 4:441-8.

[53] Rodríguez N, Alonso M, Abanades J. *Experimental investigation of a circulating fluidized□bed reactor to capture CO_2 with CaO*, AIChE J **2010**, 57:1356-66.

[54] Wang W, Ramkumar S, Li S, Wong D, Iyer M, Sakadjian BB et al. S*ubpilot Demonstration of the Carbonation− Calcination Reaction (CCR) Process: High-Temperature CO_2 and Sulfur Capture from Coal-Fired Power Plants*, Industrial Engineering Chemistry Research **2010**, 49:5094-101.

[55] Galloy A, Ströhle J, Epple B. *Design and operation of a 1 MWth carbonate and chemical looping CCS test rig*, VGB powertech **2011**, 91.

[56] Sánchez-Biezma A, Diaz L, López J, Arias B, Paniagua J, De Zárraga E. *La Pereda CO_2: a 1.7 MW Pilot to test post-combustion CO_2 capture with CaO*, **2012,** 365-72.

[57] Rodriguez N, Alonso M, Abanades JC, Grasa G, Murillo R. *Analysis of a process to capture the CO_2 resulting from the pre-calcination of the limestone feed to a cement plant*, Greenhouse Gas Control Technologies 9 **2009**;1:141-8.

[58] Rodriguez N, Murillo R, Alonso M, Martinez I, Grasa G, Abanades J. *Analysis of a Process for Capturing the CO_2 Resulting from the Precalcination of Limestone in a Cement Plant*, Industrial Engineering Chemistry Research **2011**, 50:2126-32.

[59] Rodriguez N, Murillo R, Abanades JC. *CO_2 Capture from Cement Plants Using Oxyfired Precalcination and/or Calcium Looping*, Environmental Science Technology **2012**, 46:2460-6.

[60] Trikkel A. *Estonian calcareous rocks and oil shale ash as sorbents for SO_2*, **2001**.

[61] Borgwardt RH. Calcination Kinetics and Surface Area of Dispersed Limestone Particles: Journal Version. : US Government Printing Office, 1985.

[62] Rajeswara Rao T, Gunn D, Bowen J. *Kinetics of calcium carbonate decomposition,* Chemical Engineering Research Design **1989**, 67:38-47.

[63] Hu N, Scaroni AW. *Calcination of pulverized limestone particles under furnace injection conditions*, Fuel **1996**, 75:177-86.

[64] Rao TR. *Kinetics of calcium carbonate decomposition*, Chemical Engineering Technology **1996**, 19:373-7.

[65] Stanmore BR, Gilot P. *Review of calcination and carbonation of limestone during thermal cycling for CO_2 sequestration*, Fuel Process Technology **2005**, 86:1707-43.

[66] Abanades JC, Anthony EJ, Wang JS, Oakey JE. *Fluidized bed combustion systems integrating CO_2 capture with CaO*, Environmental Science Technology **2005**, 39:2861-6.

[67] Chen C, Zhao C, Liang C, Pang K. *Calcination and sintering characteristics of limestone under O_2/ CO_2 combustion atmosphere*, Fuel Process Technology **2007**, 88:171-8.

[68] Wang Y, Lin S, Suzuki Y. *Study of limestone calcination with CO2 capture: Decomposition behavior in a CO_2 atmosphere*, Energy Fuels **2007**, 21:3317-21.

[69] Garcıa-Labiano F, Abad A, De Diego L, Gayan P, Adanez J. *Calcination of calcium-based sorbents at pressure in a broad range of CO_2 concentrations*, Chemical engineering science **2002,** 57:2381-93.

[70] Wang Y, Lin S, Suzuki Y. *Limestone calcination with CO 2 capture (II): Decomposition in CO_2/steam and CO_2/N_2 atmospheres*, Energy Fuels **2008**, 22:2326-31.

[71] Wang Y, Thomson WJ. *The effects of steam and carbon dioxide on calcite decomposition using dynamic X-ray diffraction*, Chemical Engineering Science **1995**, 50:1373-82.

[72] Dam-Johansen K, Østergaard K. *High-temperature reaction between sulphur dioxide and limestone—I. Comparison of limestones in two laboratory reactors and a pilot plant*, Chemical Engineering Science **1991**,46:827-37.

[73] H Borgwardt R. *Sintering of nascent calcium oxide*. Chemical Engineering Science **1989**, 44:53-60.

[74] Fuertes A, Alvarez D, Rubiera F, Pis J, Marban G, Palacos J. *Surface area and pore size changes during sintering of calcium oxide particles*, Chemical Engineering Communication **1991**;109:73-88.

[75] Borgwardt RH. *Calcium oxide sintering in atmospheres containing water and carbon dioxide*, I Industrial Engineering Chemistry Research **1989**, 28:493-500.

[76] Agnew J, Hampartsoumian E, Jones J, Nimmo W. *The simultaneous calcination and sintering of calcium based sorbents under a combustion atmosphere*, Fuel **2000**;79:1515-23.

[77] Lu DY, Hughes RW, Anthony EJ, Manovic V. *Sintering and reactivity of $CaCO_3$-based sorbents for in situ CO_2 capture in fluidized beds under realistic calcination conditions*. Journal Environmental Engineering **2009**, 135:404-10.

[78] Barker R. *The reversibility of the reaction $CaCO_3/CaO+CO_2$*, Journal of Applied Chemistry and Biotechnology **1973**, 23:733-42.

[79] Bhatia SK, Perlmutter DD. *Effect of the product layer on the kinetics of the CO_2-lime reaction*, AIChE J **1983,** 29:79-86.

[80] Wang C, Jia L, Tan Y, Anthony E. *Carbonation of fly ash in oxy-fuel CFB combustion*, Fuel **2008**, 87:1108-14.

[81] Sun P, Grace JR, Lim CJ, Anthony EJ. *A discrete-pore-size-distribution-based gas–solid model and its application to the CaO-CO_2 reaction*, Chemical Engineering Science **2008**, 63:57-70.

[82] Grasa G, Murillo R, Alonso M, Abanades JC. *Application of the Random Pore Model to the Carbonation Cyclic Reaction*, AICHE J **2009**, 55:1246-55.

[83] Sun P, Grace JR, Lim CJ, Anthony EJ. *Removal of CO_2 by calcium-based sorbents in the presence of SO_2*, Energy Fuels **2007**, 21:163-70.

[84] Grasa GS, Alonso M, Abanades JC. *Sulfation of CaO particles in a carbonation/calcination loop to capture CO_2*, Industrial Engineering Chemistry Research **2008**, 47:1630-5.

[85] Christensen J. *CO_2 Capture via Carbonate Looping*, **2010**.

[86] Gonzalez B, Grasa GS, Alonso M, Abanades JC. *Modeling of the Deactivation of CaO in a Carbonate Loop at High Temperatures of Calcination*, Industrial Engineering Chemistry Research **2008**, 47:9256-62.

[87] Manovic V, Anthony EJ, Loncarevic D. *SO_2 retention by CaO-based sorbent spent in CO_2 looping cycles*, Industrial Engineering Chemistry Research **2009,** 48:6627-32.

[88] Arias B, Cordero J, Alonso M, Abanades J. *Sulfation rates of cycled CaO particles in the carbonator of a Ca-looping cycle for post combustion CO_2 capture*. AIChE J **2011**, 58:2262-9.

[89] Dam-Johansen K, Østergaard K. *High-temperature reaction between sulphur dioxide and limestone—II. An improved experimental basis for a mathematical model*, Chemical Engineering Science **1991**, 46:839-45.

[90] Dam-Johansen K, Hansen P, Østergaard K. *High-temperature reaction between sulphur dioxide and limestone—III. A grain-micrograin model and its verification*, Chemical Engineering Science **1991**, 46:847-53.

[91] Dam-Johansen K, Østergaard K. *High-temperature reaction between sulphur dioxide and limestone—IV. A discussion of chemical reaction mechanisms and kinetics*, Chemical Engineering Science **1991**, 46:855-9.

[92] Hansen P, Dam-Johansen K, Østergaard K. *High-temperature reaction between sulphur dioxide and limestone—V. The effect of periodically changing oxidizing and reducing conditions,* Chemical Engineering Science **1993**, 48:1325-41.

[93] Illerup J, Dam-Johansen K, Lunden K. *High-temperature reaction between sulfur dioxide and limestone—VI. The influence of high pressure*, Chemical Engineering Science **1993**, 48:2151-7.

[94] Alvarez D, Peña M, Borrego AG. *Behavior of different calcium-based sorbents in a calcination/carbonation cycle for CO_2 capture*, Energy Fuels **2007**, 21:1534-42.

[95] Lysikov AI, Salanov AN, Okunev AG. *Change of CO_2 carrying capacity of CaO in isothermal recarbonation-decomposition cycles*, Industrial Engineering Chemistry Research **2007,** 46:4633-8.

[96] Pawlak-Kruczek H, Wieckowska K. *CO_2 capture by solid calcium sorbents the effect of properties of sorbents and process conditions on capture efficiency*, Chemical Process Engineering **2010**, 31:889-903.

[97] Laursen K, Duo W, Grace J, Lim J. *Sulfation and reactivation characteristics of nine limestones,* Fuel **2000**;79:153-63.

[98] Manovic V, Anthony EJ. *Steam reactivation of spent CaO-based sorbent for multiple CO_2 capture cycles*. Environmental Science Technology **2007,** 41:1420-5.

[99] Arias B, Grasa GS, Abanades JC. *Effect of sorbent hydration on the average activity of CaO in a Ca-looping system*, Chemical Engineering Journal **2010,** 163:324-30.

[100] Arias B, Grasa G, Abanades J, Manovic V, Anthony E. *The effect of steam on the fast carbonation reaction rates of CaO*, Industrial Engineering Chemistry Research **2012**, 51:2478-82.

[101] Wu Y, Blamey J, Anthony E, Fennell P. *Morphological changes of limestone sorbent particles during carbonation/calcination looping cycles in a thermogravimetric analyzer (TGA) and reactivation with steam*, Energy Fuels **2010,** 24:2768-76.

[102] Manovic V, Anthony EJ. *Thermal activation of CaO-based sorbent and self-reactivation during CO2 capture looping cycles,* Environmental Science Technology **2008**, 42:4170-4.

[103] Manovic V, Anthony EJ. *Improvement of CaO-based sorbent performance for CO_2 looping cycles*, Thermal Science **2009**, 13:89-104.

[104] Okunev A, Lysikov A. *Effect exerted by texture of calcined calcium oxide on its sorption capacity in the CO_2 sorption-regeneration cycles*, Russian Journal of Applied Chemistry **2011**, 84:173-8.

[105] Manovic V, Anthony EJ. *CaO-Based Pellets Supported by Calcium Aluminate Cements for High-Temperature CO_2 Capture*, Environmental Science Technology **2009**, 43:7117-22.

[106] Manovic V, Anthony EJ. *Reactivation and remaking of calcium aluminate pellets for CO_2 capture*. Fuel **2011,** 90:233-9.

[107] Fang F, Li Z, Cai N. *CO_2 capture from flue gases using a fluidized bed reactor with limestone,* Korean Journal of Chemical Engineering **2009**, 26:1414-21.

[108] Mahadzir M, Zainal Z. *Experimental Study of Hydrodynamic Characteristics and CO_2 Absorption in Producer Gas Using CaO-sand Mixture in a Bubbling Fluidized Bed Reactor*. International Journal of Chemical Reactor Engineering **2011**, 9.

[109] Fang F, Li Z, Cai N. *Experiment and Modeling of CO_2 Capture from Flue Gases at High Temperature in a Fluidized Bed Reactor with Ca-Based Sorbents*, Energy Fuels **2009**, 23:207-16.

[110] Li Z, Fang F, Cai N. *CO_2 Capture from Flue Gases Using Three Ca-Based Sorbents in a Fluidized Bed Reactor,* Journal of Environmental Engineering **2009,** 135:418-25.

[111] Felice L, Foscolo PU, Gibilaro L. *CO_2 Capture by Calcined Dolomite in a Fluidized Bed: Experimental Data and Numerical Simulations*. International Journal of Chemical Reactor Engineering **2011**, 9.

[112] Symonds RT, Lu DY, Hughes RW, Anthony EJ, Macchi A. *CO_2 capture from simulated syngas via cyclic carbonation/calcination for a naturally occurring limestone: pilot-plant testing*, Industrial Engineering Chemistry Research **2009**, 48:8431-40.

[113] Abanades J, Alonso M, Rodriguez N. *Experimental validation of in situ CO_2 capture with CaO during the low temperature combustion of biomass in a fluidized bed reactor*. International Journal of Greenhouse Gas Control **2011**, 5:512-20.

[114] Rodríguez N, Alonso M, Abanades J. *Experimental investigation of a circulating fluidized□bed reactor to capture CO_2 with CaO*, AIChE J **2011**, 57:1356-66.

[115] Vaux W. *Attrition of particles in the bubbling zone of a fluidized bed*, **1978**, 40.

[116] Scala F, Salatino P, Boerefijn R, Ghadiri M. *Attrition of sorbents during fluidized bed calcination and sulphation*, Powder Technology **2000**, 107:153-67.

[117] Shimizu T, Peglow M, Sakuno S, Misawa N, Suzuki N, Ueda H. *Effect of attrition on SO_2 capture by limestone under pressurized fluidized bed combustion conditions—comparison between a mathematical model of SO_2 capture by single limestone particle under attrition condition and SO_2 capture in a large-scale PFBC*, Chemical Engineering Science **2001**, 56:6719-28.

[118] Stendardo S, Foscolo PU. *Carbon dioxide capture with dolomite: A model for gas solid reaction within the grains of a particulate sorbent*, Chemical Engineering Science **2009**, 64:2343-52.

[119] Bhatia S, Perlmutter D. *A random pore model for fluid-solid reactions: I. Isothermal, kinetic control*, AIChE J **1980**, 26:379-86.

[120] Bhatia S, Perlmutter D. *A random pore model for fluid□solid reactions: II. Diffusion and transport effects*, AIChE J **1981**, 27:247-54.

[121] Arias B, Abanades J, Anthony E. *Model for self-reactivation of highly sintered CaO particles during CO_2 capture looping cycles*, Energy Fuels **2011**, 25:1926-30.

[122] Kunii D, Levenspiel O. *Fluidization engineering*, Butterworth-Heinemann Boston, **1991**.

[123] Alonso M, Rodriguez N, Grasa G, Abanades JC. *Modelling of a fluidized bed carbonator reactor to capture CO_2 from a combustion flue gas*, Chemical Engineering Science **2009,** 64:883-91.

[124] Lasheras A, Ströhle J, Galloy A, Epple B. *Carbonate looping process simulation using a 1D fluidized bed model for the carbonator*, International Journal of Greenhouse Gas Control **2011**, 5:686-93.

[125] Romano MC. *Modeling the carbonator of a Ca-looping process for CO_2 capture from power plant flue gas*, Chemical Engineering Science **2012**, 69:257-69.

[126] Kunii D, Levenspiel O. *Circulating fluidized-bed reactors*, Chemical Engineering Science **1997,** 52:2471-82.

[127] Kunii D, Levenspiel O. T*he KL reactor model for circulating fluidized beds*, Chemical Engineering Science **2000**, 55:4563-70.

[128] Abanades JC, Rubin ES, Anthony EJ. *Sorbent cost and performance in CO_2 capture systems*, Industrial Engineering Chemistry Research **2004**, 43:3462-6.

[129] Abanades JC, Grasa G, Alonso M, Rodriguez N, Anthony EJ, Romeo LM. C*ost structure of a postcombustion CO_2 capture system using CaO*, Environmental Science Technology **2007**, 41:5523-7.

[130] Hughes RW, Lu DY, Anthony EJ, Macchi A. *Design, process simulation and construction of an atmospheric dual fluidized bed combustion system for in situ CO_2 capture using high-temperature sorbents*. Fuel Process Technology **2005,** 86:1523-31.

[131] Rodriguez N, Alonso M, Grasa G, Abanades JC. *Heat requirements in a calciner of $CaCO_3$ integrated in a CO_2 capture system using CaO*, Chemical Engineering Journal **2008**, 138:148-54.

[132] MacKenzie A, Granatstein DL, Anthony EJ, Abanades JC. *Economics of CO_2 capture using the calcium cycle with a pressurized fluidized bed combustor*, Energy Fuels **2007**, 21:920-6.

[133] Romeo LM, Lara Y, Lisbona P, Escosa JM. *Optimizing make-up flow in a CO_2 capture system using CaO*, Chemical Engineering Journal **2009**, 147:252-8.

[134] Romeo LM, Abanades JC, Escosa JM, Pano J, Gimenez A, Sanchez-Biezma A. O*xyfuel carbonation/calcination cycle for low Cost CO2 capture in existing power plants,* Energy Conversion and Management **2008**, 49:2809-14.

[135] Yang Y, Zhai R, Duan L, Kavosh M, Patchigolla K, Oakey J. *Integration and evaluation of a power plant with a CaO-based CO_2 capture system*, International Journal of Greenhouse Gas Control **2010**, 4:603-12.

[136] Rodriguez N, Alonso M, Grasa G, Abanades JC. *Process for capturing CO_2 arising from the calcination of the $CaCO_3$ used in cement manufacture*, Environmental Science Technology **2008**, 42:6980-4.

[137] Romeo LM, Usón S, Valero A, Escosa JM. *Exergy analysis as a tool for the integration of very complex energy systems: The case of carbonation/calcination CO_2 systems in existing coal power plants*, International Journal of Greenhouse Gas Control **2010**, 4:647-54.

[138] Blamey J, Anthony EJ, Wang J, Fennell PS. *The calcium looping cycle for large-scale CO_2 capture*, Progress in Energy and Combustion Science **2010**, 36:260-79.

[139] Dean CC, Blamey J, Florin NH, Al-Jeboori M, Fennell PS. *The calcium looping cycle for CO_2 capture from power generation, cement manufacture and hydrogen production*, Chemical Engineering Research Design **2011**, 89:836-55.

[140] Telschow S. *Clinker Burning Kinetics and Mechanism*, **2012**.

[141] Taylor HFW. *Cement Chemistry*. London: Thomas Telford, **1997**.

[142] Pathi SK, Andersen MF, Lin W, Illerup JB, Dam-Johansen K, Hjuler K. C*arbonate Looping for De-Carbonization of Cement Plants*, 13.ICCC **2011**.

[143] Dean CC, Dugwell D, Fennell PS. *Investigation into potential synergy between power generation, cement manufacture and CO_2 abatement using the calcium looping cycle,* Energy Environmental Science **2011**, 4:2050-3.

[144] Lin W, Illerup JB, Dam-Johansen K, Hjuler K. *Application of Carbonate Looping to Cement Industry*, **2012,** 405.

[145] Scherrer P. *Determination of size and structure of colloidal particles by x-ray diffraction*. Gött.Nachr 1918, 2:98.

[146] Fischer HC. *Calcination of calcite*, Journal of the American Ceramic Society **1955**, 38:284-8.

[147] Rodriguez-Navarro C, Ruiz-Agudo E, Luque A, Rodriguez-Navarro A, Ortega-Huertas M. *Thermal decomposition of calcite: Mechanisms of formation and textural evolution of CaO nanocrystals,* AMER MINERAL **2009,** 94:578-93.

[148] Bartholomew CH. *Sintering kinetics of supported metals: New perspectives from a unifying GPLE treatment*, Applied Catalysis A: General **1993**, 107:1-57.

[149] Cook JL, Khang S, Lee S, Keener TC. *Attrition and changes in particle size distribution of lime sorbents in a circulating fluidized bed absorber,* Powder Technology **1996,** 89:1-8.

[150] Kyaw K, Kanamori M, Matsuda H, Hasatani M. *Study of Carbonation Reactions of Ca-Mg Oxides for High Temperature Energy Storage and Heat Transformation*, Journal Chemical Engineering Japan **1996,** 29:112-8.

[151] Kunii D, Levenspiel O. *Fluidized reactor models. 1. For bubbling beds of fine, intermediate, and large particles. 2. For the lean phase: freeboard and fast fluidization,* Industrial Engineering Chemistry Research **1990**, 29:1226-34.

[152] Charitos A, Hawthorne C, Bidwe A, Sivalingam S, Schuster A, *Spliethoff H et al. Parametric investigation of the calcium looping process for CO_2 capture in a 10kW$_{th}$ dual fluidized bed*, International Journal of Greenhouse Gas Control **2010,** 4:776-84.

[153] Cormos A, Abel S. *Dynamic Modeling of CO_2 Capture by Calcium-Looping Cycle*, **2013**, 35.

[154] Furusaki S, Kikuchi T, Miyauchi T. *Axial distribution of reactivity inside a fluid-bed contactor*, AIChE J **1976**, 22:354-61.

[155] Invensys System Inc. PRO/II **2009**.

[156] Evelien C, Wouter N. *Energy Technology System Analysis Programme*, **2010**.

[157] Jensen AD, Galborg P. *Combustion and High Temperature Processes.* : Department of Chemical and Biochemical Engineering, DTU, **2010**.

[158] Barin I, Knacke O, Kubaschewski O. *Thermochemical properties of inorganic substances: supplement,* Springer-Verlag Berlin, **1977**.

[159] Benhelal E, Zahedi G, Hashim H. A *novel design for green and economical cement manufacturing*, Journal Clean Production **2012,** 22:60-6.

[160] Engin T, Ari V. *Energy auditing and recovery for dry type cement rotary kiln systems—A case study*, Energy Conversion and Management **2005**, 46:551-62.

[161] Geldart D. *Types of gas fluidization*, Powder Technology **1973**, 7:285-92.

[162] Palfreyman D, Cottrell A, Scaife P, Wibberley L. *Techno-economics of oxygen fired PF power generation with CO_2 capture*, **2006**.

[163] Darde A, Prabhakar R, Tranier J, Perrin N. *Air separation and flue gas compression and purification units for oxy-coal combustion systems*, Energy Procedia **2009**, 1:527-34.

[164] Fan Z, Seltzer A, Hack H. O*xyfuel Power Generation with Closed-Loop to Reach Zero Emission*, **2011**.

[165] McCollum DL, Ogden JM. T*echno-economic models for carbon dioxide compression, transport, and storage & correlations for estimating carbon dioxide density and viscosity*, **2006**.

[166] Turnell VJ. *Selecting the right preheater fan and drive*, **2002**:95-106.

[167] Spliethoff H. *Power generation from solid fuels*, Springer, **2010**.

9. Appendix

9.1 Publications

- Title: Carbonate Looping for De-carbonization of Cement Plant

Authors: Pathi S.K.; Andersen F.B.; Lin W.; Illerup J.B.; Dam-Johansen K.; and Hjuler K.;

Conference: 13th International Congress on Cement Chemistry

Year: 2011

- Title: CO_2 Capture by Cement Raw Meal

Authors: Pathi S.K.; Lin W.; Illerup J.B.; Dam-Johansen K.; and Hjuler K.;

Journal: Energy and Fuels

Year: 2013

- Title: Performance of a Fast Fluidized Bed Carbonator: Experimental and Modeling

Authors: Pathi S.K.; Lin W.; Illerup J.B.; Dam-Johansen K.; and Hjuler K.;

Status: Ready for submission to a journal

- Title: Low CO_2 emission Cement Plant with Co-generation

Authors: Pathi S.K.; Lin W.; Illerup J.B.; Dam-Johansen K.; and Hjuler K.;

Status: Ready for submission to a journal

Carbonate looping for De-carbonization of Cement Plant

[1]Sharat Kumar Pathi[1]*, [1]Maria Friberg Andersen, [1]Weigang Lin, [1]Jytte Boll Illerup, [1]Kim Dam-Johansen

[1] ***CHEC Research Centre, Department of Chemical and Biochemical Engineering, DTU, Lyngby, Denmark***

[2]Klaus Hjuler

[2]***FLSmidth A/S, Research and Development, Valby, Denmark***

Abstract

Cement industry is one of the largest emitter of CO_2 other than power generation plants, which includes the emissions from combustion of fuel and also from calcination of limestone for clinker production. In order to reduce CO_2 emissions from the cement industry an effective an economically feasible technology is to be developed. The carbonate looping process is a promising technology, which is particularly suitable for the cement industry as limestone could be used for capture and release of CO_2. Integration of carbonate looping process into cement pyro-process has two advantages: 1) to capture emitted CO_2 and 2) to generate power for internal use, because high quality energy can be recovered from carbonate looping which is operated at high temperature unlike amine process. A simple carbonate looping process model was developed based on average conversion of calcined limestone defined by Abanades et al. The model is used to investigate the influence of average conversion of limestone in the carbonator on the flow rates of different streams in the looping process and energy required in the calciner for re-activation. The model developed is used for studying the carbonate looping process integrated into cement pyro-process. The energy required for regeneration in the calciner increases with increase in average conversion of calcined limestone and energy that can be extracted from carbonator decreases with increasing average conversion. Further the influence of type of limestone on the calciner capacity is also investigated. The results from this simple model show the importance of cement industry to the carbon capture technology for its application to power plants.

Originality

A major step towards sustainable production of cement is to capture carbon emitted from the process. Presently there is no technology applied on large scale for carbon capture. The carbonate looping process has the potential to be applied at industrial scale and it is especially suitable for the cement industry. So as a first step a simple model was developed to investigate the influence of the average conversion of calcined limestone in the carbonator on all flow streams in the looping process integrated to a cement plant.

Chief contributions

The model estimates the energy to be extracted from the carbonator for e.g. electricity generation by carbonate looping integrated with the cement process. The carbonation energy increases with decreasing average conversion of the calcined limestone, whereas the energy required for calcination (regeneration) decreases with decreasing average conversion. The model provides an useful tool for optimization of the carbonate looping process applied to cement industry.

Keywords: ***CO_2 capture, carbonate looping, type of limestone, cement plant***

---

* Corresponding author: Email skp@kt.dtu.dk Tel +45252839, Fax +4545882258

1. Introduction

According to IPCC carbon capture from large stationary sources is considered as the mid-term mitigation option for climate change (Metz et al., 2005). The major sources of CO_2 emitters are power plants and the other major industry is the cement plant, which involves CO_2 emissions both from combustion, calcination process and indirect emissions by consumption of electricity. One of the most promising technologies for carbon capture applicable to any process is the Carbonate looping process, which is being investigated and developed aggressively by different research groups across the world. Carbonate looping process involves calcination and re-carbonation of sorbent material i.e. limestone, which is abundantly available and distributed across the globe. The main reaction of this process is calcination and carbonation of limestone, which is governed by equilibrium expression defined in (Baker, 1962). By controlling the equilibrium conditions (Temperature and Pressure) in two inter connected reactors, carbonation and calcination reactions are carried out for continuous capture of CO_2 from flue gas and release of captured CO_2 in CO_2 atmosphere, by looping the sorbent material (Shimizu et al., 1999). The energy required for calcination can be supplied by oxy-fuel combustion or alternative energy sources (Abanades et al., 2005) and high quality energy can be recovered from the carbon capture reaction in the carbonator. However, before realizing the potential of this process, there are still many challenges to the process like: reactivity of limestone with increasing number of cycles, large circulation of sorbent particles between two inter connected reactors continuously, energy required for regeneration of sorbent material, influence of composition of limestone etc. Different research groups are focusing on these areas to overcome these challenges.

One of the critical parameter which controls the whole process is the average conversion of calcined limestone in the carbonator. A simple model is developed to evaluate the influence of this parameter on: 1) the flow rates of streams in and out of the looping process 2) the flow rates of recycle streams, 3) energy required for regeneration of limestone in the calciner and 4) the energy that can be extracted. Based on this model a case study is performed on de-carbonization of a cement plant.

2. Modeling of carbonate looping process

A simple carbonate looping process model is developed to investigate the influence of the average conversion of limestone on the calciner capacity and other flow streams in and out of the looping process. This model is applicable for any process releasing CO_2 in the flue gas.

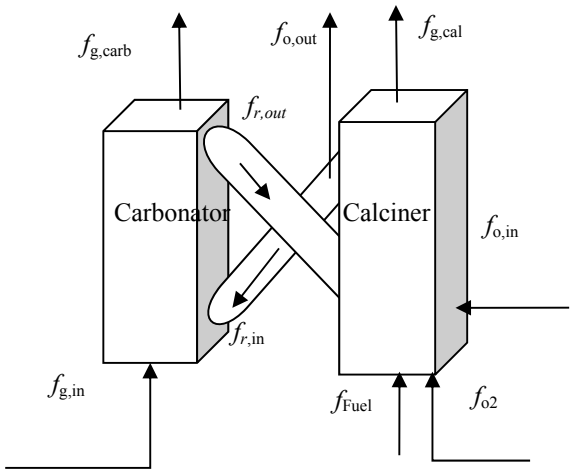

Figure 9: Schematic representation of Carbonate Looping Process

Carbonate looping process is schematically represented in the figure 1. In the process one of the important factors which influence the whole process is the reactivity of the recycled calcined limestone stream. The general characteristic of the calcined limestone is to lose its capacity to re-carbonate with increasing number of looping cycles mainly due to sintering effects (Wang and Anthony, 2005). The degree of conversion of calcined limestone to re-carbonate with respect to cycle numbers is given by the equation defined by Abanades and Alvarez, 2003.

$$X_N = f_m^N (1 - f_m) + f_w \tag{1}$$

where X_N is the degree of conversion, N is the cycle number and f_m and f_w are the characteristics constants of the type of limestone which influence the conversion based on structural properties of limestone.

The best solution to this problem of losing reactivity of limestone is to select a limestone which has high residual reactivity. The other alternative is to purge a stream of limestone from the recycle stream and replace it with fresh limestone. The influence of the addition of fresh limestone on the average conversion of calcined limestone is given by eq.4 (Abanades et al. 2005):

$$X_{ave} = \frac{f_m(1-f_w)F_O}{F_O + F_R(1-f_m)} + f_w \tag{2}$$

where X_{ave} is the average conversion of calcined limestone in the recycle stream F_R and F_O is the molar flow rate of purge stream and the fresh limestone respectively. Continuous addition of fresh limestone results in maintaining high reactivity in the carbonator and a high conversion of limestone. However, this requires more energy input to the calciner.

2.1 Assumptions for the process model

The amount of energy required for 1 kg of clinker production is around 2930 kJ, most of this energy is used for calcination of limestone (Larsen, 2007). Approximately 40% of the thermal energy consumed for clinker production is from combustion of fuel in the rotary kiln. CO_2 emission from the calcination process can be eliminated by introducing the oxy-fuel calciner. Further, a small purge stream form the oxy-fuel calciner can be fed into the carbonator for capturing the rest of CO_2 emitted from the rotary kiln. Thus cement production process can be completely free from the CO_2 emissions. The table 1 below summarizes the data related to the cement plant.

Table 1: Cement Plant Specific Data

Property	Value	Units
Energy	2,93	MW/ kg cl
Electricity	0,111	kW_h/ kg cl
Limestone	1,2	kg/kg cl
Fuel into rotary kiln	0,05	kg/kg cl
Flue gas from rotary kiln	0,48	kg/kg cl

cl: clinker

It is assumed that the fuel is coal and the flow rate of the flue gas ($f_{g,in}$) is considered as constant. The composition of fuel used is as follows C = 66 %, H = 3 %, S = 1 %, O = 8 %, H_2O = 8 % and the rest is ash. The flow rate of CO_2 ($f_{g,in}.x_{CO2}$) was estimated from the combustion of coal in the rotary kiln at excess air ratio of 1.1. The temperature of the flue gas in ($T_{fg,in}$) and out ($T_{fg,carb}$) of the system is fixed to 110 ^oC. The temperature of the inlet flue gas is considered as 110 ^oC so that this model can be applied to any process releasing flue gas to atmosphere at 110 ^oC. The temperature of fresh streams (T_{in}) is considered to be at 25 ^oC. The temperature of carbonator is 650 ^oC and the temperature of calciner is 950 ^oC. All the other parameters of the model like flow rate of recycle stream (f_r), flow rate of fresh stream (f_o), flow rate of fuel (f_{Fuel}), and flow rate of oxygen (f_{O2}) are estimated based on the average degree of conversion of calcined limestone in the recycle stream.

The characteristic values of limestone used by Abanades group, f_w is 0.17 and f_m is 0.77 are considered in the model (Abanades and Alvarez, 2003). The average conversion (X_{ave}) of calcined limestone was selected in the range of 0.2-0.7 for maximum capture of CO_2 from the flue gas. Considering the minimum and maximum degree of re-carbonation based to the characteristic values of type of limestone 'f_w' and 'f_m'. The flow rate of the recycle stream for capturing CO_2 to its thermodynamic limit is estimated by equation (Abanades et al., 2005):

$$F_R = \frac{F_{CO_2} \cdot E_{carb}}{X_{ave} \cdot X_{CaO\_cl}} \tag{3}$$

$$f_r = F_R \cdot \sum_i X_{i\_cl} \cdot M_i \tag{4}$$

E_{carb} is fixed to equilibrium capture which is 94% at 650 ^{o}C (Baker, 1962), X_{CaO_cl} is the molar fraction of limestone in the raw meal, f_r is the flow rate of recycle stream in kg/kg clinker. In raw meal 70 % of the mixture is limestone (Larsen, 2007) and the rest includes SiO_2, Al_2O_3 and Fe_2O_3, which are represented by X_{i_cl} and M_i is molecular weight of component *i*.

The flow rate of fresh raw meal into the oxy-fuel calciner or the purge stream for clinker production is given by equation:

$$F_O = F_R \cdot \left((1 - f_m) \cdot (X_{ave} - f_w) / (f_m \cdot (1 - f_w) - (X_{ave} - f_w)\right) \tag{5}$$

$$f_o = F_O \cdot \sum_i X_{i\_cl} \cdot M_i \tag{6}$$

here f_o is the flow rate of stream in kg/kg clinker.

The flow rates of all the streams are estimated based on CO_2 emitted per kg of clinker produced. Based on these assumptions the influence of the average conversion (X_{ave}) of limestone on the calciner capacity and flow rates of all the streams in and out of the carbonate looping process are estimated along with energy capacities. The specific heat capacities of the gases and the solids are taken from Yaws, Carl L., (2009).

3. Results

3.1 Influence of average conversion of calcined limestone on the streams coming in and out of carbonator.

Figure 2 and figure 3 shows the influence of average degree of re-carbonation on the streams of carbonator. Increasing the degree of re-carbonation (X_{ave}) decreases the flow rate of recycle stream (f_r) as the amount of calcined limestone required to capture CO_2 decreases with increase in average degree of re-carbonation of calcined limestone. The inlet and outlet gas streams are constant based on the assumption that the flue gas comes from combustion of fossil fuel in the rotary kiln and that maximum CO_2 is captured (see fig. 2). Since the flow rate of flue gas ($f_{g,in}$) is constant the amount of energy ($+Q_{,Fg,in}$) required to heat the flue gas to the carbonation temperature is also constant. The energy required to heat the flue gas from 110 ^oC to the carbonation temperature 650 ^oC can be supplied by the calcined recycled stream (f_r) coming into the carbonator form the calciner at 950 ^oC. The energy ($-Q_{FR}$) carried by the calcined stream decreases with increasing average conversion as the flow rate of stream decreases. The cross over for the energy required for heating flue gas by the solid stream from the calciner to the carbonator is around conversion of 0.5, which means that additional energy has to be supplied for heating the flue gas to carbonation temperature as the average conversion of the limestone increases above this value. Further the energy that can be extracted from the carbonator will also decrease with increasing average conversion of limestone (see fig. 3). However if the inlet flue gas temperature is 650 ^oC instead of 110 ^oC additional energy can be extracted from the carbonator, which could be possible because the flue gas in the rotary kiln is very high.

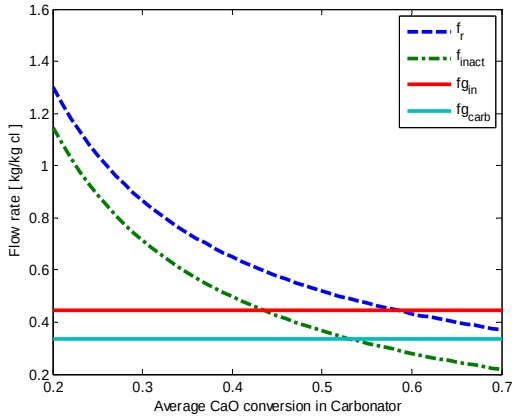

Figure 2: Flow rate of the streams in

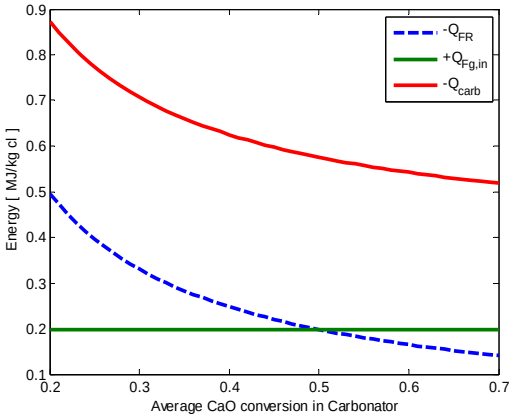

Figure 3: Energy content of the streams

3.2 Influence of average conversion of calcined limestone on the streams of the calciner

Figure 4 shows the relationship of average conversion of calcined limestone in the carbonator on the flow rate of fresh limestone stream ($f_{o,in}$), the purge stream for clinker production ($f_{o,out}$), flow rate of recycle stream (f_r) and the flow rate of oxygen (f_{o2}) which is dependent on the fuel consumption in the calciner.

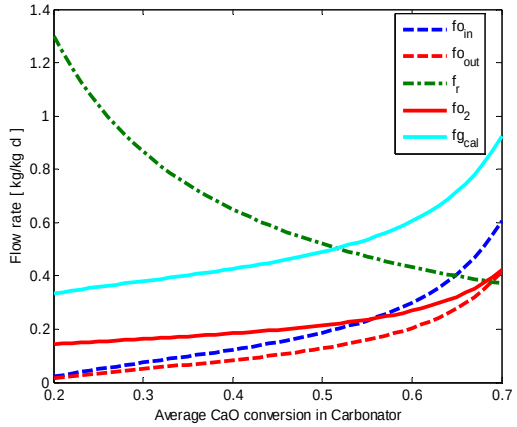

Figure 4: Flow rate of the streams in and out

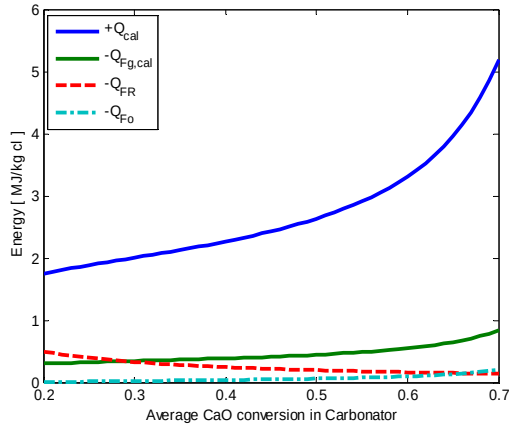

Figure 5: Energy capacity of the calciner and

The recycle stream from carbonator includes both the carbonated limestone and inactive calcined limestone. So as the average conversion in the carbonator increases the fraction of inactive calcined limestone decreases. This can be observed with flow rate of fresh limestone ($f_{o,in}$) into the calciner which influences the active fraction (X_{ave}) in the recycle stream. However, with the increasing average conversion of calcined limestone in the carbonator the amount of oxygen (f_{o2}) required for the calcination of limestone in the calciner increases. The main energy consumer in the calciner ($+Q_{cal}$) is the calcination reaction which is proportional to amount of carbonate. The amount of re-carbonated limestone is constant as the flow rate of CO_2 into the carbonator is constant. So the energy required for the calcination reaction is controlled by the flow rate of the fresh limestone stream. The other sources for energy consumers are the heating of different streams like fresh limestone stream (F_o) from room temperature to calciner temperature, recycled stream (f_r) from the carbonator temperature to calcination temperature, heating of oxygen and fuel from room temperature to calcination temperature. Thus, with increase in average conversion of calcined limestone the flow rate of fresh limestone increases which not only increases energy demand for calcination reaction but also increases energy demand for heating up the fresh stream ($f_{o,in}$) (see fig.5). This will increase the flow rate of fuel and oxygen into calciner increasing overall energy capacity of calciner.

3.3 Influence of different types of limestone

The influence of different types of limestone was simulated to estimate the energy required in the calciner. The type of limestone was determined by the values of *'f_w'* and *'f_m'* found by Andersen F.M, (2009) for different limestone compositions. These values were found from fitting curves of the degree of re-carbonation obtained in looping cycles performed in normal Thermo gravimetric Analyzer.

Table 2: Characteristic Values for Different Types of Limestone

Limestone Type	f_m	f_w
Faxe Bryozo	0.71	0.36
Obajama	0.64	0.22
Russian	0.55	0.5
Hole	0.7	0.25
Aggersund	0.6	0.48
Abanades et al.	0.77	0.17

The figure 6 below shows the energy capacity of the calciner with respect to average conversion of calcined limestone in the carbonator for different types of limestone. It can be observed that calciner required low energy at low average conversion for all the limestone mainly due to reduction in heating fresh limestone in the calciner. The type of limestone with the highest value for '*fw*' has the lowest energy requirement in the calciner with respect to average conversion in the carbonator because it reduces the flow rate of re-circulating particles required for carbon capture.

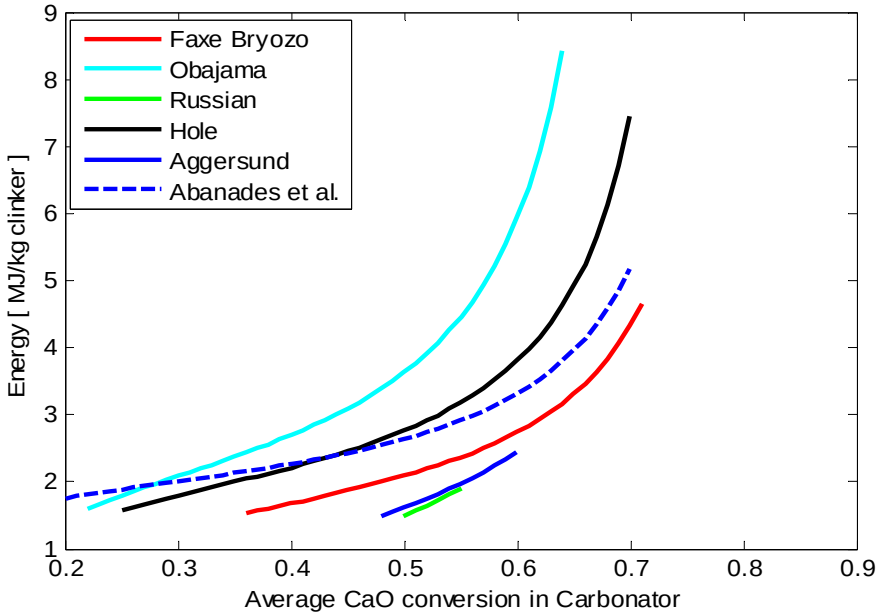

Figure 6: Influence of different types of limestone on the energy required in the calciner for reactivation for different average conversion of calcined limestone in the carbonator.

4. Conclusions and Future work

The influence of average conversion of limestone in the carbonator on the calciner capacity and energy that can be extracted in the carbonator can be observed based on this model. The amount of energy that can be extracted from the carbonator integrated to cement pyro-process for capturing CO_2 form rotary kiln is around 600 MJ/ton of clinker produced at the highest conversion (see figure 3). The global average electricity consumption is 111 kWh per ton of cement (Evelien and Wouter, 2010). Thus, integrating high pressure steam cycle into the carbonator, electricity can be produced for internal consumption, which might help in reducing overall expenses for carbon capture from cement plants.

Applying the carbonate looping process to a power plant where the flow rate of CO_2 is much higher than flow rate from rotary kiln it can be seen from this model that capacity of the calciner will be as big as the power plant at low average conversion. So the carbonate looping process is another oxy-fuel power plant with a potential to reduce the overall all emission form the existing power plants. The capacity of calciner increases with increasing average conversion in the carbonator under the assumed conditions. Further, most of the energy spent in calcination of fresh limestone for high conversion in re-carbonator cannot be recovered unless it is converted to value added product like cement. So synergy with cement plant is necessary for power plants applying carbonate looping process unless a sorbent with high residual re-carbonation capacity is used for looping.

In a cement plant maintaining high average conversion of limestone in the carbonator is not a problem owing to huge consumption of limestone in the clinker formation. The flow rate of limestone per kg of clinker produced is 1.2 kg. So the flow rate of the recycle stream is much less than the flow rate of the fresh stream which enables high activity in the recycle stream for carbon capture. However for applying the carbonate looping process to cement industry there are still many unknown factors like: oxy-fuel calcination of limestone, influence of inters from the limestone and fuel composition, influence of sulphur dioxide on re-carbonation, the size of particles in the cement production process is below 90 μm but most of the carbonate looping studies conducted until now used limestone particles much larger than 90 μm. In order to understand the influence of these factors on the looping process a circulating fluidized bed reactor setup has been built at DTU pilot facilities for conducting through studies as a PhD study with close co-operation with FLSmidth A/S.

5. References

Abanades J.C. and Alvarez D., 2003. *Conversion Limit in the Reaction of CO_2 with Lime*, Energy & Fuel, 17, 308-315.

Abanades J.C., Anthony J.C., Wang J., and Oakey J. E., 2005. *Fluidized Bed Combustion Systems Integrating CO_2 capture with CaO*, Environ. Sci. Technol., 39, 2861-2866.

Andersen M. F., 2009. *CO_2-free Cement Production*, Thesis (M.Sc). Technical University of Denmark.

Baker E. H., 1962. *The Calcium Oxide-Carbon Dioxide System in the Pressure range 1-300 atmospheres*, Journ. Chem. Soc., 70, 464-470.

Evelien C and Wouter.N, 2010. *Energy Technology System Analysis Programme*, IEA http://www.etsap.org/E-techDS/PDF/I03_cement_June%202010_GS-gct.pdf [Accessed 1st Nov 2010]

Larsen M. B, 2007. *Alternative fuel in cement production*, Thesis (PhD). Technical University of Denmark.

Metz B., Davidson O., Coninck H. de, Loos M., Meyer L, 2005. *Special report on Carbon Dioxide Capture and Storage Intergovernmental Panel on Climate Change*, Cambridge University Press.

Romeo L. M., Lara Y., Lisbona P., Escosa J. M., 2009. *Optimizing make-up flow in a CO_2 capture system using CaO*, Chem. Eng. Journ., 147, 252-258.

Shimizu T., Hirama T., Hosoda H., Kitano K., Inagaki M., Tejima K., 1999. *A Twin Fluidized Bed Reactor for Removal of CO_2 from Combustion Processes*. Trans. IChemE, 62-68.

Wang J., Anthony E.J., 2005. *On the Decay Behavior of the CO_2 Absorption Capacity of CaO-Based Sorbents*, Ind Eng Chem Res. 44, 627-629.

Yaws, Carl L., 2009. *Yaws' Handbook of Thermodynamic Properties for Hydrocarbons and Chemicals*. Knovel.

http://knovel.com.globalproxy.cvt.dk/web/portal/browse/display?_EXT_KNOVEL_DISPLAY [15th Oct 2010]

energy&fuels

Article

pubs.acs.org/EF

CO_2 Capture by Cement Raw Meal

Sharat K. Pathi,[†] Weigang Lin,[†] Jytte B. Illerup,*[,†] Kim Dam-Johansen,[†] and Klaus Hjuler[‡]

[†]Department of Chemical and Biochemical Engineering, Technical University of Denmark, Building 229, DK-2800 Kgs. Lyngby, Denmark

[‡]FLSmidth A/S, DK-2500 Valby, Denmark

ABSTRACT: The cement industry is one of the major sources of CO_2 emissions and is likely to contribute to further increases in the near future. The carbonate looping process has the potential to capture CO_2 emissions from the cement industry, in which raw meal for cement production could be used as the sorbent. Cyclic experiments were carried out in a TGA apparatus using industrial cement raw meal and synthetic raw meal as sorbents, with limestone as the reference. The results show that the CO_2 capture capacities of the cement raw meal and the synthetic raw meal are comparable to those of pure limestone. The CO_2 capture capacity of limestone in the raw meal is lower than for pure limestone. The difference in the CO_2 capture capacity decreases with an increase in cycle number. The calcination conditions and composition are major factors that influence the CO_2 capture capacity of limestone. At 850 °C in N_2, the capacity of synthetic raw meal was similar to that of pure limestone, whereas at 950 °C in N_2 and in a CO_2-rich atmosphere there was a significant difference. The SEM and BET analyses indicate that sintering is the main reason for the lower capture capacity of the limestone in the raw meal. The main components of the raw meal used along with the limestone have different effects on the CO_2 capture capacity of the limestone. Al_2O_3 has the most negative effect, followed by Fe_2O_3, whereas SiO_2 showed no effect. These interactions can be observed as a correlation between the measured surface area and the CO_2 capture capacity. The XRD results indicated an increase in crystallite size and the formation of new phases due to the reaction between the main components of the raw meal and the limestone, which also has an effect on the CO_2 capture capacity. The formation of dicalcium silicate was also observed by XRD analysis in the calcined synthetic raw meal. The effect of calcination conditions and compositions on the CO_2 capture capacity as a function of cycle number is described by a correlation equation. This equation is used to determine the decay constant (k) and residual CO_2 capture capacity (X_r). This shows that raw meal could be used as a sorbent for the easy integration of the carbonate looping process into the cement pyro process for reducing CO_2 emissions from the cement production process.

■ INTRODUCTION

Cement production is an energy-intensive process with high CO_2 emissions. It has been estimated that around 5% of the total anthropogenic CO_2 emissions is from the cement industry.[1] The energy demand comes from the calcination of limestone and the formation of the clinker. The cement industry is growing steadily, and this growth is expected to accelerate over the coming decades. Major growth is foreseen in economically growing countries[2] (i.e., China, India, etc.). At the same time, the cement industry is facing challenges of sustainable development. One of them is to reduce the amount of CO_2 emitted because 1 kg of clinker (cl) produced releases almost 1 kg of CO_2.[1]

One of the options with a significant impact on carbon emission reduction is the use of carbon capture and sequestration (CCS) technologies.[3] In CCS, carbon dioxide can be captured by precombustion, oxyfuel combustion, or postcombustion. The carbonate looping process has the potential to capture CO_2 from flue gas with a low energy penalty compared to that of other CO_2 capture processes because high-quality energy may be extracted and electricity may be produced from the heat of the absorption process.

In the carbonate looping process, CO_2 in the flue gas is captured according to the reversible reaction $CaO + CO_2 \rightleftharpoons CaCO_3$ at a thermodynamically favorable temperature. The carbonated sorbent is recycled to a regenerator,[4] in which the sorbent is calcined in a CO_2-rich atmosphere at a temperature greater than 900 °C. The carbonate looping process (CLP) for CO_2 capture from power plants has been studied extensively.[5−15] It is shown that the CO_2 capture capacity of the sorbent decreases with an increase in cycle number,[16,17] which means that the spent sorbent material has to be replaced with fresh material in order to maintain a high CO_2 capture efficiency. This is one of the main challenges in the application of the carbonate looping process in power plants. However, this may not be a serious problem for cement plants because spent sorbent (i.e., calcined limestone) can be used as the feed in clinker production. Thus, this process is especially suitable for the cement industry because the key raw material could be used as a sorbent with the possibility of producing electricity for internal use.

The cement raw meal may be used directly as a sorbent for the carbonate looping process applied to the cement production process because the major component in cement raw meal is limestone, which is approximately 70 w/w% together with SiO_2 (S), Al_2O_3 (A), and Fe_2O_3 (F).[18,19] Cement notation is used to represent raw meal components and clinker phases. The calcined raw meal might serve as both a sorbent for CO_2 capture and as a raw material in clinker production. An energy and cost analysis for integrating an oxyfuel calciner in

Received: June 7, 2013
Revised: August 19, 2013
Published: August 19, 2013

Table 1. Composition of the Limestone and Industrial Raw Meal Used in the Cyclic Experiments Given in w/w%

w/w%	CO_2	CaO	SiO_2	Al_2O_3	Fe_2O_3	K_2O	MgO	MnO	Na_2O	TiO_2
Faxe Bryozo	43.6	55.1	0.45	0.1	0.08	0.03	0.43	0.02		0.01
raw meal	35.63	43.06	13.94	3.6	2.49	0.13	0.93		0.09	0.22

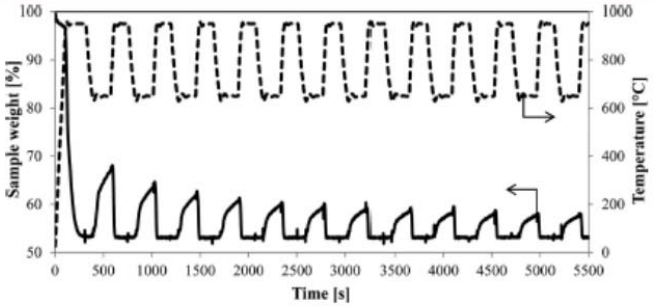

Figure 1. Sample weight % of Faxe Bryozo limestone from the cyclic experiment in the thermogravimetric analyzer. Calcination: 84% CO_2, 950 °C. Recarbonation: 14.7% CO_2 in N_2, 650 °C.

cement production was studied by Rodriguez et al.,[20] and they concluded that high CO_2 capture efficiency was feasible at a relatively low energy penalty. Results from a simple process simulation model showed that the high CO_2 capture capacity of calcined limestone in the cement raw meal will reduce the energy demand of the calciner.[21] Telschow studied the effect of temperature on clinker phase formation, indicating the formation of silicates and aluminates of calcium at 900 °C but in minor fractions.[18] It is widely accepted that the formation of dicalcium silicate (C_2S) might start at temperatures as low as 700 °C.[19] The temperature in the calciner of the carbonate looping process must be higher than 900 °C as a result of the high CO_2 concentration; therefore, it is possible that part of the clinkering reaction may commence in the calciner. Therefore, under carbonate looping conditions there might be interactions between lime and the other components in forming calcium silicates or other intermediate clinker phases; however, their effect on the CO_2 capture capacity is not known.

Dean et al.[22] discussed the possible synergy between the carbonate looping process and clinker formation. The synergy effect was observed on the fraction of the tricalcium silicate C_3S phase in the final clinker produced from spent limestone used as the sorbent in the carbonate looping process compared to fresh limestone. However, to our knowledge no information on the CO_2 capture capacity of the raw meal is reported, except in our previous study.[23] The results of our study showed that the CO_2 capture capacity was influenced by the type of clay and limestone. The CO_2 capture capacity of different clay and limestone mixtures was lower than that of limestone when cycle tests were performed under realistic conditions. The observed effect on the CO_2 capture capacity may be partially due to sintering and partially due to the solid−solid interactions between limestone and clay. However, the complexity of these interactions makes it difficult to understand the decay mechanism, so systematic studies are necessary to understand the mechanism of the CO_2 capture capacity of limestone in the raw meal. In the present work, cyclic experiments were carried out in a thermogravimetric analyzer to investigate the influence of the main components in the raw meal (i.e., silica, alumina, or iron oxide) on the CO_2 capture capacity of limestone.

EXPERIMENTAL SECTION

Materials. Faxe Bryozo limestone obtained from Faxe Kalk A/S, with a particle size of 0.09−0.25 mm, was used as the sorbent material. Silica was obtained from quartz sand, with a particle size similar to that of limestone. Al_2O_3 (purity 99.9%) and Fe_2O_3 (purity 99.9%), with particle sizes of <0.045 mm, were obtained from Sigma-Aldrich and Alfa Aesar, respectively. Cement raw meal supplied by FLSmidth A/S, with a particle size of 0.045−0.2 mm, was used for comparison. The chemical compositions of the limestone and raw meal are summarized in Table 1.

The limestone was mixed with other components in such a way that the fraction of limestone is kept close to 70 w/w%, with the remainder being single, binary, or tertiary mixtures. Because the objective was to evaluate the influence of individual and multiple components, silica, aluminum oxide, and iron oxide were included in equal weight fractions.

Experimental Setup and Methods. Cyclic experiments were performed in a thermogravimetric analyzer (Netzsch STA 449 F1 Jupiter) with rapid heating (500 °C/min) and cooling rates (300 °C/min). The amount of sample used in each experiment was around 20 mg, and the total gas flow rate was 190 N mL/min. In these cyclic experiments, carbonation was carried out at 650 °C in 14.7 vol. % CO_2 in N_2 whereas the calcination conditions were varied. Calcination was performed under mild conditions (850 °C in N_2), harsh conditions (950 °C in N_2), and realistic conditions (950 °C in 84 vol % CO_2) in order to study the influence of temperature and CO_2 concentration during calcination on the CO_2 capture capacity of the limestone. The time for calcination was 3 min for the first cycle and 2 min for the rest of the cycles under isothermal conditions, which was sufficient for complete calcination. Carbonation was carried out for 3 min for each cycle under isothermal conditions. The cyclic experiments with limestone and mixtures were repeated three times to examine the repeatability and thus to estimate the standard deviation of the experimental results. Figure 1 shows the weight % of the sample from an experiment in the thermogravimetric analyzer. The degree of carbonation was estimated from the mass change due to calcination and carbonation based on the following equations. In these equations, the weight gain due to CO_2 capture is considered relative to the amount of CO_2 released from the material, assuming that the total CO_2 released is from calcium carbonate. Thus, these equations can be used not only for pure limestone but also for any mixture for the easy comparison of CO_2 capture capacity as a function of cycle number.

$$X_{calb,N} = \frac{n_{CO_2,N}}{n_{CaCO_3,0}} \quad (1)$$

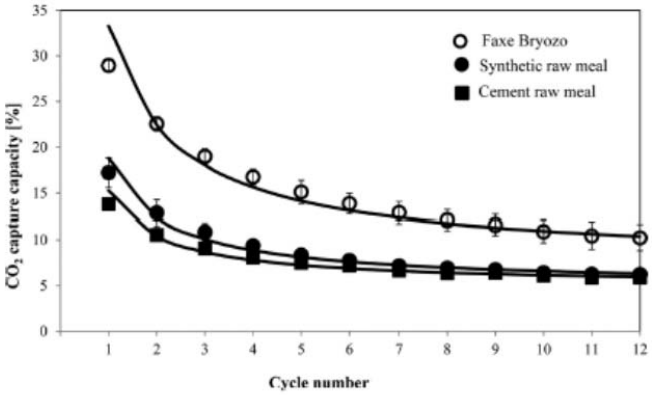

Figure 2. CO_2 capture capacity of limestone, synthetic raw meal (70% limestone and 10% each of SiO_2, Al_2O_3 and Fe_2O_3), and cement raw meal as a function of cycle number under realistic calcination conditions. Calcination: 84% CO_2, 950 °C. Recarbonation: 14.7% CO_2 in N_2, 650 °C.

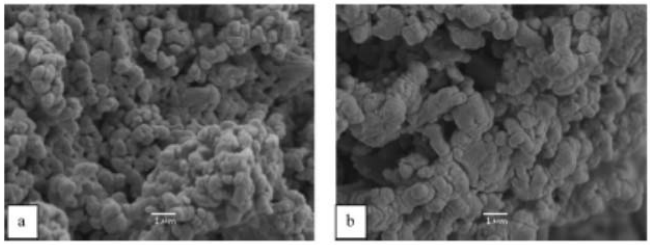

Figure 3. SEM images of calcined sorbent material after 12 cycles: (a) pure limestone and (b) limestone in the synthetic raw meal under realistic calcination conditions.

$$n_{CO_2,N} = \frac{(m_{sample,N} - m_{CaO,1})}{M_{CO_2}} \quad (2)$$

$$n_{CaCO_3,0} = \frac{(m_{sample,0} - m_{CaO,1})}{M_{CO_2}} \quad (3)$$

$X_{carb,N}$ is the degree of carbonation in the Nth cycle, $n_{CO_2,N}$ is the number of moles of CO_2 captured at the end of carbonation in the Nth cycle, $n_{CaCO_3,0}$ is the initial number of moles of $CaCO_3$, $m_{sample,N}$ is the weight of the sample at the end of the Nth carbonation cycle, $m_{CaO,1}$ is the weight of the sample at the end of the first calcination cycle, and M_{CO_2} is the molecular weight of CO_2.

To understand the mechanism of the CO_2 capture capacity of the sorbent, the calcined particles were characterized by different methods. Scanning electron microscopy (SEM) analysis was used to observe changes in the particle morphology after the looping process. The Brunauer–Emmett–Teller (BET) measurement was used to estimate the change in surface area of the sorbent, and X-ray diffraction (XRD) analysis was applied to examine the phase change of the crystalline phases during calcination. Calcination tests were performed in a tubular furnace under a gas flow rate of 1 nL/min under various conditions to obtain samples of 2 g for BET and XRD measurements.

The surface area of the samples was measured by N_2 physisorption using a Quanta Chrome Autosorb ASIQM002-1 surface area analyzer. The morphology of the sorbent particles exposed to different calcination conditions was examined by SEM (JEOL JSM-5900). The XRD spectrum was obtained from a Huber G670 diffractometer by operating in transmission mode in which a sample was placed on a piece of scotch tape. The diffraction spectrum was obtained from 2 to 100° using the Cu Kα1 radiation focused by a quartz monochromator. All of the crystalline phases were identified using the International Centre for Diffraction Data (ICDD) files.

RESULTS

The cyclic experiments were first performed with cement raw meal and with limestone as the reference under realistic calcination conditions (i.e., at 950 °C in a CO_2-rich atmosphere). The number of cycles in these experiments was restricted to 12 because this was more than sufficient when applying the looping process for the cement industry because the major fraction of the spent sorbent can be continuously fed to clinker production.[21] Figure 2 shows the CO_2 capture capacities of limestone as a function of the cycle number. The repeatability of the results was good, with very low standard deviations that were estimated from three separate experimental results obtained under the same operating conditions. The CO_2 capture capacity decreases with an increasing number of looping cycles for both the limestone and for the cement raw meal. The trend in the decay of CO_2 capture capacity is similar to the results presented in the literature (i.e., large decay in the initial cycles compared to that in later cycles).[12]

However, by comparing the CO_2 capture capacity of pure limestone with the cement raw meal it is evident that the capture capacity of limestone in the cement raw meal is approximately 50% lower than for the pure limestone already in the initial cycles. Experiments were performed with limestone mixed with the other main components (silica, aluminum oxide, and iron oxide) present in the cement raw meal, termed synthetic raw meal. The CO_2 capture capacity of synthetic raw

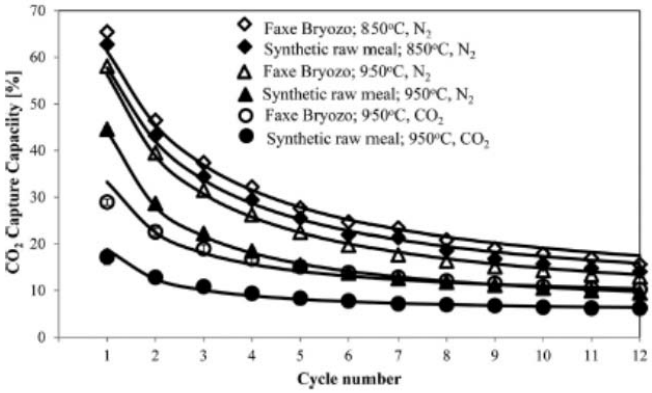

Figure 4. CO_2 capture capacity of pure limestone (open symbols) and synthetic raw meal (solid symbols) as a function of cycle number (◊) under mild calcination conditions (calcination: N_2, 850 °C; recarbonation: 14.7% CO_2 in N_2); (○) under realistic calcination conditions (calcination: 84% CO_2, 950 °C; recarbonation: 14.7% CO_2 in N_2); and (Δ) under harsh calcination conditions (calcination: N_2, 950 °C; recarbonation: 14.7% CO_2 in N_2).

meal was similar to that of cement raw meal, as shown in Figure 2.

Samples from the cyclic experiments were examined by SEM after the final calcination cycle in order to visualize the surface morphology of the pure limestone and the limestone in the synthetic raw meal (Figure 3). For the limestone, the grain sizes are uniform with clearly visible boundaries, whereas in the limestone from the synthetic raw meal the grain size appears to be larger. It appears that the presence of other main components in the raw meal influences the grain size, which might be one of the reasons for the low CO_2 capture capacity of the limestone in the synthetic raw meal compared to that of pure limestone.

To understand the deviation in the CO_2 capture capacity of the limestone compared to that of the limestone in the synthetic raw meal, cyclic experiments were performed (1) under different calcination conditions to investigate the influence of temperature and CO_2 concentration and (2) with various combinations of the main components of raw meal forming binary and tertiary mixtures to evaluate the influence of individual or multiple components present in the mixture.

Influence of Calcination Conditions. Cyclic experiments were performed at 850 and 950 °C in pure N_2 and at 950 °C in a CO_2-rich atmosphere. Figure 4 shows the CO_2 capture capacity of the limestone and the limestone in the synthetic raw meal.

When comparing the CO_2 capture capacity of the limestone under different calcination conditions, we find that the capture capacity drops from 62 to 58% when the calcination temperature is increased from 850 to 950 °C in a N_2 atmosphere. The CO_2 capture capacity of the limestone drops significantly at 950 °C when the calcination atmosphere is changed from a N_2- to a CO_2-rich atmosphere, which represents conditions closer to those of a practical system. Thus, the high concentrations of CO_2 severely enhance the decay in the CO_2 capture capacity of limestone. When comparing the CO_2 capture capacity of the limestone in the synthetic raw meal with that of pure limestone, we observed the following phenomena: (1) the decaying trend in the CO_2 capture capacity as a function of cycle number for the limestone in the synthetic raw meal was similar to that of pure limestone under different calcination conditions and (2) the CO_2 capture capacity of the synthetic raw meal was similar to that of pure limestone when the calcination was performed at 850 °C, whereas at 950 °C in a N_2- or CO_2-rich atmosphere the CO_2 capture capacity of the limestone in the synthetic raw meal was significantly lower. The lower CO_2 capture capacity for the limestone under realistic calcination conditions is the cumulative effect of the high CO_2 concentration and calcination temperature.

To study any interaction between the components, XRD analysis was carried out on the synthetic raw meal, calcined in the tubular reactor. Figure 5 shows the XRD spectra of the synthetic raw meal calcined at 850, 950, and 1050 °C in N_2 and at 950 °C in a CO_2-rich atmosphere.

The XRD spectrum data obtained were compared to the International Centre for Diffraction Data (ICDD) database using a search match program to identify the phases. All of the main components in the calcined original mixture were identified along with new phases. The calcium aluminate peak

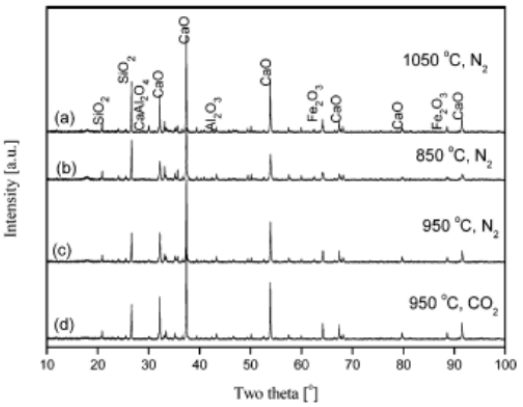

Figure 5. XRD spectra of synthetic raw meal under different calcination conditions for 20 min: (a) 1050 °C, N_2; (b) 850 °C, N_2; (c) 950 °C, N_2; and (d) 950 °C, CO_2 in N_2.

dx.doi.org/10.1021/ef4010732 | Energy Fuels 2013, 27, 5397−5406

has the highest intensity for the sample calcined at 1050 °C, whereas at 850 °C no peak was observed and at 950 °C in CO_2 and in N_2 a small-intensity peak was observed. Furthermore, there are many low-intensity peaks in the 2θ range from 30−35°, which is characteristic of C_2S peaks.[19] The low-intensity peaks of these new phases might be due to their low fraction in the sample compared to the main oxides. The C_2S phase was observed even at a temperature of 850 °C, whereas at higher temperature CS was also identified along with C_2S. On the basis of the XRD spectrum and the Crystallographic Search-Match (CSM) program, the confidence threshold for the peak search match results is estimated to be 90%. Because the possibility of forming C_2S is large compared to that of other clinker phases, XRD analysis was carried out for the mixture containing limestone and silica. For comparison, the XRD spectrum were also obtained for single components of limestone and silica as well as the mixture of limestone and silica with a weight fraction of 30% silica calcined under similar conditions. The XRD spectra for these samples are presented in Figure 6.

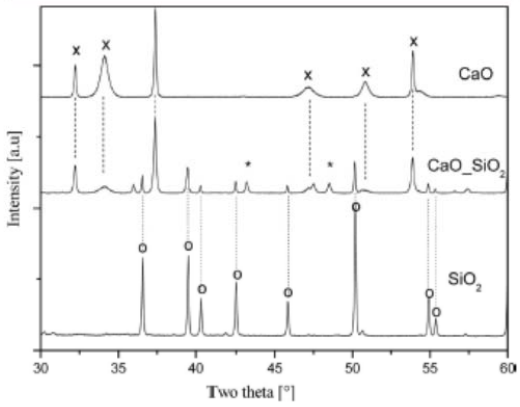

Figure 6. XRD spectra of calcined limestone (×), silica (o), and a mixture of limestone and silica calcined for 20 min under realistic calcination conditions: 950 °C, 84 vol % CO_2 in N_2.

From Figure 6, new peaks were observed for the sample containing a mixture of limestone and silica compared to data from the individual components of limestone and silica. The identified new phase peaks matched the peaks positions of calcium silicate (CS) and C_2S.[19] Even though a new phase such as C_2S could be identified by the search-match program, it is difficult to quantify the phases because of the low intensity of the peaks compared to that of the other phases. Similar experiments were performed by Telschow in a laboratory-scale rotary kiln simulator that showed the formation of C_2S, C_4AF, and C_3A at 900 °C, and their fraction increased with temperature.[19]

However, the expected amount of the new phase under the present experimental condition is low because of bad contact efficiency in the tubular furnace, so the phase formed may not be the only reason for the decay in CO_2 capture capacity. To identify other possible reasons for the drop in the CO_2 capture capacity, the crystallite size of CaO under different calcination conditions for the synthetic raw meal was estimated from the diffraction data presented in Figure 5. The crystallite size of CaO was calculated according to the Debye−Scherrer equation,[24] which uses the fwhm intensity.

$$D = \frac{K\lambda}{\beta \cos\theta} \tag{4}$$

D is the crystallite size in nanometers, K (crystallite-shape factor) = 0.9, λ (X-ray wavelength) = 0.15418 nm, θ is the observed peak angle in radians, and β is the X-ray diffraction broadening (fwhm) in radians.

According to this equation, the crystallite size was estimated for the CaO peak corresponding to 2θ = 37.4°, which had the highest intensity. The trend observed (i.e., the increase in the crystallite size of CaO in the synthetic raw meal with an increase in calcination temperature) is similar to the results for calcined limestone in the literature.[25,26] The influence of a high concentration of CO_2 on the CaO crystallite size in the synthetic raw meal during calcination was also studied. It appears that a higher CO_2 concentration increases the size of the crystallite, which is in agreement with the results of Chen et al.[27] from their study on the calcination of limestone under oxyfuel conditions. To observe the change in the particle morphology of the limestone due to the presence of the other main components in the cement raw meal, SEM analysis was carried out for the pure limestone and the synthetic raw meal. The samples were calcined in a tubular furnace under different calcination conditions. Figure 8 shows the particle surface

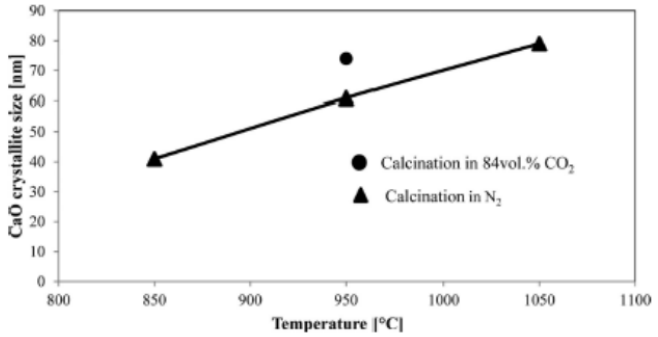

Figure 7. CaO crystallite size in synthetic raw meal determined from XRD peak broadening analysis with respect to temperature under different calcination conditions.

dx.doi.org/10.1021/ef401073p | Energy Fuels 2013, 27, 5397−5406

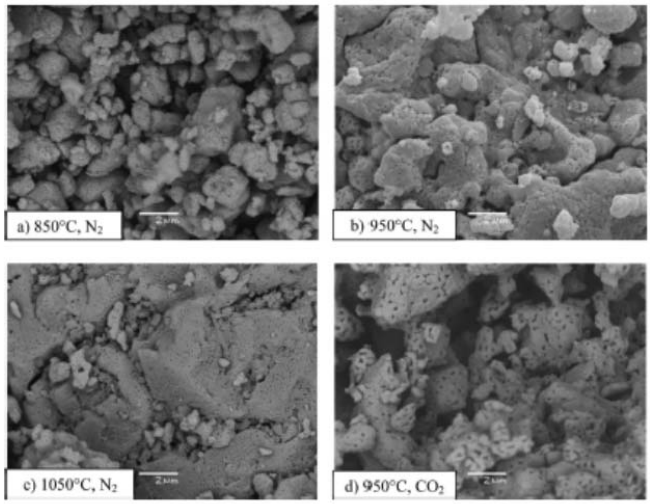

Figure 8. SEM images of pure limestone calcined at (a) 850 °C in N_2, (b) 950 °C in N_2, (c) 1050 °C in N_2, and (d) 950 °C in 84 vol. % CO_2 in N_2.

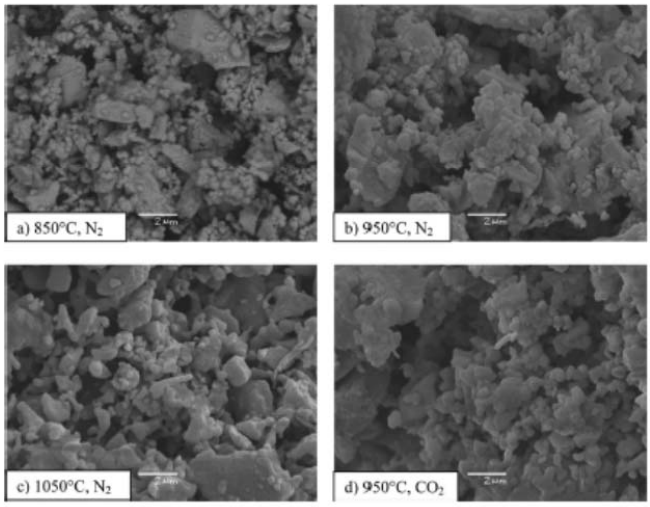

Figure 9. SEM images of limestone in the synthetic raw meal calcined for 20 min at (a) 850 °C in N_2, (b) 950 °C in N_2, (c) 1050 °C in N_2, and (d) 950 °C in 84 vol. % CO_2 in N_2.

morphology of the limestone calcined at (a) 850, (b) 950, and (c) 1050 °C in N_2 and at (d) 950 °C in a CO_2-rich atmosphere. At 850 °C, the individual grains are clearly visible, but with increasing temperature, the grains coalesce and grow in size. The effect of CO_2 concentration during calcination at 950 °C is visible in the form of large pores compared to limestone calcined in N_2.

SEM images of the synthetic raw meal calcined under different conditions are shown in Figure 9. At 850 °C, the grains are clearly visible and are similar to limestone, but with increases in temperature to 950 and 1050 °C, the grains coalesce at the contacted surfaces and grow in size. The synthetic raw meal calcined at 950 °C in a CO_2-rich gas has a surface morphology that appears to be similar to that calcined at 950 °C in N_2, which might be due to the similar interaction between limestone and the other components on the surface. However, on the nanometer scale a difference was observed in the CaO crystal size estimated from the XRD peak-widening technique as shown in Figure 7. In general, an increase in temperature or CO_2 concentration resulted in larger grains in the particles.

The SEM images presented here indicate the sintering phenomenon of the synthetic raw meal and the limestone qualitatively. To obtain quantitative information regarding the sintering phenomenon, BET measurements were carried out for the original materials and for the material calcined under different calcination conditions in a tubular furnace. First, BET measurements were performed for each component at 950 °C

in a CO_2-rich atmosphere. The surface area measurement for each component before and after calcination is summarized in Table 2. The limestone's surface area increased as a result of the release of CO_2 under calcination conditions. For the other components, aluminum oxide sintered with the surface area decreased from 10 to 1 m^2/g and iron oxide decreased from 6 to 2 m^2/g, and for silica, no change in the surface area was expected because of the very low initial surface area. The measured surface area of the pure components is used to calculate the surface area of the mixture considering no interactions.

Table 2. BET Measurements of Main Components of Cement Raw Meal under Atmospheric Conditions and Calcination at 950°C in a CO_2-Rich Atmosphere

material	original, m^2/g	calcined, m^2/g
Faxe Bryozo	1.08	4.04
Al_2O_3	10.4	0.94
Fe_2O_3	6.08	1.82
SiO_2	0.23	

If there are no interactions between the components in the synthetic raw meal, then the surface area can be estimated from the surface area of each component and its respective weight fraction. The surface area of Faxe Bryozo calcined under realistic calcination conditions was measured to be 4.04 m^2/g of calcined limestone. Because the weight fraction of the limestone was maintained at 70 w/w% in the synthetic raw meal, on calcination this reduces to 56 w/w% in the calcined sample. By estimating the surface area of the calcined synthetic raw meal based on the assumption that there are no interactions between the components, it is expected to be 2.70 m^2/g of calcined synthetic raw meal, but the measured surface area is 2.03 m^2/g of calcined synthetic raw meal. If the surface area is contributed to only by the calcined limestone in the synthetic raw meal, then it should be 2.26 m^2/g of calcined synthetic raw meal (e.g., 4.04 m^2/g times 0.56 g/g of calcined synthetic raw meal, which is greater than the measured cumulative surface area). This indicates that there may be interactions between limestone and the other components, resulting in the reduced surface area of the synthetic raw meal. In comparing the CO_2 capture capacity of limestone in the synthetic raw meal to that of pure limestone, we found that the capture capacity was lower for the raw meal, which might be because of the interaction between the components along with sintering enhanced by calcination conditions.

To verify the influence of calcination conditions on the surface area of the synthetic raw meal, BET measurements of the samples under different calcination conditions were carried out. The results from these measurements are summarized in Figure 10. For comparison, BET measurements for the pure limestone were also carried out under similar calcination conditions.

The surface areas of the synthetic raw meal calcined at 850, 950, and 1050 °C under a N_2 atmosphere were 11, 3.9, and 0.69 m^2/g of calcined synthetic raw meal, respectively. The surface areas of the calcined limestone were 21, 17, and 10 m^2/g of calcined limestone under similar calcination conditions, respectively. The decreasing trend in the surface area of limestone with an increase in temperature is due to sintering,[28] which reduces the CO_2 capture capacity of the limestone.[10] In comparing the surface area of limestone and synthetic raw meal,

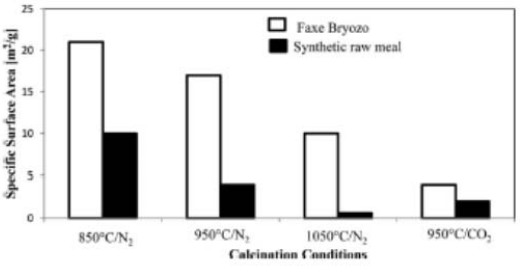

Figure 10. BET surface areas of limestone and synthetic raw meal at 850, 950, and 1050 °C in a pure N_2 atmosphere and a high-CO_2 concentration atmosphere for 20 min.

it is obvious that the surface area of the synthetic raw meal is lower than the area contributed by the limestone alone in the synthetic raw meal, and if there were there no interactions between the components, then the measured surface area must be equal to the estimated surface area using the data given in Table 2 under the respective calcination conditions as presented in Table 3.

Table 3. Measured Surface Area of the Calcined Limestone, Synthetic Raw Meal (SRM), and Estimated Surface Area of SRM Assuming No Interaction between Components

temp, °C	calcined limestone, m^2/g	SRM measured, m^2/g	SRM estimated m^2/g[a]
850	21	11	12
950	17	3.9	10
1050	10	0.69	6

[a]Based on the assumption of no interaction between components.

For all calcination temperatures, the measured surface area of the calcined synthetic raw meal is lower than the estimated value. The difference between the estimated and measured surface areas increases with temperature. The surface area results under mild calcination conditions appear to correlate with only a small difference in the CO_2 capture capacity. At 950 °C, there is a significant difference in the expected and estimated surface areas, similar to the difference in the CO_2 capture capacity results in Figure 2. This shows that the interaction between limestone and the other main components of the synthetic raw meal increases with temperature, which results in the formation of new phases along with a decrease in the surface area of the limestone.

On the basis of the observation from the crystallite size estimation, SEM images, and BET surface area measurements, the mechanisms of the sintering phenomena and their effect on the CO_2 capture capacity of limestone are observed. With increasing temperature, the SEM images show the grains coalescing, the BET surface area decreasing, and the crystallite size increasing, which confirms the sintering process. It is well known that the main parameter that influences sintering is temperature. An increase in temperature results in an increase in the vibrational energy of the atoms, which facilitates mobilization for a reduction in free surface energy. Sintering advances in different stages, increasing with time, by the initiation of neck growth between grains as observed in the SEM images and the elimination of small pores, resulting in a lower surface area as observed in the BET measurements. Along with temperature and time, atmosphere is another

dx.doi.org/10.1021/ef4010732 | Energy Fuels 2013, 27, 5397−5406

parameter that influences sintering. It was claimed[28] that the CO_2 concentration has a catalytic effect on the sintering of CaO crystallites, but no mechanism was explained. The CO_2 partial pressure during the calcination of limestone influences the calcination temperature as a result of thermodynamic equilibrium. There might be a dynamic equilibrium that enhances the movements of atoms in the crystal structure form from calcium oxide to calcium carbonate, resulting in enhanced sintering. However, this is a speculation that could be verified by performing more experiments using the in situ XRD technique. Thus under realistic calcination conditions sintering reduces the porosity of the calcined limestone, which has an effect on the carbonation as a result of the increase in the molar volume of the carbonate from oxide (36.9 from 16.9 cm^3/mol).

CaO crystallite sizes in pure limestone and in the synthetic raw meal were estimated under realistic calcination conditions to be 63 and 74 nm. This indicates that the crystallite size of CaO was influenced not only by temperature, time, and atmosphere but also by the components present in the synthetic raw meal, an effect that needs to be further investigated.

Influence of Components. A comparison of the surface area and corresponding CO_2 capture capacity of the limestone and synthetic raw meal under different calcination conditions indicates the complex nature of the solid−solid particle interaction. To elucidate the influence of each main component in the cement raw meal further, cyclic experiments were carried out under realistic calcination conditions. Because the surface area of the material appears to be the controlling parameter in the CO_2 capture capacity, BET measurements were carried out for the calcined material. The surface areas estimated by BET measurements are presented in Figure 11 for all possible

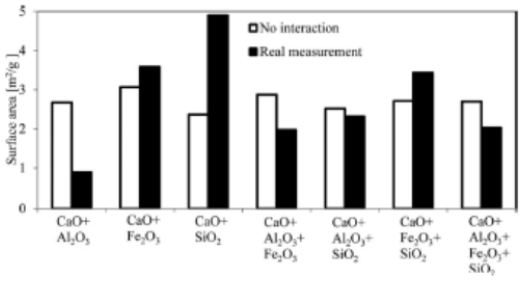

Figure 11. Comparison of measured and estimated surface areas of mixtures containing limestone and other main components of raw meal calcined under realistic calcination conditions.

combinations of limestone and the other main components of the cement raw meal and are compared to the surface area estimated by assuming no interaction between components using the data presented in Table 2.

According to the results obtained, the surface area of each mixture is different from the expected surface area of the mixture without any interactions between the components. The degree of interaction at 950 °C appears to depend on the components present along with limestone.

Considering the binary components of the synthetic raw meal, limestone with aluminum oxide has the lowest surface area and the combination of limestone with silica has the highest surface area. To verify its effect on the CO_2 capture capacity, cyclic experiments were performed. Figure 12 shows the CO_2 capture capacity of limestone and limestone with the other main component of the raw meal. The limestone with aluminum oxide has the lowest CO_2 capture capacity, similar to its measured surface area. Likewise, limestone with silica has the highest CO_2 capture capacity among the binary combinations, as expected from the surface area measured.

Cyclic experiments were performed with the tertiary mixtures to verify any relationship between the surface area measured and their respective CO_2 capture capacity. The CO_2 capture capacity of limestone mixed with the other two components is summarized in Figure 13. The tertiary mixture containing limestone, silica, and iron oxide has a higher CO_2 capture capacity compared to the other tertiary mixtures, whereas limestone mixed with aluminum oxide and iron oxide has the lowest CO_2 capture capacity. The observed trend in CO_2 capture capacity also matched the measured surface areas of the mixtures.

From the detailed analysis of the experimental results from the cyclic experiments and the BET surface area measurements of the mixture, it is possible to correlate the surface area of the mixture with the CO_2 capture capacity of the calcined limestone. Figure 14 summarizes the correlation between the CO_2 capture capacity and the surface area of the mixture calcined at 950 °C and in a CO_2-rich atmosphere. The presented correlation is for the first cycle; however, for the later cycles it might be difficult to observe the clear correlation due to the measurement uncertainties. In the cement raw meal, the main component after limestone is SiO_2, which did not show any negative effect on the CO_2 capture capacity, but the addition of Al_2O_3 or Fe_2O_3 or both decreased the CO_2 capture capacity.

The surface area of the mixture containing limestone and silica was slightly higher than that of pure limestone, and no decay in the CO_2 capacity compared to that in pure limestone is observed. The surface area of the mixture containing aluminum oxide was the lowest and also resulted in the lowest capacity, whereas the mixture containing iron oxide was slightly superior. Thus, a direct correlation between the CO_2 capture capacity and the measured surface area seems to exist. In the tertiary mixtures, a higher capture capacity was obtained for the sample with the highest surface area. The presence of Al_2O_3 in the mixture has a significant effect on the surface area, followed by Fe_2O_3, whereas SiO_2 showed no effect.

Different calcination conditions showed a correlation between the CO_2 capture capacities, the BET surface measured, and the estimated crystallite size of CaO in the synthetic raw meal. To verify the mechanism for the decay in CO_2 capture capacity influenced by the components, the CaO crystallite size was also estimated by the XRD technique, and the results are summarized in Table 4.

The results also indicate that the size of the CaO crystallite was influenced by the components present. The probable explanation for this can be drawn from the sintering of the pure components. The components that sintered most may have induced additional movement in the adjacent atoms, along with their natural tendency to move depending on the sintering temperature and atmosphere. This might have resulted in a high degree of sintering of CaO in the presence of Al_2O_3 and Fe_2O_3, contrary to the presence of SiO_2. However there is an exception for the case with the mixture containing CaO, SiO_2, and Fe_2O_3, which was expected to have a crystal size larger than that of CaO and SiO_2. This indicates the complex nature of the components, which needs to be investigated further.

dx.doi.org/10.1021/ef4010732|Energy Fuels 2013, 27, 5397−5406

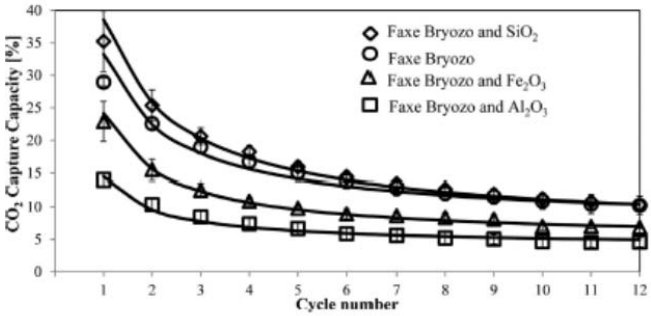

Figure 12. CO_2 capture capacity of binary components as a function of cycle number under realistic calcination conditions. Calcination: 84% CO_2, 950 °C. Recarbonation: 14.7% CO_2 in N_2.

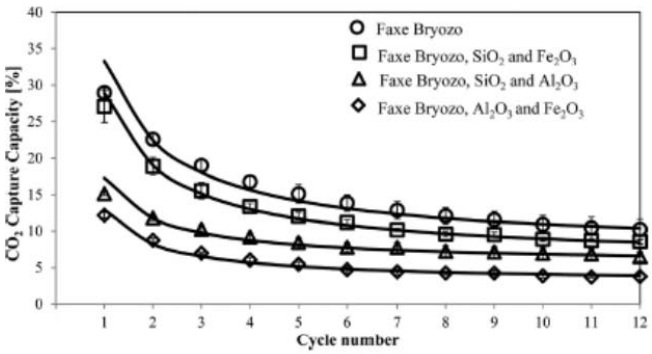

Figure 13. CO_2 capture capacity of tertiary components as a function of cycle number under realistic calcination conditions. Calcination: 84% CO_2, 950 °C. Recarbonation: 14.7% CO_2 in N_2.

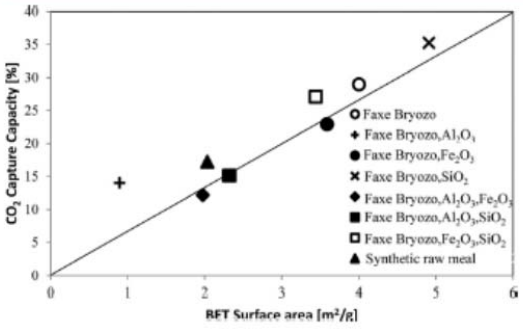

Figure 14. CO_2 capture capacity after the first cycle in the TGA apparatus as a function of the measured BET surface area for the mixtures under realistic calcination conditions: 950 °C, 84 vol. % CO_2.

Table 4. CaO Crystallite Size Estimated by the XRD Technique under Realistic Calcination Conditions

CaO crystallite	CaO	CaO + SiO_2	CaO + Fe_2O_3 + SiO_2	CaO + Al_2O_3 + SiO_2	SRM
size, nm	63	53	51	68	74

Decay in CO_2 Capture Capacity. The CO_2 capture capacity of limestone decreases with an increase in the number of cycles. The detailed analysis by SEM and BET measurements shows the textural changes in the particles. It can be concluded that the main mechanism in limestone capacity decay is sintering, and a correlation can be observed from Figure 14 between the surface area and CO_2 capture capacity. Similar decay mechanisms were observed by Abanades[16] and Wang and Anthony.[29] They formulated simple correlations to describe the decay in the CO_2 capture capacity. However, these correlations were developed for natural limestone (>95 w/w% is $CaCO_3$) unlike the complex material (raw meal) considered in this study. The main observation from the CO_2 capture capacities as a function of cycle numbers was a fast decay in the initial cycles followed by slow decay, reaching an asymptotic value that is independent of the cycle number. To formulate this trend in the decay of CO_2 capture for application to the process simulation studies, it is important to consider two parameters: (1) the degree of decay and (2) the final CO_2 capture capacity. The correlation proposed by Grasa and Abanades[30] is used to quantify the degree of decay and residual CO_2 capture capacity shown by the following equation:

$$X_N = \frac{1}{\frac{1}{1-X_r} + kN} + X_r \tag{5}$$

The decay constant (k) and residual capture capacity (X_r) were determined from curve fitting. The results of this fitting exercise are compiled in Table 5. The correlation between the experimental and predicted CO_2 capture capacities is good (R^2 – 0.98).

dx.doi.org/10.1021/ef401073p | Energy Fuels 2013, 27, 5397–5406

Table 5. CO_2 Capture Decay Constant (k) and Residual CO_2 Capture Capacity (X_r) of Limestone Mixed with the Main Components of the Raw Meal

solids	T (calcination), °C	CO_2 conc, vol. %	k	X_r
Faxe Bryozo	850	0	0.79	0.08
Faxe Bryozo	950	0	0.97	0.075
Faxe Bryozo	950	84	2.8	0.075
synthetic raw meal	850	0	0.91	0.075
synthetic raw meal	950	0	1.5	0.05
synthetic raw meal	950	84	6.2	0.05
cement raw meal	950	84	8.7	0.05
Faxe Bryozo, Al_2O_3	950	84	8.5	0.04
Faxe Bryozo, Fe_2O3	950	84	4.17	0.05
Faxe Bryozo, SiO_2	950	84	2.05	0.065
Faxe Bryozo, Al_2O_3, Fe_2O_3	950	84	9.05	0.03
Faxe Bryozo, Fe_2O_3, SiO_2	950	84	3.3	0.06
Faxe Bryozo, Al_2O_3, SiO_2	950	84	7.45	0.055

The results show that for pure limestone and for the limestone in the raw meal under the tested conditions the calcination temperature influences the residual CO_2 capacity of the limestone whereas the CO_2 concentration has a profound effect on the decay constant with no influence on the residual CO_2 capture capacity. These observations were similar to the results obtained by Grasa,[30] but the effect of the main components of the raw meal was complex and both the residual CO_2 capture capacity and decay constant were affected.

CONCLUSIONS

On the basis of the experimental work, the main conclusions are summarized as follows: (1) Raw meal could be used as the sorbent even though there are interactions between lime and the other components, especially under realistic calcination conditions. (2) SEM, XRD, and BET analyses indicated that sintering is the main reason for the observed decrease in the CO_2 capture capacity. A correlation was established between the surface area of the mixtures and the CO_2 capture capacity of the limestone in the mixture under realistic conditions. (3) XRD results show that the CaO crystallite size was influenced not only by the calcination conditions but also by the components of the cement raw meal. (4) The decay in the CO_2 capture capacity of the limestone in the raw meal is due to sintering, resulting in a change in particle morphology and a larger CaO crystal size. (5) The CO_2 capture capacity as a function of cycle number can be described by a two-parameter correlation, which can be used for process simulation studies using raw meal sorbent.

AUTHOR INFORMATION

Corresponding Author

*E-mail: jbi@kt.dtu.dk.

Notes

The authors declare no competing financial interest.

ACKNOWLEDGMENTS

This work is part of the research work of the Combustion and Harmful Emission Control (CHEC) Research Centre at the Department of Chemical and Biochemical Engineering, Technical University of Denmark. The Danish National Advanced Technology Foundation, FLSmidth A/S, and the Technical University of Denmark under the research platform of New Cement Production Technology are acknowledged for their sponsoring of the project.

REFERENCES

(1) Worrell, E.; Price, L.; Martin, N.; Hendriks, C.; Meida, L. O. *Annu. Rev. Energy Environ.* **2001**, 303−329.
(2) International Energy Agency Cement Road Map Targets. http://www.iea.org/papers/2009/Cemen_Roadmap_targets_viewing.pdf; accessed 12/31/12.
(3) Metz, B.; Davidson, O.; De Coninck, H.; Loos, M.; Meyer, L. *Intergovernmental Panel on Climate Change Special Report on Carbon Dioxide Capture and Storage*; Cambridge University Press: New York, 2005.
(4) Shimizu, T.; Hirama, T.; Hosoda, H.; Kitano, K.; Inagaki, M.; Tejima, K. *Chem. Eng. Res. Des.* **1999**, *A1*, 62−68.
(5) Pawlak-Kruczek, H.; Wiedkowska, K. *Chem. Process Eng.* **2010**, *4*, 889−903.
(6) Blamey, J.; Anthony, E. J.; Wang, J.; Fennell, P. S. *Prog. Energy Combust. Sci.* **2010**, *2*, 260−279.
(7) Dean, C. C.; Blamey, J.; Florin, N. H.; Al-Jeboori, M.; Fennell, P. S. *Chem. Eng. Res. Des.* **2011**, *6*, 836−855.
(8) Stanmore, B. R.; Gilot, P. *Fuel Process. Technol.* **2005**, *16*, 1707−1743.
(9) Ströhle, J.; Lasheras, A.; Galloy, A.; Epple, B. *Chem. Eng. Technol.* **2009**, *3*, 435−442.
(10) Abanades, J. C.; Anthony, E. J.; Wang, J. S.; Oakey, J. E. *Environ. Sci. Technol.* **2005**, *8*, 2861−2866.
(11) Fennell, P. S.; Pacciani, R.; Dennis, J. S.; Davidson, J. F.; Hayhurst, A. N. *Energy Fuels* **2007**, *4*, 2072−2081.
(12) Gonzalez, B.; Grasa, G. S.; Alonso, M.; Abanades, J. C. *Ind. Eng. Chem. Res.* **2008**, *23*, 9256−9262.
(13) Sun, P.; Grace, J. R.; Lim, C. J.; Anthony, E. J. *Environ. Sci. Technol.* **2007**, *8*, 2943−2949.
(14) Manovic, V.; Anthony, E. J. *Environ. Sci. Technol.* **2009**, *18*, 7117−7122.
(15) Abanades, J. C. *Chem. Eng. J.* **2002**, *3*, 303−306.
(16) Abanades, J. C.; Alvarez, D. *Energy Fuels* **2003**, *2*, 308−315.
(17) Grasa, G. S.; Abanades, J. C.; Alonso, M.; Gonzalez, B. *Chem. Eng. J.* **2008**, *3*, 561−567.
(18) Telschow, S. *Clinker Burning Kinetics and Mechanism*; Technical University of Denmark: Lyngby, Denmark, 2012.
(19) Taylor, H. F. W. *Cement Chemistry*; Thomas Telford: London, 1997; pp 1−456.
(20) Rodriguez, N.; Murillo, R.; Abanades, J. C. *Environ. Sci. Technol.* **2012**, *4*, 2460−2466.
(21) Pathi, S. K.; Andersen, M. F.; Lin, W.; Illerup, J. B.; Dam-Johansen, K.; Hjuler, K. *Carbonate Looping for De-carbonization of Cement Plant*, 13th International Conference of Cement Chemistry, Spain, July 2011.
(22) Dean, C. C.; Dugwell, D.; Fennell, P. S. *Energy Environ. Sci.* **2011**, *6*, 2050−2053.
(23) Lin, W.; Illerup, J. B.; Dam-Johansen, K.; Hjuler, K. *Application of Carbonate Looping to Cement Industry*, 21st International Conference on Fluidized Bed Combustion, Italy, June 2012.
(24) Scherrer, P. *Gött. Nachr* **1918**, 98.
(25) Rodriguez-Navarro, C.; Ruiz-Agudo, E.; Luque, A.; Rodriguez-Navarro, A.; Ortega-Huertas, M. *Am. Mineral.* **2009**, *4*, 578−593.
(26) Fischer, H. C. J. *Am. Ceram. Soc.* **1955**, *8*, 284−288.
(27) Chen, C.; Zhao, C.; Liang, C.; Pang, K. *Fuel Process. Technol.* **2007**, *2*, 171−178.
(28) Borgwardt, R. H. *Chem. Eng. Sci.* **1989**, *1*, 53−60.
(29) Wang, J.; Anthony, E. J. *Ind. Eng. Chem. Res.* **2005**, *3*, 627−629.
(30) Grasa, G. S.; Abanades, J. C. *Ind. Eng. Chem. Res.* **2006**, *26*, 8846−8851.

Ready for Submission

Performance of the Carbonator as a Fast Fluidized Bed Reactor: Experimental and Modeling

[1]*Sharat K. Pathi ;*[1]*Weigang Lin ;*[1]*Jytte B. Illerup*; *[1]*Kim Dam-Johansen; *[2]*Klaus Hjuler*
[1]Department of Chemical and Biochemical Engineering, Technical University of Denmark, Building 229, DK-2800 Kgs. Lyngby, Denmark
[2]FLSmidth A/S, DK-2500 Valby, Denmark

ABSTRACT

The carbonate looping process is a promising technology for CO_2 capture from flue gas. In this process the CO_2 capture efficiency depends on the performance of a carbonator that may be operated as a Circulating Fluidized Bed (CFB). In this paper, the carbonator performance is investigated by applying a new experimental method with accurate control of the particle re-circulation rate. The experimental results show that inlet Ca to C molar ratio is the main factor on the CO_2 capture efficiency by the carbonator, i.e. increasing the inlet Ca/C from 4 to 13 results in increasing the CO_2 capture efficiency from 40 to 85% with limestone having a maximum CO_2 capture capacity of only 11.5%. Furthermore, a reactor model for carbonator is developed based on the Kunii-Levenspiel's model. A key parameter in the model is the particle distribution along the height of the reactor, which is estimated from experiments under stable operating conditions with constant bed inventory, reactor temperature and exit CO_2 concentration. The validated CFB carbonator model was used to simulate different operating conditions relevant for CO_2 capture from a power plant and for a cement plant. The results show that a particle re-circulation rate of 2-5 kg/m^{2}s is sufficient for attaining 90% CO_2 capture efficiency but it depends on the inlet Ca to C ratio.

KEYWORDS: CCS, CO_2 Capture, CFB carbonator, Carbonate Looping, Cement plant, Power plant
*Corresponding Author: Jytte Boll Illerup, jbi@kt.dtu.dk

Ready for Submission

Low CO_2 Emission Cement Plant with Co-Generation

[1]Sharat K. Pathi; [1]Weigang Lin; [1]Jytte B. Illerup; [1]Kim Dam-Johansen; [2]Klaus Hjuler*

[1]Department of Chemical and Biochemical Engineering, Technical University of Denmark, Building 229, DK-2800 Kgs. Lyngby, Denmark
[2]FLSmidth A/S, DK-2500 Valby, Denmark

ABSTRACT

A process model of mass and energy flows was developed to analyze the integration of the carbonate looping process (CLP) with a cement plant using cement raw meal as sorbent for CO_2 capture. The performance of the carbonator was estimated using own experimental data for the CO_2 capture capacity of cement raw meal. It was found that a cement plant with CLP and waste heat recovery can be self-sufficient in terms of electricity at production capacities above 3400 tons clinker per day and the estimated energy penalty for CO_2 capture is 2 MJ/kg of CO_2 captured.

KEYWORDS: CO_2 Capture, Carbonate Looping, Cement plant, Co-generation

*Corresponding Author: Jytte Boll Illerup, jbi@kt.dtu.dk